4-3-2018 2:00 PM

Effects of Elevated Temperature, Elevated CO2 and Photoperiod on Conifer Carbon Fluxes

Joseph R. Stinziano, *The University of Western Ontario*

Supervisor: Way, Danielle A., *The University of Western Ontario*

A thesis submitted in partial fulfillment of the requirements for the Doctor of Philosophy degree in Biology

Abstract

Increasing temperatures due to rising atmospheric CO_2 concentrations will have direct effects on plant physiology, specifically photosynthetic carbon uptake. Changes in photosynthetic carbon uptake will alter feedbacks between vegetation and atmospheric CO_2, and changes in forest carbon dynamics will be important in determining whether vegetation amplifies or attenuates the effects of anthropogenic CO_2 emissions on climate. Coniferous trees, which are a large component of the boreal forest, are understudied in relation to thermal acclimation of photosynthesis and temperature effects on growth. In the present work, I assess the impact of rising temperatures on carbon fluxes in coniferous trees, using meta-analysis, manipulative experimentation, and *in silico* modeling. I found that photosynthetic capacity is strongly regulated by temperature in white spruce seedlings, but growth is strongly regulated by photoperiod, desynchronizing growth and carbon uptake. I found that boreal tree carbon uptake is likely to respond positively to moderate warming, particularly during autumn and at high latitudes. However, day length may restrict how much of this carbon uptake is allocated to longer-term carbon stores such as woody biomass, which could enhance the release of CO_2 from boreal forests between growing seasons. As well, thermal acclimation of photosynthesis in conifers may reduce carbon uptake, reducing the increase in carbon uptake expected with warming in conifers at high latitudes. However, modeling thermal acclimation of photosynthesis by adjusting multiple parameters of the photosynthetic temperature response equations provides diminishing returns in model performance for increased complexity. Therefore, I recommend that multifactor thermal acclimation of photosynthesis not be used in large scale modeling efforts until the underlying physiology is better understood. Overall, my data suggest that climate change will enhance the seasonality of carbon uptake in conifers, increasing the magnitude of peak carbon uptake and possibly peak carbon efflux, and may decouple photosynthetic carbon uptake and growth during autumn. However, physiological variability between boreal tree species may be introducing uncertainties in modelled boreal tree responses to climate that may propagate into unrealistic predictions of tree net carbon gain in the future. Furthermore, my work demonstrates that there is a large gap in understanding photosynthetic thermal acclimation, both on a fundamental level and in terms of the biological diversity of measured temperature responses.

Keywords

Photosynthesis, Respiration, Tree Physiology, Boreal Forest, Modeling, Thermal Acclimation, Seasonality, Carbon Cycle.

Co-Authorship Statement

Chapter 2 was published as a review article in *Botany* (reprint permission in Appendix D). I was first author for this publication, and Danielle A. Way (DAW) was the co-author, who contributed to the conception of the ideas and helped in writing the manuscript.

Chapter 3 was published in *Plant, Cell & Environment* (reprint permission in Appendix D). I was first author for this publication, and DAW was the co-author, who contributed to experimental design, manuscript writing, and discussion of ideas.

Chapter 4 was published in *Global Change Biology* (reprint permission in Appendix D). I was first author for this publication, and the co-authors were DAW and William L. Bauerle (WLB). WLB contributed to modeling design and input, and both DAW and WLB contributed to manuscript writing and discussion of ideas.

Chapter 5 is a version of a manuscript submitted to *Global Change Biology*. I was first author for this publication, and the co-authors were DAW and WLB. DAW and WLB contributed to modeling design. Both DAW and WLB contributed to manuscript writing and discussion of ideas.

Acknowledgments

Pursuing a Ph.D. is often stereotyped as a lonely endeavor to push the boundary of human knowledge, but it is far from lonely, and cannot be done alone. There are many people that I must thank for my success thus far. I would like to begin by thanking my family: my parents, Catherine and Alfred Stinziano, for your unceasing support even if you did not quite understand what or why I was doing what I was doing, and for teaching me to be open and perceptive to new ideas, which were the sparks that put me on this journey; my grandmother, Eleanor Kasawan, for teaching me the importance of patience, which sustained me through the challenging moments of this journey; my cousin, Alex Heibein, for providing comic relief and advice when I needed it most; and my brothers, Tony and Nick Stinziano, for your advice and encouragement when I needed it.

I have been told that your mood in grad school reflects the mood of your supervisor: how lucky I was, then, to have Danielle Way as my supervisor. Enthusiastic and excited even at the worst of times, your encouragement and support, combined with your piercing intellect, have opened my mind and creativity in a way that I never imagined. You helped me tame my enthusiasm and sometimes impulsive curiosity, which otherwise would have put me in quite the sticky pickle. But most of all, I am grateful for your unwavering commitment to my success, providing me with amazing opportunities and connections.

Sometimes working on a Ph. D. can get really stressful, and you need someone there providing unconditional support. I want to thank my partner, Megan Swafford, for providing such unconditional love and support, keeping me up when things were down, and your enthusiasm and patience in supporting my goals and ambitions.

If you are lucky, your lab members become family and I would like to thank all the past and present members of the Way lab: Vi Bui, for your intellectual and emotional support, thought-provoking ideas, and silliness in Sweden #WaylabgoestoSweden; Yulia Kroner, for our discussions that stimulated greater clarity of thought; Eric Dusenge, for those thoughtful and eager discussions on our long road trips to Minnesota; Andre Duarte, for injecting optimism and skepticism when each was most needed; and Bridget Murphy, for placating me when my ideas exceeded the bounds of sensibility.

I would like to thank everyone (past and present) in BGS 2035 for their intellectual, social, emotional, and mental support: Laura Ferguson, Ruth Jakobs, Alex McKinnon, Lauren Des Marteaux, Jantina Toxopeus, Jackie Lebenzon, Alex Cooper, Kurtis Turnbull, Susan Anthony, Kate Mathers, Sasha Madhavji, and Joshua Frank. And of course, my scientific role models and BGS 2035 alumni: Heath MacMillan, Katie Marshall, and Caroline Williams, all of whom are paragons of modern science.

I would like to thank past and present members of the Hüner lab: Lauren Hollis, Beth Szyszka, and Avery McCarthy, for providing invaluable experimental advice and a sounding board for my ideas, however crazy they were.

I would like to thank everyone that I met during my time in Fort Collins, specifically: my mentor, William Bauerle, for encouraging my ambition and enthusiasm; my friends, Lauren Wearsch, Meghan Denny, Ale Romero, and Dominic Cossentino for making me feel at home in Fort Collins; and to the members of Café Philosophique, for stimulating discussions on topics so far removed from my work. It was a short time, but all that support helped me to produce most of my thesis.

I would also like to thank everyone that I worked with and met on my Fulbright exchange in Albuquerque, specifically: my advisor, David Hanson, for encouraging and amplifying my unbridled curiosity; Samantha Stutz, for helping me think of things from a different perspective; Jeremiah Anderson, for making my life a lot easier with your technical know-how; and Monique and Jacob Swafford for helping make Albuquerque feel like home. I'd also like to thank Kathleen Hill and Jeremy McNeil for encouraging me to apply for the Fulbright award in the first place.

I'd like to thank the staff in the Biology Department main office: Diane Gauley, Carol Curtis, and Hillary Bain for making university bureaucracy seem trivial, and Arzie Chant for your hilarious and morale boosting off-the-cuff remarks about everything.

Lastly, I'd like to thank all my scientific advisors, supervisors, and mentors throughout my degree: Danielle Way, Norman Hüner, Brent Sinclair, Hugh Henry, William Bauerle, and David Hanson. This group covers the whole range of approaches to science, from careful conservatism to diving headfirst into controversial topics, and all of them have a deep

passion for what they do. Your diverse perspectives on science have cultivated within me an open mind and healthy skepticism for new ideas, and encouraged me to push the limits and boundaries of my science both methodologically and philosophically.

Table of Contents

List of Tables

List of Figures

List of Appendices

List of Abbreviations

[Car] – carotenoid concentration

[Chl a] – chlorophyll a concentration

[Chl b] – chlorophyll b concentration

[Total Chl] – total concentration of Chl a and Chl b

a – coefficient for the relationship between photosynthetic capacity and day of year for *Picea glauca*

ADP – adenosine diphosphate

ADVJ – deactivation energy of the maximum electron transport rate

AIC – Akaike's Information Criterion

AJQ – quantum yield of electron transport

ALLAREA – leaf area

ALLDIAM – stem diameter

ALLHTCROWN – height

ALLHTTRUNK – trunk height

ALLRADX – crown radius in the x-direction

ALLRADY – crown radius in the y-direction

A_{net} – net CO_2 assimilation rate

ANOVA – analysis of variance

ARHO – needle reflectance

A_{sat} – light saturated rate of net CO_2 assimilation

ATAU – needle transitivity

ATP – adenosine triphosphate

b - coefficient for the relationship between photosynthetic capacity and day of year for *Picea glauca*

b_1 – intercept of the Ball-Berry stomatal conductance model

BIC – Bayesian Information Criterion

BPT – beta distribution coefficients for leaf area density

C Gain – carbon gain

C_3 – photosynthesis where the first stable product of CO_2 fixation is a three-carbon sugar

C_a – ambient CO_2 concentration at the leaf surface

Car – carotenoids

C_c – chloroplastic carbon dioxide concentration

CH_2O – a carbohydrate molecule

Chl a – chlorophyll a

Chl b – chlorophyll b

C_i – intercellular CO_2 concentration

CO_2 – carbon dioxide

C_s – CO_2 concentration outside the leaf

d – constant for the relationship between ΔS of V_{cmax} or J_{max} and acclimation temperature

DAYRESP – fraction by which dark respiration is reduced in the light

DELSJ – entropy term of the maximum electron transport rate

df – degrees of freedom

DL – day length

DOY – day of year

e – slope for the relationship between ΔS of V_{cmax} or J_{max} and acclimation temperature

E_a – activation energy of the Arrhenius temperature response

$E_{a,Jmax}$ – activation energy of the maximum electron transport rate

$E_{a,Vcmax}$ – activation energy of the maximum Rubisco carboxylation rate

Eav (-) – acclimation of the activation energy of V_{cmax} with the unmodified Arrhenius equation describing V_{cmax}

Eav (+) – acclimation of the activation energy of V_{cmax} with the modified Arrhenius equation describing V_{cmax}

Eav/ΔS – acclimation of the activation energy of V_{cmax} and the entropy parameter of the modified Arrhenius equation for V_{cmax} and J_{max}

EAVC – activation energy of V_{cmax}

EAVJ – activation energy of J_{max}

Eavj (-) – acclimation of the activation energies of V_{cmax} and J_{max} with the unmodified Arrhenius equation describing V_{cmax}

Eavj (+) – acclimation of the activation energies of V_{cmax} and J_{max} with the modified Arrhenius equation describing V_{cmax}

Eavj/ΔS – acclimation of the activation energies of V_{cmax} and J_{max} and the entropy parameter of the modified Arrhenius equation for V_{cmax} and J_{max}

ELIP – ellipsoid canopy shape

ENDDATE – end date of MAESTRA simulations

f – fraction of light absorbed by the light harvesting complexes

$f(T_k)$ – the rate of a biological process at a given leaf temperature

$FADH_2$ – flavin adenine dinucleotide

FOLQ10 – foliage Q_{10} values

g - constant for the relationship between photosynthetic capacity and day of year for *Picea glauca*

G0 – input parameter for the intercept of the Ball-Berry stomatal conductance model

G1 – input parameter for the slope of the Ball-Berry stomatal conductance model

GAMMA – CO_2 compensation point in the absence of mitochondrial respiration at 25 °C

g_m – mesophyll conductance

GPP – gross primary productivity

GPP_{meas} – measured gross primary productivity

GPP_{mod} – modelled gross primary productivity

g_s – stomatal conductance

H – seedling height

H_d – the deactivation energy of the modified Arrhenius temperature response

hv – photon of visible light energy

I – irradiance

IR – infrared radiation

j – potential rate of electron transport

J_{max} – maximum rate of electron transport

J_{max25} – maximum rate of electron transport at 25 °C

JMAXA – slope of the relationship between J_{max} and foliar nitrogen

JMAXB – intercept of the relationship between J_{max} and foliar nitrogen

k_{25} – basal photosynthetic capacity at 25 °C

k_{25} (-) – acclimation of basal photosynthetic capacity with the unmodified Arrhenius equation describing V_{cmax}

k_{25} (+) – acclimation of basal photosynthetic capacity with the modified Arrhenius equation describing V_{cmax}

K_c – the Michaelis-Menten constant for Rubisco carboxylation

K_o – the Michaelis-Menten constant for Rubisco oxygenation

k_{opt} – photosynthetic capacity at the thermal optimum temperature of the leaf

LA – leaf area

lat. – latitude

LMA – leaf mass area

LMR – leaf mass ratio

long. – longitude

m_1 – slope of the Ball-Berry stomatal conductance model

MA – modified Arrhenius temperature response

N – sample size

$N_{2(l)}$ – liquid nitrogen

NA (-) – non-acclimated scenario with the unmodified Arrhenius equation describing V_{cmax}

NA (+) – non-acclimated scenario with the modified Arrhenius equation describing V_{cmax}

NAD^+ – oxidized nicotinamide adenine dinucleotide

NADH – nicotinamide adenine dinucleotide

$NADP^+$ – oxidized nicotinamide adenine dinucleotide phosphate

NADPH – nicotinamide adenine dinucleotide phosphate

N_{area} – foliar nitrogen concentration on an area basis

NAZ – number of azimuth angles in MAESTRA

NFOL – foliar nitrogen concentration for each canopy layer

NIR – near-infrared radiation

NL – night length

NOLAY – number of layers in the tree crown in MAESTRA

NOTREES – number of shading trees in MAESTRA

NOTREES – number of simulated trees in the plot

NPP – net primary productivity

NSIDES – number of sides to a leaf

NUE – nitrogen use efficiency

NZEN – number of zenith angles in MAESTRA

O.D. – Optical density

O_i – intercellular O_2

OTC – open top chamber

P – the rate of photosynthesis

PAR – photosynthetically active radiation

PC – photosynthetic capacity, either V_{cmax} or J_{max}

P_i – inorganic phosphate

P_m – the maximum capacity for photosynthesis

P_{max} – maximum value of photosynthetic capacity for a given species

$P_{max,pg}$ – maximum value of photosynthetic capacity for *Picea glauca*

Pn – photosynthetic acclimation

PPLAY – number of points per crown layer in MAESTRA

PTOX – plastoquinol terminal oxidase

Q – maximum quantum yield

Q_{10} – thermal sensitivity of a biological process

R – the universal gas constant

R_1 – respiration rate at temperature T_1

R_2 – respiration rate at temperature T_2

R_{25} – respiration rate at 25 °C

RD – foliar dark respiration at a reference temperature

R_{dark} – foliar respiration in the dark

R_{day} – foliar respiration in the light

RHOSOL – Soil reflectance

RMR – root mass ratio

Rn – respiratory thermal acclimation

R_{night} – night time foliar respiration

R_{root} – root respiration

$R_{root, day}$ – root respiration during the day

$R_{root, night}$ – root respiration during the night

RTEMP – reference temperature at which RD is specified

Rubisco – ribulose-1,5-bisphosphate carboxylase oxygenase

s.e.m. – standard error of the mean

SD – standard deviation

SLA – specific leaf area

SMR – stem mass ratio

STARTDATE – start date of MASTRA simulations

T – temperature

T_1 –leaf temperature at R_1

T_2 – leaf temperature at R_2

T_{air} – air temperature

T_{avg} – average daily temperature in a given week

T_{Day} – day time temperature

T_g – growth temperature

T_{growth} – previous ten-day running mean air temperature

THETA – curvature of the light response curve of electron transport

T_k – leaf temperature in Kelvin

T_{Night} – night time temperature

T_{opt} – thermal optimum temperature of A_{net}

T_{optk} – thermal optimum temperature of V_{cmax} or J_{max}

TPU – triose phosphate limitation

UA – unmodified Arrhenius temperature response

v_c – the rate of carboxylation

V_{cmax} – maximum rate of Rubisco carboxylation

V_{cmax25} – maximum rate of Rubisco carboxylation at 25 °C

VCMAXA – slope of the relationship between V_{cmax} and foliar nitrogen

VCMAXB– intercept of the relationship between V_{cmax} and foliar nitrogen

v_o – the rate of oxygenation

WLEAF – width of the leaf

x – coefficient describing the acclimation response of activation energy for V_{cmax} or J_{max} to growth temperature

XMAX – length of the plot in the x-direction

XSLOPE – slope of the plot in the x-direction

y – coefficient describing the acclimation response of activation energy for V_{cmax} or J_{max} to growth temperature

YMAX – length of the plot in the y-direction

YSLOPE – slope of the plot in the y-direction

z – constant describing the acclimation response of activation energy for V_{cmax} or J_{max} to growth temperature

Z0HT – roughness length

ZHT – measurement height

ZPD – zero-plane displacement

α – proportion of irradiance absorbed by the leaf

Γ^* – CO_2 compensation point in the absence of mitochondrial respiration

ΔS – the entropy parameter of the modified Arrhenius temperature response

Θ – curvature of the photosynthetic light response

Φ – the ratio of oxygenation to carboxylation

Chapter 1

1 General introduction

Anthropogenic CO_2 emissions are causing the global climate system to warm, which is associated with changing seasonal patterns of, and enhanced variability in, air temperature and precipitation (Collins *et al*., 2013; IPCC, 2013). These climatic changes are affecting the biosphere, which responds to and interacts with the rest of the Earth system, primarily through coupled vegetation-atmosphere feedbacks (Ciais *et al*., 2013). Vegetation-atmosphere feedbacks occur because vegetation consumes CO_2 from the atmosphere through photosynthesis and water from the hydrosphere through root systems, and releases CO_2 through respiratory processes and water through transpiration (Ciais *et al*., 2013; Hartmann *et al*., 2013). Vegetation thus can alter radiative forcing (through photosynthesis and transpiration, which affect atmospheric concentrations of two greenhouse gases, CO_2 and water vapor) and precipitation patterns (through transpiration) (Myhre *et al*., 2013). Understanding how plants respond to a changing environment is crucial to our ability to predict and prepare for the future state of the Earth system (Collins *et al*., 2013; Rogers *et al*., 2017). The focus of this work is on understanding the responses of photosynthesis, net carbon gain (the balance of photosynthesis and respiratory processes), and growth in high latitude tree species, an influential vegetative component of the Earth system, to increasing temperatures.

1.1 Climate change

Anthropogenic activities are causing a steady rise in atmospheric CO_2 concentrations from 280 μmol mol^{-1} at the beginning of the Industrial Revolution to over 400 μmol mol^{-1} today (Ciais *et al*., 2013; Duglokencky & Tans, 2017). CO_2 is a greenhouse gas, as it increases heat retention in the atmosphere and affects the energy balance of the Earth system (Stocker *et al*., 2013). Radiative forcing, defined as changes in the energy balance of the planet, is determined by much more than CO_2 concentrations in the atmosphere, and includes concentrations of methane, halocarbons, N_2O, aerosols, land surface reflectance, and changes in solar irradiance (Stocker *et al*., 2013).

Predictions of future climate warming are made using Earth system models (with terrestrial biosphere models coupling the biosphere to the rest of the Earth system) (Friedlingstein *et al*., 2006; Fisher *et al*., 2014). Current Earth System Models predict average global surface temperatures will rise between 0.3 and 4.8 °C by 2100, depending on the socio-economic emissions scenario used (Stocker *et al*., 2013). Socio-economic emissions scenarios are required to drive current-generation Earth System Models because it is unknown whether, what, and how climate change mitigations measured will be implemented (Stocker *et al*., 2013). The commitments of the 2015 Paris Climate agreement suggest that large-scale implementation of climate change mitigation measures may be achieved this century (Rogelj *et al.*, 2016). The most recent assessment report from the Intergovernmental Panel on Climate Change (Stocker *et al*., 2013) established four socio-economic emissions scenarios termed representative concentration pathways. These representative concentration pathways range from extensive mitigation (representative concentration pathway 2.6), intermediate mitigation (representative concentration pathway 4.5 and representative concentration pathway 6.0), through to a business-as-usual scenario (representative concentration pathway 8.5), where the numbers indicate the expected increase in radiative forcing in W m^{-2} for the year 2100, relative to 1750 (Stocker *et al*., 2013). The projected global average annual climate warming for 2100 ranges from ~1.0 °C under representative concentration pathway 2.6 to ~3.7 °C for representative concentration pathway 8.5 (Collins *et al*., 2013). Climate projections are typically cited regarding average annual global changes, which is misleading, since spatiotemporal warming projections are highly variable with greater warming projected at high latitudes and during winter compared to low latitudes and during summer (Collins *et al*., 2013; IPCC, 2013).

One major source of uncertainty in climate projections is the response of the biosphere, specifically vegetation, to climate change, since the biosphere has strong effects on the global carbon and water cycles, which affect total radiative forcing (Pearson *et al.*, 2013; Willeit *et al.*, 2014; Rogers *et al.*, 2017). Understanding and modeling vegetative responses to environmental change is thus pertinent to modeling the entire Earth system. Forests, due to their long-term carbon storage in woody biomass and soils, and their

ecological dominance (covering ~30% of Earth's land surface; FAO, 2016), are key drivers of the Earth system and atmospheric CO_2 concentrations concentrations, and are largely responsible for the magnitude of seasonal oscillations in atmospheric CO_2 concentrations (Forkel *et al.*, 2016; Wenzel *et al.*, 2016). Henceforth, I will focus on forest-climate feedbacks whenever possible instead of general vegetation-climate feedbacks.

1.2 Boreal forests

Boreal forests (synonym: taiga) occur in high latitude regions across North America and Eurasia, accounting for ~30% of globally forested area (FAO, 2001; Brandt *et al.*, 2013). These forests contain 28 Pg of terrestrial carbon in Canada alone (Kurz *et al.*, 2013), with most of the carbon stored in soil and peatlands (Davidson & Janssens, 2006). Carbon stocks of boreal forests increase with age with net carbon uptake peaking in the range of 100 years and declining thereafter (Litvak *et al*., 2003; Luyssaert *et al*., 2008). Estimates of net boreal carbon flux vary from a net uptake of 0.5 to 0.8 Pg of carbon per year (Bradshaw & Warkentin, 2015), while net terrestrial carbon uptake has ranged from 0.4 to 1.0 Pg of carbon per year (Houghton, 2007). Changes in boreal carbon flux thus have the potential to cause relatively large changes in net terrestrial carbon fluxes.

Soil microbial activity has a strong impact on boreal carbon fluxes by affecting decomposition rates, soil respiration and methane flux (Chapin *et al*., 2009). Climate warming is expected to increase carbon inputs into boreal soils by vegetation, which may 'prime' soil microbial and fungal activity by increasing energy available for microbial and soil respiration (Clemmensen *et al*., 2013; Karhu *et al*., 2016). This increased soil respiration could lead to greater efflux of carbon from the soil, releasing more carbon stored in the soil, potentially tipping the balance of whether boreal forests are a source or sink for carbon. Mosses may counterbalance increases in soil respiration by reducing decomposition rates, stabilizing boreal soil carbon, and modulating soil nitrogen availability (Turetsky *et al*., 2008; Turetsky *et al*., 2012), while contributing substantially to boreal forest carbon uptake (Harden *et al*., 1997). CO_2 released from soil respiration may stimulate moss photosynthesis, offsetting the increase in soil respiration expected

with climate change (Turetsky & Wieder, 1999). However, for the remainder of my thesis, I will focus on the impacts of climate on vegetation.

1.2.1 Disturbance impacts on boreal carbon balance

Disturbance, including fire and insects, plays a crucial role in boreal forest carbon balance (Goetz *et al*., 2005; Bond-Lamberty *et al*., 2007; Magnani *et al*., 2007). Boreal forests frequently burn, causing forest loss (Potapov *et al*., 2008), directly leading to an increase in carbon efflux as well as an increased turnover of soil carbon (Clemmensen *et al*., 2013). Projections of future fire regimes in the boreal forest predict an increase in fire severity due to climate change this century, with total burned area increasing between 200 and 500% of current levels (de Groot *et al*., 2013) and reaching levels unprecedented in the past 10,000 years (Kelly *et al*., 2013). While fire may initially increase radiative forcing of the region (through reduced albedo and carbon efflux, amplifying climate warming), after 80 years there may be a reduction in radiative forcing in some cases (dampening warming; Randerson *et al*., 2006). Given that the frequency of stand-replacing disturbances in the boreal forest (Larsen, 1998), the increasing frequency and intensity of fires (Kasischke & Turetsky, 2006), and that young forest stands have relatively low to negligible carbon uptake (Litvak *et al*., 2003), understanding seedling responses to climate change will become increasingly important for understanding the persistence and future carbon sequestration potential of boreal forests.

In addition to fire, insect outbreaks can dramatically affect forests: a western spruce budworm (*Choristoneura occidentalis*) outbreak in the late 20th century led to the infection of over 80% of trees in a mixed conifer stand (Swetnam *et al*., 1995). In the early 2000s, Canada's boreal forests switched from a carbon sink to a carbon source, which is attributed to an increase in insect outbreaks (Kurz *et al*., 2008b). The severity of mountain pine beetle (*Dendroctonus ponderosae*) infection has increased from less than 2 million ha in the 1980s to over 10 million ha in the 2000s, and has the potential to spread further with climate warming (Safranyik *et al*., 2010). Estimates of the carbon balance effect of the current mountain pine beetle outbreak from 2000 to 2020 are on the order of 370 Gg, and historically can rival the impact of fire (Kurz *et al*., 2008a). Furthermore, insect and fire disturbance are interconnected: insect attack can increase the availability

of fuel for, and risk of, fire, while fire can leave trees vulnerable to insect attack (McCullough *et al*., 1998). Thus, fire and insect outbreaks are of considerable importance to boreal forest carbon balance.

1.2.2 Nitrogen and water limitations on boreal carbon balance

Nitrogen and water are often limiting resources in boreal forests (Kljun *et al*., 2006; Blaško *et al*., 2015). Due to relatively low nitrogen availability, atmospheric nitrogen deposition is relatively important in the boreal nitrogen cycle, especially after fire-related disturbances (Palviainen *et al*., 2017). Lim *et al*. (2015) showed that nitrogen fertilization of stands of *Pinus sylvestris* (a dominant Eurasian boreal tree species) can increase net carbon uptake by over 25%, suggesting a strong nitrogen limitation on carbon uptake in this system. Furthermore, a 10% reduction in precipitation in this system can prevent a response of carbon uptake to nitrogen, while a 33% increase in precipitation may double carbon uptake (Lim *et al*., 2015), indicating strong interactions between nutrient and moisture limitations on carbon uptake for boreal trees. However, the rate of change in nitrogen availability also matters in affecting vegetation growth. Höberg *et al*. (2006) found that over 30 years of nitrogen fertilization of Scots pine (*Pinus sylvestris*) plots, the lowest rate of nitrogen addition led to the greatest increase in growth. This suggests a more complex relationship between nitrogen and growth in boreal trees.

Water availability is thought to contrain the southern range of boreal forests (Hogg, 1994). Archambault and Bergeron (1992) found a strong correlation between growth of northern white cedar (*Thuja occidentalis*) and precipitation for over 800 years based on tree-ring analysis in the Quebec, Canada. This suggests that precipitation has historically limited growth in the boreal forest. In terms of boreal forest carbon balance, drought can limit carbon uptake (Kljun *et al*., 2006): in an Alaskan boreal forest, a severe summer drought in 2004 reduced net carbon uptake of deciduous sites by 56% and evergreen sites by 38% (Welp *et al*., 2007). Furthermore, increasing water stress since 1970 has not only decreased growth in the boreal forest of western Canada, it has also inceased mortality (Peng *et al*., 2011), leading to a reduction in the carbon sink capacity of this boreal system (Ma *et al*., 2012). The prevalence of drought is projected to increase with climate

change in the boreal forest, excacerbating the risk of fire-related disturbance and carbon efflux to the atmosphere (de Groot *et al*., 2013).

1.2.3 Boreal vegetation and carbon fluxes

Boreal forests are characterized by predominantly needle-leaf conifers, large seasonal changes in temperature and photoperiod, and extensive land-use management for forestry, particularly in Europe (Brandt *et al.*, 2013; Gauthier *et al.*, 2015). Trees in the boreal forest exhibit seasonality in their growth: buds are produced and set for the next year's growth during late summer/autumn, the trees become cold hardened to survive winter, and the buds burst the subsequent spring to initiate new growth, with each of these processes being regulated by a combination of temperature and photoperiod (Öquist & Hüner, 2003; Schwartz *et al*., 2006; Hamilton *et al*., 2016). Along with a highly seasonal climate, projected climate warming is greater for boreal forests than for all other forest biomes (Collins *et al*., 2013).

Seasonal changes in temperature and photoperiod regulate growth and carbon uptake in boreal forest tree species, and the relative influence of these environmental variables on plant physiology can change with latitude. For example, in Norway spruce (*Picea abies* (L.) H. Karst.), more northern populations exhibit greater photoperiod control of growth than more southern populations (Clapham *et al.*, 1998; Sogaard *et al.*, 2008). This is likely because photoperiod is a more reliable seasonal signal of imminent low temperatures, since photoperiod at a given point in the year is constant (Dumberry & Bloxham, 2006), while seasonal temperatures can vary from year to year (IPCC, 2014). Temperature can also override photoperiod cues in some populations of Norway spruce, either extending growth through warming or inducing growth cessation through low nighttime temperatures (Heide, 1974), and there is evidence that temperature controls autumnal shutdown in carbon uptake (Stinziano *et al*., 2015).

Large-scale changes in growth and carbon fluxes in the boreal forests could serve to attenuate or amplify changes in atmospheric CO_2 concentrations. Warming is often expected to increase growth and carbon uptake in the boreal forest as this biome is assumed to be limited by low temperature (Myeni *et al*., 1997; Jarvis & Linder, 2000;

Tanja *et al*., 2003; Way & Oren, 2010). Since the boreal forest consistently contributes a net carbon sink of 0.5 Pg carbon $year^{-1}$ to the global net forest sink of 1.1 Pg carbon $year^{-1}$ (Pan *et al*., 2011), changes in boreal carbon fluxes can strongly impact global forest net carbon sinks and atmospheric CO_2 concentrations. Graven *et al*. (2013) found that the magnitude of the seasonal oscillations in atmospheric CO_2 concentrations have increased over the last 50 years, and that this effect is driven by increased seasonality in ecosystem CO_2 exchange in northern forests. However, while individual tree species show specific growth responses to climate change across the boreal forest, overall there has been no net effect of climate change on the overall growth of trees in Canada's boreal forest over the past 50 years (Girardin *et al*., 2016).

Climate warming has advanced the onset of the spring growing season in the Northern Hemisphere over the past 60 years by ~2 days per decade (Schwartz *et al*., 2006), and may create a permissible thermal environment for growth later into the autumn by delaying bud set. However, photoperiod may limit growth at northern latitudes in the boreal forest (Way & Montgomery, 2015) by inducing bud formation and growth cessation at a consistent date in the year regardless of temperature (e.g. Oleksyn *et al*., 2001; Chen *et al*., 2012; Hamilton *et al*., 2016). However, in some cases an interaction between temperature and photoperiod signaling can affect the timing of bud formation and growth cessation (e.g. Heide, 1974). If photoperiod control on growth is plastic, warming might increase growth in boreal tree species during autumn, otherwise autumn growth could be unaffected or negatively affected by increasing temperatures. Given that photosynthetic capacity (and therefore carbon uptake) is strongly correlated to photoperiod in deciduous broadleaf tree species (Bauerle *et al*., 2012), it is possible that photoperiod may exert direct control on photosynthesis. However, there have been few direct tests of the effect of photoperiod on photosynthetic capacity (but see Bauerle *et al*., 2012).

The impact of boreal forests on future global carbon cycling lies primarily in their ability to store carbon in wood and soil; woody biomass accumulation removes carbon from the global carbon cycle for years to centuries, depending on tree longevity, mortality, and decomposition rates (Körner, 2017). The accumulation of woody biomass depends, first

and foremost, on the balance of primary metabolic processes: photosynthesis, respiration, and nitrogen assimilation. Given that our mechanistic understanding of the carbon balance implications of nitrogen assimilation is in its infancy (Busch *et al*., 2018), my thesis will focus on photosynthesis and respiration.

1.3 Photosynthesis and respiration

The simplest conception of plant growth is that total growth is the carbon balance of photosynthesis, respiration, and photorespiration. Net carbon gain can be estimated through gas exchange; however, this does not account for the carbon cost of secondary metabolism (Ramakrishna & Ravishankar, 2011). Growth itself may be limited by available nutrients (e.g. Sigurdsson *et al.*, 2013), especially nitrogen since it is required for amino acids and nucleotides. Thus, net carbon gain represents the carbon available for all processes beyond maintenance respiration and photorespiration, and without consideration of possible constraints for building plant tissues due to the stoichiometry of plant carbon to nitrogen. Below, I review the processes that set the upper bound on tree net carbon gain: photosynthesis and respiration.

1.3.1 Biochemical basis of photosynthesis and respiration

Photosynthesis occurs in the chloroplasts of plants and is the conversion of light energy into electrochemical potential energy (in the form of electrons and carbohydrates) (Fig. 1.1). The whole process can be described by the following equation (Hüner & Hopkins, 2009):

$$CO_2 + H_2O + h\nu \rightarrow CH_2O + O_2 \qquad \text{Equation 1.1}$$

where *hv* represents a photon of visible light energy, and CH_2O represents a carbohydrate molecule where the ratio of carbon to hydrogen to oxygen is 1:2:1. This equation, while stoichiometrically correct, is an oversimplification of the myriad processes involved in photosynthesis.

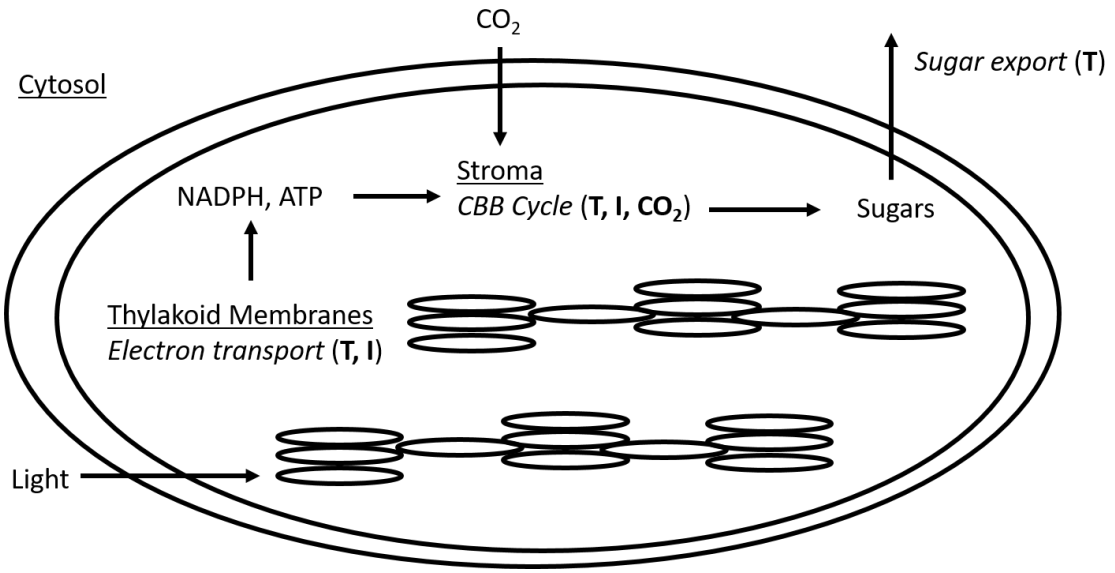

Figure 1.1. Overview of photosynthesis in the chloroplasts of plants. Photosynthetic electron transport occurs in the thylakoid membranes (ellipsoid structures) where light is absorbed and is affected by temperature (T) and irradiance (I) (Buchanan, 1991). Electron transport produces nicotinamide adenine dinucleotide phosphate (NADPH) and adenosine triphosphate (ATP), which are used in the Calvin-Benson-Bessham (CBB) cycle to fix CO_2 in the stroma (Bassham *et al*., 1954). The Calvin-Benson-Bessham cycle produces sugars for export from the chloroplast, and is sensitive to T, I (through redox regulation of enzyme activities), and CO_2. Sugars are exported from the chloroplast to the cytosol, in a process that is highly sensitive to T. Compartments are underlined, processes are italicized, environmental parameters affecting a process are in bold, and substrates are unemphasized text.

To understand and predict how photosynthesis will respond to changing environments, it is necessary to understand the processes involved and how these can respond to environmental perturbations. On the most basic level, these processes can be divided between light harvesting and carbon fixation, which involve different proteins, processes, and timescales.

Light is absorbed by pigments (where the primary pigments for photosynthetic light absorption by terrestrial plants are chlorophyll a and b, while carotenoids are involved in dissipating excess light energy) embedded in large protein structures called photosystems (Grossman *et al.*, 1995; Vasil'ev & Bruce, 2004). There are two photosystems in plants, photosystem I and photosystem II, which are each composed of a reaction centre and light harvesting complexes (Alfonso *et al.*, 1994; Grossman *et al.*, 1995; Krauß *et al.*, 1996; Vasil'ev & Bruce, 2004). Light absorbed by the light harvesting complexes is converted into redox potential energy in the reaction centres of the photosystems, facilitated by special pigment pairs: P680 for photosystem II and P700 for photosystem I (Kok, 1957, 1961; Thornber, 1975; Vinyard *et al.*, 2013; Wei *et al.*, 2016; Mazor *et al.*, 2017). Electrons flow from photosystem II to photosystem I through a series of coupled redox reactions, starting with the photo-oxidation of P680 and P700. The electron generated by the photo-oxidation of P680 ($P680 + \text{absorbed light energy} \rightarrow P680^{+} + e^{-}$) results in the reduction of plastoquinone (Haehnel, 1984; Krause & Weis, 1991) to plastoquinol in the plastoquinone pool, the reduction of cytochrome b_6/f by plastoquinol, the reduction of plastocyanin by cytochrome b_6/f (Hurt & Hauska, 1981). The photo-oxidation of P700 ($P700 + \text{absorbed light energy} \rightarrow P700^{+} + e^{-}$), reduces ferredoxin, and ferredoxin can then be used to reduce the NADP reductase complex, which subsequently reduces oxidized nicotinamide adenine dinucleotide phosphate ($NADP^{+}$) to NADPH (Zanetti & Curti, 1981), an electron carrier molecule needed for CO_2 fixation (Bassham et al., 1954; Buchanan, 1991). Reduced plastocyanin subsequently reduces $P700^{+}$ back to P700. Ferredoxin can also be used to reduce thioredoxin, which is involved in redox regulation of enzymes (Buchanan, 1991). $P680^{+}$ is reduced through the oxygen evolving complex which oxidizes water through a water-splitting reaction to release O_2 (Haehnel, 1984).

The electron cycling of the plastoquinone pool in the thylakoid membranes transfers hydrogen ions (i.e. protons) from the stroma to the thylakoid lumen of the chloroplast, creating a proton-motive force across the thylakoid membrane (Arnon *et al.*, 1981). The proton motive force across the thylakoid membrane is collapsed in a controlled manner through an adenosine triphosphate (ATP)-synthase, which uses protons to drive a motor that produces ATP from adenosine diphosphate, ADP, and inorganic phosphate, P_i (Arnon *et al.*, 1957; Hill & Bendall, 1960; Junge, 1999; McCarty *et al.*, 2000; reviewed by Allen, 2002). This ATP is then used for energy-requiring functions, including carbon fixation (Fig. 1.2).

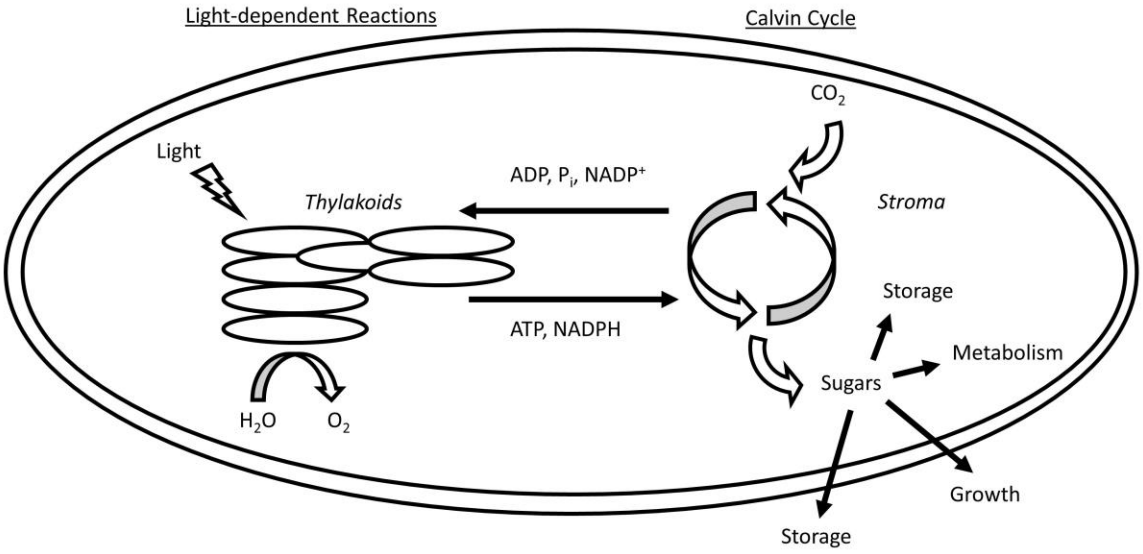

Figure 1.2. Overview of photosynthesis in the chloroplasts of plants, split between the light-dependent reactions (left side) and Calvin cycle (right side). Light absorbed by the thylakoids is used to drive electron transport to produce ATP and NADPH, which are subsequently used to regenerate RuBP in the Calvin cycle. CO_2 is fixed by Rubisco in the Calvin cycle, and sugars produced through the Calvin cycle can be stored inside or outside the chloroplast, or used for metabolism or growth.

In addition to the linear photosynthetic electron transport between photosystem II and photosystem I described above, there are other electron transport pathways through the thylakoid membranes. Cyclic photosynthetic electron transport around photosystem I is used to balance the ratio of ATP to NADPH in the chloroplast stroma (Shikanai, 2007) by redirecting electron flow from photosystem I to the plastoquinone pool via either 1) the NADH dehydrogenase-like dependent pathway which uses NADPH to reduce plastoquinone via the NADH dehydrogenase-like complex (Strand *et al*., 2017), or 2) the proton gradient regulation 5-dependent pathway where reduced ferredoxin is used to reduce plastoquinone via proton gradient regulation 5 and proton gradient regulation 5-like photosynthetic phenotype complexed with photosystem I (Munekage *et al*., 2002; DalCorso *et al*., 2008; Hertle *et al*., 2013). While cyclic electron transport represents an important component of photosynthetic electron flow in responding to specific stress conditions (i.e. high light stress; Wang *et al*., 2015), some evidence suggests that it may not play a large role in affecting carbon uptake and biomass accumulation (Nishikawa *et al*., 2012). There are also alternative electron transport pathways related to high light stress including the water-water cycle (Asada, 1999), the Mehler reaction (Schreiber & Neubauer, 1990), and a plastoquinol terminal oxidase (PTOX) (McDonald *et al*., 2011). However, the remainder of my thesis will focus primarily on carbon dynamics and modeling that does not account for electron sinks beyond linear photosynthetic electron transport.

Carbon fixation occurs via the Calvin-Benson-Bessham (CBB) Cycle (Bassham *et al*., 1954), which uses the ATP and NADPH generated through photosynthetic electron transport to regenerate intermediate products in the cycle and produce triose phosphates. The primary carboxylating enzyme, ribulose-1,5-bisphosphate carboxylase/oxygenase (Rubisco), fixes CO_2 onto ribulose-1,5-bisphosphate, which generates an unstable six carbon intermediate that splits into the three-carbon sugar 3-phosphoglycerate (Jakoby *et al.*, 1956; Weissbach *et al.*, 1956). Next, 3-phosphoglycerate kinase uses ATP to phosphorylate 3-phosphoglycerate to 1,3-phosphoglycerate (Bassham *et al*., 1954), followed with reduction and dephosphorylation by glyceraldehyde 3-phosphate dehydrogenase to glyceraldehyde-3-phosphate (Bassham *et al*., 1954). Glyceraldehyde-3-phosphate can then be interconverted to dihydroxyacetone phosphate through triose

phosphate isomerase. Most of the glyceraldehyde-3-phosphate and dihydroxyacetone phosphate produced through these reactions are used to regenerate intermediates to maintain the Calvin-Benson-Bessham cycle (requiring the consumption of one further ATP to regenerate ribulose-1,5-bisphosphate). These triose phosphates can be used to synthesize sucrose (in the cytoplasm; Bird *et al*., 1974) and starch (in the chloroplast; Stitt & Heldt, 1981) for growth, development, and energy storage (Bassham *et al*., 1954). Triose phosphates are exported from the chloroplast in exchange for inorganic phosphate from the cytoplasm (Heber & Heldt, 1981), while starch synthesis releases inorganic phosphate in the chloroplast (Stitt & Heldt, 1981). Thus, starch and sucrose synthesis are required to maintain sufficient inorganic phosphate in the chloroplasts for continued photosynthesis (Walker & Herold, 1977). For reviews regarding the enzymes involved in the Calvin-Benson-Bessham cycle, see Woodrow and Berry (1988) and Raines (2003).

The Calvin-Benson-Bessham cycle has three primary limitations to its function: Rubisco substrate availability (CO_2-limited), ATP and NADPH availability (photosynthetic electron transport- or ribulose-1,5-bisphosphate regeneration-limited), and export of sugars from the chloroplast (triose phosphate utilization-limited). These limitations are addressed in more detail below (section 1.3.2)

Rubisco does not solely fix CO_2, it can also fix O_2 in a process called photorespiration that leads to a net CO_2 release (Ogren & Bowes, 1971). However, Rubisco has far greater specificity for CO_2 than O_2 (Jordan & Ogren, 1984). Increasing CO_2 is expected to suppress photorespiration (Whittingham *et al*., 1963; Bowes, 1991; Sage *et al.*, 2008), while increasing temperature may increase photorespiration, since O_2 solubility declines more slowly with increasing temperature than does the solubility of CO_2 (Ku & Edwards, 1977). Due to its role as the primary carboxylating enzyme for plants (and indeed the whole biosphere), maximum Rubisco carboxylation capacity, V_{cmax}, is of central interest in modeling and predicting photosynthesis (Rogers *et al*., 2017).

In addition to the Calvin-Benson-Bessham cycle, chloroplasts also use an oxidative pentose phosphate cycle to metabolize carbon, and the oxidative pentose phosphate cycle is crucial for producing carbon skeletons in the chloroplast (Herrmann & Weaver, 1999).

The oxidative pentose phosphate cycle converts glucose-6-phosphate to ribose-5-phosphate through three reactions, producing NADPH and releasing CO_2 in the process, and regenerates glucose-6-phosphate by processing ribose-5-phosphate using reactants and enzymes from the Calvin-Benson-Bessham cycle (Kruger & von Schaewen, 2003). While this pathway is important to plant metabolism, particularly with respect to generating carbon skeletons for biosynthesis (Herrmann & Weaver, 1999), in the remainder of my thesis I will be focusing on photosynthesis and respiration, as these processes are more easily related to plant gas exchange measurements and modeling of plant carbon uptake.

Respiration occurs in the mitochondria of plant cells, and results in the net consumption of oxygen and an energy-containing substrate (e.g. carbohydrates, lipids, proteins) with the release of CO_2 and H_2O (Goddard & Meeuse, 1950; Millerd, 1953). Respiration of carbohydrates starts with pyruvate, which is decarboxylated (releasing CO_2), oxidized (to reduce nicotinamide adenine dinucleotide (NAD^+) to NADH) and condensed with Coenzyme A to form acetyl-Coezyme A via the pyruvate dehydrogenase complex (Miernyk *et al*., 1985). Citrate synthase condenses oxaloacetate and form acetyl-Coezyme A in the mitochondrial matrix, producing citrate and CoA (Millar *et al*., 2011). The tricarboxylic acid cycle then involves a series of oxidation reactions to produce NADH and flavin adenine dinucleotide ($FADH_2$), releasing CO_2 and regenerating oxaloacetate in the process (Krebs & Lowenstein, 1960; Sweetlove *et al*., 2010; Millar *et al*., 2011). NADH and $FADH_2$ are used to drive respiratory electron transport, reducing O_2 to water and generating a proton gradient that is used for ATP production (Michalecka *et al*., 2003; Moore *et al*., 2003; Miller *et al*., 2011). However, for the consideration of respiration in my thesis, respiration will be addressed in relation to its rate of CO_2 production. One important note for respiration rates of plants is that respiration can be suppressed (Kok, 1948; Laisk, 1977; Atkin *et al*., 2000) or stimulated (Kroner & Way, 2016) in the light, complicating efforts to measure respiration in the light in plants.

Given the contribution of photosynthesis and respiration to carbon uptake, when discussing photosynthesis and CO_2 fixation, we can define three different rates: gross photosynthesis (total photosynthetic carboxylation at the leaf level, while at the whole plant and ecosystem levels this is termed gross primary productivity), apparent photosynthesis (gross photosynthesis minus photorespiration), and net photosynthesis (apparent photosynthesis minus respiration) (Wohlfahrt & Gu, 2015).

1.3.2 Models of photosynthetic CO_2 assimilation

Photosynthetic carbon uptake responds to many environmental variables, both directly (light, temperature, CO_2) and indirectly (H_2O, stressors). These responses can be modeled based on our understanding of the biochemistry of the processes involved.

1.3.2.1 The photosynthetic CO_2 response

The concentration of CO_2 affects photosynthetic carbon uptake by affecting substrate availability for Rubisco. The CO_2 response of net photosynthesis is modelled using a rectangular hyperbola, which can be used to estimate maximum rates of Rubisco carboxylation capacity (V_{cmax}) and maximum rates of electron transport to CO_2 (J_{max}) according to the model of Farquhar *et al*. (1980):

$$A_{net} = V_{cmax}\frac{C_c - \Gamma^*}{C_c + K_c\left(1 + {}^{O}/_{K_o}\right)} - R_{day} \qquad \text{Equation 1.2}$$

where A_{net} is the net CO_2 assimilation rate (μmol m^{-2} s^{-1}), C_c is the chloroplastic CO_2 concentration (μmol mol^{-1}), Γ^* is the CO_2 compensation point in the absence of mitochondrial respiration (μmol mol^{-1}), K_c is the Michaelis-Menten constant for Rubisco carboxylation (μmol mol^{-1}), O is the chloroplastic [O_2] (mmol mol^{-1}), K_o is the Michaelis-Menten constant for Rubisco oxygenation (mmol mol^{-1}), R_{day} is the rate of mitochondrial respiration in the light (μmol m^{-2} s^{-1}).

Photosynthetic electron transport is described by a pair of equations (Farquhar *et al*., 1980):

$$j = 0.5(1 - f)I \qquad \text{Equation 1.3}$$

where j is the potential rate of electron transport (μmol m^{-2} s^{-1}), f is the fraction of light not absorbed by the light harvesting complexes, I is the incident irradiance (μmol m^{-2} s^{-1})

$$J_{max} = \frac{j}{2(2+2\Phi)} \quad \text{Equation 1.4}$$

where J_{max} is the maximum rate of carboxylation limited by electron transport (μmol m^{-2} s^{-1}), Φ is the ratio of oxygenation to carboxylation, and the 2 is the number of electrons required per NADPH (Farquhar *et al.*, 1980).

Equations 1.2 to 1.4 describe different biochemical limitations to photosynthesis, either CO_2 limitations (V_{cmax}) or ribulose-1,5-bisphosphate regeneration limitations (J_{max}). A third type of limitation, triose phosphate limitation (TPU), occurs at extremely high CO_2 concentrations and/or at low temperatures, and is rarely studied, although it can be important at low temperatures (Sharkey, 1985a, 1985b; Sage *et al*., 1988; Busch & Sage, 2017). This third type of limitation occurs under limitations of free phosphate in the chloroplast stroma and can be described as (Sharkey, 1985a; Harley & Sharkey, 1991):

$$TPU = \frac{v_c}{3} - \frac{v_o}{6} \quad \text{Equation 1.5}$$

where v_c is the rate of carboxylation (μmol m^{-2} s^{-1}), v_o is the rate of oxygenation (μmol m^{-2} s^{-1}), and the numbers in the denominators reflect phosphate consumption and release by the CBB and photorespiratory cycles, respectively.

To calculate each of these limitations, net photosynthesis must be measured within each zone of limitation (Fig. 1.3a; Gu *et al.*, 2010).

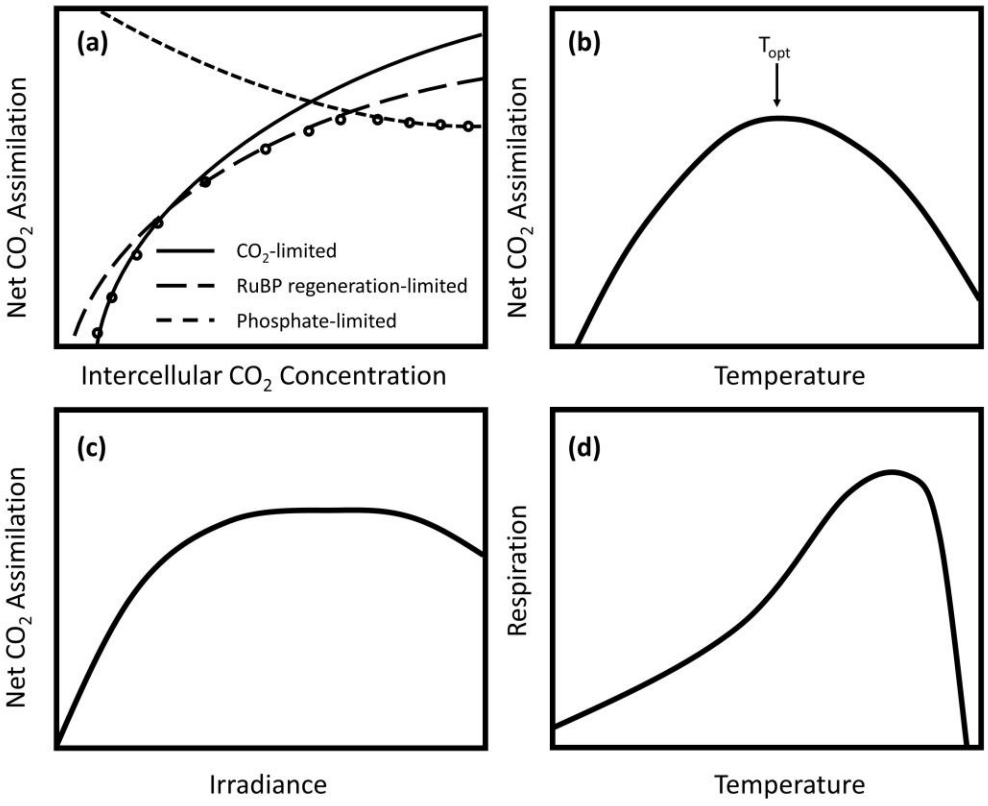

Figure 1.3. The response of net CO_2 assimilation (A_{net}) to (a) intercellular CO_2 concentration (C_i), (b) temperature, and (c) irradiance, and (d) the response of respiration to temperature (T). (a) The CO_2-limited region (solid line) of the A_{net}-C_i response is used to calculate Rubisco-limited carboxylation and its maximum rate (V_{cmax}), the ribulose-1,5-bisphosphate-limited region (long dashed line) is used to calculated photosynthetic electron transport limitations on A_{net} to derive the maximum rate of electron transport, J_{max}, and the phosphate-limited portion of the response is used to calculate triose phosphate utilization limitations (TPU). (b) The temperature response of A_{net} is characterized by a peaked response with the maximum rate at an optimal temperature, T_{opt}. (c) The light response of A_{net} is characterized by a linear region at low irradiance, a light-saturated region where A_{net} is relatively constant across a range of irradiances, and a decline at very high irradiance due to photoinhibition. (d) The temperature response of respiration is characterized by an exponential region at low temperatures, peaking at a high temperature, and then declining rapidly at very high temperatures.

Estimating the CO_2 concentrations within the chloroplast for the Farquhar model requires estimating CO_2 diffusion and supply within the leaf. The CO_2 supply into the intercellular airspace can be modelled using an equation based on Fickian diffusion (Moss & Rawlins, 1963):

$$A_{net} = g_s(C_s - C_i) \qquad \text{Equation 1.6}$$

where g_s is stomatal conductance to CO_2 (mol m^{-2} s^{-1}), C_s is the CO_2 concentration outside the leaf (μmol mol^{-1}), and C_i is the CO_2 concentration in the intercellular airspace (μmol mol^{-1}). The stomatal conductance component allows estimation of the intercellular CO_2 concentration via the measurement of water flux across a leaf (Moss & Rawlins, 1963). To further estimate the supply of CO_2 to the chloroplast, mesophyll conductance (g_m, the flow of CO_2 from the intercellular airspace (gas phase) into the chloroplasts of the mesophyll cells (liquid phase)) must be measured to calculate chloroplastic CO_2 concentrations according to (Harley *et al.*, 1992):

$$A_{net} = g_m(C_i - C_c) \qquad \text{Equation 1.7}$$

where g_m is mesophyll conductance to CO_2 (mol m^{-2} s^{-1}), and C_c is the CO_2 concentration inside the chloroplast (μmol mol^{-1}). Mesophyll conductance can be measured through combined gas exchange and fluorescence (Harley *et al.*, 1992), or through on-line isotope discrimination of CO_2 during gas exchange measurements (Flexas *et al.*, 2007). However, these techniques assume that only leaf tissue is being measured, which introduces significant difficulties when applying these techniques to needle-leaf species where stem gas exchange is necessarily included when measuring leaf gas exchange. Therefore, modeling of the photosynthetic CO_2 response in conifers typically proceeds by assuming either infinite g_m or a previously measured g_m, such that the C_c term in the photosynthetic CO_2 response model is replaced with C_i instead when infinite g_m is assumed. When V_{cmax} and J_{max} are fit on a C_i basis, it is important to recognize that these values are only apparent rates of photosynthetic capacity due to the assumption of infinite g_m.

1.3.2.2 Photosynthetic light responses

Photosynthesis increases with light intensity up to a saturating limit (A_{sat}), beyond which photosynthesis can decline due to photoinhibition and photodamage (Fig. 1.2c). The photosynthetic light response can be described according to the equation (Ögren & Evans, 1993):

$$\Theta P^2 - (Q\alpha IP_m)P - Q\alpha IP_m = 0 \qquad \text{Equation 1.8}$$

where Θ is the curvature of the photosynthetic light response (unitless), P is the rate of photosynthesis in μmol m^{-2} s^{-1}, Q is the maximum quantum yield (mol CO_2 fixed per mol photon absorbed), α is the proportion of irradiance absorbed by the leaf (unitless), I is the irradiance in μmol m^{-2} s^{-1}, and P_m is the maximum capacity for photosynthesis in μmol m^{-2} s^{-1}. Oftentimes this model replaces photosynthesis on a gas exchange basis with photosynthetic electron transport, j, and maximum photosynthetic electron transport capacity, J_{max}. This model parameterizes the steady-state light response, and such light responses are used to determine the saturating light intensity for photosynthesis, which must be known for gas exchange measurements to parameterize the photosynthetic CO_2 response model (Farquhar *et al.*, 1980). It is important to note that Equations 1.3 and 1.4 address electron transport needed to reduce CO_2, while Equation 1.8 can be used with chlorophyll a fluorescence measurements of electron transport to estimate total electron flow through the linear photosynthetic electron transport chain (Maxwell & Johnson, 2000). Furthermore, these equations ignore other potential electron acceptors from photosynthetic electron transport, including O_2 and thioredoxin (Schreiber & Neubauer, 1990; Buchanan, 1991; Asada, 1999). Thus, when modeling carbon dynamics of vegetation, terminology referencing 'photosynthetic electron transport' typically means 'photosynthetic electron transport to CO_2'.

1.3.2.3 Photosynthetic and respiratory temperature responses

The temperature response of photosynthesis is determined by a combination of the thermal sensitivity of photosynthetic enzymes and thylakoid membranes, temperature responses of stomatal conductance (affecting CO_2 supply), temperature responses of photosynthetic enzymes, and the capacity for chaperone proteins to ameliorate

temperature stress (Schreiber & Berry, 1977; Bunce, 2000; Salvucci & Crafts-Brandner, 2004). Photosynthesis exhibits a peaked response to changing leaf temperature (Fig. 1.3b), and the temperature responses of V_{cmax} and J_{max} can be described with a modified Arrhenius function (Medlyn *et al*., 2002):

$$f(T_k) = k_{25}\exp\left[\frac{E_a(T_k-298)}{298RT_k}\right]\frac{1+\exp\left(\frac{298\Delta S-H_d}{298R}\right)}{1+\exp\left(\frac{T_k\Delta S-H_d}{T_kR}\right)} \qquad \text{Equation 1.10}$$

where k_{25} is photosynthetic capacity at 25 °C (μmol m^{-2} s^{-1}), E_a is the activation energy (J mol^{-1}), T_k is the leaf temperature (K), 298 is the reference temperature in K, R is the universal gas constant (8.314 J K^{-1} mol^{-1}), ΔS is the entropy parameter (J mol^{-1}), and H_d is the deactivation energy (J mol^{-1}). In cases where peak photosynthetic capacity is outside the measured temperature range, a regular Arrhenius function can be used:

$$f(T_k) = k_{25}\exp\left[\frac{E_a(T_k-298)}{298RT_k}\right] \qquad \text{Equation 1.11}$$

These equations describe the acute response of photosynthetic capacity to temperature. To model acclimatory responses of photosynthetic capacity to growth temperatures, there are several options available (Hikosaka *et al*., 2006; Kattge & Knorr, 2007; Dillaway & Kruger, 2010), involving acclimation of E_a or ΔS, although these are discussed in detail in Chapter 4 and introduced in section 1.3.3.

Photosynthetic function is lost in species at temperatures as low as 33°C, although function can be maintained as high as 75°C depending on thermal adaptations (O'Sullivan *et al.*, 2017), and these limits may be due to protein denaturation and breakdown of thylakoid membranes (Schreiber & Berry, 1977). Rubisco carboxylation rate is sensitive to more than the thermal stability of the enzyme's protein structure: the CO_2/O_2 ratio in the chloroplast and the activation status of Rubisco are important contributors to total carboxylation rates (Salvucci & Crafts-Brandner, 2004; Carmo-Silva *et al.*, 2012). At high temperatures, solubility of gases in aqueous solutions declines, with the solubility of CO_2 declining faster than the solubility of O_2, such that temperature drives down the CO_2/O_2 ratio. Due to the oxygenase function of Rubisco and shifts in the enzyme's specificity for its substrates, Rubisco carboxylation rates decrease with

increasing temperature relative to oxygenation rates (i.e. photorespiration), contributing to net reductions in carbon fixation at high temperatures (Laing *et al.*, 1974; Badger & Collatz, 1977; Brooks & Farquhar, 1985). The main chaperone protein involved in activating Rubisco, Rubisco activase, is thermally sensitive and often denatures at high temperatures (Salvucci & Crafts-Brandner, 2004; Carmo-Silva *et al.*, 2012). While Rubisco activase is not necessary to activate Rubisco *per se* (Scales *et al.*, 2014), it is necessary to maintain active Rubisco to maximize carbon fixation.

The acute temperature response of respiration exhibits a sharper peaked response compared to the acute temperature response of A_{net} (Fig. 1.2d): respiratory rates increase exponentially at low temperatures, peaking at high temperatures (with a higher T_{opt} relative to photosynthesis), and rapidly decline at very high temperatures due to heat-induced damage. The acute temperature response over the exponential range is often described according to (Wager, 1941; Atkin & Tjoelker, 2003):

$$Q_{10} = \left({R_2}/{R_1}\right)^{{10}/{(T_2 - T_1)}} \qquad \text{Equation 1.12}$$

where Q_{10} is a thermal sensitivity coefficient that describes the fold-change in the rate of respiration for every 10°C (or 10 K) change in temperature (for example, a Q_{10} of 2 means that the rate doubles every 10°C), while R_1 and R_2 are the rates of respiration at temperatures T_1 and T_2 in μmol m^{-2} s^{-1}, respectively.

1.3.3 Temperature and CO_2 responses of photosynthesis and respiration

While photosynthesis and respiration respond to acute changes in temperature (respiration and photosynthesis) and CO_2 (photosynthesis only), longer-term responses of these processes to changes in air temperature or CO_2 concentration involve acclimation. While acute responses of metabolism to temperature involve changes in biochemical equilibria and post-translational modifications of enzymes, acclimation of metabolism involves longer-term changes in gene and protein expression. First, I will review

photosynthetic and respiratory acclimation to temperature, then I will review photosynthetic acclimation to high CO_2 concentrations.

Thermal acclimation of photosynthesis leads to changes in the temperature optimum of photosynthesis (Way & Yamori, 2014; Yamori *et al.*, 2014) and temperature response parameters describing the acute temperature response of photosynthetic capacity (Hikosaka *et al.*, 2006; Kattge & Knorr, 2007; Dillaway & Kruger, 2010). The mechanisms of these effects include changes in thermal stability of enzymes in the Calvin-Benson-Bassham cycle and photosynthetic electron transport (reviewed in Berry & Björkman, 1980; Badger *et al.*, 1982), thlykoid membrane lipids (Raison & Berry, 1979), Rubisco concentrations (Scafaro et al., 2017), and possible changes in Rubisco small subunit expression (Hikosaka *et al*., 2006). Thermal acclimation can also occur through modifications of sink strength for carbon metabolism to prevent phosphate limitations at low temperature (Hurry *et al*., 1992; Strand *et al*., 2003), or through modifications in electron transport to ensure adequate regeneration of ribulose-1,5-bisphosphate in the cold (Hurry *et al*., 1996). The net effect of acclimation can lead to a constructive adjustment (where A_{net} at the growth temperature increases at higher growth temperatures), detractive adjustment (where A_{net} at the growth temperature decreases at higher growth temperatures), or homeostasis (where A_{net} at the growth temperature remains the same across growth temperatures) of A_{net} (Way & Yamori, 2014).

Several studies include equations to describe acclimation of the temperature response of photosynthetic capacity. Kattge and Knorr (2007) found a general acclimatory response in the ΔS parameter of the temperature response for V_{cmax} and J_{max}:

$$\Delta S = d + e \times T_{growth} \qquad \text{Equation 1.13}$$

where d is 668.39 and 659.70 for V_{cmax} and J_{max}, respectively, e is -1.07 and -0.75 for V_{cmax} and J_{max}, respectively, and T_{growth} is the growth temperature to which the plant is acclimated. Hikosaka *et al*. (2006) investigated acclimation of the activation energy for V_{cmax} and found the following relationship:

$$E_a = 34.1 + 1.01 \times T_{growth} \qquad \text{Equation 1.14}$$

In contrast, Dillaway and Kruger (2010) used a nonlinear equation to describe the activation energy of both V_{cmax} and J_{max}:

$$E_a = \frac{x}{T_{growth}^{\ 2}} - \frac{y}{T_{growth}} + z \qquad \text{Equation 1.15}$$

where x, y, and z are constants equal to 45322 kJ mol^{-1} °C, 3368.2 kJ mol^{-1} °C, and 119.9 kJ mol^{-1} for V_{cmax}, and 80318.9 kJ mol^{-1} °C, 6093.6 kJ mol^{-1} °C, and 134.7 kJ mol^{-1} for J_{max} (Dillaway & Kruger, 2010).

There has been little investigation into how these acclimatory responses operate together, and whether deactivation energies (H_d) in the temperature response function acclimate to different growth temperatures. However, given the evidence that ΔS thermally acclimates (Kattge & Knorr, 2007), and that ΔS is a function of both the activation and deactivation energies of the temperature response of photosynthetic capacity (Medlyn *et al*., 2002), it is likely that both activation and deactivation energies of V_{cmax} and J_{max} acclimate to temperature.

Thermal acclimation of respiration involves changes to the basal rate of respiration (respiration at 25 °C, R_{25}) as well as the acute temperature response of respiration which could involve changes in the quantity of enzymes or properties of the inner mitochondrial membrane (Atkin & Tjoelker, 2003; Way & Oren, 2010). In trees, R_{25} in the dark tends to decline with increasing temperatures (Way & Oren, 2010), while the thermal sensitivity of respiration is also suppressed (Atkin & Tjoelker, 2003; Slot & Kitajima, 2015; Heskel *et al*., 2016). The net effect of these changes is that while respiration at growth temperatures may be higher in warm-grown vegetation, the rate of respiration in these plants is suppressed relative to what would be expected without acclimation (e.g. Slot & Kitajima, 2015). Atkin and Tjoelker (2003) found the following relationships for thermal acclimation of leaf respiration across species from all biomes:

$$Q_{10} = 3.090 - 0.043T_{growth} \qquad \text{Equation 1.16}$$

Acclimation of photosynthesis to high CO_2 concentrations involves metabolic feedbacks that shift the balance between light harvesting and the Calvin-Benson-Bessham cycle.

Since Rubisco carboxylation is usually limiting under current atmospheric CO_2 concentrations, plants invest significantly in Rubisco, which is one of the most abundant proteins on the planet (Ellis, 1979). Under elevated CO_2 concentrations, when Rubisco limitations are removed, plants tend to invest less nitrogen into Rubisco, distributing the N to other rate-limiting processes instead (Long & Drake, 1992; Ainsworth & Long, 2005). This generally results in a down-regulation of V_{cmax} due to a reduction in Rubisco protein concentration (Ainsworth & Long, 2005). At the same time, elevated CO_2 directly stimulates photosynthesis (Ainsworth & Long, 2005; Ainsworth & Rogers, 2007; Leakey *et al.*, 2009; Ellsworth *et al.*, 2017). The mechanism by which photosynthesis is regulated by elevated CO_2 is thought to involve an imbalance between sugar export and production in the chloroplast (Ainsworth & Rogers, 2007). Specifically, at high CO_2 concentrations, sugar production is stimulated and can exceed the rate at which the sugars can be exported from the chloroplast, and excess sugars are stored as starch (Paul & Foyer, 2001). Once starch stores are saturated in chloroplasts, there can be feedback inhibition of photosynthesis, causing a down-regulation in carbon fixation to rebalance sugar production and export (Moore *et al.*, 1999; Paul & Foyer, 2001; Long *et al.*, 2004). Over the long term, this involves a rebalancing of nitrogen allocation to proteins involved in carbon fixation and sugar export (Paul & Foyer, 2001).

1.4 Plant growth responses to environmental change

While the first step in understanding plant-growth responses to environmental change requires understanding the response of photosynthesis and respiratory processes to those changes, actual growth can exhibit a disconnect with primary metabolism (i.e. photosynthesis plus respiration does not equal carbon gain allocated to growth). This is because plants divert energy equivalents away from primary metabolism to secondary metabolic processes such as the regulation of enzymes (Carmo-Silva & Salvucci, 2011; Scales *et al.*, 2014), root exudates (Baetz & Martinoia, 2014), and volatile organic compound production (Ryan *et al.*, 2014; Jardine *et al.*, 2014).

Plant growth under elevated CO_2 concentrations is generally stimulated at high CO_2 (Norby *et al*., 2004; Ainsworth & Long, 2005; Gielen *et al*., 2005; McCarthy *et al*., 2010), however in some cases there is no stimulation of growth (Sigurdsson *et al*., 2013;

Klein *et al*., 2016; Ellsworth *et al*., 2017). In *Eucalyptus* forests, Ellsworth *et al*. (2017) found that phosphorus limitation prevented an increase in growth under elevated CO_2, while phosphorus fertilization stimulated growth even under ambient CO_2. Similarly, in Norway spruce (*Picea abies*), nitrogen limitations can prevent growth responses to temperature and CO_2 (Sigurdsson *et al.*, 2013). Such data suggest that nutrient limitations may prevent vegetative responses to rising CO_2 concentrations, and since nutrient requirements should increase proportionally to growth, forests that currently do not experience nutrient limitations may become nutrient limited from CO_2-stimulation of growth.

Temperature has mixed effects on growth, depending on the evolutionary history and developmental environment of the plant. Meta-analyses however, show some general trends. Way and Oren (2010) found that trees show a positive response of growth, measured as biomass, to increasing temperatures, but that evergreen trees often do not benefit as much from increased temperatures.

1.5 Boreal tree responses to environmental change

Boreal forests are often assumed to be temperature-limited due to their northern location and low temperatures experienced throughout the year (Myeni *et al*., 1997; Jarvis & Linder, 2000; Tanja *et al*., 2003; Way & Oren, 2010), such that warming is expected to increase growth and carbon uptake, while elevated CO_2 concentration is expected to promote enhanced photosynthesis and growth (Ceulemans & Mousseau, 1994; Wullschleger *et al*., 1995; Hyvönen *et al*., 2007; Temme *et al.*, 2015). Boreal tree responses to warming are generally more positive, but more variable, than trees from lower latitudes, while deciduous trees show more positive growth responses than evergreen trees (Way & Oren, 2010). Tree-ring analyses suggest that temperature may be especially limiting growth in the northern boreal forest, while moisture limitations may play a larger role in limiting growth in the southern boreal forest (Brooks *et al*., 1998).

The responses of boreal trees to climate change are complicated by myriad other environmental factors, including nutrients (Sigurdsson *et al.*, 2013), water (Hogg *et al.*,

2008; Ma *et al.*, 2012), and disturbance (Bond-Lamberty *et al.*, 2007). Satellite observations suggest that the North American boreal forest is browning due to reduced precipitation, such that drought constrains growth and carbon uptake in these forests (Bi et al., 2013), while tree-ring analyses support both precipitation- and temperature-driven browning (Lloyd & Bunn, 2007; Huang *et al*., 2010). Nutrients can provide further limitations on carbon uptake in forests, with reduced nutrient availability reducing photosynthetic carbon uptake relative to respiration (Fernández-Martínez *et al*., 2014). Given the nutrient limitations on carbon uptake present in the boreal forest even after accounting for disturbance (Magnani *et al*., 2007), boreal trees may show attenuated responses to climate change (Sigurdsson *et al*., 2013).

Furthermore, the seasonality (i.e. intra-annual changes in temperature, day length, water availability) of the boreal forest adds complexity to any predictions of forest-level responses, since limitations to growth and carbon uptake may change over the year. Therefore, to understand the effects of global change on the boreal forest, we should account for possible limitations due to environmental seasonality. In Chapter 2, I review boreal tree responses to warming and CO_2 in more detail.

1.6 MAESTRA: modeling carbon gain

Photosynthesis is the primary source of carbon for the biosphere, and carbon allocated into recalcitrant living biomass (e.g. wood) is carbon that is removed from the atmosphere for decades to hundreds of years. Increased carbon storage into woody biomass is one potential carbon sink that could attenuate climate warming by carbon efflux to the atmosphere. Therefore, modeling the carbon dynamics of woody species is crucial to understanding how atmospheric CO_2 concentrations will change in the future.

MAESTRA (Multi Array Evaporation Stand Tree Radiation A), is a three-dimensional model that simulates the carbon gain of individual trees within a predefined landscape, and accounts for interactions between trees to simulate a forest stand (Wang & Jarvis, 1990a,b; Medlyn *et al.*, 1999; Duursma & Medlyn, 2012; Fig. 1.4). The model accounts for radiative energy partitioning (Weiss & Norman, 1985; Spitters *et al*., 1986) and

transfer (Norman, 1979, 1980; Steven & Unsworth, 1979), canopy structure (Campbell, 1986, 1990; Wang & Jarvis, 1988; Baldwin & Peterson, 1997), environmental responses of photosynthesis, respiration, and stomatal conductance, and shading effects of trees within the canopy (Wang & Jarvis, 1990a,b). Important environmental inputs to MAESTRA for each of the above components include air temperature, CO_2 concentration, atmospheric pressure, humidity, windspeed, day length, latitude and longitude, solar irradiance, and day of year.

MAESTRA accounts for structural aspects of tree canopies (number of layers, number of pixels per layer, leaf area, leaf angle distribution, specific leaf area, number of leaf age classes, shape, physical size, physical location of each tree on a simulated plot) while assuming that stems do not interfere with the light environment (Wang & Jarvis, 1990a,b; Medlyn *et al.*, 1999; Duursma & Medlyn, 2012). Canopy structure is used in determining light absorbance, transmittance, and reflectance through the tree canopy, which allows shading between neighbouring trees. The absorbance, transmittance, and reflectance of the soil is also used in calculating the light environment for leaves, however this is the extent of the impact of soil on MAESTRA calculations. The interactions between each component of the light environment, along with leaf-level transpiration, can be used to calculate leaf temperature for input into the gas exchange models.

MAESTRA uses the CO_2, temperature, and light response models of photosynthesis and the temperature response of respiration outlined above (Equations 1.2–1.12), and closes the system of equations with the Ball-Berry model of stomatal conductance (Equation 1.17, described below) to calculate leaf level carbon and water exchange, as well as stem and root respiration (Wang & Jarvis, 1990a,b; Medlyn *et al.*, 1999; Duursma & Medlyn, 2012). Leaf-level carbon balance for each canopy pixel is summed to the canopy-level of each tree, to which stem and root respiration are subtracted out to obtain whole-tree carbon balance. The carbon balance of every tree can then be summed to obtain whole-stand carbon balance. Windspeed is also incorporated which, along with leaf water balance and the radiation environment for each canopy pixel, can be used to calculate latent heat loss at the leaf-, tree- and stand- level.

There is no spin-up period (i.e. model training on a test data set), so MAESTRA can be run and the output interpreted once parameters are set, without having to train the model. The coding of MAESTRA is modular, which increases the flexibility of MAESTRA to incorporate new developments and to be highly tailored to an experimental system or question. The mechanistic basis of the physiology in MAESTRA, and its modular structure, make MAESTRA a useful *in silico* tool for testing new approaches for modeling environmental responses of vegetation and for scaling plant physiology from the leaf level to the ecosystem level. MAESTRA has been successfully used to inform best-practices for tree nurseries (Bauerle *et al.*, 2004), and to model the water balance responses of trees (Barnard & Bauerle, 2013).

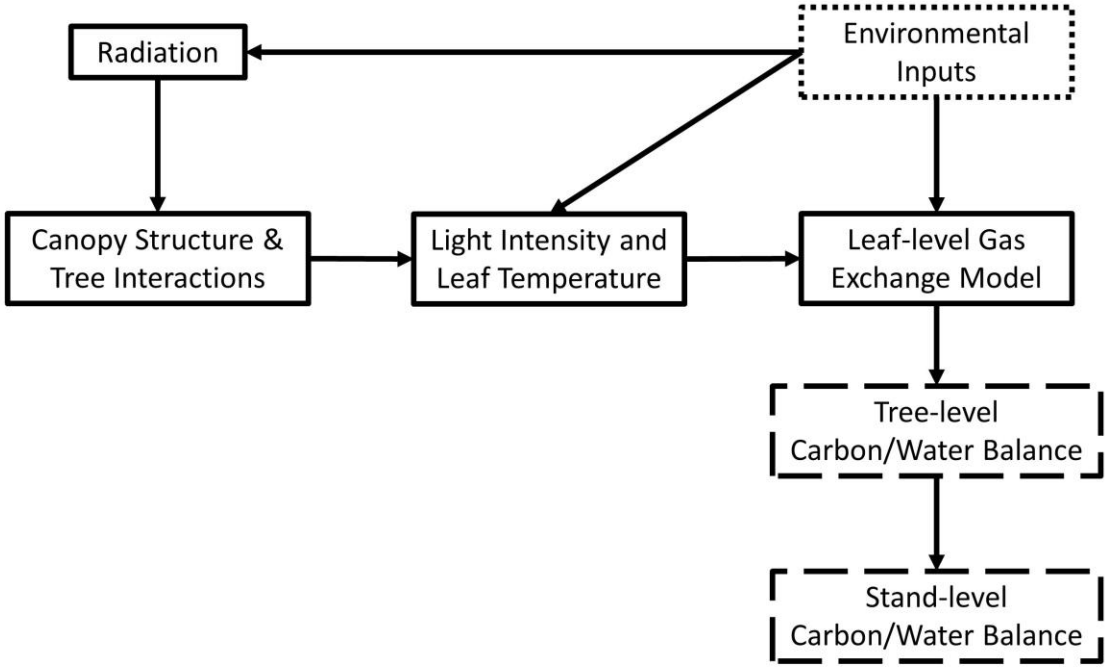

Figure 1.4. Overview of MAESTRA. MAESTRA takes environmental inputs (e.g. air temperature, irradiance, relative humidity, windspeed), calculates the radiation components incident on the canopy, scales the radiation environment throughout the canopy based on structural inputs and neighbouring trees, calculates leaf temperature and incident light intensity on leaves, feeds data into a leaf-level gas exchange model to calculate leaf-level, then tree- and stand- level carbon and water balance. The technical manual for MAESTRA and the most recent update, MAESPA, can be found on the MAESPA model GitHub webpage (maespa.github.io/index.html).

Stomatal conductance is often modelled as a response to relative humidity (Ball *et al.*, 1987), which requires defining stomatal responses *a priori*. In MAESTRA, the Ball-Berry model of stomatal conductance can be used (Ball *et al*., 1987):

$$g_s = m_1 \frac{A}{C_a - \Gamma^*} \text{relative humidity} + b_1 \qquad \text{Equation 1.17}$$

where g_s is stomatal conductance, A is net CO_2 assimilation rate, C_a is the CO_2 concentration at the leaf surface, and m_1 and b_1 are empirically-derived treatment/species-specific parameters.

Modeling with MAESTRA can provide information on whether there is a fundamental shift in the underlying biology. For example, if MAESTRA cannot predict the net carbon gain of a given tree species under particularly hot conditions, that may indicate an element of heat stress that is unaccounted for in the model.

1.7 Questions and hypotheses

The primary goal of my thesis was to understand how climate change, day length, and temperature acclimation affect carbon dynamics in the boreal forest and its dominant species. To do this, I sought answers to the following questions:

1.7.1 Questions

1) What do we know about boreal tree photosynthetic and growth responses to changes in temperature and CO_2? (Chapter 2)

2) How do temperature and day length interact in regulating autumnal photosynthesis and growth in a boreal conifer? (Chapter 3)

3) Do models that include multi-factor acclimation of photosynthesis improve estimates of gross primary productivity in conifers? (Chapter 4)

4) How do climate variation (seasonal and annual) and physiological variation interact to affect projections of net carbon gain responses of boreal trees to climate change? (Chapter 5)

1.7.2 Hypotheses

1) Boreal trees are limited in growth and photosynthesis by low temperatures.
   Predictions: elevated temperatures should increase carbon gain, growth and photosynthetic capacity (addressed in Chapters 2, 3, 5)

2) Day length, not temperature, controls seasonal changes in photosynthetic capacity in evergreen conifers.
   Predictions: photosynthetic capacity should be better correlated with day length than temperature, and manipulations of day length should alter photosynthetic capacity (addressed in Chapters 3, 4).

3) Evergreen conifers acclimate to multiple parameters of the temperature response of photosynthetic capacity.
   Prediction: multifactor thermal acclimation should improve predictions of gross primary productivity over that of single factor acclimation (addressed in Chapter 4).

1.8 References

Ainsworth EA, Long SP. **2005**. What have we learned from 15 years of free-air CO_2 enrichment (FACE)? A meta-analytic review of the responses of photosynthesis, canopy properties and plant production to rising CO_2. *New Phytologist* **165**, 351–371.

Ainsworth EA, Rogers A. **2007**. The response of photosynthesis and stomatal conductance to rising [CO_2]: mechanisms and environmental interactions. *Plant, Cell & Environment* **30**, 258–270.

Alfonso M, Montoya G, Cases R, Rodríguez R, Picorel R. **1994**. Core antenna complexes, CP43 and CP47, of higher plant photosystem II. Spectral properties, pigment stoichiometry, and amino acid composition. *Biochemistry* **33**, 10494–10500.

Allen J. **2002**. Photosynthesis of ATP-electrons, proton pumps, rotors, and poise. *Cell* **110**, 273–276.

Archambault S, Bergeron Y. **1992**. An 802-year tree-ring chronology from the Quebec boreal forest. *Canadian Journal of Forest Research* **22**, 674–682.

Arnon DI, Tsujimoto HY, Tang GM. **1981**. Proton transport in photooxidation of water: a new perspective on photosynthesis. *Proceedings of the National Academy of Sciences of the United States of America* **78**, 2942–2946.

Arnon DI, Whatley FR, Allen MB. **1957**. Triphosphopyridine nucleotide as a catalyst of photosynthetic phosphorylation. *Nature* **180**, 182–185.

Asada K. **1999**. The water-water cycle in chloroplasts: scavenging of active oxygens and dissipation of excess photons. *Annual Review of Plant Physiology & Plant Molecular Biology* **50**, 601–639.

Atkin OK, Evans JR, Ball MC, Lambers H, Pons TL. **2000**. Leaf respiration of snow gum in the light and dark. Interactions between temperature and irradiance. *Plant Physiology* **122**, 915–923.

Atkin OK, Tjoelker MG. **2003**. Thermal acclimation and the dynamic response of plant respiration to temperature. *Trends in Plant Science* **8**, 343–351.

Badger MR, Collatz GJ. **1977**. Studies on the kinetic mechanism of ribulose-1,5-bisphosphate carboxylase and oxygenase reactions, with particular reference to the effect of temperature on kinetic parameters. *Carnegie Institute of Washington Yearbook* **76**, 355–366.

Badger MR, Bjorkman O, Armond PA. **1982**. An analysis of photosynthetic response and adaptation to temperature in higher plants: temperature acclimation in the desert evergreen *Nerium oleander* L. *Plant, Cell & Environment* **5**, 85–99.

Baetz U, Martinoia E. **2014**. Root exudates: the hidden part of plant defense. *Trends in Plant Science* **19**, 90–98.

Baldwin VC Jr, Peterson KD. **1997**. Predicting the crown shape of loblolly pine trees. *Canadian Journal of Forest Research* **27**, 102–107.

Ball JT, Woodrow IE, Berry JA. **1987**. A model predicting stomatal conductance and its contribution to the control of photosynthesis under different environmental conditions. In: *Progress in Photosynthesis Research, Proceedings of the VII International Congress on Photosynthesis*, vol. 4, edited by **Biggins I**, pp. 221–224. Martinus Nijhoff: Dordrecht, Netherlands.

Barnard DM, Bauerle WL. **2013**. The implications of minimum stomatal conductance on modeling water flux in forest canopies. *Journal of Geophysical Research: Biogeosciences* **118**, 1322–1333.

Bassham JA, Benson AA, Kay LD, Harris AZ, Wilson AT, Calvin M. **1954**. The path of carbon in photosynthesis. XXI. The cyclic regeneration of carbon dioxide acceptor. *Journal of the American Chemical Society* **76**, 1760–1770.

Bauerle WL, Oren R, Way DA, Qian SS, Stoy PC, Thornton PE, Bowden JD, Hoffman FM, Reynolds RF. **2012**. Photoperiodic regulation of the seasonal pattern of photosynthetic capacity and the implications for carbon cycling. *Proceedings of the National Academy of Sciences of the United States of America* **109**, 8612–8617.

Bauerle WL, Bowden JD, McLeod MF, Toler JE. **2004**. Modeling intra-crown and intra-canopy interactions in red maple: assessment of light transfer on carbon dioxide and water vapor exchange. *Tree Physiology* **24**, 589–597.

Berry J, Björkman O. **1980**. Photosynthetic response and adaptation to temperature in higher plants. *Annual Review of Plant Physiology* **31**, 491–543.

Bi J, Xu L, Samanta A, Zhu Z, Myneni R. **2013**. Divergent arctic-boreal vegetation changes between North American and Eurasia over the past 30 years. *Remote Sensing* **5**, 2093–2112.

Bird IF, Cornelius MJ, Keys AJ, Whittingham CP. **1971**. Intracellular site of sucrose synthesis in leaves. *Phytochemistry* **13**, 59–64.

Blaško R, Bach LH, Yarwood SA, Trumbore SE, Högberg P, Högberg MN. **2015**. Shifts in soil microbial community structure, nitrogen cycling and the concomitant declining N availability in agein primary boreal forest ecosystems. *Soil Biology & Biochemistry* **91**, 200–211.

Bond-Lamberty B, Peckham SD, Ahl DE, Gower ST. **2007**. Fire as the dominant driver of central Canadian boreal forest carbon balance. *Nature* **450**, 89–92.

Bowes G. **1991**. Growth at elevated CO_2: photosynthetic responses mediated through Rubisco. *Plant, Cell & Environment* **14**, 795–806.

Bradshaw CJA, Warkentin IG. **2015**. Global estimates of boreal forest carbon stocks and flux. *Global and Planetary Change* **128**, 24–30.

Brandt JP, Flannigan MD, Maynard DG, Thompson ID, Volney WJA. **2013**. An introduction to Canada's boreal zone: ecosystem processes, health, sustainability, and environmental issues. *Environmental Reviews* **21**, 207–226.

Brooks A, Farquhar GD. **1985**. Effect of temperature on the CO_2/O_2 specificity of ribulose-1,5-bisphosphate carboxylase/oxygenase and the rate of respiration in the light. *Planta* **165**, 397–406.

Brooks JR, Flanagan LB, Ehleringer JR. **1998**. Responses of boreal conifers to climate fluctuations: indications from tree-ring widths and carbon isotope analyses. *Canadian Journal of Forest Research* **28**, 524–533.

Buchanan BB. **1991**. Regulation of CO_2 assimilation in oxygenic photosynthesis: The ferredoxin/thioredoxin system. *Archives of Biochemistry & Biophysics* **288**, 1–9.

Bunce JA. **2000**. Responses of stomatal conductance to light, humidity and temperature in winter wheat and barley grown at three concentrations of carbon dioxide in the field. *Global Change Biology* **6**, 371–382.

Busch FA, Sage RF. **2017**. The sensitivity of photosynthesis to O_2 and CO_2 concentration identifies strong Rubisco control above the thermal optimum. *New Phytologist* **213**, 1036–1051.

Busch FA, Sage RF, Farquhar GD. **2018**. Plants increase CO_2 uptake by assimilating nitrogen via the photorespiratory pathway. *Nature Plants* **4**, 46–54.

Campbell GS. **1986**. Extinction coefficients for radiation in plant canopies calculated using an ellipsoidal inclination angle distribution. *Agricultural & Forest Meteorology* **36**, 317–321.

Campbell GS. **1990**. Derivation of an angle density function for canopies with ellipsoidal leaf angle distributions. *Agricultural & Forest Meteorology* **49**, 173–176.

Carmo-Silva AE, Gore MA, Andrade-Sanchez P, French AN, Hunsaker DJ, Salvucci ME. **2012**. Decreased CO_2 availability and inactivation of Rubisco limit photosynthesis in cotton plants under heat and drought stress in the field. *Environmental & Experimental Botany* **83**, 1–11.

Carmo-Silva AE, Salvucci ME. **2011**. The activity of Rubisco's molecular chaperone, Rubisco activase, in leaf extracts. *Photosynthesis Research* **108**, 143–155.

Ceulemans R, Mousseau M. **1994**. Effects of elevated atmospheric CO_2 on woody plants. *New Phytologist* **127**, 425–446.

Chapin III FS, McFarland J, McGuire AD, Euskirchen ES, Ruess RW, Kielland K. **2009**. The changing global carbon cycle: linking plant-soil carbon dynamics to global consequences. *Journal of Ecology* **97**, 840–850.

Chen J, Källman T, Ma X, *et al*. 2012. Disentangling the roles of history and local selection in shaping clinal variation of allele frequencies and gene expression in Norway spruce (*Picea abies*). *Genetics* **191**, 865–881.

Ciais P, Sabine C, Bala G, *et al*. 2013. Carbon and other biogeochemical cycles. In: *Climate Change 2013: The Physical Science Basis. Contribution of Working Group I to the Fifth Assessment Report of the Intergovernmental Panel on Climate Change*, edited **Stocker TF, Qin D, Plattner G-K, Tignor M, Allen SK, Boschung J, Nauels A, Xia Y, Bex V, Midgley PM**. Cambridge University Press: Cambridge, UK.

Clapham DH, Dormling I, Ekberg L, Eriksson G, Qamaruddin M, Vince-Prue D. **1998**. Latitudinal cline of requirement for far-red light for the photoperiodic control of budset and extension growth in *Picea abies* (Norway spruce). *Physiologia Plantarum* **102**, 71–78.

Clemmensen KE, Bahr A, Ovaskainen O, *et al*. 2013. Roots and associated fungi drive long-term carbon sequestration in boreal forest. *Science* **339**, 1615–1618.

Collins M, Knutti R, Arblaster J, *et al*. 2013. Long-term climate change: projections, commitments and irreversibility. In: *Climate Change 2013: The Physical Science Basis. Contribution of Working Group I to the Fifth Assessment Report of the Intergovernmental Panel on Climate Change*, edited **Stocker TF, Qin D, Plattner G-K, Tignor M, Allen SK, Boschung J, Nauels A, Xia Y, Bex V, Midgley PM**. Cambridge University Press: Cambridge, UK.

DalCorso G, Pesarai P, Masiero S, Aseeva E, Schünemann D, Finazzi G, Joliot P, Barbato R, Leister D. **2008**. A complex containing PGRL1 and PGR5 is involved in the switch between linear and cyclic electron flow in *Arabidopsis*. *Cell* **132**, 273–285.

Davidson EA, Janssens IA. **2006**. Temperature sensitivity of soil carbon decomposition and feedbacks to climate change. *Nature* **440**, 165–173.

de Groot WJ, Flannigan MD, Cantin AS. **2013**. Climate change impacts on future boreal fire regimes. *Forest Ecology and Management* **294**, 35–44.

Dillaway DN, Kruger EL. **2010**. Thermal acclimation of photosynthesis: a comparison of boreal and temperate tree species along a latitudinal transect. *Plant, Cell & Environment* **33**, 888–899.

Duglokencky E, Tans P. **2017**. Trends in atmospheric carbon dioxide. *Earth System Research Laboratory, Global Monitoring Division, National Oceanic & Atmospheric Administration* https://www.esrl.noaa.gov/gmd/ccgg/trends/ [accessed November 8, 2017].

Dumberry M, Bloxham J. **2006**. Azimuthal flows in the Earth's core and changes in length of day at millennial timescales. *Geophysical Journal International* **165**, 32–46.

Duursma R, Medlyn B. **2012**. MAESPA: a model to study interactions between water limitation, environmental drivers and vegetation function at tree and stand levels, with an example application to [CO_2] x drought interactions. *Geoscientific Model Development* **5**, 919–940.

Ellis RJ. **1979**. The most abundant protein in the world. *Trends in Biochemical Sciences* **4**, 241–244.

Ellsworth D, Anderson I, Crous K, *et al.* 2017. Elevated CO_2 does not increase eucalypt forest productivity on a low-phosphorus soil. *Nature Climate Change* **7**, 279–282.

Farquhar GD, von Caemmerer S, Berry JA. **1980**. A biochemical model of photosynthetic CO_2 assimilation in leaves of C_3 species. *Planta* **149**, 78–90.

Fisher JB, Huntzinger DN, Schwalm CR, Sitch S. **2014**. Modeling the terrestrial biosphere. *Annual Review of Environment & Resources* **39**, 91–123.

Flexas J, Diaz-Espejo A, Galmés J, Kaldenhoff R, Medrano H, Ribas-Carbo M. **2007**. Rapid variations of mesophyll conductance in response to changes in CO_2 concentration around leaves. *Plant, Cell & Environment* **30**, 1284–1298.

Food & Agriculture Organization of the United Nations (FAO). **2001**. State of the world's forests 2001. FAO: Rome, Italy.

FAO. **2016**. State of the world's forests 2016. Forests and agriculture: land-use challenges and opportunities. FAO: Rome, Italy.

Fernández-Martínez M, Vicca S, Janssens IA, *et al*. 2014. Nutrient availability as the key regulator of global forest carbon balance. *Nature Climate Change* **4**, 471–476.

Forkel M, Carvalhais N, Rödenbeck C, Keeling R, Heimann M, Thonicke K, Zaehle S, Reichstein M. **2016**. Enhanced seasonal CO_2 exchange caused by amplified plant productivity in northern ecosystems. *Science* **351**, 696–699.

Friedlingstein P, Cox P, Betts R, *et al*. 2006. Climate-carbon cycle feedback analysis: results from the C^4MIP model intercomparison. *Journal of Climate* **19**, 3337–3353.

Gauthier S, Bernier P, Kuuluvainen T, Shvidenko AZ, Schepaschenko DG. **2015**. Boreal forest health and global change. *Science* **349**, 819–822.

Gielen B, Calfapietra C, Lukac M, *et al*. 2005. Net carbon storage in a poplar plantation (POPFACE) after three years of free-air CO_2 enrichment. *Tree Physiology* **25**, 1399–1408.

Girardin MP, Hogg EH, Bernier PY, Kurs WA, Guo XJ, Cyr G. **2016**. Negative impacts of high temperatures on growth of black spruce forests intensify with the anticipated climate warming. *Global Change Biology* **22**, 627–643.

Goddard DR, Meeuse JD. **1950**. Respiration of higher plants. *Annual Review of Plant Physiology* **1**, 207–232.

Goetz SJ, Bunn AG, Fiske GJ, Houghton RA. **2005**. Satellite-observed photosynthetic trends across boreal North America associated with climate and fire disturbance. *Proceedings of the National Academy of Sciences of the United States of America* **102**, 13521–13525.

Graven HD, Keeling RF, Piper SC, *et al.* 2013. Enhanced seasonal exchange of CO_2 by northern ecosystems since 1960. *Science* **341**, 1085–1089.

Grossman AR, Bhaya D, Apt KE, Kehoe DM. **1995**. Light-harvesting complexes in oxygenic photosynthesis: diversity, control, and evolution. *Annual Review of Genetics* **29**, 231–288.

Gu L, Pallardy SG, Tu K, Law BE, Wullschleger SD. **2010**. Reliable estimation of biochemical parameters from C_3 leaf photosynthesis-intercellular carbon dioxide response curves. *Plant, Cell & Environment* **33**, 1852–1874.

Haehnel W. **1984**. Photosynthetic electron transport in higher plants. *Annual Review of Plant Physiology* **35**, 659–693.

Hamilton JA, El Kayal W, Hart AT, Runcie DE, Arango-Velez A, Cooke JEK. **2016**. The joint influence of photoperiod and temperature during growth cessation and development of dormancy in white spruce (*Picea glauca*). *Tree Physiology* **36**, 1432–1448.

Harden JW, O'Neill KP, Trumbore SE, Veldhuis H, Stocks BJ. **1997**. Moss and soil contributions to the annual net carbon flux of a maturing boreal forest. *Journal of Geophysical Research* **102**, 28805–28816.

Harley PC, Sharkey TD. **1991**. An improved model of C_3 photosynthesis at high CO_2: reversed O_2 sensitivity explained by lack of glycate reentry into the chloroplast. *Photosynthesis Research* **27**, 169–178.

Harley PC, Loreto F, Di Marco G, Sharkey TD. **1992**. Theoretical considerations when estimating the mesophyll conductance to CO_2 flux by analysis of the response of photosynthesis to CO_2. *Plant Physiology* **98**, 1429–1436.

Hartmann DL, Tank AMGK, Rusticucci M, *et al*. 2013. Observations: atmosphere and surface. In: *Climate Change 2013: The Physical Science Basis. Contribution of Working Group I to the Fifth Assessment Report of the Intergovernmental Panel on Climate*

Change, edited by **Stocker TF, Qin D, Plattner G-K, Tignor M, Allen SK, Boschung J, Nauels A, Xia Y, Bex V, Midgley PM**. Cambridge University Press: Cambridge, UK.

Heber U, Heldt HW. **1981**. The chloroplast envelope: structure, function and role in leaf metabolism. *Annual Review of Plant Physiology* **32**, 139–168.

Heide OM. **1974**. Growth and dormancy in Norway spruce ecotypes (*Picea abies*). 1. Interaction of photoperiod and temperature. *Physiologia Plantarum* **30**, 1–12.

Herrmann KM, Weaver LM. **1999**. The shikimate pathway. *Annual Review of Plant Physiology & Plant Molecular Biology* **50**, 473–503.

Hertle AP, Blunder T, Wunder T, Pesaresi P, Pribil M, Armbruster U, Leister D. **2013**. PGRL1 is the elusive ferredoxin-plastoquinone reductase in photosynthetic cyclic electron transport. *Molecular Cell* **49**, 511–523.

Heskel MA, O'Sullivan OS, Reich PB, *et al*. **2016**. Convergence in the temperature response of leaf respiration across biomes and plant functional types. *Proceedings of the National Academy of Sciences of the United States of America* **113**, 3832–3837.

Hikosaka K, Ishikawa K, Borjigidai A, Muller O, Onoda Y. **2006**. Temperature acclimation of photosynthesis: mechanisms involved in the changes in temperature dependence of photosynthetic rate. *Journal of Experimental Botany* **57**, 291–302.

Hill R, Bendall F. **1960**. Function of the two cytochrome components in chloroplasts: A working hypothesis. *Nature* **186**, 136–137.

Höberg P, Fan H, Quist M, Binkley D, Tamm CO. **2006**. Tree growth and soil acidification in response to 30 years of experimental nitrogen loading on boreal forest. *Global Change Biology* **12**, 489–499.

Hogg EH, Brandt JP, Michaelian M. **2008**. Impacts of a regional drought on the productivity, dieback, and biomass of western Canadian aspen forests. *Canadian Journal of Forest Research* **38**, 1373–1384.

Hogg EH. **1994**. Climate and the southern limit of the western Canadian boreal forest. *Canadian Journal of Forest Research* **24**, 1835–1845.

Houghton RA. **2007**. Balancing the global carbon budget. *Annual Review of Earth and Planetary Sciences* **35**, 313–347.

Huang J, Tardif JC, Bergeron Y, Denneler B, Berninger F, Girardin MP. **2010**. Radial growth response of four dominant boreal tree species to climate along a latitudinal gradient in the eastern Canadian boreal forest. *Global Change Biology* **16**, 711–731.

Hüner NPA, Hopkins WG. **2009**. *Introduction to Plant Physiology* (4th Ed.). John Wiley & Sons: New York, NY.

Hurry VM, Garderström P, Öquist G. **1992**. Reduced sensitivity to photoinhibition following frost-hardening of winter rye is due to increased phosphate availability. *Planta* **190**, 484–490.

Hurry VM, Keerberg O, Pärnik T, Öquist G, Garderström P. **1996**. Effect of cold hardening on the components of respiratory decarboxylation in the light and in the dark in leaves of winter rye. *Physiologia Plantarum* **111**, 713–179.

Hurt E, Hauska G. **1981**. A cytochrome f/b6 complex of five polypeptides with plastoquinol-plastocyanin-oxidoreductase activity from spinach chloroplasts. *European Journal of Biochemistry / FEBS* **117**, 591–595.

Hyvönen R, Ågren GI, Linder S, *et al*. 2007. The likely impact of elevated [CO_2], nitrogen deposition, increased temperature and management on carbon sequestration in temperate and boreal forest ecosystems: a literature review. *New Phytologist* **173**, 463–480.

Intergovernmental Panel on Climate Change (IPCC). **2014**. Climate Change Synthesis Report. *Contribution of Working Groups I, II and III to the Fifth Assessment Report of the Intergovernmental Panel on Climate Change*, edited by **Core Writing Team, Pachauri RK, Meyer LA**. IPCC: Geneva, Switzerland, 151 pp.

IPCC. **2013**. Annex I: atlas of global and regional climate projections supplementary material RCP8.5. In: *Climate Change 2013: The Physical Science Basis. Contribution of Working Group I to the Fifth Assessment Report of the Intergovernmental Panel on Climate Change*, edited by **van Oldenborgh GJ, Collins M, Arblaster J, Christensen JH, Marotzke J, Power SB, Rummukainen M, Zhou T**. Cambridge University Press: Cambridge, UK.

Jakoby WB, Brummond DO, Ochoa S. **1956**. Formation of 3-phosphoglyceric acid by carbon dioxide fixation with spinach leaf enzymes. *The Journal of Biological Chemistry* **218**, 811–822.

Jardine K, Chambers J, Alves EG, *et al.* 2014. Dynamic balancing of isoprene carbon sources reflects photosynthetic and photorespiratory responses to temperature stress. *Plant Physiology* **166**, 2051–2064.

Jarvis PG, Linder S. **2000**. Constraints to growth of boreal forests. *Nature* **405**, 904–905.

Jordan DB, Ogren WL. **1984**. The CO_2/O_2 specificity of ribulose 1,5-bisphosphate carboxylase/oxygenase. *Planta* **161**, 308–313.

Junge W. **1999**. ATP synthase and other motor proteins. *Proceedings of the National Academy of Sciences of the United States of America* **96**, 4735–4737.

Karhu K, Hilsavuori E, Fritze H, Biasi C, Nykänen H, Liski J, Vanhala P, Heinonsalo J, Pumpanen J. **2016**. Priming effect increases with depth in a boreal forest soil. *Soil Biology & Biochemistry* **99**, 104–107.

Kasischke ES, Turetsky MR. **2006**. Recent changes in the fire regime across the North American boreal region – spatial and temporal patterns of burning across Canada and Alaska. *Geophysical Research Letters* **33**, L09703.

Kattge J, Knorr W. **2007**. Temperature acclimation in a biochemical model of photosynthesis: a reanalysis of data from 36 species. *Plant, Cell & Environment* **30**, 1176–1190.

Kelly R, Chipman ML, Higuera PE, Stefanova I, Brubaker LB, Hu FS. **2013**. Recent burning of boreal forests exceeds fire regime limits of the past 10,000 years. *Proceedings of the National Academy of Sciences of the United States of America* **110**, 13055–13060.

Klein T, Bader MK-F, Leuzinger S, Mildner M, Schleppi P, Siegwolf RTW, Körner C. **2016**. Growth and carbon relations of mature *Picea abies* tres under 5 years of free-air CO_2 enrichment. *Journal of Ecology* **104**, 1720–1733.

Kljun N, Black TA, Griffis TJ, Barr AG, Gaumont-Guay D, Morgenstern K, McCaughney JH, Nesic Z. **2006**. Response of net ecosystem productivity of three boreal forest stands to drought. *Ecosystems* **9**, 1128–1144.

Kok B. **1948**. A critical consideration of the quantum yield of *Chlorella*-photosynthesis. *Enzymology* **13**, 1–56.

Kok B. **1957**. Absorption changes induced by the photochemical reaction of photosynthesis. *Nature* **179**, 583–584.

Kok B. **1961**. Partial purification and determination of oxidation reduction potential of the photosynthetic chlorophyll complex absorbing at 700 mμ. *Biochimica et Biophysica Acta* **48**, 527–533.

Körner C. **2017**. A matter of tree longevity. *Science* **355**, 130–131.

Krause GH, Weis E. **1991**. Chlorophyll fluorescence and photosynthesis: the basics. *Annual Review of Plant Physiology & Plant Molecular Biology* **42**, 313–349.

Krauß N, Schubert W-D, Klukas O, Fromme P, Witt HT, Saenger W. **1996**. Photosystem I at 4 Å resolution represents the first structural model of a joint photosynthetic reaction centre and core antenna system. *Nature Structural & Molecular Biology* **3**, 965–973.

Krebs HA, Lowenstein JM. **1960**. Chapter 4: the tricarboxylic acid cycle. *Metabolic Pathways*, vol. 1, edited by **Greenberg DM**, pp. 129–204. Academic Press Inc.: New York, NY.

Kroner Y, Way DA. **2016**. Carbon fluxes acclimate more strongly to elevated growth temperatures than to elevated CO_2 concentrations in a northern conifer. *Global Change Biology* **22**, 2913–2928.

Kruger NJ, von Schaewen A. **2003**. The oxidative pentose phosphate pathway: structure and organisation. *Current Opinion in Plant Biology* **6**, 236–246.

Ku SB, Edwards GE. **1977**. Oxygen inhibition of photosynthesis. 1. Temperature dependence and relation to O_2/CO_2 solubility ratio. *Plant Physiology* **59**, 986–990.

Kurz WA, Shaw CH, Boisvenue C, Stinson G, Metsaranta J, Leckie D, Dyk A, Smyth C, Neilson ET. **2013**. Carbon in Canada's boreal forest — A synthesis. *Environmental Reviews* **21**, 260–292.

Kurz WA, Dymond CC, Stinson G, Rampley GJ, Neilson ET, Carroll AL, Ebata T, Safranyik L. **2008a**. Mountain pine beetle and forest carbon feedback to climate change. *Nature* **452**, 987–990.

Kurz WA, Stinzon G, Rampley GJ, Dymond CC, Neilson ET. **2008b**. Risk of natural disturbances makes future contribution of Canada's forests to the global carbon cycle highly uncertain. *Proceedings of the National Academy of Sciences of the United States of America* **105**, 1551–1555.

Laing WA, Ogren WL, Hageman RH. **1974**. Regulation of soybean net photosynthetic CO_2 fixation by the interaction of CO_2, O_2, and ribulose 1,5-diphosphate carboxylase. *Plant Physiology* **54**, 678–685.

Laisk A. **1977**. Kinetics of photosynthesis and photorespiration in C_3-plants. Nauka, Moscow (in Russian).

Larsen CPS. **1998**. Spatial and temporal variations in boreal forest fire frequency in northern Alberta. *Journal of Biogeography* **24**, 663–673.

Leakey ADB, Ainsworth EA, Bernacchi CJ, Rogers A, Long SP, Ort DR. **2009**. Elevated CO_2 effects on plant carbon, nitrogen, and water relations: six important lessons from FACE. *Journal of Experimental Botany* **60**, 2859–2876.

Lim H, Oren R, Palmroth S, *et al*. 2015. Inter-annual variability of precipitation constrains the production response of boreal *Pinus sylvestris*to nitrogen fertilization. *Forest Ecology & Management* **348**, 31–45.

Litvak M, Miller S, Wofsy SC, Goulden M. **2003**. Effect of stand age on whole ecosystem CO_2 exchange in the Canadian boreal forest. *Journal of Geophysical Research: Atmospheres* **108**, 8225.

Lloyd AH, Bunn AG. **2007**. Responses of the circumpolar boreal forest to 20^{th} century climate variability. *Environmental Research Letters* **2**, 045013.

Long SP, Ainsworth EA, Rogers A, Ort DR. **2004**. Rising atmospheric carbon dioxide: plants FACE the future. *Annual Review of Plant Biology* **55**, 591–628.

Long SP, Drake BG. 1992 Photosynthetic CO_2 assimilation and rising atmospheric CO_2 concentrations. *Topics in Photosynthesis* **12**, 69–103.

Luyssaert S, Schulze E-D, Börner A, Knohl A, Hessenmöller D, Law BE, Ciais P, Grace J. **2008**. Old-growth forests as global carbon sinks. *Nature* **455**, 213–215.

Ma Z, Peng C, Zhu Q, Chen H, Yu G, Li W, Zhou X, Wang W, Zhang W. **2012**. Regional drought-induced reduction in the biomass carbon sink of Canada's boreal forests. *Proceedings of the National Academy of Sciences of the United States of America* **109**, 2423–2427.

Magnani F, Mencuccini M, Borghetti M, *et al*. 2007. The human footprint in the carbon cycle of temperate and boreal forests. *Nature* **447**, 849–851.

Maxwell K, Johnson GN. **2000**. Chlorophyll fluorescence – a practical guide. *Journal of Experimental Botany* **51**, 659–668.

Mazor Y, Borovikova A, Caspy I, Nelson N. **2017**. Structure of the plant photosystem I supercomplex at 2.6 Å resolution. *Nature Plants* **3**, 17014.

McCarthy HR, Oren R, Johnsen KH, Gallet-Budynek A, Pritchard SG, Cook CW, LaDeau SL, Jackson RB, Finzi AC. **2010**. Re-assessment of plant carbon dynamics at the Duke free-air CO_2 enrichment site: interactions of atmospheric [CO_2] with nitrogen and water availability over stand development. *New Phytologist* **185**, 514–528.

McCarty RE, Evron Y, Johnson EA. **2000**. The chloroplast ATP synthase: a rotary enzyme? *Annual Review of Plant Physiology & Plant Molecular Biology* **51**, 83–109.

McCullough DG, Werner RA, Neumann D. **1998**. Fire and insects in northern and boreal forest ecosystems of North America. *Annual Review of Entomology* **43**, 107–127.

McDonald AE, Ivanov AG, Bode R, Maxwell DP, Rodermel SR, Hüner NPA. **2011**. Flexibility in photosynthetic electron transport: the physiological role of plastoquinol terminal oxidase (PTOX). *Biochimica et Biophysica Acta – Bioenergetics* **1807**, 954–967.

Medlyn BE, Badeck F-W, De Pury DGG, *et al.* 1999. Effects of elevated [CO_2] on photosynthesis in European forest species: a meta-analysis of model parameters. *Plant, Cell & Environment* **22**, 1475–1495.

Medlyn BE, Dreyer E, Ellsworth D, *et al*. 2002. Temperature response of parameters of a biochemically based model of photosynthesis. II. A review of experimental data. *Plant, Cell & Environment* **25**, 1167–1179.

Michalecka AM, Svensson AS, Johansson FI, *et al*. 2003. *Arabidopsis* genes encoding mitochondrial type II NAD(P)H dehydrogenases have different evolutionary origin and show distinct responses to light. *Plant Physiology* **133**, 642–652.

Miernyk JA, Camp PJ, Randall DD. **1985**. Regulation of plant pyruvate dehydrogenase complexes. *Current Topics in Plant Biochemistry & Physiology* **4**, 175–190.

Millar AH, Whelan J, Soole KL, Day DA. **2011**. Organization and regulation of mitochondrial respiration in plants. *Annual Review of Plant Biology* **62**, 79–104.

Millerd A. **1953**. Respiratory oxidation of pyruvate by plant mitochondria. *Archives of Biochemistry & Biophysics* **42**, 149–163.

Moore BD, Cheng S-H, Sims D, Seemann JR. **1999**. The biochemical and molecular basis for photosynthetic acclimation to elevated atmospheric CO_2. *Plant, Cell & Environment* **22**, 567–582.

Moore CS, Cook-Johnson R, Rudhe C, *et al*. 2003. Identification of AtNDl1: an internal nonphosphorylating NAD(P)H dehydrogenase in *Arabidopsis thaliana* mitochondria. *Plant Physiology* **133**, 1968–1978.

Moss DN, Rawlins SL. **1963**. Concentration of Carbon Dioxide inside Leaves. *Nature* **197**, 1320–1321.

Munekage Y, Hojo M, Meurer J, Endo T, Tasaka M, Shikanai T. **2002**. PGR5 is involved in cyclic electron flow around photosystem I and is essential for photoprotection in *Arabidopsis*. *Cell* **110**, 361–371.

Myeni RB, Keeling CD, Tucker CJ, Asrar G, Nemani RR. **1997**. Increased plant growth in the northern high latitudes from 1981 to 1991. *Nature* **386**, 698–702

Myhre G, Shindell D, Bréon F-M, *et al*. 2013. Anthropogenic and natural radiative forcing. In: *Climate Change 2013: The Physical Science Basis. Contribution of Working Group I to the Fifth Assessment Report of the Intergovernmental Panel on Climate Change*, edited by **Stocker TF, Qin D, Plattner G-K, Tignor M, Allen SK, Boschung J, Nauels A, Xia Y, Bex V, Midgley PM**. Cambridge University Press: Cambridge, UK.

Nishikawa Y, Yamamoto H, Okegawa Y, Wada S, Sato N, Taira Y, Sugimoto K, Makino A, Shikanai T. **2012**. PGR5-dependent cyclic electron transport around PSI contributes to the redox homeostasis in chloroplasts rather than CO_2 fixation and biomass production in rice. *Plant Cell Physiology* **53**, 2117–2126.

Norby RJ, Ledford J, Reilly CD, Miller NE, O'Neill EG. **2004**. Fine-root production dominates response of a deciduous forest to atmospheric CO_2 enrichment. *Proceedings of the National Academy of Sciences of the United States of America* **101**, 9689–9693.

Norman JM. **1979**. Modelling the complete crop canopy. In: *Modification of the Aerial Environment of Crops*, edited by **Barfield BJ, Gerber JF**, pp. 249–277. American Society of Agricultural Engineers: Saint Joseph, MI, USA.

Norman JM. **1980**. Interfacing leaf and canopy light interception models. In: *Predicting Photosynthesis for Ecosystem Models*, vol. 2, edited by **Hesketh JD, Jones JW**. CRC Press: Boca Raton, FL, USA.

O'Sullivan OS, Heskel MA, Reich PB, *et al.* 2017. Thermal limits of leaf metabolism across biomes. *Global Change Biology* **23**, 209–223.

Ogren WL, Bowes G. **1971**. Ribulose diphosphate carboxylase regulates soybean photorespiration. *Nature* **230**, 159–160.

Ögren E, Evans JR. **1993**. Photosynthetic light-response curves. *Planta* **189**, 182–190.

Oleksyn J, Reich PB, Tjoelker MG, Chalupka W. **2001**. Biogeographic differences in shoot elongation pattern among European Scots pine populations. *Forest Ecology & Management* **148**, 207–220.

Öquist G, Hüner NPA. **2003**. Photosynthesis of overwintering evergreen plants. *Annual Review of Plant Biology* **54**, 329–55.

Palviainen M, Pumpanen J, Berninger F, Ritala K, Duan B, Helnonsalo J, Sun H, Köster E, Köster K. **2017**. Nitrogen balance alond a northern boreal forest fire chronosequence. *PLoS ONE* **12**, e0174720.

Pan Y, Birdsey RA, Fang J, *et al*. 2011. A large and persistent carbon sink in the world's forests. *Science* **333**, 988–993.

Paul MJ, Foyer CH. **2001**. Sink regulation of photosynthesis. *Journal of Experimental Botany* **52**, 1383–1400.

Pearson RG, Phillips SJ, Loranty MM, Beck PSA, Damoulas T, Knight SJ, Goetz SJ. **2013**. Shifts in Arctic vegetation and associated feedbacks under climate change. *Nature Climate Change* **3**, 673–677.

Peng C, Ma Z, Lei X, Zhu Q, Chen H, Wang W, Liu S, Li W, Fang X, Zhou X. **2011**. A drought-induced pervasive increase in tree mortality across Canada's boreal forests. *Nature Climate Change* **1**, 467–471.

Potapov P, Hansen MC, Stehman SV, Loveland TR, Pittman K. **2008**. Combining MODIS and Landsat imagery to estimate and map boreal forest cover loss. *Remote Sensing of Environment* **112**, 3708–3719.

Raines CA. **2003**. The Calvin cycle revisited. *Photosynthesis Research* **75**, 1–10.

Raison JK, Berry JA. **1979**. Viscotropic denaturation of chloroplast membranes and acclimation to temperature by adjustment of lipid viscosity. *Carnegie Institute of Washington Yearbook* **78**, 149–152.

Ramakrishna A, Ravishankar GA. **2011**. Influence of abiotic stress signals on secondary metabolites in plants. *Plant Signaling & Behavior* **6**, 1720–1731.

Randerson JT, Liu H, Flanner MG, *et al*. 2006. The impact of boreal forest fire on climate warming. *Science* **314**, 1130–1132.

Rogelj J, den Elzen M, Höhne N, Fransen T, Fekete H, Winkler H, Schaeffer R, Sha F, Riahi K, Meinshausen M. **2016**. Paris Agreement climate proposals need a boost to keep warming well below 2 °C. *Nature* **534**, 631–639.

Rogers A, Medlyn BE, Dukes JS, *et al.* 2017. A roadmap for improving the representation of photosynthesis in Earth system models. *New Phytologist* **213**, 22–42.

Ryan AC, Hewitt CN, Possell M, Vickers CE, Purnell A, Mullineaux PM, Davies WJ, Dodd IC. **2014**. Isoprene emission protects photosynthesis but reduces plant productivity during drought in transgenic tobacco (*Nicotiana tabacum*) plants. *New Phytologist* **201**, 205–216.

Safranyik L, Carroll AL, Régnière J, *et al*. 2010. Potential for range expansion of mountain pine beetle into the boreal forest of North America. *The Canadian Entomologist* **142**, 415–442.

Sage RF, Sharkey TD, Seemann JR. **1988**. The *in vivo* response of the ribulose-1,5-bisphosphate carboxylase activation state and the pool sizes of photosynthetic metabolites to elevated CO_2 in *Phaseolus vulgaris* L. *Planta* **174**, 407–416.

Sage RF, Way DA, Kubien DS. **2008**. Rubisco, Rubisco activase, and global climate change. *Journal of Experimental Botany* **59**, 1581–1595.

Salvucci ME, Crafts-Brandner SJ. **2004**. Inhibition of photosynthesis by heat stress: the activation state of Rubisco as a limiting factor in photosynthesis. *Physiologia Plantarum* **120**, 179–186.

Scafaro AP, Xiang S, Long BM, Bahar NHA, Weerasinghe LK, Creek D, Evans JR, Reich PB, Atkin OK. **2017**. Strong thermal acclimation of photosynthesis in tropical and temperate wet-forest tree species: the importance of altered Rubisco content. *Global Change Biology* **23**, 2783–2800.

Scales JC, Parry MAJ, Salvucci ME. **2014**. A non-radioactive method for measuring Rubisco activase activity in the presence of variable ATP: ADP ratios, including modifications for measuring the activity and activation state of Rubisco. *Photosynthesis Research* **119**, 355–365.

Schreiber U, Berry JA. **1977**. Heat-induced changes of chlorophyll fluorescence in intact leaves correlated with damage of the photosynthetic apparatus. *Planta* **136**, 233–238.

Schreiber U, Neubauer C. **1990**. O_2-dependent electron flow, membrane energization and the mechanism of nonphotochemical quenching of chlorophyll fluorescence. *Photosynthesis Research* **25**, 279–293.

Schwartz MD, Ahas R, Aasa A. **2006**. Onset of spring starting earlier across the Northern Hemisphere. *Global Change Biology* **12**, 343–351.

Sharkey TD. **1985a**. Photosynthesis in intact leaves of C_3 plants: physics, physiology and rate limitations. *The Botanical Review* **51**, 53–105.

Sharkey TD. **1985b**. O_2-insensitive photosynthesis in C_3 plants. *Plant Physiology* **78**, 71–75.

Sigurdsson BD, Medhurst JL, Wallin G, Eggertsson O, Linder S. **2013**. Growth of mature boreal Norway spruce was not affected by elevated [CO_2] and/or air temperature unless nutrient availability was improved. *Tree Physiology* **33**, 1192–1205.

Slot M, Kitajima K. **2015**. General patterns of acclimation of leaf respiration to elevated temperatures across biomes and plant types. *Oecologia* **177**, 885–900.

Sogaard G, Johnsen O, Nilsen J, Junttila O. **2008**. Climatic control of bud burst in young seedlings of nine provenances of Norway spruce. *Tree Physiology* **28**, 311–320.

Spitters CJT, Toussaint HAJM, Goudriaan J. **1986**. Separating the diffuse and direct component of global radiation and its implications for modeling canopy photosynthesis. I. Components of incoming radiation. *Agricultural & Forest Meteorology* **38**, 217–229.

Steven MD, Unsworth MH. **1979**. The diffuse solar irradiance of slopes under buttless skies. *Quarterly Journal of the Royal Meteorological Society* **105**, 593–602.

Stinziano JR, Hüner NPA, Way DA. **2015**. Warming delays autumn declines in photosynthetic capacity in a boreal conifer, Norway spruce (*Picea abies*). *Tree Physiology* **35**, 1303–1313.

Stitt M, Heldt HW. **1981**. Simultaneous synthesis and degradation of starch in spinach chloroplasts in the light. *Biochimica et Biophysica Acta* **638**, 1–11.

Stocker TF, Dahe Q, Plattner G-K, *et al*. **2013**. Technical summary. In: *Climate Change 2013: The Physical Science Basis. Contribution of Working Group I to the Fifth Assessment Report of the Intergovernmental Panel on Climate Change*, edited by **Stocker TF, Qin D, Plattner G-K, Tignor M, Allen SK, Boschung J, Nauels A, Xia Y, Bex V, Midgley PM**. Cambridge University Press: Cambridge, UK.

Strand Å, Foyer CH, Gustafsson P, Garderström P, Hurry V. **2003**. Altering flux through the sucrose biosynthesis pathway in transgenic *Arabidopsis thaliana* modifies photosynthetic acclimation at low temperatures and the development of freezing tolerance. *Plant, Cell & Environment* **26**, 523–535.

Strand DD, Fisher N, Kramer DM. **2017**. The higher plant plastid NAD(P)H dehydrogenase-like complex (NDH) is a high efficiency proton pump that increase ATP production by cyclic electron flow. *Journal of Biological Chemistry* **292**, 11850–11860.

Sweetlove LJ, Beard KFM, Nunes-Nesi A, Fernie AR, Ratcliffe RG. **2010**. Not just a circle: flux modes in the plant TCA cycle. *Trends in Plant Science* **15**, 462-470.

Swetnam TW, Wickman BE, Paul HG, Baisan CH. **1995**. Historical patterns of western spruce budworm and Douglas fir tussock moth outbreaks in the Northern Blue Mountains, Oregon, since A.D. 1700. *Res. Pap. PNW-RP-484*. USDA Pac. Northwest. Res. Stn. 27 pp.

Tanja S, Berninger F, Vesala T, *et al*. 2003. Air temperature triggers the recovery of evergreen boreal forest photosynthesis in spring. *Global Change Biology* **9**, 1410–1426.

Temme AA, Liu JC, Cornwell WK, Cornelissen JHC, Aerts R. **2015**. Winners always win: growth of a wide range of plant species from low to future high CO_2. *Ecology & Evolution* **5**, 4949–4961.

Thornber JP. **1975**. Chlorophyll-proteins: light-harvesting and reaction center components of plants. *Annual Review of Plant Physiology* **26**, 127–158.

Turetsky MR, Bond-Lamberty B, Euskirchen E, Talbot J, Frokling S, McGuire AD, Tuittila E-S. **2012**. The resilience and functional role of moss in boreal and arctic ecosystems. *New Phytologist* **196**, 49–67.

Turetsky MR, Crow SE, Evans RJ, Vitt DH, Wieder RK. **2008**. Trade-offs in resource allocation among moss species control decomposition in boreal peatlands. *Ecology* **96**, 1297–1305.

Turetsky MR, Wieder RK. **1999**. Boreal bog *Sphagnum* refixes soil-produced and respired $^{14}CO_2$. *Ecoscience* **6**, 587–591.

Vasil'ev S, Bruce D. **2004**. Optimization and evolution of light harvesting in photosynthesis: the role of antenna chlorophyll conserved between photosystem II and photosystem I. *The Plant Cell* **16**, 3059–3068.

Vinyard DJ, Ananyev GM, Dismukes GC. **2013**. Photosystem II: the reaction center of oxygenic photosynthesis. *Annual Review of Biochemistry* **82**, 577–606.

Wager HG. **1941**. On the respiration and carbon assimilation rates of some arctic plants as related to temperature. *New Phytologist* **40**, 1–19.

Walker DA, Herold A. **1977**. Can the chloroplast support photosynthesis unaided? *Plant & Cell Physiology* **Special Issue**, 1–7.

Wang C, Yamamoto H, Shikanai T. **2015**. Role of cyclic electron transport around photosystem I in regulating proton motive force. *Biochimica et Biophysica Acta – Bioenergetics* **1847**, 931–938.

Wang YP, Jarvis PG. **1988**. Mea leaf angles for the ellipsoidal inclination angle distribution. *Agricultural & Forest Meteorology* **49**, 173–176.

Wang YP, Jarvis PG. **1990a**. Description and validation of an array model — MAESTRO. *Agricultural & Forest Meteorology* **51**, 257–280.

Wang YP, Jarvis PG. **1990b**. Influence of crown structural properties on PAR absorption, photosynthesis, and transpiration in Sitka spruce: application of a model (MAESTRO). *Tree Physiology* **7**, 297–316.

Way DA, Montgomery RA. **2015**. Photoperiod constraints on tree phenology, performance and migration in a warming world. *Plant, Cell & Environment* **38**, 1725–1736.

Way DA, Oren R. **2010**. Differential responses to changes in growth temperature between trees from different functional groups and biomes: a review and synthesis of data. *Tree Physiology* **30**, 669–688.

Way DA, Yamori W. **2014**. Thermal acclimation of photosynthesis: on the importance of adjusting our definitions and accounting for thermal acclimation of respiration. *Photosynthesis Research* **119**, 89–100.

Wei X, Su X, Cao P, Liu X, Chang W, Zhang X, Liu Z. **2016**. Structure of spinach photosystem II-LHCII supercomplex at 3.2 Å resolution. *Nature* **534**, 69–74.

Weiss A, Norman JM. **1985**. Partitioning solar radiation into direct and diffuse, visible and near-infrared components. *Agricultural & Forest Meteorology* **34**, 205–213.

Weissbach A, Horecker BL, Hurwitz J. **1956**. The enzymatic formation of phosphoglyceric acid from ribulose diphosphate and carbon dioxide. *The Journal of Biological Chemistry* **218**, 795–810.

Welp LR, Randerson JT, Liu HP. **2007**. The sensitivity of carbon fluxes to spring warming and summer drought depends on plant functional type in boreal forest ecosystems. *Agricultural and Forest Meteorology* **147**, 172–185.

Wenzel S, Cox PM, Eyring V, Friedlingstein P. **2016**. Projected land photosynthesis constrained by changes in the seasonal cycle of atmospheric CO_2. *Nature* **538**, 499–501.

Whittingham CP, Pritchard GG, Walker DA, Fogg GE, Nalewajko C. **1963**. The production of glycolate during photosynthesis in *Chlorella*. *Proceedings of the Royal Society of London. Series B, Biological Sciences* **157**, 366–382.

Willeit M, Ganopolski A, Feulner G. **2014**. Asymmetry and uncertainties in biogeophysical climate–vegetation feedback over a range of CO_2 forcings. *Biogeosciences* **11**, 17–32.

Wohlfahrt G, Gu L. **2015**. The many meanings of gross photosynthesis and their implication for photosynthesis research from leaf to globe. *Plant, Cell & Environment* **38**, 2500–2507.

Woodrow IE, Berry JA. **1988**. Ezymatic regulation of photosynthetic CO_2 fixation in C_3 plants. *Annual Review of Plant Physiology & Plant Molecular Biology* **39**, 533–594.

Wullschleger SD, Post WM, King AM. **1995**. On the potential for a CO_2 fertilization effect in forests: estimates of the biotic growth factor based on 58 controlled-exposure studies. In: *Biotic Feedbacks in the Global Climatic System: Will the Warming Feed the Warming?* Edited by **Woodwell GM, Mackenzie FT**. Oxford University Press: New York, NY.

Yamori W, Hikosaka K, Way DA. **2014**. Temperature response of photosynthesis in C_3, C_4, and CAM plants: temperature acclimation and temperature adaptation. *Photosynthesis Research* **119**, 101–117.

Zanetti G, Curti B. **1981**. Interactions between ferredoxin-$NADP^+$ reductase and ferredoxin at different reduction levels of the two proteins. *FEBS Letters* **129**, 201–204.

Chapter 2

2 Combined effects of rising CO_2 concentrations and temperature on boreal forests: growth, physiology and limitations

This review and meta-analysis was published in a similar form in *Botany* (Stinziano & Way, 2017, "Combined effects of rising [CO_2] and temperature on boreal forests: growth, physiology and limitations", *Botany* **92**(6), 425–436), and addresses **Question 1** (what do we know about boreal tree photosynthetic and growth responses to changes in temperature and CO_2) and **Hypothesis 1** (boreal trees are limited in growth and photosynthesis by low temperatures) from Chapter 1.

2.1 Introduction

Atmospheric CO_2 concentrations are projected to reach 730–1020 μmol mol^{-1} by the year 2100, mainly due to anthropogenic fossil fuel burning and land use change (Meehl *et al.*, 2007). This in turn will lead to a global mean temperature increase of 1.5 to 6 °C in that same period, but even greater warming at high latitudes, with increases of up to 8 °C in boreal regions (Serreze *et al.*, 2000; Meehl *et al.*, 2007). Significant climate warming has already occurred, with four of the five hottest decades in the last 150 years occurring in the last 60 years (Kaufman *et al.*, 2009). Not only will there be increases in temperature and CO_2 concentrations, but temperature variability and precipitation patterns are also expected to change in coming decades (Meehl *et al.* 2007). Precipitation may increase in parts of the boreal forest; however, it is likely to become more variable, such that there is a greater risk of both droughts and flooding (Meehl *et al.*, 2007). These environmental changes will alter the productivity of high latitude forests, but predicting how climate change will affect these systems requires both a deeper understanding of how key tree species will respond to rising temperature and CO_2 concentrations, and what factors might limit their ability to respond to climate change.

The boreal forest accounts for ~30% of the Earth's total forested area (FAO, 2001). Given the extent of this ecosystem, changes in forest carbon fluxes and productivity driven by climate change can in turn impact global carbon cycling and climate. A recent

study found increases in the seasonal amplitude of atmospheric CO_2 concentration, indicating a significant and unexpected shift in the global carbon cycle (Graven *et al.*, 2013). While the underlying cause of this shift is not known, the alterations in seasonal atmospheric CO_2 concentration patterns have been attributed to fluxes from high latitude forests, implying dramatic changes in the physiological and ecological functions that determine carbon cycling in boreal forest landscapes.

Current simulations suggest that increasing temperatures and CO_2 levels will stimulate net primary productivity (NPP) in high latitude forests (Qian *et al.*, 2010). However, interactions between environmental variables other than CO_2 and temperature will complicate our ability to predict boreal forest growth under future climates (Kurz *et al.*, 2008). In 2002, North American boreal forests switched from being a carbon sink (that absorbed more CO_2 than they emitted) to being a carbon source, owing to increased fire damage and insect outbreaks (Kurz *et al.*, 2008), both disturbances that are likely to become more common in the future. More frequent water stress, caused by changes in precipitation regimes and a warmer environment with a higher vapor pressure deficit, is also expected in coming decades. At the same time, one key environmental factor, photoperiod, will remain stable as the climate changes. Photoperiod could constrain the response of trees to a changing climate, as day length is an important cue for determining the beginning and end of the growing season (Körner & Basler, 2010). The purpose of this paper is, therefore, to review the potential impacts of elevated temperature and CO_2 concentrations on photosynthesis and growth in high latitude forests, and use meta-analytical techniques to provide a synthesis of experimental results of the effects of these climate change factors on boreal tree species.

2.2 Impact of elevated temperatures

2.2.1 Effects of warming on physiology

Warming is expected to impact both photosynthesis and respiration, thereby affecting boreal carbon fluxes. Elevated temperatures can impact photosynthesis positively (e.g., by stimulating enzyme function) and negatively (e.g., through heat lability of key enzymes or membrane stability) (Sage & Kubien, 2007; Yamori *et al.*, 2014). Because

photosynthesis is not linearly related to leaf temperature, the direct effect of warming on CO_2 assimilation rates depends on how close the tree already is to its thermal optimum: slight temperature increases will stimulate carbon gain if the tree is below the photosynthetic thermal optimum, while a greater degree of warming will inhibit CO_2 uptake by pushing the system into supraoptimal temperatures (Yamori *et al.*, 2014).

While short-term increases in temperature impact photosynthesis, trees acclimate to warmer growth environments, and this response includes acclimation of the photosynthetic apparatus (Berry & Björkman, 1980; Yamori *et al.*, 2014). Overall, photosynthetic capacity in trees is not altered by growth at elevated temperatures (Way & Oren, 2010): this means that maximum carboxylation rates of Rubisco (V_{cmax}), a key Calvin cycle enzyme, and maximum rates of electron transport (J_{max}) measured at 25 °C are similar in trees that develop at current or future temperatures. But because temperature directly affects enzyme kinetics, V_{cmax} and J_{max} assessed at the higher leaf temperatures predicted for the future are usually increased in warming experiments (Way & Oren, 2010). This potential stimulation of carbon fixation capacity with warming could enhance photosynthetic rates in forests that experience elevated temperatures, but will likely not occur equally in all species. In a recent meta-analysis, Way and Yamori (2014) found that evergreen woody species, like those that dominate boreal forests, showed the least ability to acclimate photosynthesis to high growth temperatures. Indeed, photosynthesis in many boreal species appears to be either unaffected by elevated temperatures or susceptible to heat inhibition under realistically warmer future temperatures. Light-saturated rates of photosynthesis in *Picea mariana* did not respond to warming in the field (Bronson & Gower, 2010), and neither net photosynthetic rates nor V_{cmax} were affected by an 8 °C increase in growth temperature in *Populus balsamifera* (Silim *et al.*, 2010). In *Populus deltoides* and *Populus balsamifera*, temperatures above 33 °C decreased net photosynthetic rates, driven by a decline in ATPase activity in Rubisco activase and a subsequent reduction in the Rubisco activation state (Hozain *et al.*, 2010). Heat inhibition of the activation state of Rubisco has also been implicated in reduced photosynthetic capacity in *Picea mariana* seedlings grown at elevated temperatures (Sage *et al.*, 2008; Way & Sage, 2008b).

Unlike photosynthesis, respiration rates increase exponentially with temperature, up to a threshold. This means that warming might be expected to increase rates of respiration in trees: unless CO_2 fixation rates keep pace, this response would lead to a decrease in net CO_2 assimilation rates (A_{net}) (Way & Yamori, 2014). However, as with photosynthesis, respiration can acclimate to elevated growth temperatures (Atkin *et al.*, 2005). Tjoelker *et al.* (1999) found that respiration measured at a common temperature was lower in trees grown at 30 °C (day) – 24 °C (night) than for those grown at lower temperatures (18 °C (day) – 12 °C (night), and 24 °C (day) – 18 °C (night)) in five North American boreal tree species (*Populus tremuloides, Betula papyrifera, Larix laricina, Pinus banksiana,* and *Picea mariana*). Leaves of *Populus balsamifera* also acclimate respiration to high temperatures (Silim *et al.*, 2010), and Bronson and Gower (2010) found acclimation of both foliar and stem respiration in *Picea mariana* to elevated growth temperatures. This reduction in respiration in warm-grown trees can offset reductions in photosynthesis: lower respiration rates in *Picea mariana* seedlings grown at high temperatures allowed them to achieve higher net CO_2 assimilation rates than seedlings grown at ambient temperature, but only for temperatures above 30 °C (Way & Sage, 2008a).

2.2.2 Effects of warming on phenology

The high latitude warming that has occurred in the last 60 years exhibits substantial temporal variability, with the most extreme warming during winter (Serreze *et al.*, 2000). Winter warming is an important factor in treeline advance (Harsch *et al.*, 2009), and the boreal treeline in Canada may be expected to advance significantly this century as the climate warms. This expectation is based on both a climate-envelope approach, as well as on movements of trees in past geological periods of warming. But a meta-analysis of changes in treelines since 1900 found that while they advanced in over half of the studies, the rest of the studies reported a stable treeline, with two studies even reporting a retreat (Harsch *et al.*, 2009).

So why might treelines not advance in response to rising temperatures in coming decades? In North America, the main treeline-forming species are *Picea glauca,* which dominates in the northwest (Walker *et al.*, 2012), and *Picea mariana,* which forms the treeline in the lower Mackenzie Valley and eastern Canada (Rowe, 1972; Burns &

Honkala, 1990). Cone production and seed germination rates in *Picea glauca* decrease toward the treeline, and reproductive capacity is thought to be limited by low temperatures, as higher summer temperatures increase reproductive output (Walker *et al.*, 2012). Warming is also expected to increase growth rates in *Picea glauca* (Danby & Hik, 2007), which may allow for greater reproductive output at the northern edge of the boreal forest. However, the northern limit of *Picea glauca* has yet to respond to warming, likely due to the difficulty of stand establishment at the forest–tundra ecotone (Walker *et al.*, 2012). Environmental conditions are harsher outside of the moderating influences of an existing forest, owing to increased wind shear, vapor pressure deficit s, and irradiance close to the ground. For *Picea mariana*, seeds produced from trees in the forest–tundra region had lower masses than seeds from forest regions and were unable to germinate (Black & Bliss, 1980), indicating that stand establishment may also be limited by reproductive ability. Germination in this species is inhibited by low temperatures (<15 °C), and only occurs in the field after burning, both traits that may prevent substantial increases in recruitment north of the treeline in coming decades (Black & Bliss, 1980). As well, *Picea mariana* germlings are sensitive to soil water potential (Black & Bliss, 1980), such that warmer conditions in the future may restrict recruitment above the treeline by increasing evapotranspiration and drying the soils. Taken together, the results from these two species indicate that boreal treelines may not advance as fast or as far as is often expected based purely on a climate-envelope approach.

2.2.3 Constraints on tree responses to warming

The same types of interactions that limit treeline movement can also constrain the ability of boreal tree species to respond to warming *in situ*. In particular, constraints imposed by photoperiod and water availability are likely to be two of the biggest limitations to increases in carbon uptake and productivity in northern forests in response to warming.

The cues used by trees in northern latitudes to sense seasonality and regulate the length of the growing season include both temperature and day length. For example, the timing of spring bud burst in trees reflects a composite of interacting factors: seasonal temperatures, photoperiod, temperature by photoperiod interactions, and a genotype-dependent response to the environment (Hänninen & Tanino, 2011; Way, 2011; Cooke *et*

al., 2012). Thus, while climate change can lead to earlier spring growth and delayed fall senescence/dormancy where temperature is the dominant cue, species that rely on photoperiod to regulate the growing season may show little change in their growing season length under warming.

Which species are most likely to be constrained in their response to warming by photoperiod? In a recent study, Basler and Körner (2012) investigated the effects of different photoperiod treatments on dormancy release in 14 tree species. In late-successional species, including *Picea abies* and *Abies alba*, short photoperiods delayed bud burst, implying that the ability to increase the growing season length under a warmer climate will be limited by day length cues. In contrast, the bud burst of early-successional tree species (such as *Larix decidua*) was not photoperiod-limited (Basler & Körner, 2012). It is thus possible that photoperiod may constrain phenological responses to rising temperatures in dominant late-successional coniferous species to a greater extent than in the deciduous species that tend to appear early in succession.

While day length cues are likely to limit the duration of leaf presence in the canopy, they can also regulate the physiological activity of those leaves. In temperate, deciduous trees, seasonal variation in photosynthetic capacity is tightly correlated with photoperiod, more so than with changes in temperature (Bauerle *et al.*, 2012). This means that even though deciduous leaves may remain green later into the autumn in a warmer climate, those leaves have lost most of their ability to fix CO_2 under the short photoperiods that occur late in the season. This may explain recent reports of asymmetric responses of northern forests to warming in spring versus autumn (Barichivich *et al.*, 2013). The photosynthetic activity of high latitude forests is closely coupled to temperature, such that warming over the last 60 years has allowed photosynthetic activity to occur about 6 days earlier in the spring. However, in the autumn, the photosynthetically active season is only growing at half the pace at which thermal limitations to growth are being lifted by climate warming (Barichivich *et al.*, 2013), which may indicate that photoperiodic constraints are limiting CO_2 uptake in boreal forests late in the year.

Overall, there are few studies looking at the interaction of day length and temperature on growing season length in trees, and none to my knowledge investigating this in a boreal species. I put forward four possible scenarios regarding this interaction. (i) No temperature stimulation, no photoperiodic constraints (Fig. 2.1a): in this scenario, net carbon uptake rates are not enhanced by warming; however, the growing season is lengthened, leading to a total increase in carbon fixation over the year. (ii) Temperature stimulation, no photoperiodic constraints (Fig. 2.1b): in this "best case" situation, net carbon uptake of northern forest species will increase, owing to both a longer growing season and higher net photosynthetic rates. (iii) Temperature inhibition, photoperiodic constraints (Fig. 2.1c): in this "worst case" scenario, net carbon fixation is reduced by warming and the current growing season length is maintained through photoperiod constraints, resulting in a net reduction in annual forest carbon uptake. (iv) Temperature by photoperiod interactions lead to asymmetric effects (Fig. 2.1d): in this scenario, there is an advance in the start of the growing season, as has already been observed (Beaubien & Hamann, 2011; Barichivich *et al.*, 2013), but in the autumn, photoperiod constrains leaf retention or physiological activity, such that the end of the growing season is relatively unresponsive to warming (Fig. 2.1d). This last scenario is consistent with the response of temperate trees (Bauerle *et al.*, 2012).

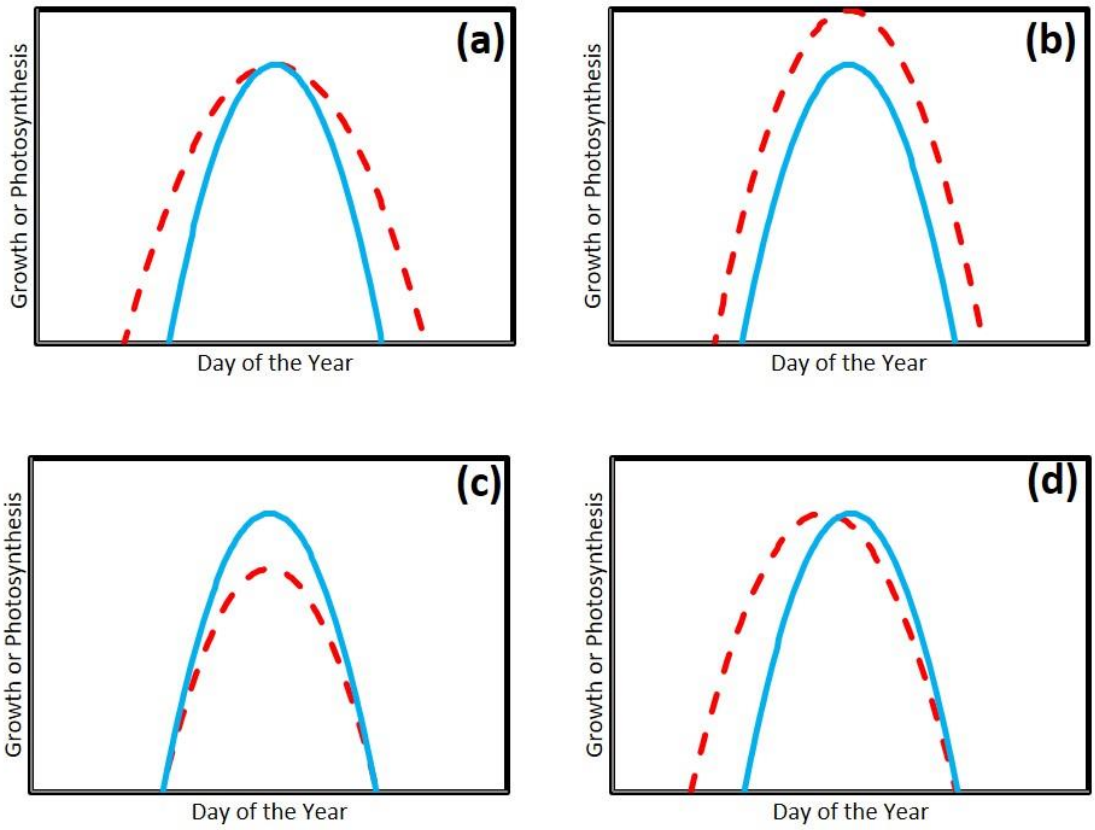

Figure 2.1. Possible responses of boreal tree function to warming and increases in atmospheric CO_2 concentration. Broken lines (red, online only) indicate a warming scenario; solid lines (blue, online only) indicate the current ambient conditions. (a) Climate change may extend growing season length in both the spring and autumn, with no effect on tree performance, leading to enhanced annual productivity. (b) Climate change may stimulate tree performance and extend the growing season length, leading to a more dramatic increase in annual productivity. (c) Photoperiod may constrain the length of the growing season, and climate change may inhibit photosynthesis or growth, leading to a net decline in annual productivity. (d) Climate change may advance the growing season in spring, but there may be no response of physiological activity in the autumn, owing to photoperiodic constraints.

In boreal forests, there could be more than a decoupling of earlier spring onsets of the growing season with later autumnal ends to the growing season. Earlier springs are correlated with declines in midsummer productivity in boreal forests, likely due to greater evapotranspiration and associated water deficits when spring arrives early (Buermann *et al.*, 2013). Thus, we may expect to see a shift in the growing season towards earlier dates in these forests (Fig. 2.1d), but an overall suppression of annual productivity due to greater drought stress (Buermann *et al.*, 2013), although warmer springs can also enhance boreal tree growth (Wilmking *et al.*, 2004). Plant water demand is greater at high temperatures: a linear rise in air temperature exponentially increases the vapor pressure deficit, greatly enhancing the driving force for transpirational water loss. If water becomes more limiting in a warmer climate, then lower stomatal conductance may limit CO_2 uptake, potentially offsetting any temperature-related enhancements of photosynthetic rates. For example, in Alaskan *Picea glauca*, late 20th century drought stress has led to a negative correlation between high temperatures and radial tree ring width, which implies a reduction in carbon uptake for *Picea glauca* forests as the climate warms and dries (Barber *et al.*, 2000); higher summer temperatures are also associated with growth declines in *Picea glauca* (Wilmking *et al.*, 2004). High temperatures combined with water stress can increase the ratio of day respiration to photosynthesis, which could reduce net carbon uptake in a warmer and drier climate (Centritto *et al.*, 2011). Transpiration is also important for leaf thermoregulation through latent heat loss: under the condition of water stress, low stomatal conductance limits not only the ability to fix CO_2, but the ability to cool the leaf as well (Ainsworth & Long, 2005). In *Populus fremontii*, water stress imposed stomatal limitations on photosynthesis, but also exacerbated the negative effects of high temperatures on photosynthesis, causing heat stress to occur at air temperatures 10 °C cooler than in trees with ample water (Tozzi *et al.*, 2013). However, not all heat × drought interactions are negative: in *Picea mariana*, exposure to elevated temperatures reduced the severity of drought-induced damage to the photosynthetic apparatus, potentially due to similar acclimation mechanisms between water and heat stresses (Way *et al.*, 2013a).

While there is reason to believe that a higher vapor pressure deficit in a warmer world will be the dominant driver of increases in transpiration, temperature itself can affect

water loss in boreal tree species. Higher temperatures increased canopy transpiration in *Picea mariana* even when vapor pressure deficit was held constant (Van Herk *et al.*, 2011); saplings of this same species have higher drought-induced mortality when grown at elevated growth temperatures than at current temperature regimes (Balducci *et al.*, 2013). As well, Way *et al.* (2013b) showed that hydraulic traits of *Populus tremuloides* were affected by growth temperature, such that seedlings that developed at warmer conditions had higher hydraulic conductance and thus the ability to transport (and lose) water more quickly through their roots and leaves. The unexpected flip side of increasing drought is the possibility of too much water: warmer temperatures are thawing permafrost sites in northern regions, which can lead to forest loss due to waterlogging (Baltzer *et al.*, 2014). Given the uncertainty in future precipitation patterns, and the recent evidence that warmer years are already decreasing productivity in northern forests via increased water stress (Buermann *et al.*, 2013), it would be dangerous to assume that rising temperatures will benefit these ecosystems.

2.3 Impact of elevated CO_2 concentration

2.3.1 Effects of CO_2 on physiology

Increasing atmospheric CO_2 concentration has a strong impact on tree physiology. Under current ambient CO_2 concentrations, photosynthesis is limited by Rubisco carboxylation capacity, such that greater CO_2 substrate availability increases photosynthetic rates (Bernacchi *et al.*, 2001; Sage & Kubien, 2007) and plant productivity. It is therefore unsurprising that studies show that elevated CO_2 concentration generally stimulates photosynthesis in boreal species. For example, elevated CO_2 concentration increased the leaf area index and operating efficiency of photosystem II of *Populus tremuloides* (McGrath *et al.*, 2010), while in a study comparing five boreal species, Tjoelker *et al.*, (1998b) found that photosynthesis was stimulated more strongly by elevated CO_2 concentration in slow-growing species such as *Picea mariana, Pinus banksiana,* and *Larix laricina* than in rapidly growing species such as *Populus tremuloides* and *Betula papyrifera*. These differences in growth response were due to a strong initial, transient increase in growth in the broadleaf species that declined through time, while increased growth rates in response to elevated CO_2 concentration in the conifers were maintained

(Tjoelker *et al.*, 1998b). Given that this suite of species dominates the North American boreal forest, the results suggest that the relative dominance of each species may change as CO_2 concentrations increase.

In response to elevated CO_2 concentration, trees often show increased A_{net} (when measured at growth CO_2 concentrations), but a down-regulation of photosynthesis indicated by declines in both V_{cmax} and J_{max} (Medlyn *et al.*, 1999). This photosynthetic down-regulation is common in studies of high CO_2 concentrations: the enhanced efficiency of photosynthesis achieved through greater CO_2 substrate availability increases sugar concentrations, which instigates a negative feedback to suppress Rubisco expression (Gunderson & Wullschleger, 1994; Moore *et al.*, 1999). As Rubisco operates more efficiently at high CO_2 concentrations, the nitrogen use efficiency (NUE, the amount of carbon fixed per unit leaf nitrogen) of the plant is increased; the lower Rubisco concentration also returns the photosynthetic rate towards the pre-high CO_2 concentration carbon fixation rate and helps rebalance carbohydrate supply with demand. Declines in V_{cmax} and J_{max} at elevated CO_2 concentrations increased with needle age in boreal species (Medlyn *et al.*, 1999), an effect that has been confirmed in *Pinus sylvestris* (Jach & Ceulemans, 2000), *Picea abies* (Urban *et al.*, 2012), and *Pinus taeda* (Crous *et al.*, 2008). These data suggest that net CO_2 uptake rates in northern forests may be initially stimulated by a high CO_2 atmosphere, but that the effect will likely decline over time. Furthermore, elevated CO_2 concentration leads to an increase in light use efficiency (the ability of a plant to use light to fix CO_2) in *Pinus taeda* (Kellomäki & Wang, 1997) which contributes, along with higher leaf CO_2 concentrations, to the stimulation of net CO_2 assimilation despite downregulation of V_{cmax} and J_{max}. Even if photosynthetic rates are not strongly stimulated by rising CO_2 concentrations in the long run, if high CO_2 concentration leads to a longer growing season, owing to delayed autumn leaf senescence (as seen in *Populus*; Taylor *et al.*, 2008), this may still increase forest productivity in these strongly seasonal forests.

However, it is unclear from these studies whether enhancements of leaf-level photosynthesis will scale reliably to the ecosystem level. This is hard to address without large-scale experiments in boreal forests, but there are some data we can use to

extrapolate potential responses. Rising atmospheric CO_2 concentrations over a 50-year timespan increased growth rates by ~50% in natural stands of *Populus tremuloides* (Cole *et al.*, 2010). On a more experimental level, free-air CO_2 enrichment sites in temperate forests show that elevated CO_2 concentration (~550 μmol mol^{-1}) increases net primary productivity (NPP) by almost 25% (Norby *et al.*, 2005), suggesting a strong response to CO_2 fertilization in forest systems. However, temperate free air CO_2 enrichment results may not be representative of boreal forests. Hickler *et al.* (2008) could model realistic NPP changes in temperate free air CO_2 enrichment sites, but found only a 15% average enhancement of modeled NPP in boreal systems, much less than is expected for more equatorial regions. Results from eddy flux measurements also imply that elevated CO_2 concentration has increased the magnitude of net ecosystem exchange over time in temperate and boreal forest stands, primarily due to increased CO_2 uptake during the summer (Keenan *et al.*, 2013), but the boreal sites appear to show the weakest increase in net ecosystem exchange of the stands studied. Overall, the lack of field studies investigating the effects of high CO_2 concentrations on boreal species, and conifers in particular, leaves a gap in knowledge about the dominant components of high latitude forests. Work in other boreal forest systems has shown that applying an elevated CO_2 treatment alone to *Picea abies* in the field did not alter tree growth (Sigurdsson *et al.*, 2013). Taken together, these studies imply that rising CO_2 concentrations will have less of an effect on the productivity of high latitude forests than in other regions, although fast-growing species like poplars may be more responsive than evergreen conifers.

Aside from its direct effects on photosynthesis and growth, elevated CO_2 concentration enhances water use efficiency (the amount of CO_2 fixed per unit water lost), potentially increasing drought tolerance (Ainsworth & Long, 2005). Increases in water use efficiency are due to an increase in A_{net} and a decline in stomatal conductance in response to elevated CO_2, responses that are commonly reported in free air CO_2 enrichment experiments (Ainsworth & Long, 2005). Recently, data from ~15 years of eddy flux covariance at northern temperate and boreal sites indicated enhancements in water use efficiency, with increases in CO_2 over that time being the primary driving factor (Keenan *et al.*, 2013). There is thus good evidence that water use efficiency is increasing as CO_2 concentration increases, but this does not necessarily correlate with increased growth in

boreal tree species. A meta-analysis looking at changes in water use efficiency across biomes world-wide since 1960 found that while water use efficiency increased ~20% owing to increases in atmospheric CO_2 concentrations, tree growth (measured as annual ring width) did not (Peñuelas *et al.*, 2011); further, there were no differences between biomes in the growth response to elevated atmospheric CO_2 concentrations. A similar dendrochronological study showed that water use efficiency increased ~50% in *Quercus rubra, Acer rubrum, Picea mariana,* and *Pinus resinosa* since 1950, as atmospheric CO_2 concentrations increased (Silva *et al.*, 2010). But there was a concurrent net decline in basal area increment in these species, suggesting that other environmental variables are limiting the growth response of trees to CO_2 concentration.

2.3.2 Constraints on responses of boreal trees to high CO_2 concentrations

While the direct effects of rising CO_2 concentrations on photosynthetic physiology are usually positive, higher CO_2 concentration can also negatively impact the performance of high latitude tree species. One such effect is through changes in freeze tolerance. In treeline species, elevated CO_2 concentration increased freezing sensitivity in *Larix decidua*, although it had no such effect on the evergreen species *Pinus uncinata* and *Empetrum hermaphroditum* (Martin *et al.*, 2010). Elevated CO_2 concentration also increases freezing damage in other alpine species (Rixen *et al.*, 2012), possibly by increasing the ice nucleation temperature (Beerling *et al.*, 2001).

Although the expectation is that higher CO_2 concentrations will reduce water demand in forests by reducing stomatal conductance, the ability of trees to respond to elevated CO_2 concentration is often dependent on water availability. In a free air CO_2 enrichment study with *Pinus taeda*, interannual variations in aboveground NPP and fecundity were driven by water demand, and this effect was stronger in plots with elevated CO_2 concentrations than in stands with ambient CO_2 concentrations (Way *et al.*, 2010). The CO_2-induced growth stimulation of *Populus tremuloides* stands was also more pronounced when water availability was high, suggesting that drought may be an important limitation in growth responses to CO_2 concentration in high latitude forests (Cole *et al.*, 2010). And while elevated CO_2 concentrations may improve drought tolerance, extreme moisture stress

could be a different issue. During an intense summer drought at the Oak Ridge free air CO_2 enrichment site, canopy net CO_2 uptake in *Liquidambar styraciflua* declined faster in plots with elevated CO_2 concentrations than in plots with ambient CO_2 concentrations, and leaf drop was greater in stands with elevated CO_2 concentrations after the drought relative to the plots with ambient CO_2 concentrations (Warren *et al.*, 2011). These data suggest that elevated CO_2 concentrations could reduce tree resiliency to drought stress that co-occurs with heat events. While elevated CO_2 concentration reduces leaf-level stomatal conductance, canopy leaf area often increases, which can increase whole tree water loss, while the reduced transpiration rates can increase leaf temperatures and thereby exacerbate heat stress (Way, 2011). Given that more variable and extreme weather is projected for the future (Gao *et al.*, 2012), water availability will be a key factor in limiting how forests respond to rising atmospheric CO_2 concentrations in coming decades.

And it's not just water. Nutrient availability, in particular nitrogen, is a primary constraint on forest and ecosystem responses to CO_2 (Oren *et al.*, 2001; Reich *et al.*, 2006; Norby *et al.*, 2010). At the Oak Ridge free air CO_2 enrichment site, elevated CO_2 concentrations initially stimulated CO_2 uptake and NPP. However, soil nitrogen limitations did not lead to differences in NPP between plots with elevated or with ambient CO_2 concentrations after several years (Norby *et al.*, 2010). This effect is common in high CO_2 experiments, and is termed progressive nitrogen limitation (Luo *et al.*, 2004; Johnson, 2006). Increased biomass under high CO_2 concentrations requires more nitrogen, even accounting for increases in NUE, and initially available soil nitrogen becomes sequestered in tree biomass and less labile soil pools, limiting further nitrogen uptake. In a *Pinus taeda* free air CO_2 enrichment site, CO_2 enrichment stimulated annual nitrogen requirements by ~30% (Finzi *et al.*, 2002). While NPP was increased over the 4-year study period, the authors predicted (based on the increase in nitrogen requirements) that NPP would eventually decline in the CO_2-enriched plots (Finzi *et al.*, 2002). However, after 11 years of CO_2 enrichment, NPP was still higher in plots with high CO_2 concentrations compared with the ambient CO_2 concentration plots, although plot-level variation in NPP was strongly dependent on nutrient availability (McCarthy *et al.*, 2010; Way *et al.*, 2010). The results above suggest that a sustained response to elevated CO_2 concentrations requires

additional nitrogen inputs. Norby *et al.* (2010) hypothesized that evergreen forests might have a more prolonged increase in NPP under elevated CO_2 concentrations, owing to their lower nitrogen requirements compared with deciduous forests. But even in evergreen conifer species, the CO_2 concentration-dependent growth response and its interaction with nitrogen supply varies. Soil fertilization enhanced the positive growth response of *Pinus taeda* stands to CO_2 enrichment (Oren *et al.*, 2001), and the high CO_2 concentration-induced enhancement of growth in *Picea mariana* also increased with greater nitrogen supply (Li *et al.*, 2013). Lastly, in one of the only studies to examine the responses of a boreal conifer to high CO_2 concentrations *in situ*, growth was not stimulated at all under elevated CO_2 concentrations unless the trees were fertilized (Sigurdsson *et al.*, 2013), which corresponds well to the earlier suggestion that there may not be a response to CO_2 enrichment in nutritionally poor soils (Oren *et al.*, 2001).

2.4 Combined effects of elevated temperature and CO_2 concentration on boreal species: a meta-analysis

As I described in the preceding sections of this review, understanding how a combination of elevated CO_2 concentrations and temperature will alter boreal tree growth and performance is critical, since both environmental factors are changing simultaneously. To determine whether there are trends in the response of either photosynthetic traits or tree growth to future climate scenarios in boreal trees, I collected studies that imposed elevated CO_2 concentrations and/or elevated temperature regimes on these species. I conducted a meta-analysis using 58 studies involving 15 boreal tree species (number of studies in parentheses): *Abies alba* (1), *Betula papyrifera* (11), *Betula pendula* (6), *Larix laricina* (1), *Picea abies* (8), *Picea glauca* (4), *Picea mariana* (9), *Picea sitchensis* (4), *Pinus banksiana* (5), *Pinus contorta* (1), *Pinus sylvestris* (8), *Populus balsamifera* (1), *Populus tremuloides* (6), *Pseudotsuga menziesii* (8), and *Tsuga heterophylla* (1) (Table 2.1). Studies were selected using Google Scholar with the following criteria: (i) a boreal tree species; (ii) an experimental manipulation of elevated temperature and/or CO_2 concentrations; (iii) the study collected data on total biomass, net CO_2 assimilation rates (A_{net}) measured at the growth conditions, and/or photosynthetic capacity (V_{cmax}, and/or J_{max}). For growth chamber studies, the current ambient temperature or CO_2 treatment was

considered the control. For studies in which multiple temperatures were used, the average June day/night temperatures from the site nearest to the seed source was used as the control treatment (see Way & Oren, 2010); for field studies, the control temperature was the average day/night temperatures of the month during which data were collected. Data where growth temperature was reduced below this control temperature were included in the study to increase the range of temperature change and aid in visualizing the overall pattern of response to changing temperature. For studies that manipulated other variables (e.g., nutrients, water availability), only data from the well-watered, well-fertilized subset of treatments were used.

Owing to variation in growth temperatures between studies and variation in atmospheric CO_2 concentrations across studies over time (as CO_2 concentration continues to rise annually), all physiological parameters were analyzed against the respective change in temperature and CO_2 concentration (treatment – control values) from the study. The response ratio of the measured parameters (treatment/control) were calculated: a response ratio = 1 means there was no change in the parameter, <1 means that there was a decrease in the parameter in the high CO_2 concentration/temperature plants relative to the control, while >1 means that there was an increase in the parameter in trees grown at future climates compared with the control trees. Because there were few data on V_{cmax} and J_{max} from temperature × CO_2 concentration experiments, temperature terms were left out of the analysis.

Table 2.1. Summary of the studies used in the meta-analysis.

Species	Ontogenic Stage	Variable(s) Manipulated	Response(s) Measured	Treatment Location	Reference
Abies alba	Seedling	CO_2	Biomass	OTC	Hattenschwiler & Körner, 2000
Betula papyrifera	Seedling	CO_2	A_{net}, J_{max}, V_{cmax}	Greenhouse	Ambebe & Dang, 2009
	Seedling	CO_2	A_{net}, J_{max}, V_{cmax}	Greenhouse	Ambebe *et al.*, 2010
	Seedling	CO_2	A_{net}	Greenhouse	Cao *et al.*, 2007
	Seedling	CO_2	Biomass	Greenhouse	Cao *et al.*, 2008
	Mature	CO_2	A_{net}	Field	Riikonen *et al.*, 2008
	Seedling	CO_2, T	A_{net}, Biomass	Chamber	Tjoelker *et al.*, 1998a
	Seedling	CO_2	A_{net}, J_{max}, V_{cmax}	Greenhouse	Zhang & Dang, 2005
	Seedling	CO_2	A_{net}, J_{max}, V_{cmax}	Greenhouse	Zhang & Dang, 2006
	Seedling	CO_2, T	Biomass	Greenhouse	Zhang & Dang, 2007
	Seedling	CO_2	A_{net}, J_{max}, V_{cmax}	Greenhouse	Zhang & Dang, 2013
	Seedling	CO_2	A_{net}, J_{max}, V_{cmax}	Greenhouse	Zhang *et al.*, 2013
Betula pendula	Seedling	CO_2, T	A_{net}, Biomass	Chamber	Kellomäki & Wang, 2001
	Seedling	CO_2, T	Biomass	Chamber	Kuokkanen *et al.*, 2001
	Seedling	CO_2, T	Biomass	WTC	Lavola *et al.*, 2013
	Seedling	CO_2	A_{net}, Biomass	Chamber	Pettersson & McDonald, 1992
	Seedling	CO_2	J_{max}, V_{cmax}	OTC	Rey & Jarvis, 1998
	Seedling	CO_2	Biomass, J_{max}, V_{cmax}	OTC	Rey & Jarvis, 1997
Larix laricina	Seedling	CO_2, T	A_{net}, Biomass	Chamber	Tjoelker *et al.*, 1998a
Picea abies	Mature	CO_2, T	Biomass	WTC	Kostiainen *et al.*, 2009
	Seedling	CO_2	A_{net}, Biomass	Chamber	Lippert *et al.*, 1996
	Seedling	CO_2	Biomass	Chamber	Liu *et al.*, 2004
	Seedling	CO_2, T	A_{net}, Biomass	Chamber	Pumpanen *et al.*, 2012

	Mature	CO_2	A_{net}	Field	Roberntz, 2001
	Seedling	CO_2, T	Biomass	Chamber	Sallas *et al.*, 2003
	Mature	CO_2	A_{net}	OTC	Špunda *et al.*, 2005
	Seedling	CO_2	J_{max}, V_{cmax}	Field	Urban *et al.*, 2012
Picea glauca	Seedling	CO_2	A_{net}, J_{max}, V_{cmax}	Greenhouse	Dang *et al.*, 2008
	Seedling	CO_2	Biomass	Greenhouse	Marfo & Dang, 2009
	Seedling	CO_2	Biomass	Chamber	Yakimchuk & Hoddinott, 1994
	Seedling	CO_2, T	Biomass	Greenhouse	Zhang & Dang, 2007
Picea mariana	Mature	T	A_{net}	Field	Bronson & Gower, 2010
	Seedling	CO_2	A_{net}, Biomass	Chamber	Johnsen, 1993
	Seedling	CO_2	A_{net}, Biomass	Greenhouse	Johnsen & Seiler, 1996
	Seedling	CO_2	Biomass	Greenhouse	Li *et al.*, 2013
	Seedling	CO_2	Biomass	Greenhouse	Marfo & Dang, 2009
	Seedling	CO_2, T	A_{net}, Biomass	Chamber	Tjoelker *et al.*, 1998a
	Seedling	T	Biomass	Greenhouse	Way & Sage, 2008b
	Seedling	CO_2	Biomass	Chamber	Yakimchuk & Hoddinott, 1994
	Seedling	CO_2, T	Biomass	Greenhouse	Zhang & Dang, 2007
Picea sitchensis	Sapling	CO_2	A_{net}, J_{max}, V_{cmax}	OTC	Centritto & Jarvis, 1999
	Seedling	CO_2	Biomass, J_{max}, V_{cmax}	OTC	Murray *et al.*, 2000
	Seedling	CO_2	Biomass	Greenhouse	Townend, 1995
	Sapling	CO_2	Biomass	OTC	Centritto *et al.*, 1999
Pinus banksiana	Seedling	T	Biomass	Chamber	Cantin *et al.*, 1997
	Seedling	CO_2, T	A_{net}, Biomass	Chamber	Tjoelker *et al.*, 1998a
	Seedling	CO_2	Biomass	Chamber	Yakimchuk & Hoddinott, 1994
	Seedling	CO_2	A_{net}, J_{max}, V_{cmax}	Greenhouse	Zhang & Dang, 2005
	Seedling	CO_2, T	Biomass	Greenhouse	Zhang & Dang, 2007
Pinus contorta	Seedling	CO_2	Biomass, V_{cmax}	Chamber	Higginbotham *et al.*, 1985

Pinus sylvestris	Seedling	CO_2	Biomass	OTC	Hattenschwiler & Körner, 2000
	Seedling	CO_2	Biomass	OTC	Jach *et al.*, 2000
	Mature	CO_2, T	A_{net}, J_{max}, V_{cmax}	Field	Kellomäki & Wang, 1996
	Seedling	CO_2	Biomass	Chamber	Perez-Soba *et al.*, 1995
	Seedling	T	A_{net}, Biomass	Chamber	Pumpanen *et al.*, 2012
	Seedling	CO_2, T	Biomass	Chamber	Sallas *et al.*, 2003
	Seedling	CO_2	Biomass	OTC	Utriainen *et al.*, 2000
	Sapling	CO_2	J_{max}, V_{cmax}	OTC	Wang *et al.*, 1996
Populus balsamifera	Seedling	T	A_{net}	Greenhouse	Silim *et al.*, 2010
Populus tremuloides	Mature	CO_2	A_{net}	Field	Kets *et al.*, 2010
	Seedling	CO_2	A_{net}, Biomass	Greenhouse	Liu *et al.*, 2006
	Mature	CO_2	A_{net}	Field	Riikonen *et al.*, 2008
	Seedling	CO_2	A_{net}	Chamber	Sharkey *et al.*, 1991
	Seedling	CO_2, T	A_{net}, Biomass	Chamber	Tjoelker *et al.*, 1998a
	Seedling	CO_2	Biomass	OTC	Zak *et al.*, 2000
Pseudotsuga menziesii	Seedling	T	A_{net}	Chamber	Brix, 1967
	Seedling	T	Biomass	Chamber	Brix, 1971
	Seedling	CO_2	A_{net}, Biomass	Chamber	Hollinger, 1987
	Seedling	CO_2, T	A_{net}	Mesocosm	Lewis *et al.*, 1999
	Seedling	CO_2, T	Biomass	Field	Olszyk *et al.*, 2003
	Seedling	CO_2, T	Biomass	Field	Olszyk *et al.*, 2005
	Seedling	T	Biomass	Chamber	Sorenson & Ferrell, 1973
	Seedling	CO_2, T	A_{net}	Mesocosm	Tingey *et al.*, 2007
Tsuga heterophylla	Seedling	T	Biomass	Chamber	Brix, 1971

Note: Studies are grouped by species used and may appear more than once. T, temperature; A_{net}, net CO_2 assimilation rate; J_{max}, maximum rate of electron transport; V_{cmax}, maximum rate of Rubisco carboxylation; OTC, open top chamber; WTC, whole tree chamber.

Data were analyzed using multiple regressions with R (version 2.13.0, R Development Core Team). Linear models were run on measured parameters using the following predictor variables (where applicable): evergreen or deciduous leaf form; broad-leaf or needle growth form; chamber type (open-top chamber, whole tree chamber, greenhouse, growth chamber, open field); life stage (seedling, sapling, mature); species; day temperature change; night temperature change; and CO_2 concentration change. Candidate models were first constructed using the leaps package in R to select the best additive model containing numerical predictors with the lowest Bayesian information criterion (BIC) (Quinn & Keough, 2002); BIC was chosen over Akaike's information criterion (AIC) because BIC is more conservative and penalizes the complexity (i.e., number of terms) in a model more intensely than does AIC. Next, all possible interaction terms and categorical explanatory variables were added to the model, which was then reduced stepwise by removing nonsignificant predictor variables and/or interaction terms until BIC was minimized. The top two models (those with the lowest BIC) are shown for comparison; the best model is that which has the lowest BIC and is significant. Three points (two for *Pinus banksiana*, one for *Pinus contorta*) had biomass response ratios >4 under elevated CO_2 concentration, and these points are not shown in the figures but were used in the analysis; these points were not significant in the best model.

The biomass response ratio was best explained by increases in day temperature and CO_2 concentration. Biomass responded positively to increases in day temperature ($P < 0.001$) and elevated CO_2 concentrations ($P < 0.0001$; Fig. 2.2; Table 2.2); however, the best model did not show an interaction between temperature and CO_2 concentrations and the general response of biomass gain in boreal species to rising temperatures does not therefore depend on CO_2 concentration. There was no significant difference between evergreen and deciduous growth forms or between species, suggesting that boreal trees may respond similarly to increasing temperature and CO_2 concentration, in contrast to the overall pattern seen in Way and Oren (2010). Given that there was no significant effect of chamber type or life stage, it therefore may be possible to generalize across life stages and studies in regard to CO_2 concentration × warming manipulations. The biomass of trees exposed to elevated CO_2 concentration was stimulated above the ambient CO_2-

treated tree biomass (Fig. 2.2). Much of the significant temperature response was driven by reduced biomass in trees grown at cooler than current growth temperatures; in fact, the median biomass was similar in trees grown at high growth temperatures and ambient CO_2 concentrations compared with the control temperature and CO_2-treated trees (Fig. 2.2). Viewing the data in Fig. 2.2 as a growth-response curve therefore implies that increased temperatures (of +1–5 °C) may increase future growth in these species at elevated CO_2 concentrations, but that the more extreme warming predicted for these regions may offset this effect, as median biomass is barely stimulated above control values when elevated CO_2 concentration is combined with the elevated temperatures of 5–10 °C (Fig. 2.2). However, more data are needed on extreme warming (>+6 °C) with elevated CO_2 concentrations to verify whether growth will be reduced at higher temperatures despite CO_2 fertilization.

The A_{net} of boreal species showed a different response to changes in climate factors than biomass. A_{net} was positively correlated with increases in CO_2 concentration ($P < 0.0001$), but unaffected by growth temperature changes (Fig. 2.3a; Table 2.2). As with biomass, there was no effect of evergreen/deciduous leaf type, species, chamber type, or life stage suggesting that A_{net} exhibits the same response for all boreal trees in these studies. While the effect of CO_2 concentration on A_{net} was strong, that of temperature was not significant, indicating that photosynthetic rates in boreal tree species were not affected by an increase in growth temperature, consistent with the discussion presented earlier in the paper (see section 2.2.1 Effects of warming on physiology).

There were not enough data on the responses of photosynthetic capacity (either V_{cmax} or J_{max}) to increased temperature for analysis, so all data were pooled into ambient or elevated CO_2 concentration categories. Growth CO_2 concentration significantly reduced V_{cmax} by ~10% on average (i.e., down-regulation of photosynthetic capacity; Fig. 2.3b; Table 2.2), while J_{max} was not significantly affected by either growth temperature or CO_2 concentration (Table 2.2). As my data show that A_{net} is stimulated by elevated CO_2 concentration, this down-regulation of V_{cmax} is generally more than compensated for by the direct effect of high CO_2 concentrations on photosynthesis. Chamber type, evergreen/deciduous growth form, species, and life stage were not significant

components of any of the models. Thus, the balance between V_{cmax} and J_{max} may decrease with elevated CO_2 concentrations in boreal tree species, but the temperature (and temperature × CO_2 concentration) response of V_{cmax} and J_{max} remains unclear.

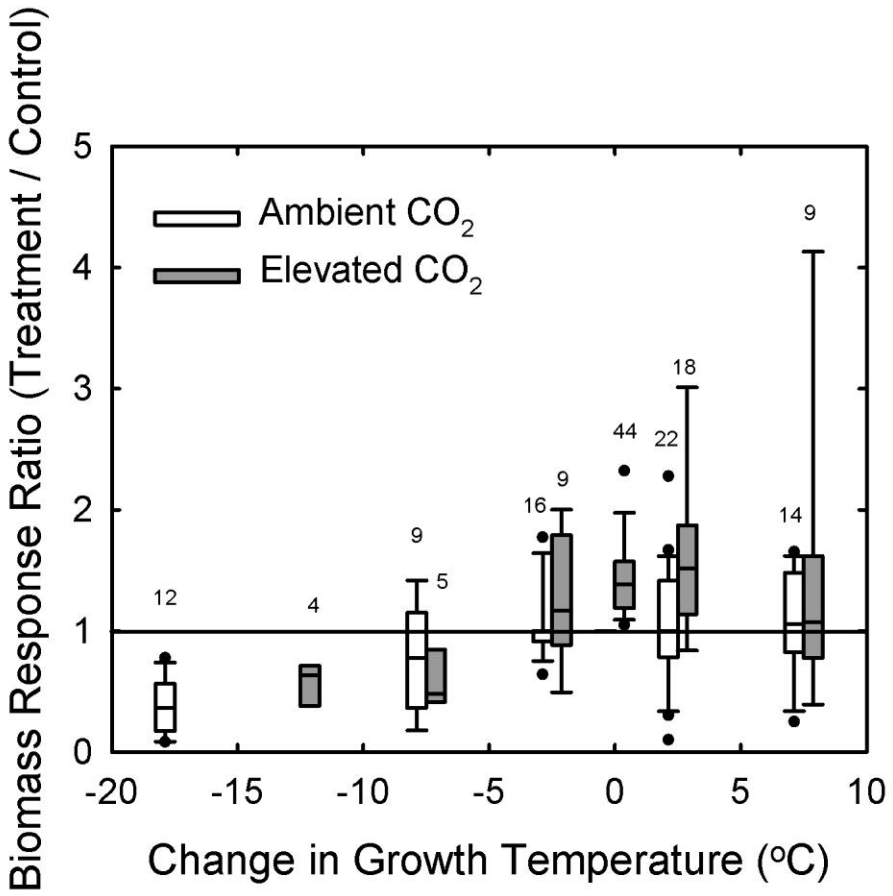

Figure 2.2. Effects of changes in growth temperature at either ambient (open boxes) or elevated CO_2 concentrations (filled boxes) on the biomass response ratio in boreal tree species. Average level of CO_2 concentration elevation was 316 ± 165 µmol mol^{-1} (mean ± SD). Horizontal line indicates biomass response ratio = 1; *N* = 203 measurements from 47 studies. Boxplots show temperature bins in 5 °C intervals, see text for details. Numbers associated with boxplots indicate sample size (*N* = 4–44, *N* = 46 for 0 °C temperature change and ambient CO_2 concentrations); boxplots indicate median, 25th, and 75th percentiles; whiskers indicate 10th and 90th percentiles.

Table 2.2. Summary of best general linear models for responses of biomass, net CO_2 assimilation rate (A_{net}), maximum Rubisco carboxylation rate (V_{cmax}), and maximum electron transport rate (J_{max}) to changes in growth temperature and CO_2 concentrations according to Bayesian Information Criterion (BIC).

		Model					
	F	*P*-value	BIC	T_{Day}	T_{Night}	CO_2	Species
Biomass	$F_{2,207}$ = 22.8	<0.0001	518	<0.001		<0.0001	
	$F_{3,206}$ = 16.0	<0.0001	521	<0.0005	0.151	<0.0001	
A_{net}	$F_{1,129}$ = 50.6	<0.0001	-9.27			<0.0001	
	$F_{2,128}$ = 25.3	<0.0001	-4.59	0.661		<0.0001	
V_{cmax}	$F_{1,32}$ = 20.1	<0.0001	-47.0			<0.0001	
	$F_{9,24}$ = 4.66	<0.005	-36.6			<0.0001	<0.05[a]
J_{max}	$F_{1,29}$ = 0.59	0.4496	-24.0			0.45	
	$F_{7,23}$ = 2.34	0.0582	-19.5				<0.05[a]

Note: other parameters used in construction of the models were chamber type (open top chamber, whole tree chamber, greenhouse, growth chamber, open field), life stage (seedling, sapling, mature), evergreen/deciduous, broadleaf/needleleaf; these parameters did not appear in the best models. T_{Day}, day temperature warming; T_{Night}, night temperature warming; CO_2, CO_2 elevation. [a]*Picea glauca* and *Pinus banksiana* both had significant effects in the model, such that they responded differently than the other species.

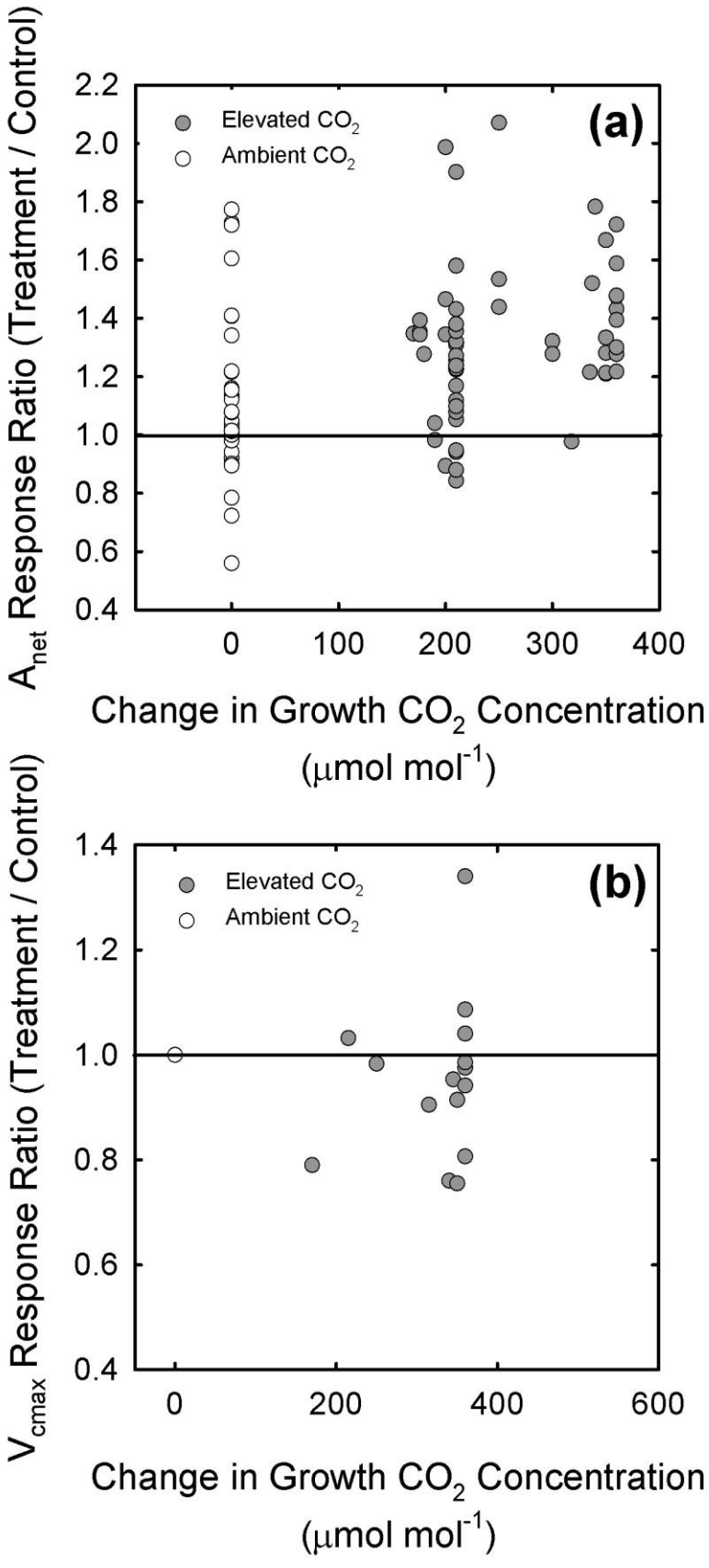
(a)
Elevated CO2
Ambient CO2
Anet Response Ratio (Treatment / Control)
Change in Growth CO2 Concentration
(μmol mol-1)
(b)
Elevated CO2
Ambient CO2
Vcmax Response Ratio (Treatment / Control)
Change in Growth CO2 Concentration
(μmol mol-1)

Figure 2.3. (a) The effect of elevated CO_2 concentrations on the response ratio of net CO_2 assimilation rates (A_{net}) measured at growth levels of temperature and CO_2 concentration; *N* = 131 measurements from 29 studies. (b) The effect of elevated CO_2 concentrations (excluding a CO_2 elevation of 1670 µmol mol^{-1}) on the response ratios for photosynthetic capacity (V_{cmax}) measured at growth temperature; *N* = 34 from 15 studies. Filled circles represent elevated CO_2 concentrations; open circles represent ambient CO_2 concentrations. The solid horizontal lines indicate response ratio = 1.

2.5 Implications for boreal forests

As the climate warms, the boreal treeline is expected to advance northward (Grace *et al.*, 2002) and forest NPP is projected to increase (Qian *et al.*, 2010). My data suggest that boreal tree species do have the potential for positive physiological and growth responses to moderate combined increases in temperature and CO_2 concentrations. However, forest responses to these climate factors may not be realistically predicted from these results if tree responses to rising CO_2 and temperature are limited by water stress, nutrient availability, or photoperiod in the field. As discussed above, there is a positive correlation between warmer, earlier springs and drier growing seasons that can limit tree productivity (Buermann *et al.*, 2013). A study on drought-induced mortality in North American boreal forests found that mortality rates have increased 2–5% since 1963 (Peng *et al.*, 2011), reinforcing the message that water may be the primary limiting factor on forest productivity in the future. Recent evidence of asymmetry between positive spring growth responses and negative autumn growth responses to warming also point to the need to better understand the role of photoperiod in these forests. Lastly, the strong nutrient limitations seen on growth responses to elevated CO_2 concentrations and temperature in *Picea abies* in whole-tree chambers indicate that small-scale studies are unlikely to capture the true environmental dynamics controlling growth in the field (Ryan, 2013; Sigurdsson *et al.*, 2013). Low nutrient availability strongly limited photosynthesis and growth in high latitude *Picea glauca* as well: fertilizer addition enhanced growth at the treeline, but not in sites with warmer soils, likely due to reduced rates of nitrogen fixation by soil microbes in cold soils (McNown & Sullivan, 2013).

The likelihood of negative responses to warming in the boreal is also borne out by remote sensing data and tree ring analyses. Widespread browning trends are evident in central boreal zones in North America, and greening is generally limited to the very northern edges of the ecosystem and is attributable to shrub expansion on the tundra (Goetz *et al.*, 2005; Verbyla, 2008; Beck *et al.*, 2011). Dendrochronology work shows that these browning trends are common in dominant spruce species and in the warmest regions of species' ranges, implying that elevated temperatures alone or warming-associated drying is responsible for tree declines (Lloyd & Bunn, 2007).

Understanding how key environmental limitations will affect boreal forests in coming decades is therefore a key to improving our ability to predict how northern forests will respond to climate change in coming decades. Most greenhouse and chamber experiments, like those analyzed here, provide ample water and nutrients, factors that are likely to limit photosynthetic and growth responses to warming and elevated CO_2 in natural forest systems. To fully address how boreal forests will respond to a changing climate will therefore require a combination of (i) multifactor experiments manipulating CO_2 concentrations and temperature along with nutrients and water supply; (ii) field experiments that address the role of CO_2 concentrations and rising temperatures on tree performance under natural conditions; and (iii) better linkages between researchers who work on these experiments with those studying larger scale processes, such as the eddy flux, remote sensing, and modeling communities, to better guide research questions.

2.6 References

(* Indicates a reference used in data analysis)

Ainsworth EA, Long SP. **2005**. What have we learned from 15 years of free-air CO_2 enrichment (FACE)? A meta-analytic review of the responses of photosynthesis, canopy properties and plant production to rising CO_2. *New Phytologist* **165**, 351–371.

***Ambebe TF, Dang Q-L**. **2009**. Low moisture availability inhibits the enhancing effect of increased soil temperature on net photosynthesis of white birch (*Betula papyrifera*) seedlings grown under ambient and elevated carbon dioxide concentrations. *Tree Physiology* **29**, 1341–1348.

***Ambebe TF, Dang Q-L, Li J**. **2010**. Low soil temperature inhibits the effect of high nutrient supply on photosynthetic response to elevated carbon dioxide concentration in white birch seedlings. *Tree Physiology* **30**, 234–243.

Atkin OK, Bruhn D, Hurry VM, Tjoelker MG. **2005**. The hot and the cold: unravelling the variable response of plant respiration to temperature. *Functional Ecology* **32**, 87–105.

Balducci L, Deslauriers A, Giovannelli A, Rossi S, Rathgeber CBK. **2013**. Effects of temperature and water deficit on cambial activity and woody ring features in *Picea mariana* saplings. *Tree Physiology* **33**, 1006–1017.

Baltzer JL, Veness T, Chasmer LE, Sniderhan AE, Quinton WL. **2014**. Forests on thawing permafrost: fragmentation, edge effects, and net forest loss. *Global Change Biology* **20**, 824–834.

Barber VA, Juday GP, Finney BP. **2000**. Reduced growth of Alaskan white spruce in the twentieth century from temperature-induced drought stress. *Nature* **405**, 668–673.

Barichivich J, Briffa KR, Myneni RB, Osborn TJ, Melvin TM, Ciais P, Piao S, Tucker C. **2013**. Large-scale variations in the vegetation growing season and annual cycle of atmospheric CO_2 at high northern latitudes from 1950 to 2011. *Global Change Biology* **19**, 3167–3183.

Basler D, Körner C. **2012**. Photoperiod sensitivity of bud burst in 14 temperate forest tree species. *Agricultural & Forest Meteorology* **165**, 73–81.

Bauerle WL, Oren R, Way DA, Qian SS, Stoy PC, Thornton PE, Bowden JD, Hoffman FM, Reynolds RF. **2012**. Photoperiodic regulation of the seasonal pattern of photosynthetic capacity and the implications for carbon cycling. *Proceedings of the National Academy of Sciences of the United States of America* **109**, 8612–8617.

Beaubien E, Hamann A. **2011**. Spring flowering response to climate change between 1936 and 2006 in Alberta, Canada. *Bioscience* **61**, 514–524.

Beck PS, Juday GP, Alix C, Barber V, Winslow SE, Sousa EE, Heiser P, Herriges JD, Goetz SJ. **2011**. Changes in forest productivity across Alaska consistent with biome shift. *Ecology Letters* **14**, 373–379.

Beerling DJ, Terry AC, Mitchell PL, Callaghan TV, Gwynn-Jones D, Lee JA. **2001**. Time to chill: effects of simulated global change on leaf ice nucleation temperatures of subarctic vegetation. *American Journal of Botany* **88**, 628–633.

Bernacchi CJ, Singsaas EL, Pimentel C, Portis AR Jr, Long SP. **2001**. Improved temperature response functions for models of Rubisco-limited photosynthesis. *Plant, Cell & Environment* **24**, 253–259.

Berry J, Björkman O. **1980**. Photosynthetic response and adaptation to temperature in higher plants. *Annual Review of Plant Physiology* **31**, 491–543.

Black RA, Bliss LC. **1980**. Reproductive ecology of *Picea mariana* (Mill.) BSP., at tree line near Inuvik, Northwest Territories, Canada. *Ecological Monographs* **50**, 331–354.

***Brix H**. **1967**. An analysis of dry matter production of Douglas-fir seedlings in relation to temperature and light intensity. *Canadian Journal of Botany* **45**, 2063–2072.

***Brix H**. **1971**. Growth response of western hemlock and Douglas-fir seedlings to temperature regimes during day and night. *Canadian Journal of Botany* **49**, 289–294.

***Bronson DR, Gower ST**. **2010**. Ecosystem warming does not affect photosynthesis or aboveground autotrophic respiration for boreal black spruce. *Tree Physiology* **30**, 441–449.

Bronson DR, Gower ST, Tanner M, Van Herk I. **2009**. Effect of ecosystem warming on boreal black spruce bud burst and shoot growth. *Global Change Biology* **15**, 1534–1543.

Buermann W, Bikash PR, Jung M, Burn DH, Reichstein M. **2013**. Earlier springs decrease peak summer productivity in North American boreal forests. *Environmental Research Letters* **8**, 024027.

Burns R, Honkala B. **1990**. Silvics of North America: 1. Conifers; 2. Hardwoods. *Agriculture Handbook 654*. U.S. Department of Agriculture, Forest Service: Washington, D.C.

***Cantin D, Tremblay MF, Lechowicz MJ, Potvin C**. **1997**. Effects of CO_2 enrichment, elevated temperature, and nitrogen availability on the growth and gas exchange of

different families of Jack pine seedlings. *Canadian Journal of Forest Research* **27**, 510–520.

***Cao B, Dang Q-L, Zhang S**. **2007**. Relationship between photosynthesis and leaf nitrogen concentration in ambient and elevated [CO_2] in white birch seedlings. *Tree Physiology* **27**, 891–899.

***Cao B, Dang Q-L, Yü X, Zhang S**. **2008**. Effects of [CO_2] and nitrogen on morphological and biomass traits of white birch (*Betula papyrifera*) seedlings. *Forest Ecology & Management* **254**, 217–224.

***Centritto M, Jarvis P**. **1999**. Long-term effects of elevated carbon dioxide concentration and provenance on four clones of Sitka spruce (*Picea sitchensis*). II. Photosynthetic capacity and nitrogen use efficiency. *Tree Physiology* **19**, 807–814.

***Centritto M, Lee H, Jarvis P**. **1999**. Long-term effects of elevated carbon dioxide concentration and provenance on four clones of Sitka spruce (*Picea sitchensis*). I. Plant growth, allocation and ontogeny. *Tree Physiology* **19**, 799–806.

Centritto M, Brilli F, Fodale R, Loreto F. **2011**. Different sensitivity of isoprene emission, respiration and photosynthesis to high growth temperature coupled with drought stress in black poplar (*Populus nigra*) saplings. *Tree Physiology* **31**, 275–286.

Cole CT, Anderson JE, Lindroth RL, Waller DM. **2010**. Rising concentrations of atmospheric CO_2 have increased growth in natural stands of quaking aspen (*Populus tremuloides*) *Global Change Biology* **16**, 2186–2197.

Cooke JEK, Eriksson ME, Junttila O. **2012**. The dynamic nature of bud dormancy in trees: environmental control and molecular mechanisms. *Plant, Cell & Environment* **35**, 1707–1728.

Crous KY, Walters MB, Ellsworth DS. **2008**. Elevated CO_2 concentration affects leaf photosynthesis–nitrogen relationships in *Pinus taeda* over nine years in FACE. *Tree Physiology* **28**, 607–614.

Danby RK, Hik DS. **2007**. Responses of white spruce (*Picea glauca*) to experimental warming at a subarctic alpine treeline. *Global Change Biology* **13**, 437–451.

***Dang Q-L, Maepea JM, Parker WH**. **2008**. Genetic variation of ecophysiological responses to CO_2 in *Picea glauca* seedlings. *Open Forest Science Journal* **1**, 68–79.

Finzi A, DeLucia E, Hamilton J, Schlesinger W, Richter D. **2002**. The nitrogen budget of a pine forest under free air CO_2 enrichment. *Oecologia* **132**, 567–578.

Food & Agricultural Organization of the United Nations (FAO). **2001**. State of the World's Forests. FAO: Rome, Italy.

Gao Y, Fu JS, Drake JB, Liu Y, Lamarque J-F. **2012**. Projected changes of extreme weather events in the eastern United States based on a high resolution climate modeling system. *Environmental Research Letters* **7**, 044025.

Goetz SJ, Bunn AG, Fiske GJ, Houghton RA. **2005**. Satellite-observed photosynthetic trends across boreal North America associated with climate and fire disturbance. *Proceedings of the National Academy of Sciences of the United States of America* **102**, 13521.

Grace J, Berninger F, Nagy L. **2002**. Impacts of climate change on the tree line. *Annals of Botany* **90**, 537–544.

Graven HD, Keeling RF, Piper SC, *et al*. **2013**. Enhanced seasonal exchange of CO_2 by northern ecosystems since 1960. *Science* **341**, 1085–1089.

Gunderson CA, Wullschleger SD. **1994**. Photosynthetic acclimation in trees to rising atmospheric CO_2: a broader perspective. *Photosynthesis Research* **39**, 369–388.

Hall M, Räntfors M, Slaney M, Linder S, Wallin G. **2009**. Carbon dioxide exchange of buds and developing shoots of boreal Norway spruce exposed to elevated or ambient CO_2 concentration and temperature in whole-tree chambers. *Tree Physiology* **29**, 467–481.

Hänninen H, Tanino K. **2011**. Tree seasonality in a warming climate. *Trends in Plant Science* **16**, 412–416.

Harsch MA, Hulme PE, McGlone MS, Duncan RP. **2009**. Are treelines advancing? A global meta-analysis of treeline response to climate warming. *Ecology Letters* **12**, 1040–1049.

***Hattenschwiler S, Körner C**. **2000**. Tree seedling responses to *in situ* CO_2-enrichment differ among species and depend on understorey light availability. *Global Change Biology* **6**, 213–226.

Hickler T, Smith B, Prentice IC, Mjöfors K, Miller P, Arneth A, Sykes MT. **2008**. CO_2 fertilization in temperate FACE experiments not representative of boreal and tropical forests. *Global Change Biology* **14**, 1531–1542.

***Higginbotham KO, Mayo JM, L'Hirondelle S, Krystofiak DK**. **1985**. Physiological ecology of lodgepole pine (*Pinus contorta*) in an enriched CO_2 environment. *Canadian Journal of Forest Research* **15**, 417–421.

***Hollinger DY**. **1987**. Gas exchange and dry matter allocation responses to elevation of atmospheric CO_2 concentration in seedlings of three tree species. *Tree Physiology* **3**, 193–202.

Hozain MI, Salvucci ME, Fokar M, Holaday AS. **2010**. The differential response of photosynthesis to high temperature for a boreal and temperate *Populus* species relates to differences in Rubisco activation and Rubisco activase properties. *Tree Physiology* **30**, 32–44.

Jach ME, Ceulemans R. **2000**. Effects of season, needle age and elevated atmospheric CO_2 on photosynthesis in Scots pine (*Pinus sylvestris*). *Tree Physiology* **20**, 145–157.

***Jach M, Laureysens I, Ceulemans R**. **2000**. Above- and below-ground production of young Scots pine (*Pinus sylvestris* L.) trees after three years of growth in the field under elevated CO_2. *Annals of Botany* **85**, 789–798.

***Johnsen KH**. **1993**. Growth and ecophysiological responses of black spruce seedlings to elevated CO_2 under varied water and nutrient additions. *Canadian Journal of Forest Research* **23**, 1033–1042.

***Johnsen KH, Seiler JR**. **1996**. Growth, shoot phenology and physiology of diverse seed sources of black spruce: I. Seedling responses to varied atmospheric CO_2 concentrations and photoperiods. *Tree Physiology* **16**, 367–373.

Johnson DW. **2006**. Progressive N limitation in forests: review and implications for long-term responses to elevated CO_2. *Ecology* **87**, 64–75.

Kaufman DS, Schneider DP, McKay NP, *et al*. 2009. Recent warming reverses long-term arctic cooling. *Science* **325**, 1236–1239.

Keenan TF, Hollinger DY, Bohrer G, Dragoni D, Munger JW, Schmid HP, Richardson AD. **2013**. Increase in forest water-use efficiency as atmospheric carbon dioxide concentrations rise. *Nature* **499**, 324–327.

***Kellomäki S, Wang KY**. **1996**. Photosynthetic responses to needle water potentials in Scots pine after a four-year exposure to elevated CO_2 and temperature. *Tree Physiology* **16**, 765–772.

Kellomäki S, Wang KY. **1997**. Effects of long-term CO_2 and temperature elevation on crown nitrogen distribution and daily photosynthetic performance of Scots pine. *Forest Ecology & Management* **99**, 309–326.

***Kellomäki S, Wang KY**. **2001**. Growth and resource use of birch seedlings under elevated carbon dioxide and temperature. *Annals of Botany* **87**, 669–682.

***Kets K, Darbah JNT, Sober A, Riikonen J, Sober J, Karnosky DF**. **2010**. Diurnal changes in photosynthetic parameters of *Populus tremuloides*, modulated by elevated concentrations of CO_2 and/or O_3 and daily climatic variation. *Environmental Pollution* **158**, 1000–1007.

Körner C, Basler D. **2010**. Phenology under global warming. *Science* **365**, 3247–3260.

***Kostiainen K, Kaakinen S, Saranpää P, Sigurdsson BD, Lundqvist S-O, Linder S, Vapaavuori E**. **2009**. Stem wood properties of mature Norway spruce after 3 years of continuous exposure to elevated [CO_2] and temperature. *Global Change Biology* **15**, 368–379.

***Kuokkanen K, Julkunen-Tiitto R, Keinänen M, Niemelä P, Tahvanainen J**. **2001**. The effect of elevated CO_2 and temperature on the secondary chemistry of *Betula pendula* seedlings. *Trees* **15**, 378–384.

Kurz WA, Stinson G, Rampley GJ, Dymond CC, Neilson ET. **2008**. Risk of natural disturbances makes future contribution of Canada's forests to the global carbon cycle highly uncertain. *Proceedings of the National Academy of Sciences of the United States of America* **105**, 1551–1555.

Kvaalen H, Johnsen O. **2008**. Timing of bud set in *Picea abies* is regulated by a memory of temperature during zygotic and somatic embryogenesis. *New Phytologist* **177**, 49–59.

***Lavola A, Nybakken L, Rousi M, Pusenius J, Petrelius M, Kellomäki S, Julkunen-Tiitto R**. **2013**. Combination treatment of elevated UVB radiation, CO_2 and temperature has little effect on silver birch (*Betula pendula*) growth and phytochemistry. *Physiologia Plantarum* **149**, 499–514.

***Lewis JD, Olszyk D, Tingey DT**. **1999**. Seasonal patterns of photosynthetic light response in Douglas-fir seedlings subjected to elevated atmospheric CO_2 and temperature. *Tree Physiology* **19**, 243–252.

***Li J, Dang Q-L, Man R, Marfo J**. **2013**. Elevated CO_2 alters N-growth relationship in spruce and causes unequal increases in N, P and K demands. *Forest Ecology & Management* **298**, 19–26.

***Lippert M, Haberle K-H, Steiner K, Payer H-D, Rehfuess K-E**. **1996**. Interactive effects of elevated CO_2 and O_3 on photosynthesis and biomass production of clonal 5-

year-old Norway spruce [*Picea abies* (L.) Karst.] under different nitrogen nutrition and irrigation treatments. *Trees* **10**, 382–392.

***Liu N, Dang Q-L, Parker WH**. **2006**. Genetic variation of *Populus tremuloides* in ecophysiological responses to CO_2 elevation. *Canadian Journal of Botany* **84**, 294–302.

***Liu X, Kozovits AR, Grams TEE, Blaschke H, Rennenberg H, Matyssek R**. **2004**. Competition modifies effects of enhanced ozone/carbon dioxide concentrations on carbohydrate and biomass accumulation in juvenile Norway spruce and European beech. *Tree Physiology* **24**, 1045–1055.

Lloyd AH, Bunn AG. **2007**. Responses of the circumpolar boreal forest to 20th century climate variability. *Environmental Research Letters* **2**, 045013.

Luo Y, Su B, Currie WS, *et al*. **2004**. Progressive nitrogen limitation of ecosystem responses to rising atmospheric CO_2. *Bioscience* **54**, 731–739.

***Marfo J, Dang Q-L**. **2009**. Interactive effects of carbon dioxide concentration and light on the morphological and biomass characteristics of black spruce and white spruce seedlings. *Botany* **87**, 67–77.

Martin M, Gavazov K, Körner C, Hättenschwiler S, Rixen C. **2010**. Reduced early growing season freezing resistance in alpine treeline plants under elevated atmospheric CO_2. *Global Change Biology* **16**, 1057–1070.

McCarthy HR, Oren R, Johnsen KH, Gallet-Budynek A, Pritchard SG, Cook CW, Ladeau SL, Jackson RB, Finzi AC. **2010**. Re-assessment of plant carbon dynamics at the Duke free-air CO_2 enrichment site: interactions of atmospheric [CO_2] with nitrogen and water availability over stand development. *New Phytologist* **185**, 514–528.

McGrath JM, Karnosky DF, Ainsworth EA. **2010**. Spring leaf flush in aspen (*Populus tremuloides*) clones is altered by long-term growth at elevated carbon dioxide and elevated ozone concentration. *Environmental Pollution* **158**, 1023–1028.

McNown RW, Sullivan PF. **2013**. Low photosynthesis of treeline white spruce is associated with limited soil nitrogen availability in the Western Brooks Range, Alaska. *Functional Ecology* **27**, 672–683.

Medlyn BE, Badeck F, Pury DGGDE, Barton CVM, Broadmeadow M, Ceulemans R. **1999**. Effects of elevated [CO_2] on photosynthesis in European forest species: a meta-analysis of model parameters. *Plant, Cell & Environment* **22**, 1475–1495.

Meehl G, Stocker T, Collins W, *et al*. **2007**. Global climate projections. In: *Climate Change 2007: The Physical Science Basis. Contribution of Working Group I to the Fourth Assessment Report of the Intergovernmental Panel on Climate Change*, edited by **Solomon S, Qin D, Manning M, Chen Z, Marquis M, Averyt KB, Tignor M, Miller HL**. Cambridge University Press: Cambridge, UK. pp. 747–845.

Moore BD, Cheng S-H, Sims D, Seemann JR. **1999**. The biochemical and molecular basis for photosynthetic acclimation to elevated atmospheric CO_2. *Plant, Cell & Environment* **22**, 567–582.

***Murray MB, Smith RI, Friend A, Jarvis PG**. **2000**. Effect of elevated [CO_2] and varying nutrient application rates on physiology and biomass accumulation of Sitka spruce (*Picea sitchensis*). *Tree Physiology* **20**, 421–434.

Norby RJ, DeLucia EH, Gielen B, *et al*. **2005**. Forest response to elevated CO_2 is conserved across a broad range of productivity. *Proceedings of the National Academy of Sciences of the United States of America* **102**, 18052–18056.

Norby RJ, Warren JM, Iversen CM, Medlyn BE, McMurtrie RE. **2010**. CO_2 enhancement of forest productivity constrained by limited nitrogen availability. *Proceedings of the National Academy of Sciences of the United States of America* **107**, 19368–19373.

***Olszyk DM, Johnson MG, Tingey DT, Rygiewicz PT, Wise C, Vaness E, Benson A, Storm MJ, King R**. **2003**. Whole-seedling biomass allocation, leaf area, and tissue

chemistry for Douglas-fir exposed to elevated CO_2 and temperature for 4 years. *Canadian Journal of Forest Research* **33**, 269–278.

***Olszyk D, Apple M, Gartner B, Spicer R, Wise C, Buckner E, Benson-Scott A, Tingey D**. **2005**. Xeromorphy increases in shoots of *Pseudotsuga menziesii* (Mirb.) Franco seedlings with exposure to elevated temperature but not elevated CO_2. *Trees* **19**, 552–563.

Oren R, Ellsworth DS, Johnsen KH, *et al*. **2001**. Soil fertility limits carbon sequestration by forest ecosystems in a CO_2-enriched atmosphere. *Nature* **411**, 469–472.

Peng C, Ma Z, Lei X, Zhu Q, Chen H, Wang W, Liu S, Li W, Fang X, Zhou X. **2011**. A drought-induced pervasive increase in tree mortality across Canada's boreal forests. *Nature Climate Change* **1**, 467–471.

Peñuelas J, Canadell JG, Ogaya R. **2011**. Increased water-use efficiency during the 20th century did not translate into enhanced tree growth. *Global Ecology & Biogeography* **20**, 597–608.

***Perez-Soba M, Dueck TA, Puppi G, Kuiper PJC**. **1995**. Interactions of elevated CO_2, NH_3 and O_3 on mycorrhizal infection, gas exchange and N metabolism in saplings of Scots pine. *Plant & Soil* **176**, 107–116.

***Pettersson R, McDonald AJS**. **1992**. Effects of elevated carbon dioxide concentration on photosynthesis and growth of small birch plants (*Betula pendula* Roth.) at optimal nutrition. *Plant, Cell & Environment* **15**, 911–919.

***Pumpanen J, Heinonsalo J, Rasilo T, Villemot J, Ilvesniemi H**. **2012**. The effects of soil and air temperature on CO_2 exchange and net biomass accumulation in Norway spruce, Scots pine and silver birch seedlings. *Tree Physiology* **32**, 724–736.

Qian H, Joseph R, Zeng N. **2010**. Enhanced terrestrial carbon uptake in the northern high latitudes in the 21st century from the Coupled Carbon Cycle Climate Model Intercomparison Project model projections. *Global Change Biology* **16**, 641–656.

Quinn GP, Keough M. **2002**. *Experimental design and data analysis for biologists*. Cambridge University Press: Cambridge, UK.

R Development Core Team. **2011**. R: a language and environment for statistical computing. R Foundation for Statistical Computing: Vienna Austria. http://R–project.org.

Reich PB, Hobbie SE, Lee T, Ellsworth DS, West JB, Tilman D, Knops JMH, Naeem S, Trost J. **2006**. Nitrogen limitation constrains sustainability of ecosystem response to CO_2. *Nature* **440**, 922–925.

***Rey AN, Jarvis PG**. **1997**. An overview of long-term effects of elevated atmospheric CO_2 concentration on the growth and physiology of birch (*Betula pendula* Roth.). *Botanical Journal of Scotland* **49**, 325–340.

***Rey A, Jarvis PG**. **1998**. Long-term photosynthetic acclimation to increased atmospheric CO_2 concentration in young birch (*Betula pendula*) trees. *Tree Physiology* **18**, 441–450.

***Riikonen J, Kets K, Darbah J, Oksanen E, Sober A, Vapaavuori E, Kubiske ME, Nelson N, Karnosky DF**. **2008**. Carbon gain and bud physiology in *Populus tremuloides* and *Betula papyrifera* grown under long-term exposure to elevated concentrations of CO_2 and O_3. *Tree Physiology* **28**, 243–254.

Rixen C, Dawes MA, Wipf S, Hagedorn F. **2012**. Evidence of enhanced freezing damage in treeline plants during six years of CO_2 enrichment and soil warming. *Oikos* **121**, 1532–1543.

***Roberntz P**. **2001**. Atmospheric carbon dioxide concentration, nitrogen availability, temperature and the photosynthetic capacity of current-year Norway spruce shoots. *Tree Physiology* **21**, 931–940.

Rowe, J. **1972**. Forest regions of Canada. *Forestry Service Publication 1300*. Department of the Environment: Ottawa, Ontario.

Ryan MG. **2013**. Three decades of research at Flakaliden advancing whole-tree physiology, forest ecosystem and global change research. *Tree Physiology* **33**, 1123–1131.

Sage RF, Kubien DS. **2007**. The temperature response of C_3 and C_4 photosynthesis. *Plant, Cell & Environment* **30**, 1086–1106.

Sage RF, Way DA, Kubien DS. **2008**. Rubisco, Rubisco activase, and global climate change. *Journal of Experimental Botany* **59**, 1581–1595.

***Sallas L, Luomala E-M, Ultriainen J, Kainulainen P, Holopainen JK**. **2003**. Contrasting effects of elevated carbon dioxide concentration and temperature on Rubisco activity, chlorophyll fluorescence, needle ultrastructure and secondary metabolites in conifer seedlings. *Tree Physiology* **23**, 97–108.

Serreze MC, Walsh JE, Osterkamp T, Dyurgerov M, Romanovsky V, Oechel WC, Morison J, Zhang T, Barry RG. **2000**. Observational evidence of recent change in the northern high-latitude environment. *Climate Change* **46**, 159–207.

***Sharkey TD, Loreto F, Delwiche CF**. **1991**. High carbon dioxide and sun/shade effects on isoprene emission from oak and aspen tree leaves. *Plant, Cell & Environment* **14**, 333–338.

Sigurdsson BD, Medhurst JL, Wallin G, Eggertsson O, Linder S. **2013**. Growth of mature boreal Norway spruce was not affected by elevated [CO_2] and/or air temperature unless nutrient availability was improved. *Tree Physiology* **33**, 1192–1205.

***Silim SN, Ryan N, Kubien DS**. **2010**. Temperature responses of photosynthesis and respiration in *Populus balsamifera* L.: acclimation versus adaptation. *Photosynthesis Research* **104**, 19–30.

Silva LCR, Anand M, Leithead MD. **2010**. Recent widespread tree growth decline despite increasing atmospheric CO_2. *PLoS ONE* **5**, e11543.

***Sorenson FC, Ferrell WK**. **1973**. Photosynthesis and growth of Douglas-fir seedlings when grown in different environments. *Canadian Journal of Botany* **51**, 1689–1698.

***Špunda V, Kalina J, Urban O, Luis VC, Sibisse I, Puértolas J, Šprtová M, Marek MV**. **2005**. Diurnal dynamics of photosynthetic parameters of Norway spruce trees cultivated under ambient and elevated CO_2: the reasons of midday depression in CO_2 assimilation. *Plant Science* **168**, 1371–1381.

Taylor G, Tallis MJ, Giardina CP, *et al*. 2008. Future atmospheric CO_2 leads to delayed autumnal senescence. *Global Change Biology* **14**, 264–275.

***Tingey DT, Lee EH, Phillips DL, Rygiewicz PT, Waschmann RS, Johnson MG, Olszyk DM**. **2007**. Elevated CO_2 and temperature alter net ecosystem C exchange in a young Douglas fir mesocosm experiment. *Plant, Cell & Environment* **30**, 1400–1410.

***Tjoelker M, Oleksyn J, Reich P**. **1998a**. Temperature and ontogeny mediate growth response to elevated CO_2 in seedlings of five boreal tree species. *New Phytologist* **140**, 197–210.

Tjoelker MG, Oleksyn J, Reich PB. **1998b**. Seedlings of five boreal tree species differ in acclimation of net photosynthesis to elevated CO_2 and temperature. *Tree Physiology* **18**, 715–726.

Tjoelker M, Oleksyn J, Reich P. **1999**. Acclimation of respiration to temperature and CO_2 in seedlings of boreal tree species in relation to plant size and relative growth rate. *Global Change Biology* **5**, 679–691.

***Townend J**. **1995**. Effects of elevated CO_2, water and nutrients on *Picea sitchensis* (Bong.) Carr seedlings. *New Phytologist* **130**, 193–206.

Tozzi ES, Easlon HM, Richards JH. **2013**. Interactive effects of water, light and heat stress on photosynthesis in Fremont cottonwood. *Plant, Cell & Environment* **36**, 1423–1434.

***Urban O, Hrstka M, Zitová M, Holišová P, Sprtová M, Klem K, Calfapietra C, De Angelis P, Marek MV**. **2012**. Effect of season, needle age and elevated CO_2 concentration on photosynthesis and Rubisco acclimation in *Picea abies*. *Plant Physiology & Biochemistry* **58**, 135–141.

***Utriainen J, Janhunen S, Helmisaari H-S, Holopainen T**. **2000**. Biomass allocation, needle structural characteristics and nutrient composition in Scots pine seedlings exposed to elevated CO_2 and O_3 concentrations. *Trees* **14**, 475–484.

Van Herk IG, Gower ST, Bronson DR, Tanner MS. **2011**. Effects of climate warming on canopy water dynamics of a boreal black spruce plantation. *Canadian Journal of Forest Research* **41**, 217–227.

Verbyla D. **2008**. The greening and browning of Alaska based on 1982–2003 satellite data. *Global Ecology & Biogeography* **17**, 547–555.

Walker X, Henry GHR, McLeod K, Hofgaard A. **2012**. Reproduction and seedling establishment of *Picea glauca* across the northernmost forest-tundra region in Canada. *Global Change Biology* **18**, 3202–3211.

***Wang K-Y, Kellomäki S, Laitinen K**. **1996**. Acclimation of photosynthetic parameters in Scots pine after three years exposure to elevated temperature and CO_2. *Agricultural & Forest Meteorology* **82**, 195–217.

Warren JM, Norby RJ, Wullschleger SD. **2011**. Elevated CO_2 enhances leaf senescence during extreme drought in a temperate forest. *Tree Physiology* **31**, 117–130.

Way DA. **2011**. The bigger they are, the harder they fall: CO_2 concentration and tree size affect drought tolerance. *Tree Physiology* **31**, 115–116.

Way DA, Oren R. **2010**. Differential responses to changes in growth temperature between trees from different functional groups and biomes: a review and synthesis of data. *Tree Physiology* **30**, 669–688.

Way DA, Sage RF. **2008a**. Thermal acclimation of photosynthesis in black spruce [*Picea mariana* (Mill.) B.S.P.]. *Plant, Cell & Environment* **31**, 1250–1262.

***Way DA, Sage RF**. **2008b**. Elevated growth temperatures reduce the carbon gain of black spruce [*Picea mariana* (Mill.) B.S.P.]. *Global Change Biology* **14**, 624–636.

Way DA, Yamori W. **2014**. Thermal acclimation of photosynthesis: on the importance of adjusting our definitions and accounting for thermal acclimation of respiration. *Photosynthesis Research* **119**, 89–100.

Way DA, Ladeau SL, McCarthy HR, Clark JS, Oren R, Finzi AC, Jackson RB. **2010**. Greater seed production in elevated CO_2 is not accompanied by reduced seed quality in *Pinus taeda* L. *Global Change Biology* **16**, 1046–1056.

Way DA, Crawley C, Sage RF. **2013a**. A hot and dry future: warming effects on boreal tree drought tolerance. *Tree Physiology* **33**, 1003–1005.

Way DA, Domec J-C, Jackson RB. **2013b**. Elevated growth temperatures alter hydraulic characteristics in trembling aspen (*Populus tremuloides*) seedlings: implications for tree drought tolerance. *Plant, Cell & Environment* **36**, 103–115.

Wilmking M, Juday GP, Barber VA, Zald HSJ. **2004**. Recent climate warming forces contrasting growth responses of white spruce at treeline in Alaska through temperature thresholds. *Global Change Biology* **10**, 1724–1736.

***Yakimchuk R, Hoddinott J**. **1994**. The influence of ultraviolet-B light and carbon dioxide enrichment on the growth and physiology of seedlings of three conifer species. *Canadian Journal of Forest Research* **24**, 1–8.

Yamori W, Hikosaka K, Way DA. **2014**. Temperature response of photosynthesis in C_3, C_4, and CAM plants: temperature acclimation and temperature adaptation. *Photosynthesis Research* **119**, 101–117.

***Zak DR, Pregitzer KS, Curtis PS, Vogel CS, Holmes WE, Lussenhop J**. **2000**. Atmospheric CO_2, soil-N availability, and allocation of biomass and nitrogen by *Populus tremuloides*. *Ecological Applications* **10**, 34–46.

***Zhang S, Dang Q-L**. **2005**. Effects of soil temperature and elevated atmospheric CO_2 concentration on gas exchange, in vivo carboxylation and chlorophyll fluorescence in Jack pine and white birch seedlings. *Tree Physiology* **25**, 523–531.

***Zhang S, Dang Q-L**. **2006**. Effects of carbon dioxide concentration and nutrition on photosynthetic functions of white birch seedlings. *Tree Physiology* **26**, 1457–1467.

***Zhang S, Dang Q**. **2007**. Interactive effects of soil temperature and [CO_2] on morphological and biomass traits in seedlings of four boreal tree species. *Forest Science* **53**, 453–460.

***Zhang S, Dang Q-L**. **2013**. CO_2 elevation improves photosynthetic performance in progressive warming environment in white birch seedlings. *F1000Research* **2**, 1–10.

***Zhang S, Dang Q-L, Cao B**. **2013**. Nutrient supply has greater influence than sink strength on photosynthetic adaptation to CO_2 elevation in white birch seedlings. *Plant Science* **203–204**, 55–62.

Chapter 3

3 Autumn photosynthetic decline and growth cessation in seedlings of white spruce are decoupled under warming and photoperiod manipulations

This article was published in a similar form in *Plant, Cell & Environment* (Stinziano & Way, 2017, "Autumn photosynthetic decline and growth cessation in seedlings of white spruce are decoupled under warming and photoperiod manipulations", *Plant, Cell & Environment* **40**(8), 1296–1316), and addresses **Question 2** (how do temperature and day length interact in regulating autumnal photosynthesis and growth in a boreal conifer?) and **Hypotheses 1** and **2** (**1**: boreal trees are limited in growth and photosynthesis by low temperatures; **2**: day length, not temperature, drives seasonal changes in photosynthetic capacity in evergreen conifers) from Chapter 1.

3.1 Introduction

Global mean air temperature increases of up to 4.5 °C are predicted by the year 2100, but even greater warming is projected for mid to high northern latitudes (Collins *et al.*, 2013). At these latitudes, evergreen conifers overwinter in a state of dormancy, which is associated with a reorganization of the photosynthetic apparatus, and a suppression of photosynthetic capacity (Öquist & Hüner, 2003). The physiological changes associated with preparing for winter dormancy are induced during the summer and autumn as temperatures drop and days become shorter (Hänninen & Tanino, 2011). Increasing temperatures could therefore delay the induction of dormancy in conifers, extending the period of growth in northern forests and increasing ecosystem-level carbon uptake (Stinziano & Way, 2014). Delays in autumn phenology due to recent warming in northern forests have already increased ecosystem carbon uptake, in agreement with expectations, though this effect is weakest in evergreen-dominated sites (Keenan *et al.*, 2014).

While the projected impacts of moderate climate warming on northern temperate and boreal forests are often assumed to be positive, the effects of warming on northern conifers are mixed. Experimentally imposed elevated temperatures can increase

photosynthetic carbon uptake (Danby & Hik, 2007; Zhao & Liu, 2009; Hall *et al*., 2013; Deslauriers *et al*., 2014), allowing new shoots to reach the carbon break-even point sooner (Hall *et al*., 2009), maintain photosynthetic rates under short photoperiods (Stinziano *et al.*, 2015; Hamilton *et al*., 2016), and stimulate growth (Danby & Hik, 2007; Yin *et al*., 2008; Zhao & Liu, 2009; Reich *et al*., 2015) or the length of the active growing season in conifers (Bronson *et al*., 2009; Hamilton *et al*., 2016). But warming can also suppress photosynthetic rates (Busch *et al.*, 2007, 2008; Way & Sage, 2008a; Deslauriers *et al*., 2014) and growth (Kang *et al*., 1994; Way & Sage, 2008b; Reich *et al*., 2015) in both young and mature northern conifers, and higher temperatures are correlated with increased tree mortality rates in boreal forest stands (Zhang *et al.*, 2015a), which could lead to species range shifts at southern range limits where high temperatures may limit growth and survival. Lastly, in other cases, warming imposed on mature trees may have little or no effect on photosynthesis and growth (Slaney *et al*., 2007; Sigurdsson *et al*., 2013) due to nutrient limitations, particularly in boreal sites (Sigurdsson *et al.*, 2013). Warming in autumn has been linked to decreases in net CO_2 uptake in high latitude systems (Piao *et al*., 2008; Barichivich *et al*., 2013), a result attributed to the greater stimulation of respiration than of photosynthesis by high temperatures in autumn, which may be partly due to the low capacity of evergreen trees to thermally acclimate photosynthesis to elevated temperatures (Way & Yamori, 2014; Yamori *et al.*, 2014). These results cast doubt on the notion that northern forests will necessarily become stronger carbon sinks as the climate warms.

Despite these concerns, warming could still stimulate tree carbon uptake and growth in mid to high latitudes if it primarily relieves cold limitations during autumn on these processes, without suppressing carbon fixation and growth in the summer (Buermann *et al*., 2013). But plant phenology responds to photoperiod as well as temperature. Since photoperiod cues will not be affected by climate change, trees may experience a desynchronization between the temperature and day length cues that normally lead to the cessation of growth and the down-regulation of photosynthesis (Busch *et al*., 2007, 2008). If photoperiod is a stronger regulator of these changes over the season than is temperature, then warming may have little effect on the length of the active growing season or the duration of active carbon uptake in northern forests (Chapter 2; Stinziano &

Way, 2014; Way & Montgomery, 2015). This effect could explain remote sensing data showing a decoupling between the end of the potential growing season, based on thermal conditions, and the end of the photosynthetically active season in the autumn in high latitude forests (Barichovich *et al.*, 2013).

Photoperiod is known to be a strong regulator of plant growth: increasing day lengths promote bud burst (Basler & Körner, 2012) and continued growth (Kramer, 1936; Downs & Borthwick, 1956), while declining day lengths in the autumn promote growth cessation and dormancy (Kramer, 1936; Heide, 1974; Öquist & Hüner, 2003; Hamilton *et al.*, 2016). However, temperature can also regulate growth cessation in conifers (Hänninen & Tanino, 2011), and the relative importance of photoperiod and temperature cues for inducing growth cessation varies by species (Delpierre *et al.*, 2016). In Norway spruce (*Picea abies* (L.) H. Karst.) seedlings, low temperatures can induce shoot growth cessation (Dormling *et al.*, 1968), while in white spruce (*Picea glauca* (Moench) Voss) this is modulated by short photoperiods (Hamilton *et al.*, 2016). When photoperiod and temperature signals are conflicting, the coordination of the timing of growth cessation in roots and shoot tissues can become disrupted (Hamilton *et al.*, 2016), as shoot tissue growth may be more strongly regulated by photoperiod, while root growth appears to be better correlated with temperature (Bigras & D'Aoust, 1993).

There is also evidence that photoperiod may play a role in regulating photosynthesis. Photoperiod explained more seasonal variability in photosynthetic capacity (the maximum rate of Rubisco carboxylation, V_{cmax}, and the maximum rate of electron transport, J_{max}) across 23 broadleaf deciduous tree species than did temperature, implying that the seasonal duration of carbon uptake would be unresponsive to warming (Bauerle *et al.*, 2012). In the same study, red maple (*Acer rubrum* L.) exposed to longer photoperiods maintained a higher V_{cmax} than control trees (Bauerle *et al.*, 2012). In agreement with these findings, warming had no effect on the autumn induction of photosynthetic down-regulation in *Pinus sylvestris* L. in a free air temperature experiment with natural photoperiod (Chang *et al.*, 2015). Studies such as these that assess how changes in photoperiod or temperature affect photosynthetic dynamics often use large step-changes in photoperiod (e.g. Caspar *et al.*, 1985; Öquist & Hüner, 1991; Busch *et*

al., 2007, 2008; Hamilton *et al*., 2016) or make monthly measurements of photosynthetic performance (e.g. Chang *et al*., 2015). However, detecting shifts in the timing of autumn photosynthetic down-regulation may require frequent measurements of plants experiencing ecologically realistic declines in photoperiod and temperature: when Norway spruce seedlings were exposed to weekly changes in photoperiod and temperature based on field conditions, a 4°C warming treatment delayed the autumn down-regulation of photosynthesis (Stinziano *et al.*, 2015), although all trees experienced the same photoperiods. The relative roles of temperature and photoperiod on photosynthetic capacity in evergreen conifers are therefore still unclear, and there is currently no proposed mechanism to explain how seasonal changes in photosynthetic capacity might be regulated by photoperiod.

Changes in photosynthetic capacity over the growing season are underlain by changes in the relationships between leaf nitrogen, nitrogen investment in photosynthetic machinery, and realized photosynthetic capacity, which can be altered by enzyme activation states and other processes (Reich *et al.*, 1991; Niinemets & Tenhunen, 1997; Wilson *et al.*, 2000). Work on the leaf economic spectrum has demonstrated strong correlations between photosynthetic rates and leaf nitrogen concentrations across a broad range of plants (Amundson *et al*., 1992; Reich *et al.*, 1997; Wright *et al*., 2004; Zhang *et al*., 2015b), and the correlation between photosynthetic capacity and both chlorophyll and nitrogen concentrations has been known for decades (e.g. Evans, 1989; Reich *et al.*, 1995). While these patterns hold across species, correlations between leaf nitrogen and photosynthesis are not constant within a species over a growing season (Reich *et al.*, 1991; Niinemets & Tenhunen, 1997), especially in evergreen conifers (Wilson *et al.*, 2000). In seedlings of Norway spruce (*Picea abies*), photosynthetic capacity decreased sharply near the end of the growing season, although leaf nitrogen concentrations remained stable (Stinziano *et al.*, 2015), and in a suite of deciduous temperate tree species, declines in photosynthetic capacity after the summer solstice were coupled with constant estimates of leaf greenness (Bauerle *et al*., 2012). Understanding how the relationships between photosynthetic capacity, chlorophyll, and leaf nitrogen change seasonally has implications for our ability to estimate carbon uptake from remote sensing

data, where photosynthetic activity is derived from spectral data by assuming relationships between light absorption by leaf pigments, leaf nitrogen concentrations and primary productivity (Gitelson *et al*., 2015; Park *et al*., 2016).

In the present study, I measured the effects of realistically-based weekly changes in photoperiod and temperature on photosynthetic capacity, leaf biochemistry, and growth in seedlings of white spruce (*Picea glauca*), a dominant conifer in the North American boreal forest. My goals were to determine: 1) the relative importance of photoperiod and temperature in regulating autumn declines in photosynthetic capacity; 2) how leaf chlorophyll and nitrogen concentrations are correlated with photosynthetic capacity across a simulated autumn when temperature and photoperiod were manipulated; and 3) the effect of increases in temperature (and photoperiod) on biomass and growth.

3.2 Materials and methods

3.2.1 Plant material and growing conditions

White spruce (*Picea glauca* (Moench) Voss) seeds from a southern provenance located near Belleville, Ontario (lat.: 44.216 N, long.: 77.133 W) were obtained from the Canadian National Tree Seed Centre. This seed lot was chosen because, while it still represents a broadly distributed boreal tree species, it has a relatively long growing season compared to more northerly provenances, allowing for a longer experiment to disentangle photoperiod and temperature effects. Seeds were moist-chilled for 21 days at 3 °C and then planted in 2 L pots filled with PRO-MIX BX Mycorrhizae (Premier Tech Horticulture Rivière-du-Loup, QC, Canada) mixed with Miracle-GRO slow release fertilizer (as per product instructions, 12-4-8, Miracle-Gro, Marysville, OH, USA). Temperature and photoperiod conditions during the first 16 weeks of growth were based on summer solstice conditions for the provenance (based on ten-year historical averages for Trenton, ON, the closest Environment Canada climate data available for the seed lot), and seedlings were grown at a light intensity of 558 ± 122 μmol photons m^{-2} s^{-1} in four growth chambers (GCW15, Environmental Growth Chambers, Chagrin Falls, OH). Chambers were kept at 60% relative humidity, and pots were watered daily as needed to maintain moist growth medium. After 16 weeks, when the seedlings were large enough

(~15 cm tall) to measure gas exchange, four treatments were imposed. The *control* treatment consisted of weekly changes in temperature and photoperiod representing field conditions from the summer solstice to the week of October 8, where the photoperiod and day/night temperatures used were ten-year historical averages from the seed source site. The *warming* treatment was the same as the control treatment, except that the day/night temperatures were 5 °C warmer than the control treatment. The *constant photoperiod* treatment had the same weekly temperatures as the control treatment, but with a constant summer solstice photoperiod, and the *constant temperature* treatment had the same weekly photoperiod as the control and warming treatments, but with constant summer solstice day/night temperatures (Fig. 3.1). The experiment was run twice to obtain two independent replications (trial 1 & 2). Four seedlings per week per treatment per trial were randomly selected for gas exchange, biomass, and biochemical analyses.

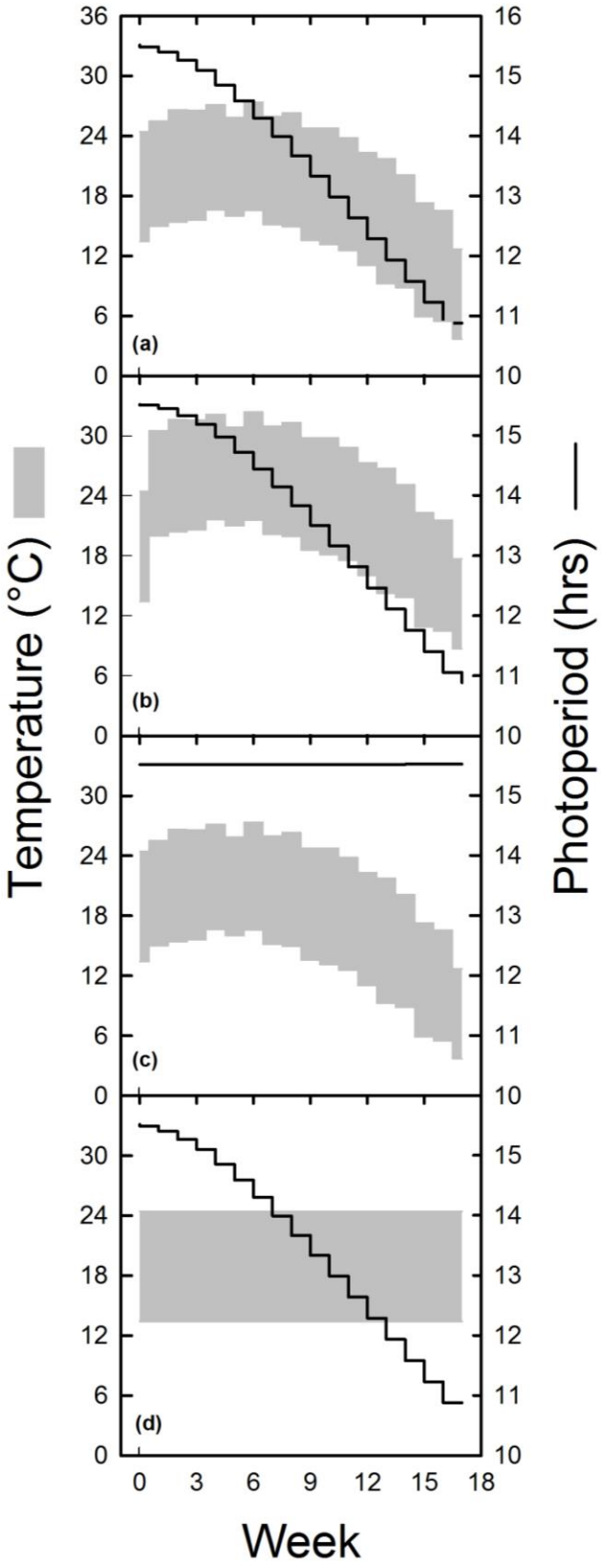
Temperature (°C)
Photoperiod (hrs)
Week
(a)
(b)
(c)
(d)
0
3
6
9
12
15
18
0
6
12
18
24
30
36
10
11
12
13
14
15
16

Figure 3.1. The day/night temperatures (bounding the shaded region) and photoperiod (solid lines) treatments for white spruce (*Picea glauca*). All seedlings were grown under summer solstice temperature and photoperiod conditions for 16 weeks; treatments began at week 0. (a) Control treatment, with day/night temperatures and photoperiod for the provenance; (b) warming treatment, with control treatment day/night temperatures +5 °C and control treatment photoperiod; (c) constant photoperiod treatment, with control treatment day/night temperatures and a constant summer solstice photoperiod; and (d) constant temperature treatment, with constant summer solstice day/night temperatures and control treatment weekly photoperiod. Note: temperature and photoperiod refer to the weekly temperature and photoperiod experienced by the seedlings, while treatment denotes the integrated temperature and photoperiod regimes (i.e. control, warming, constant photoperiod, and constant temperature).

3.2.2 Gas exchange measurements

Gas exchange measurements were performed weekly (seven days after the weekly photoperiod/temperature condition was imposed in each treatment) using a portable photosynthesis system (Licor 6400XT, 6400-22L opaque conifer chamber and 6400-02B LED light source, Licor Biosciences, Lincoln, NE). The response of net CO_2 assimilation rate (A_{net}) to intercellular CO_2 concentrations (C_i) under saturating light intensity (1500 μmol photons m^{-2} s^{-1}) was measured by changing ambient CO_2 concentrations sequentially (from 400, 200, 150, 100, 50, 400, 1500, 2000, and 2200 μmol mol^{-1} CO_2) and holding leaf temperature at 25 °C and the vapor pressure deficit between 1.0 and 1.6 kPa. The A_{net}-C_i curves were then used to calculate both the maximum rate of Rubisco carboxylation (V_{cmax}) and the maximum rate of electron transport (J_{max}) according to Farquhar *et al.* (1980). As V_{cmax} and J_{max} were determined on a C_i basis, rather than on a chloroplastic CO_2 basis or from *in vitro* assays, I refer to these parameters as apparent V_{cmax} and apparent J_{max}. Leaf dark respiration (R_{dark}) was measured at 25 °C and a CO_2 concentration of 400 μmol mol^{-1} in the middle of the dark period (i.e. between 00:00 and 03:00 hours) during the last three weeks of the experiment.

Needles used for gas exchange were harvested and projected leaf area was measured by photographing the needles and analyzing the photographs using ImageJ (NIH, Bethesda, MD). A subsample of the needles was dried at 60 °C until constant mass, and weighed for dry mass to calculate specific leaf area (SLA); another subsample was immediately frozen in $N_{2(l)}$ and stored at -80 °C for biochemical analysis. Seedling height and stem diameter were measured, and the rest of the seedling was harvested, divided into leaves, stems and roots, and dried at 60 °C until constant mass for growth analysis. Leaf mass ratio, stem mass ratio and root mass ratios were calculated by dividing the dry mass of leaves, stems, and roots (respectively) by total biomass.

3.2.3 Modeling of V_{cmax}, A_{net}, R_{dark}, and carbon gain

Values for V_{cmax} at the growth temperature (growth V_{cmax}) of each treatment in each week were estimated from the weekly measured V_{cmax} at 25 °C. The temperature dependency of V_{cmax} was modelled with an Arrhenius function (Medlyn *et al.*, 2002):

$$f(T_g) = k_{25} \times \exp\left[\frac{E_a \times (T_g - 298)}{(298 \times R \times T_g)}\right]$$ Equation 3.1

where T_g is growth temperature in Kelvin; R is the universal gas constant (8.314 J mol^{-1} K^{-1}); k_{25} is the measured parameter value at 25 °C, and E_a is the activation energy (64.8 kJ mol^{-1}; Badger & Collatz, 1977).

Net CO_2 assimilation rates (A_{net}) were also calculated for each week for each treatment. The A_{net} was assumed to be Rubisco limited and calculated using (Farquhar *et al.*, 1980):

$$A_{net} = \frac{V_{cmax} \times (C_i - \Gamma^*)}{\left[C_i + K_c\left(1 + \frac{O_i}{K_o}\right)\right]} - R_{day}$$ Equation 3.2

where A_{net} is in μmol CO_2 m^{-2} s^{-1}, O_i is the intercellular O_2 concentration (assumed to be 210,000 μmol mol^{-1} based on an atmospheric pressure of 95.3 kPa and O_2 concentration of 21%), and C_i is the intercellular CO_2 concentration (set at 280 μmol mol^{-1}, with an assumed C_i/C_a of 0.7 based on Farquhar & Wong, 1984). Values for K_c and K_o (the Michaelis-Menten constants for Rubisco carboxylation and oxygenation, respectively) and for the photorespiratory CO_2 compensation point, Γ*, were calculated for each weekly growth temperature in each treatment. The K_c and K_o values were derived using Equation 3.1 with k_{25} values of 419 μmol mol^{-1} for K_c and 381 mmol mol^{-1} for K_o (Jordan & Ogren, 1981, 1984) and E_a values of 81,655 kJ mol^{-1} and 15,632 kJ mol^{-1} for K_c and K_o, respectively (Jordan & Ogren, 1981,1984). The temperature dependency of Γ* was modelled according to Yamori *et al*. (2006):

$$\Gamma^* = 0.0021 * (T_g - 273.15)^3 - 0.1083 * (T_g - 273.15)^2 + 2.5821 * (T_g - 273.15) + 9.837$$ Equation 3.3

R_{day}, mitochondrial respiration in the light, was calculated as described below.

Weekly measured R_{dark} values at 25 °C were temperature-acclimated using (Atkin & Tjoelker, 2003):

$$Q_{10} = 3.09 - 0.043 \times T_{avg}$$ Equation 3.4

where the thermal sensitivity coefficient, Q_{10}, was determined for each week based on T_{avg}, the average daily temperature for that week in each treatment. The measured R_{dark} was then temperature-scaled to the nightly temperatures (T_{night}) for each week in each treatment according to Atkin & Tjoelker (2003):

$$R_{night} = 10^{\left[\frac{T_{night}-25}{10}\times \log Q_{10} + \log R_{25}\right]} \quad \text{Equation 3.5}$$

where R_{night} is R_{dark} at T_{night} (in μmol CO_2 m^{-2} s^{-1}), and R_{25} is the treatment-specific dark respiration rate at 25 °C. Leaf respiration during the day (R_{day}) was assumed to be 0.7 times R_{dark} (Ayub *et al*., 2011), but calculated with daytime temperatures (T_{day}) instead of T_{night} in Equation 3.5.

I modelled the weekly carbon gain of seedling tissues for each seedling as:

$$\text{Weekly carbon gain} = \frac{A_{net}*DL - R_{night}*NL}{1{,}000{,}000\ \mu\text{mol mol } CO_2{}^{-1}} * 7 \text{ days week}^{-1} *$$
$$12.01 \text{ g carbon mol } CO_2{}^{-1} * LA - \frac{R_{root,day}*DL - R_{root,night}*NL}{1{,}000{,}000\ \mu\text{mol mol } CO_2{}^{-1}} * 7 \text{ days week}^{-1} *$$
$$12.01 \text{ g carbon mol } CO_2{}^{-1} * \text{Root mass} \quad \text{Equation 3.6}$$

where weekly carbon gain is in g carbon; DL and NL are day length and night length per day in seconds, respectively; dividing by 1,000,000 converts A_{net}, R_{night} and R_{root} from μmol to mol; the constant 7 converts daily carbon gain into a weekly value; 12.01 converts carbon gain from mol CO_2 to g C; and LA is seedling leaf area in m^{-2}; $R_{root,\ day}$ and $R_{root,\ night}$ are root respiration rates during the day and night, respectively, with a rate of 0.02948 μmol CO_2 g^{-1} s^{-1} at 23.5 °C (Reich *et al*., 1998) scaled to growth temperatures with the leaf Q_{10}; root mass is in g dry mass. I then summed weekly carbon gain across the experiment to obtain cumulative net carbon gain. I estimated a 1:1 relationship between measured dry biomass and cumulative net carbon gained by assuming that dry biomass is 50% carbon to determine whether differences in modeled cumulative net carbon gain explained differences in measured dry biomass.

3.2.4 Carbon, nitrogen and chlorophyll analysis

Dried needles were ground using a Wiley mill, and analyzed for % carbon and % nitrogen (Thermo Finnigan Delta Plus XL continuous flow mass spectrometer, Thermo Fisher Scientific, Waltham, MA, USA). Frozen needle samples were ground in $N_{2(l)}$, and chlorophylls and carotenoids were extracted in 100% methanol under dim light at 4 °C for 2 h, followed by two more extractions with 100% methanol for 15 min each, with each extraction followed by centrifugation for 5 min at 16,100 x g (protocol modified from Busch *et al.*, 2007). Chlorophyll a and b, and total carotenoid concentrations were determined using a spectrophotometer (Varian Cary 50 UV-Vis Spectrophotometer, Agilent Technologies, Inc., Santa Clara, CA, USA) according to equations in Wellburn (1994).

3.2.5 Rubisco quantification and immunoblotting

To determine whether Rubisco concentrations correlated with the observed patterns in V_{cmax}, Rubisco was quantified for a subset of weeks for each treatment (weeks 0, 5, 9, 13, and 17), with two individuals randomly selected from each trial for each chosen week (for a total of four individuals/week). Frozen leaf tissue was ground in $N_{2(l)}$, and proteins were extracted by grinding in 2 ml of 4% (w/v) sodium dodecyl sulfate containing 3 mg ml^{-1} dithiothreitol per 1 cm^2 of leaf tissue using a Ten-Broeck glass homogenizer. Crude extracts were heated at 95 °C for 5 minutes then diluted two-fold with loading buffer containing 4% (w/v) sodium dodecyl sulfate, 0.3 M Trizma base and bromophenol blue dye prior to sodium dodecyl sulfate polyacrylamide gel electrophoresis. Proteins from crude extracts were separated on 12.5% (w/v) polyacrylamide gels using sodium dodecyl sulfate polyacrylamide gel electrophoresis in a protocol modified from Laemmli (1970). Proteins were electrotransferred for 1 h at 100 V onto nitrocellulose membranes, which were then blocked with milk powder in Trizma-buffered saline followed by three 5 minute washes of Trizma-buffered saline. Rabbit primary antibodies toward the Rubisco large subunit (donated by NPA Hüner) were diluted to 1:5000 and used to incubate blocked membranes for 1 h followed by four 10 minute washes in Trizma-buffered saline. Secondary goat antibodies toward rabbit proteins conjugated to horseradish protein (A6154, Sigma-Aldrich, Oakville, ON, Canada) were diluted 1:5000, and

incubated with the membrane for 1 h, followed by four 10 minute washes in Trizma-buffered saline. Enhanced chemiluminescence reagent (RPN2109, GE Life Sciences, Mississauga, ON, Canada) was used to detect horseradish peroxidase antibodies on film. Rubisco large subunit standard (AS01 017S, Agrisera, Vännäs, Sweden) was used to create a standard curve to quantify Rubisco on each immunoblot. Immunoblot bands were quantified against the Rubisco standard curve using ImageJ (NIH, Bethesda, MD, USA; Appendix A; Fig. A.1).

3.2.6 Statistical analyses

Data were analyzed in R GUI Version 3.0.2 (R Core Development Team, 2013). To test for responses to photoperiod and temperature, as well as treatment effects, ANOVA models were used to test for effects of weekly photoperiod, weekly temperature, treatment, week, trial, and all relevant interactions, treating each variable as a fixed effect. ANOVA models with the lowest Bayesian Information Criterion (BIC) were selected for final interpretation. To meet the ANOVA model assumptions, ratio and compositional data were $\log_{10}$-transformed according to Aitchison (1986), however these data are presented in untransformed units. *P*-values from ANOVA outputs were adjusted for control of family-wise error rates using the Holm method, which gives more power than a standard Bonferroni correction (Holm, 1979).

Correlations between V_{cmax} and J_{max} with weekly growth temperature and photoperiod were calculated using data from the control, constant photoperiod, and constant temperature treatments, with means and standard errors calculated for each unique photoperiod and temperature. The warming treatment was excluded from this analysis to maintain a balanced design of equal data points with manipulated temperature or photoperiod in each week. Values of R_{dark} were analyzed using a two-way ANOVA to test the effects of week and treatment. Biomass data were also analyzed using an ANOVA to test for the effects of treatment and trial and either accumulated temperature sum (calculated as the number of degrees Celsius above 0 °C times the number of days) or irradiance (calculated as the number of hours of accumulated light based on the photoperiod). Rubisco concentrations were analyzed using an ANOVA testing the effects of treatment along with time, V_{cmax}, and nitrogen concentration. Rubisco concentrations

on week 0 were tested for differences using an ANOVA for treatment effects. Curve fitting was performed using SigmaPlot Version 11.0 (Systat Software Inc., California, USA). Data are presented as means ± s.e.m. (standard error of the mean).

3.3 Results

White spruce seedlings were exposed to changing weekly temperature and photoperiod regimes in the following treatment combinations: control changes in temperature and photoperiod (*control*), 5 °C warming with control changes in photoperiod (*warming*), control changes in temperature with constant summer solstice photoperiod (*constant photoperiod*), and constant summer solstice temperature with control changes in photoperiod (*constant temperature*). The control and constant photoperiod treatments had a common temperature regime, while the warming and constant temperature treatments both represent elevated temperature treatments.

3.3.1 Photosynthetic capacity is maintained under warmer temperatures at low photoperiods, but respiration is stimulated by long photoperiods

Both apparent V_{cmax} and J_{max} changed over the experiment in all treatments (Week; $P < 0.001$; Table 3.1). Photosynthetic capacity peaked in the control and constant photoperiod treatments near week 13, but plateaued or continued to increase at short photoperiods in the treatments with elevated temperatures (warming and constant temperature treatments) (Table 3.1; Fig. 3.2). Apparent V_{cmax} and J_{max} were higher in the warming and constant temperature treatments than in the control and constant photoperiod treatments (treatment; $P < 0.001$; Table 3.1) due to high photosynthetic capacity late in the experiment. There was a linear relationship between apparent V_{cmax} and J_{max} across all treatments ($P < 0.001$; $R^2 = 0.86$; Fig. 3.3), with a slope of 1.96, indicating that a high apparent V_{cmax} was associated with even higher apparent J_{max}. This resulted in effects of treatment ($P < 0.0001$), week ($P < 0.0005$), and a treatment x week interaction on the ratio of apparent J_{max}:apparent V_{cmax} ($P < 0.05$; Table 3.1), as the ratio was highest in the treatments and weeks where apparent V_{cmax} was high. Photosynthetic capacity was significantly correlated with both photoperiod and temperature across the pooled data from the control, constant temperature and constant photoperiod treatments ($P < 0.0001$

for both; Fig. 3.4), although the relationship was stronger for photoperiod than for temperature.

Table 3.1. ANOVA of photosynthetic responses of *Picea glauca* to different autumn temperature and photoperiod regimes.

		V_{cmax}	J_{max}	J_{max} : V_{cmax}	R_{dark}	LMA	Nitrogen conc.	Rubisco conc.	V_{cmax} / nitrogen conc.	V_{cmax} / Rubisco conc.
Temperature	df	1,563	1,562	1,560					1,563	
	F	5.24	3.89	0.77					107.63	
	P	0.07	0.10	0.38					**<0.0001**	
Photoperiod	df	1,563	1,562	1,560			1,565		1,563	
	F	216.64	207.62	3.29			20.98		3.28	
	P	**<0.0001**	**<0.0001**	**0.0340**			**<0.0001**		0.34	
Trial	df	1,563	1,562	1,560		1,566	1,565		1,563	
	F	10.69	4.83	0.12		47,37	0.01		1.20	
	P	**0.0091**	0.20	1.00		**<0.0001**	1.00		1.00	
Treatment	df	3,563	3,562	3,560	3,40	3,566	3,565	3,72	3,563	3,72
	F	22.67	24.27	12.20	17.0	8.07	4.95	0.18	2.96	0.20
	P	**<0.0001**	**<0.0001**	**<0.0001**	**<0.0001**	**0.0003**	**0.0170**	1.00	0.16	1.00
Week	df	1,563	1,562	1,560	1,40	1,566	1,565	1,72	1,563	1,72
	F	80.45	109.98	16.31	2.41	438.70	4.41	16.08	31.74	0.13
	P	**<0.0001**	**<0.0001**	**0.0003**	0.128	**<0.0001**	0.11	**0.0006**	**<0.0001**	1.0000
Temperature x Photoperiod	df	1,563	1,562	1,560					1,563	
	F	20.54	29.65	7.85					11.27	
	P	**<0.0001**	**<0.0001**	**0.0053**					**0.0025**	
Temperature x Trial	df								1,563	
	F								9.35	
	P								**0.0094**	

Photoperiod x Trial	df	1,563	1,562							
	F	27.34	23.47							
	P	**<0.0001**	**<0.0001**							
Treatment x Week	df	3,563	3,562	3,560	3,40			1,72		3,72
	F	3.11	4.23	4.33	0.26			16.36		7.26
	P	0.0602	**0.0248**	**0.0248**	0.857			0.0602		**0.0020**
Treatment x Trial	df			3,560		3,566	3,565		3,563	
	F			6.59		7.27	10.03		4.50	
	P			**0.0015**		**0.0007**	**<0.0001**		**0.0157**	
Week x Trial	df		1,562	1,560		1,566	1,565			
	F		7.27	4.81		74.38	22.03			
	P		**0.0289**	0.09		**<0.0001**	**<0.0001**			
Treatment x Week x Trial	df									
	F									
	P									
BIC		4416	5270	-1542	150	6280	-740	1090	-400	453

V_{cmax}, apparent maximum rate of Rubisco carboxylation; J_{max}, apparent maximum rate of electron transport; R_{dark}, dark respiration; LMA, leaf mass area; conc., concentration. Significant *P*-values are bolded ($P < 0.05$). Note that temperature and photoperiod refer to the weekly temperature and photoperiod experienced by the seedlings, while treatment denotes the integrated temperature and photoperiod regimes (i.e. control, warming, constant photoperiod and constant temperature).

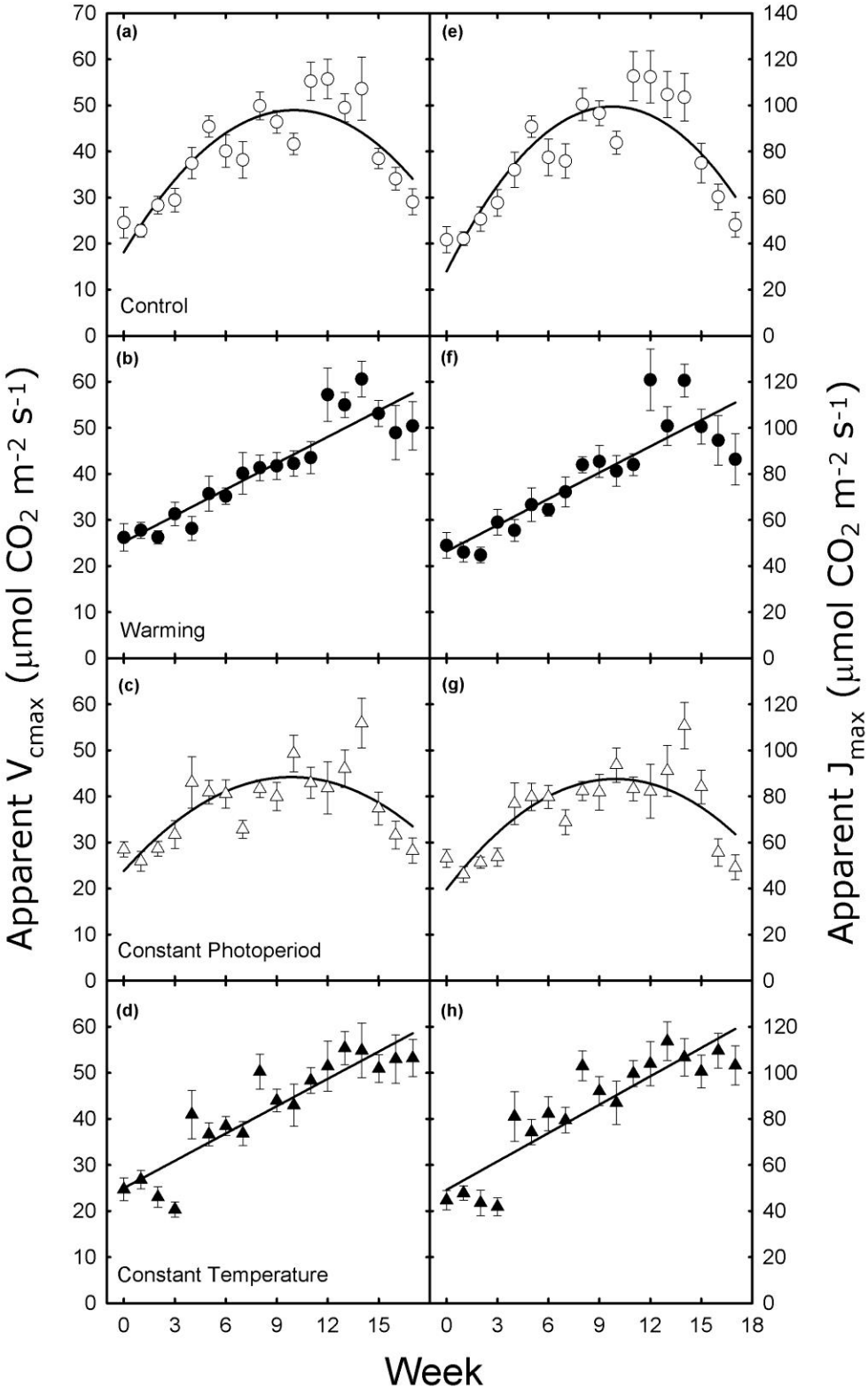
(a)
(e)
Control
(b)
(f)
Warming
(c)
(g)
Constant Photoperiod
(d)
(h)
Constant Temperature
Apparent V_{cmax} (μmol CO_2 m^{-2} s^{-1})
Apparent J_{max} (μmol CO_2 m^{-2} s^{-1})
Week

Figure 3.2. Apparent maximum Rubisco carboxylation (apparent V_{cmax}) and apparent maximum electron transport rates (apparent J_{max}) across time since the beginning of the experiment. Data presented as means ± s.e.m. (of total number of individuals, *N* = 8). *N* = 4 seedlings per chamber and two chambers per point. Regression equations: (a) $V_{cmax} = 18.2 + 6.1 \times week - 0.3 \times week^2$, $R^2 = 0.43$, $P < 0.0001$; (b) $V_{cmax} = 35.2 + 1.9 \times week$, $R^2 = 0.48$, $P < 0.0001$; (c) $V_{cmax} = 23.8 + 4.1 \times week - 0.2 \times week^2$, $R^2 = 0.23$, $P < 0.0001$; (d) $V_{cmax} = 25.0 + 2.0 \times week$, $R^2 = 0.47$, $P < 0.0001$; (e) $J_{max} = 28.0 + 14.6 \times week - 0.7 \times week^2$, $R^2 = 0.45$, $P < 0.0001$; (f) $J_{max} = 46.4 + 3.8 \times week$, $R^2 = 0.44$, $P < 0.0001$; (g) $J_{max} = 39.6 + 9.6 \times week - 0.5 \times week^2$, $R^2 = 0.29$, $P < 0.0001$; (h) $J_{max} = 49.2 + 4.1 \times week$, $R^2 = 0.49$, $P < 0.0001$.

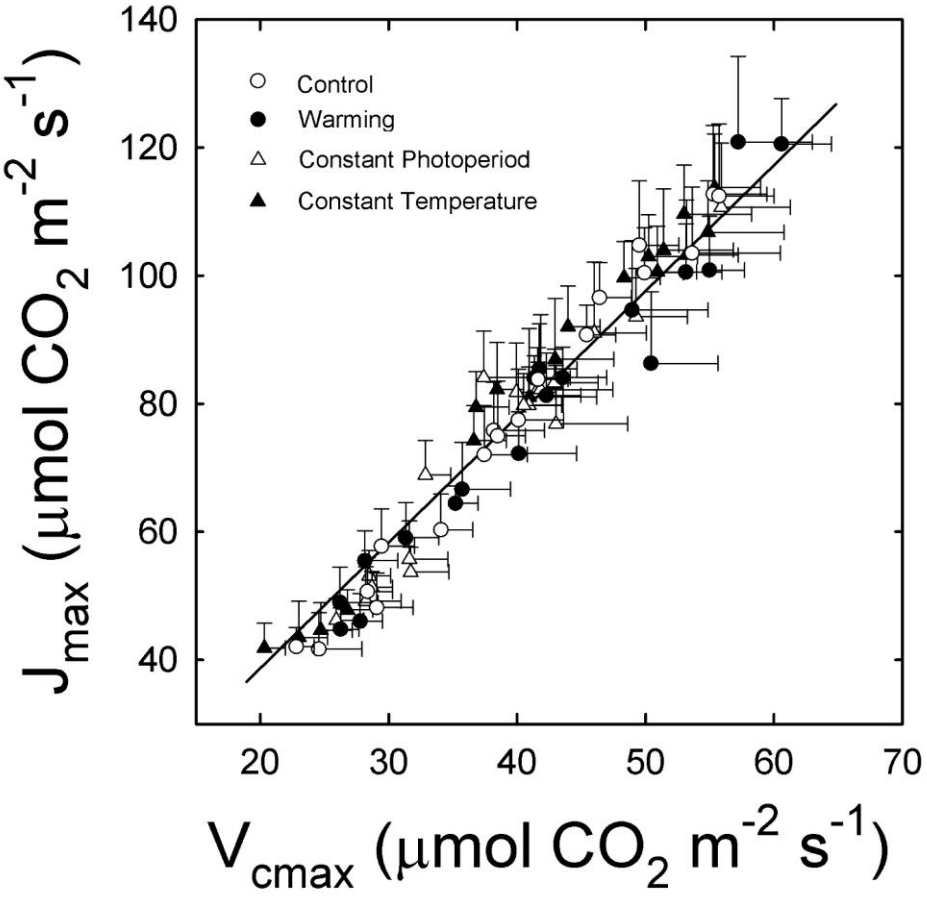

Figure 3.3. Correlation between apparent maximum rates of Rubisco carboxylation (V_{cmax}) and electron transport (J_{max}) rates. Data presented as means ± s.e.m. *N* = 8 (four seedlings per chamber and two chambers per point). Regression equation: $J_{max} = 1.96 \times V_{cmax} - 0.59$, $R^2 = 0.86$, $P < 0.0001$.

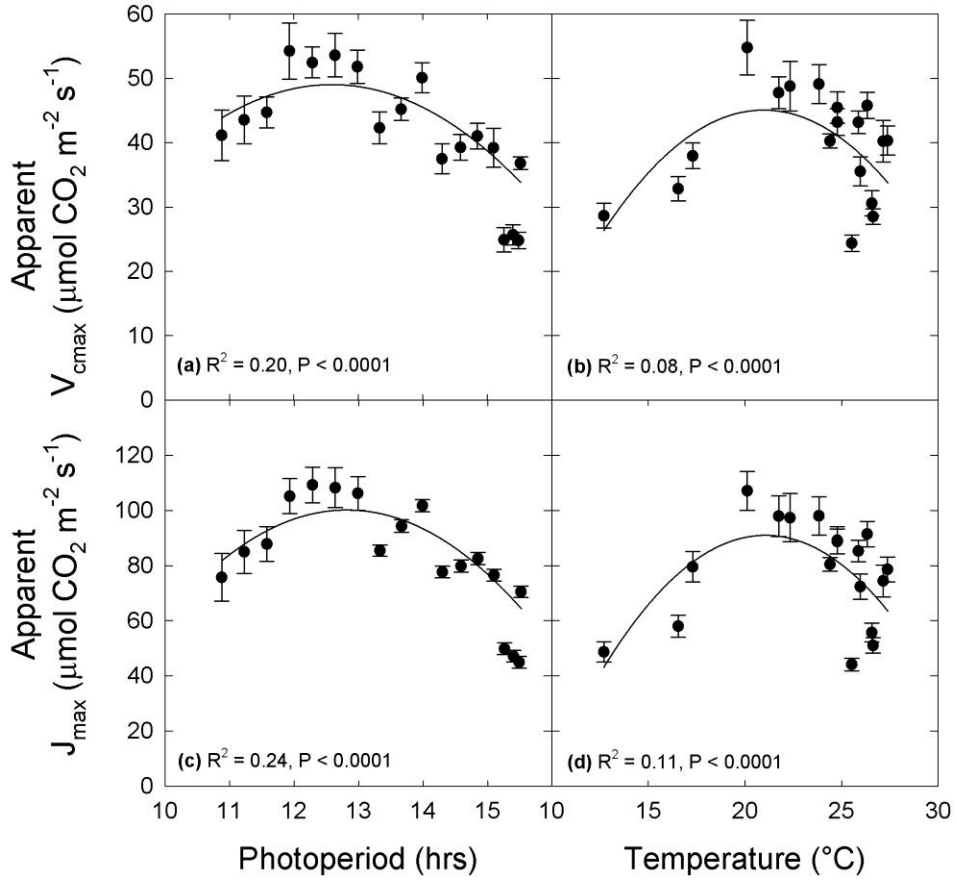

Figure 3.4. The apparent maximum rates of Rubisco carboxylation rate (apparent V_{cmax}, a, b) and electron transport (apparent J_{max}, c, d) correlated to photoperiod and temperature across the control, constant photoperiod and constant temperature treatments. Data presented as means ± s.e.m. *N* = 16 (for a and c: four seedlings per chamber, two chambers per treatment and two treatments per point, except at the highest photoperiod, which includes all seedlings in the constant photoperiod treatment so that *N* = 144; for b and d: four seedlings per chamber, two chambers per treatment and up to two treatments per point, except for week 0, which includes all seedlings from the constant temperature treatment). Regression equations: (a) $V_{cmax} = -231.7 + 44.6 \times \text{photoperiod} - 1.8 \times \text{photoperiod}^2$ (peak V_{cmax} at 12.4 hr photoperiod); (b) $V_{cmax} = -75.4 + 11.5 \times \text{temperature} - 0.3 \times \text{temperature}^2$ (peak V_{cmax} at 19.2 °C); (c) $J_{max} = -705.4 + 125.7 \times \text{photoperiod} - 4.9 \times \text{photoperiod}^2$ (peak J_{max} at 12.8 hr photoperiod); (d) $J_{max} = -212.8 + 28.8 \times \text{temperature} - 0.7 \times \text{temperature}^2$ (peak J_{max} at 20.6 °C).

When the apparent V_{cmax} was scaled to reflect the weekly growth temperatures (growth V_{cmax}; Fig. 3.5; Table 3.2), the pattern of V_{cmax} over time was similar in the control and constant photoperiod treatments, but there was a delayed decline in V_{cmax} in the warming seedlings, and a maintenance of V_{cmax} in the constant temperature treatment. Modelled A_{net} at growth temperatures diverged between treatments at the end of the experiment, with a higher A_{net} in the elevated temperature treatments relative to the control and constant photoperiod treatments (Fig. 3.5, Table 3.2).

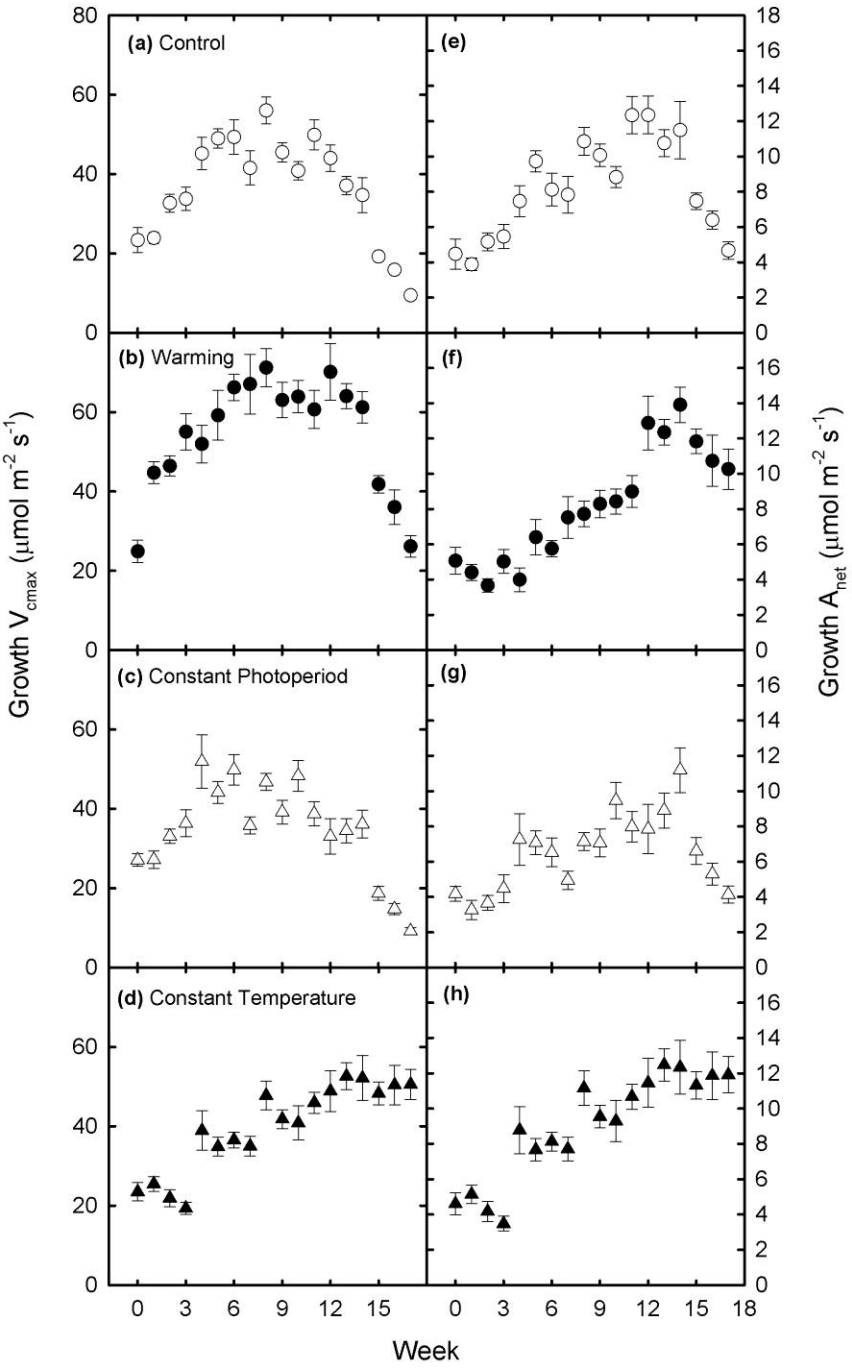

Figure 3.5. Apparent maximum rates of Rubisco carboxylation (Growth V_{cmax}; a, b, c, d) and net CO_2 assimilation rates (Growth A_{net}; e, f, g, h) modelled under weekly growth temperatures for the control (a, e), warming (b, f), constant photoperiod (c, g), and constant temperature (d, h) treatments. Data presented as means ± s.e.m. $N = 8$ (four seedlings per chamber and two chambers per point).

Table 3.2. ANOVA of photosynthetic and respiratory responses of *Picea glauca* to different autumn temperature and photoperiod regimes at their respective growth temperatures along with modelled weekly and cumulative carbon gain.

		Growth V_{cmax}	Growth A_{net}	Night R_{dark}	Weekly Net Carbon Gain	Net Cumulative Carbon Gain
Temperature	df	1,565	1,561		1,557	1,555
	F	20.2	15.5		46.85	3426
	P	**<0.0001**	**<0.0001**		**<0.0001**	**<0.0001**
Photoperiod	df	1,565	1,561		1,557	1,555
	F	87.3	27.4		9.38	1183
	P	**<0.0001**	**<0.0001**		0.064	**<0.0001**
Trial	df	1,565	1,561		1,557	1,555
	F	5.62	6.88		86.45	888
	P	**0.018**	**0.0090**		**<0.0001**	**<0.0001**
Treatment	df	3,565	3,561	3,40	3,557	3,555
	F	39.1	19.9	28.32	10.72	195
	P	**<0.0001**	**<0.0001**	**<0.0001**	**<0.0001**	**<0.0001**
Week	df	1,565	1,561	1,40	1,557	1,555
	F	7.50	0.007	0.026	100.079	1230
	P	**0.0064**	0.93	0.873	**<0.0001**	**<0.0001**
Temperature x Photoperiod	df		1,561		1,557	1,555
	F		35.4		19.90	13.46
	P		**<0.0001**		**0.0002**	**0.0075**
Temperature x Trial	df		1,561		1,557	1,555
	F		1.39		1.16	294
	P		0.24		0.99	**<0.0001**

Photoperiod x Trial	df		1,561		1,557	1,555
	F		0.034		0.09	129
	P		0.85		0.99	**<0.0001**
Treatment x Week	df	3,565	3,561	3,40	3,557	3,555
	F	20.82	12.2	1.35	3.99	82.03
	P	**<0.0001**	**<0.0001**	0.273	0.22	**<0.0001**
Treatment x Trial	df				3,557	3,555
	F				5.33	114
	P				**0.0017**	**<0.0001**
Week x Trial	df				3,557	1,555
	F				7.51	34.92
	P				0.60	**<0.0001**
Treatment x Week x Trial	df					3,555
	F					12.20
	P					**<0.0001**
Temperature x Photoperiod x Trial	df		1,561		1,557	
	F		4.08		9.01	
	P		0.44		0.079	
BIC		4753	3082	-32	1298	2407

Growth V_{cmax}: apparent maximum rate of Rubisco carboxylation at growth temperature; Growth A_{net}: net CO_2 assimilation rate at growth temperature; Night R_{dark}: dark respiration at night time growth temperature. Significant *P*-values are bolded ($P < 0.05$). Note: temperature and photoperiod refer to the weekly temperature and photoperiod experienced by the seedlings, while treatment denotes the integrated temperature and photoperiod regimes (i.e. control, warming, constant photoperiod, and constant temperature).

Leaf R_{dark} did not vary with time ($P > 0.05$). Averaged over the three measured weeks, R_{dark} in the control, warming and constant temperature seedlings was 2.64 ± 0.08 μmol m^{-2} s^{-1}, but R_{dark} was 79% greater than this in the constant photoperiod seedlings (4.73 ± 0.44 μmol m^{-2} s^{-1}) ($P < 0.0001$; Table 3.1). When R_{dark} was scaled to the growth temperatures, there were still no effects of time ($P > 0.05$, Table 3.2), but control seedlings had lower R_{dark} (0.34 ± 0.02 μmol m^{-2} s^{-1}) and constant temperature seedlings had higher R_{dark} (0.84 ± 0.04 μmol m^{-2} s^{-1}) than the constant photoperiod (0.59 ± 0.05 μmol m^{-2} s^{-1}) and warming (0.54 ± 0.03 μmol m^{-2} s^{-1}) treatment seedlings.

3.3.2 Foliar nitrogen did not change over time, while pigment concentrations increased

Mass-based foliar nitrogen concentrations did not respond to time (week, $P > 0.1$; Table 3.1; Fig. 3.6), and nitrogen concentration was slightly higher in the constant temperature treatment than in the other treatments (treatment, $P < 0.05$; Table 3.1). The leaf mass area (LMA) increased over time in all treatments (week, $P < 0.0001$; Table 3.1; Fig. 3.6) and seedlings from the constant temperature treatment generally had higher LMA than those from other treatments ($P < 0.0005$; Table 3.1). Because LMA increased over time, the constant mass-based nitrogen concentration translates to an increase in N per unit leaf area over the experiment in all treatments (data not shown).

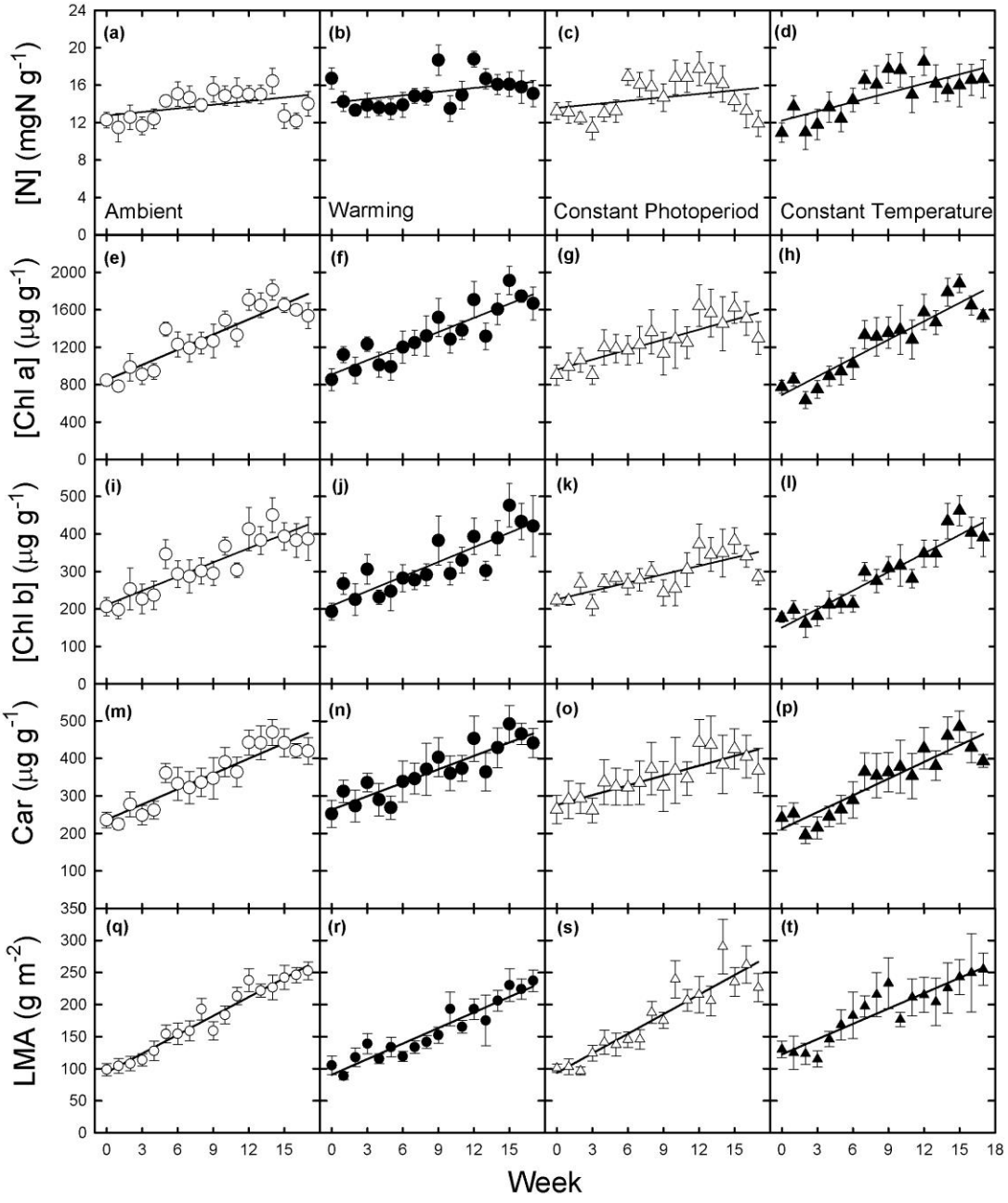

Figure 3.6. Foliar nitrogen concentrations, chlorophyll a and b concentrations (Chl a and b), carotenoid concentrations (Car), and leaf mass area (LMA) across time for the control (a, e, i, m, q), warming (b, f, j, n, r), constant photoperiod (c, g, k, o, s), and constant temperature (d, h, l, p, t) treatments. Data presented as means ± s.e.m. *N* = 8 (4 seedlings per chamber and 2 chambers per point).

Mass–based Chl a, Chl b, and carotenoid concentrations increased over time in all treatments (week, $P < 0.0001$; Table 3.3; Fig. 3.6), and were lower in the constant photoperiod treatment relative to other treatments (treatment, $P < 0.0001$), leading to significant effects of photoperiod and temperature on pigment concentrations ($P < 0.0001$ for all; Fig. 3.6). Although there were significant effects of trial on pigment concentrations, due to lower Chl a and carotenoid concentrations in trial 2, and higher Chl b concentrations toward the end of the experiment in trial 1 (Table 3.3), all pigments increased in concentration over time in both trials ($P < 0.05$, Table 3.3; Fig. 3.6). The Chl a:Chl b ratio was constant (4.4 ± 0.1) across weeks and treatments ($P > 0.05$ for both; Table 3.3).

Table 3.3. ANOVA of photosynthetic pigment responses of *Picea glauca* to different autumn temperature and photoperiod regimes.

		[Chl a]	[Chl b]	Chl a : Chl b	[Car]	J_{max} / [Total Chl]
Temperature	df	1,563	1,562		1,563	1,557
	F	69.94	54.76		73.41	7.09
	P	**<0.0001**	**<0.0001**		**<0.0001**	**0.0320**
Photoperiod	df	1,563	1,562		1,563	1,557
	F	181.66	168.00		171.99	0.19
	P	**<0.0001**	**<0.0001**		**<0.0001**	0.66
Trial	df	1,563	1,562	1,560	1,563	1,557
	F	258.58	67.05	8119.81	790.37	89.58
	P	**<0.0001**	**<0.0001**	**<0.0001**	**<0.0001**	**<0.0001**
Treatment	df	3,563	3,562	3,560	3,563	3,557
	F	20.84	14.05	3.50	25.67	2.19
	P	**<0.0001**	**<0.0001**	0.0918	**<0.0001**	0.27
Week	df	1,563	1,562	1,560	1,563	1,557
	F	56.32	29.12	0.10	57.15	192.52
	P	**<0.0001**	**<0.0001**	1.00	**<0.0001**	**<0.0001**
Temperature x Photoperiod	df					
	F					
	P					
Temperature x Trial	df		1,562			
	F		7.94			
	P		**0.010**			
Photoperiod x Trial	df	1,563	1,562		1,563	1,557

	F	16.05	53.75		5.14	4.30
	P	**0.0002**	**<0.0001**		**0.0480**	**0.0480**
Treatment x Week	df			3,560		
	F			6.08		
	P			**0.0031**		
Treatment x Trial	df	3,563	3,562	3,560	3,563	3,557
	F	16.44	12.11	6.59	19.62	0.70
	P	**<0.0001**	**<0.0001**	**0.0015**	**<0.0001**	0.5500
Week x Trial	df	1,563	1,562	1,560	1,563	
	F	9.00	9.29	4.52	12.00	
	P	**0.0145**	**0.0145**	0.09	**0.0040**	
Treatment x Week x Trial	df			3,560		3,557
	F			5.00		3.56
	P			**0.0039**		**0.0140**
BIC		8437	6963	-1225	6773	-377

[Chl a]: chlorophyll a concentration; [Chl b]: chlorophyll b concentration; [Car]: carotenoid concentration. Significant *P*-values are bolded ($P < 0.05$). Note: temperature and photoperiod refer to the weekly temperature and photoperiod experienced by the seedlings, while treatment denotes the integrated temperature and photoperiod regimes (i.e. control, warming, constant photoperiod, and constant temperature).

3.3.3 Declines in photosynthetic capacity were associated with changes in nitrogen allocation

The ratio of apparent V_{cmax} to nitrogen concentration (an indication of the investment of N in Rubisco carboxylation) declined over time ($P < 0.0001$), an effect driven by the trends in the control and constant photoperiod treatments, with no significant effects of photoperiod, trial or treatment ($P > 0.05$) (Table 3.1; Fig. 3.7). There was a significant effect of temperature ($P < 0.0001$) and a temperature × photoperiod interaction ($P < 0.005$) on the ratio of apparent V_{cmax} to nitrogen concentration, indicating that high growth temperatures, even under short photoperiods, maintain a high apparent V_{cmax}/nitrogen concentration ratio (Table 3.1; Fig. 3.7). In contrast, the ratio of apparent J_{max}/[total Chl] (an indication of electron transport capacity relative to light capture, such that a decrease would suggest increased energy dissipation) declined in a similar manner across time in all treatments (week, $P < 0.0001$; treatment, $P = 0.27$; Table 3.3; Fig. 3.7).

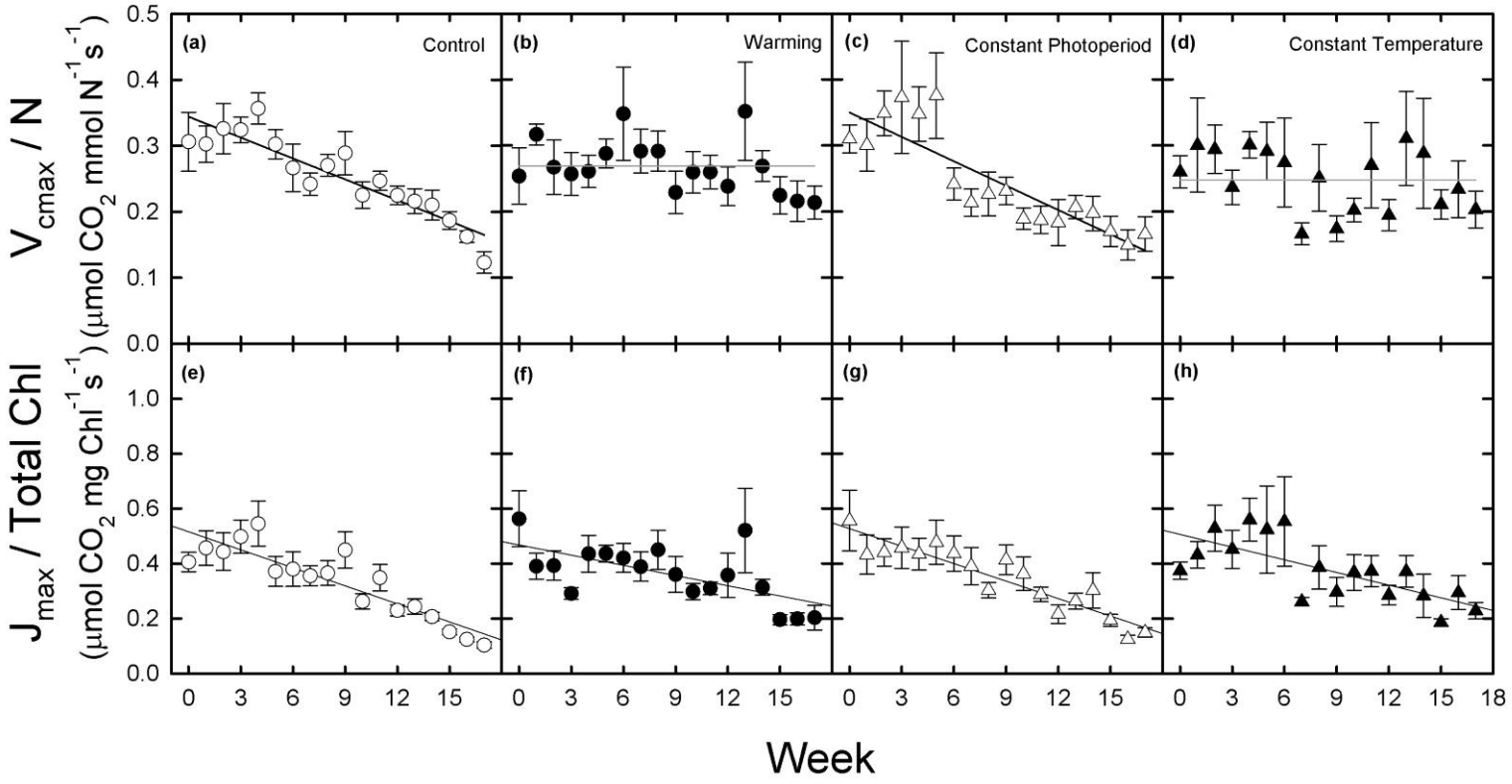

Figure 3.7. Apparent V_{cmax} on a nitrogen-basis (V_{cmax} /N; a, b, c, d) and apparent J_{max} on a chlorophyll-basis (J_{max}/total Chl; e, f, g, h) across time for the control (a, e), warming (b, f), constant photoperiod (c, g), and constant temperature (d, h) treatments. Data presented as means ± s.e.m. *N* = 8 (4 seedlings per chamber and 2 chambers per point).

3.3.4 Decreases in apparent V_{cmax} were associated with increases in Rubisco

Initial Rubisco concentrations (at week 0) did not differ among treatments ($F_{3,12}$ = 2.19, P = 0.142) and while Rubisco concentrations generally increased over time (week, P < 0.001; Table 3.1), this was driven by increases in Rubisco concentration in the control and constant photoperiod treatments (Fig. 3.8), which both experienced control temperatures. Rubisco concentration was not correlated with V_{cmax} (P = 0.20; Fig. 3.8; Table 3.4). However, when the Rubisco-V_{cmax} relationship was examined through time, there was an initial linear relationship between V_{cmax} and Rubisco concentration in the two control temperature treatments (control and constant photoperiod treatments) that was disrupted late in the experiment when weekly day/night temperatures dropped to 12.7/3.7 °C; this trajectory was not seen in the elevated temperature treatments (Fig. 3.8). Rubisco concentration was correlated with nitrogen concentration across the entire data set (P < 0.001; Table 3.4), a relationship also driven by correlations between Rubisco concentrations and nitrogen concentrations in the control and constant photoperiod treatments (P = 0.028; Table 3.4; Fig. 3.8), but not in the treatments with elevated growth temperatures.

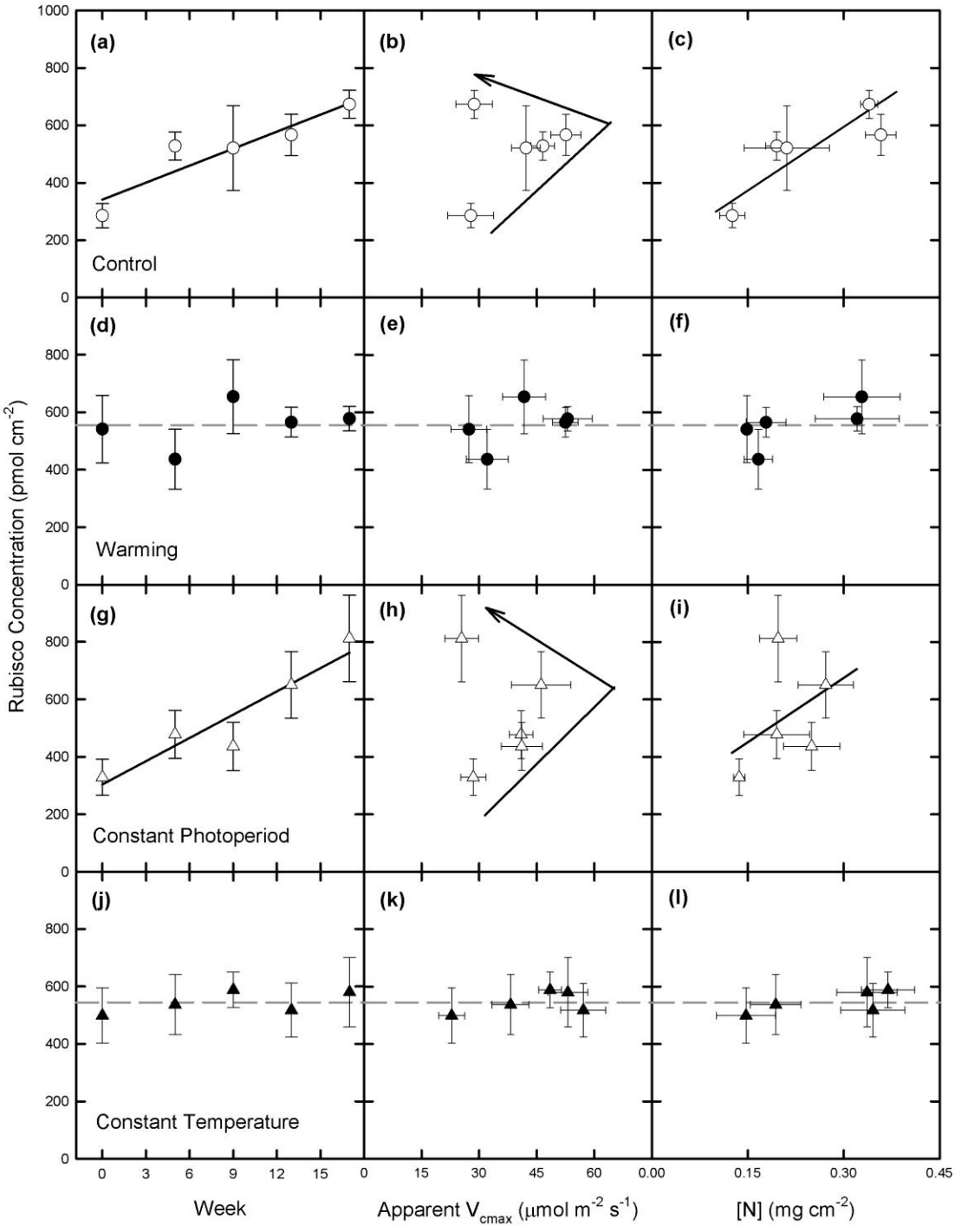

Figure 3.8. Rubisco concentrations versus (a, d, g, j) time, b, e, h, k) apparent V_{cmax} and (c, f, i, l) leaf N for the control (a, b, c), warming (d, e, f), constant photoperiod (g, h, i) and constant temperature (j, k, l) treatments. Rubisco content is significantly

correlated with: time in a) $R^2 = 0.38$, $P < 0.005$ and b) $R^2 = 0.42$, $P < 0.005$ and nitrogen in g) $R^2 = 0.69$, $P < 0.001$ and i) $R^2 = 0.24$, $P < 0.05$. Dashed grey lines indicate means, and vectors in b) and h) indicate time to illustrate the relationship between Rubisco and V_{cmax} over the experiment. Data presented as means ± s.e.m. $N = 4$ seedlings per point (2 seedlings per chamber and 2 chambers per point).

Table 3.4. ANOVA of Rubisco concentrations as a function of foliar nitrogen concentration or maximum Rubisco carboxylation rate (V_{cmax}) across treatments. Significant P-values are bolded ($P < 0.05$).

		Rubisco concentration vs. nitrogen concentration	Rubisco concentration vs. V_{cmax}
(V_{cmax} or nitrogen concentration)	df	1,72	1,72
	F	16.4	1.64
	P	**0.0001**	0.2
Treatment	df	3,72	3,72
	F	0.18	0.13
	P	0.91	0.94
(V_{cmax} or nitrogen concentration) * Treatment	df	3,72	3,72
	F	3.22	0.38
	P	**0.028**	0.77
BIC		1089	1111

3.3.5 Biomass accumulation responds to photoperiod, not temperature

Seedlings in the constant photoperiod treatment had significantly higher biomass (43.5 ± 5.3 g) and height (28.7 ± 6.0 cm) by the end of the experiment than those in the control (30.0 ± 6.5 g, 20.8 ± 3.9 cm) and warming treatments (26.7 ± 5.1 g, 20.7 ± 4.4 cm), while seedlings from the constant temperature treatment were smaller and shorter than all other treatments (24.5 ± 4.0 g, 18.1 ± 1.6 cm) (treatment; $P < 0.001$; Table 3.5; Figs. 3.9a-d,i-l). Despite differences in growth trajectory, allocation to leaves and roots was consistent across treatments over time ($P > 0.5$; Table 3.5, Figs. 3.9e-h). Allocation to stems significantly varied between treatments (Table 3.5), but this was due to small variance around the means and not considerable variation in stem mass ratio (SMR; 0.199 ± 0.004, 0.189 ± 0.003, 0.206 ± 0.004, 0.202 ± 0.004 for the control, warming, constant photoperiod, and constant temperature seedlings, respectively). When biomass was plotted against either accumulated temperature sums or accumulated irradiance, the constant photoperiod treatment seedlings had significantly faster growth compared to other treatments ($P < 0.0001$; Table 3.6; Fig. 3.10). This indicates that the constant photoperiod treatment seedlings were not larger because they had more hours of light to photosynthesize, a result that also held when the last two weeks of growth (where seedling biomass increased considerably in the constant photoperiod treatment) were omitted from the analysis (data not shown). In contrast, the warming treatment had the lowest growth rate of all treatments, a response that occurred even before the seedlings accumulated a greater temperature sum than the other treatments (Table 3.6, Fig. 3.10).

Table 3.5. ANOVA for leaf mass ratio (LMR), stem mass ratio (SMR), root mass ratio (RMR), and seedling height (H).

Parameter		Biomass	LMR	SMR	RMR	H
Week	df	1,560	1,560	1,566	1,560	1,560
	F	424.58	686	113	371	47.8
	P	**<0.0001**	**<0.0001**	**<0.0001**	**<0.0001**	**<0.0001**
Treatment	df	3,560	3,560	3,566	3,560	3,560
	F	23.27	0.762	4.56	0.716	13.7
	P	**<0.0001**	0.52	**0.0036**	0.54	**<0.0001**
Trial	df	1,560	1,560	1,566	1,560	1,560
	F	42.73	38.3	2.6	27.4	611
	P	**<0.0001**	**<0.0001**	0.11	**<0.0001**	**<0.0001**
Week * Treatment	df	3,560	3,560		3,560	3,560
	F	16.11	8.26		5.14	4.42
	P	**<0.0001**	**<0.0001**		**0.0016**	**0.0044**
Week * Trial	df	1,560	1,560	1,566	1,560	1,560
	F	0.31	1.63	10.5	0.186	47.8
	P	0.58	0.2	**0.0013**	0.67	**<0.0001**
Treatment * Trial	df	3,560	3,560	3,566	3,560	3,560
	F	24.92	0.467	4.15	1.19	14.7
	P	**<0.0001**	0.71	**0.0064**	0.31	**<0.0001**
Week * Treatment * Trial	df	3,560	3,560		3,560	3,560
	F	15.08	8		7.42	4.65
	P	**<0.0001**	**<0.0001**		**<0.0001**	**0.0032**
BIC		4326	-1136	-1973	-1048	3735

Significant P-values are bolded ($P < 0.05$). Note: temperature and photoperiod refer to the weekly temperature and photoperiod experienced by the seedlings, while treatment denotes the integrated temperature and photoperiod regimes (i.e. control, warming, constant photoperiod, and constant temperature).

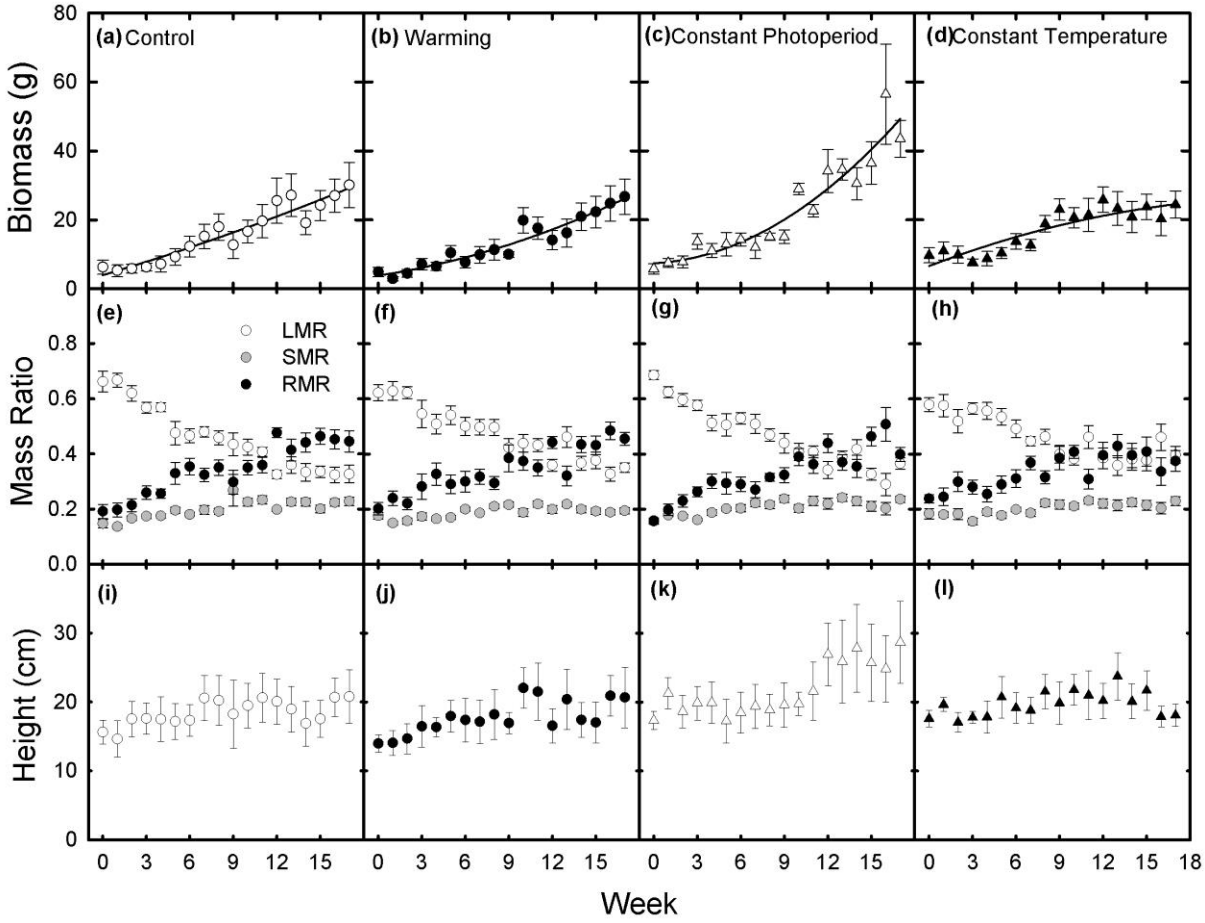

Figure 3.9. Weekly changes in (a, b, c, d) biomass, (i, j, k, l) height, (e, f, g, h) leaf mass ratio (LMR), stem mass ratio (SMR), and root mass ratio (RMR) for the control (a, e, i), warming (b, f, j), constant photoperiod (c, g, k), and constant temperature (d, h, l) treatments. *N* = 8 (4 seedlings per chamber and 2 chambers per point).

Table 3.6. ANOVA of biomass as a function of accumulated irradiance or degree days across treatments. Significant P-values are bolded ($P < 0.05$).

Parameter		Biomass vs. Irradiance	Biomass vs. Degree Days
Irradiance or Degree Days	df	1,560	1,560
	F	624	534
	P	**<0.0001**	**<0.0001**
Treatment	df	3,560	3,560
	F	23.7	53.7
	P	**<0.0001**	**<0.0001**
Trial	df	1,560	1,560
	F	176	176
	P	**<0.0001**	**<0.0001**
(Irradiance or Degree Days) * Treatment	df	3,560	3,560
	F	7.72	9
	P	**<0.0001**	**<0.0001**
(Irradiance or Degree Days) * Trial	df	1,560	1,560
	F	20.8	11.3
	P	**<0.0001**	**0.0008**
Treatment * Trial	df	3,560	3,560
	F	29.6	32.1
	P	**<0.0001**	**<0.0001**
(Irradiance or Degree Days) * Treatment * Trial	df	3,560	3,560
	F	5.1	5.85
	P	**0.0017**	**0.0006**
BIC		1078	1076

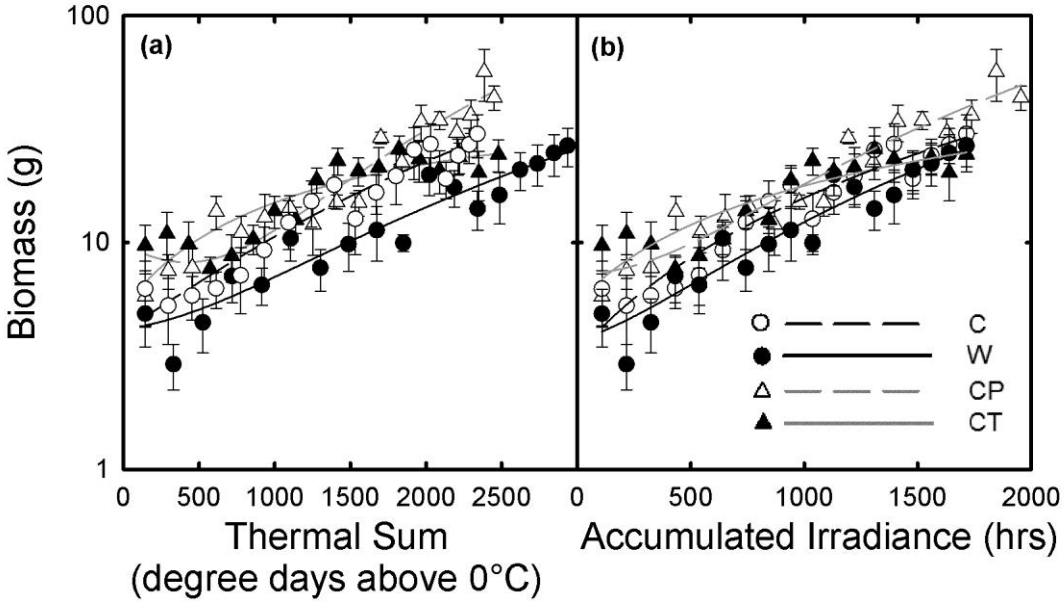

Figure 3.10. Biomass as a function of (a) thermal sum and (b) accumulated irradiance. Treatments are coded as follows: C, control; W, warming; CP, constant photoperiod; CT, constant temperature. Data presented as means ± s.e.m. *N* = 8 (4 seedlings per chamber and 2 chambers per point). Note the log scale for biomass.

Modelled weekly net carbon gain showed a peaked seasonal trajectory that differed among treatments ($P < 0.0001$) and with weekly growth temperature ($P < 0.0001$) (Table 3.2; Fig. 3.11). The modelled cumulative net carbon gain showed complex statistical interactions (Table 3.2), but seedlings in the control and warming treatments had lower cumulative net carbon gain than those from the constant temperature and constant photoperiod treatments (Fig. 3.11). Measured biomass was consistent with modeled cumulative net carbon gain in the control, warming, and constant photoperiod treatments, but not in the constant temperature treatment, suggesting that carbon was allocated to carbon sinks other than growth in the constant temperature seedlings (Fig. 3.12).

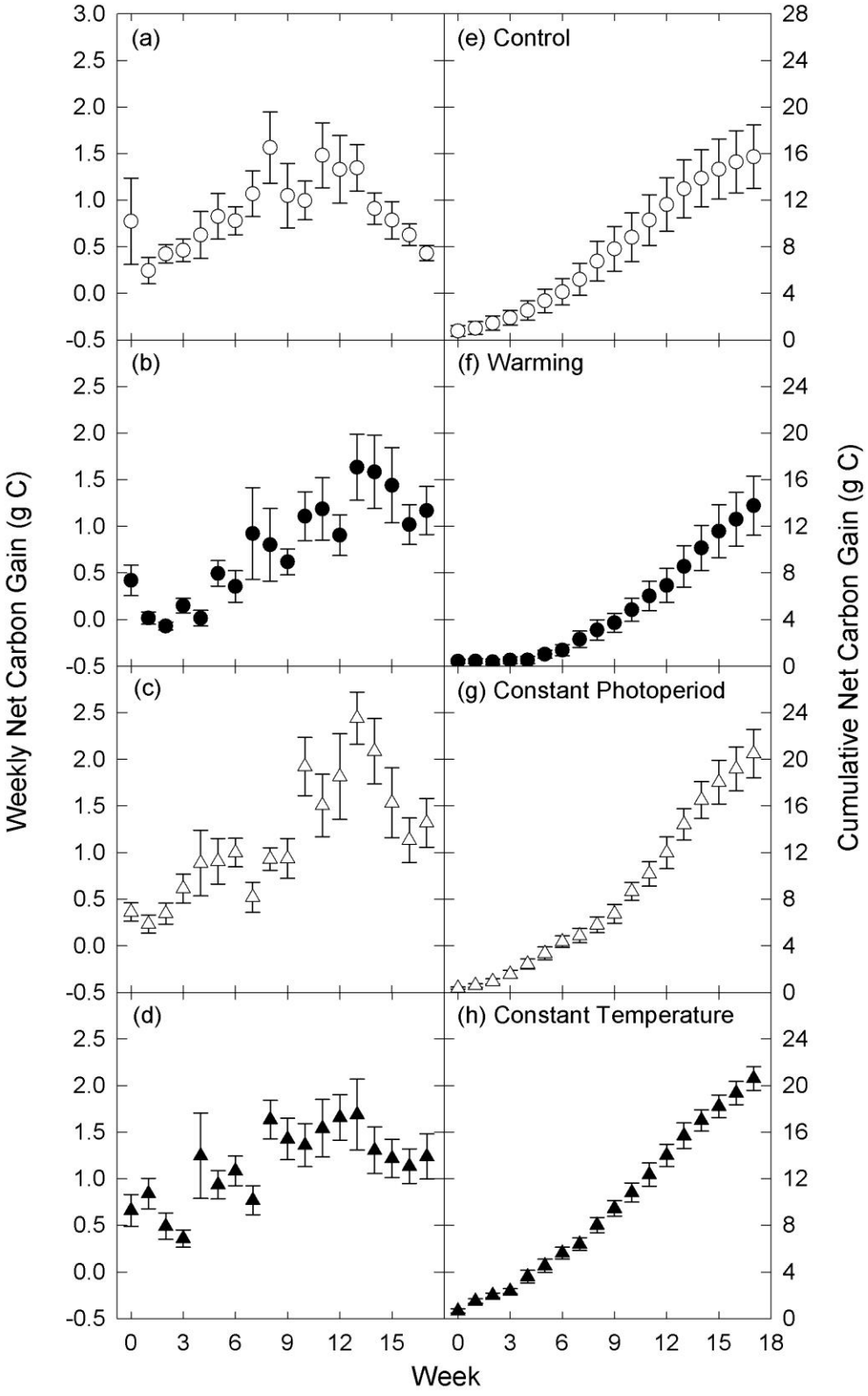
(a)
(e) Control
(b)
(f) Warming
(c)
(g) Constant Photoperiod
(d)
(h) Constant Temperature
Weekly Net Carbon Gain (g C)
Cumulative Net Carbon Gain (g C)
Week
3.0
2.5
2.0
1.5
1.0
0.5
0.0
-0.5
28
24
20
16
12
8
4
0
0 3 6 9 12 15
0 3 6 9 12 15 18

Figure 3.11. Modelled (a, b, c, d) weekly net carbon gain and (e, f, g, h) cumulative net carbon gain across the experiment for the control (a, e), warming (b, f), constant photoperiod (c, g), and constant temperature (d, h) treatments. Data presented as means ± s.e.m (of total number of individuals, *N* = 8). *N* = 4 seedlings per chamber and 2 chambers per point.

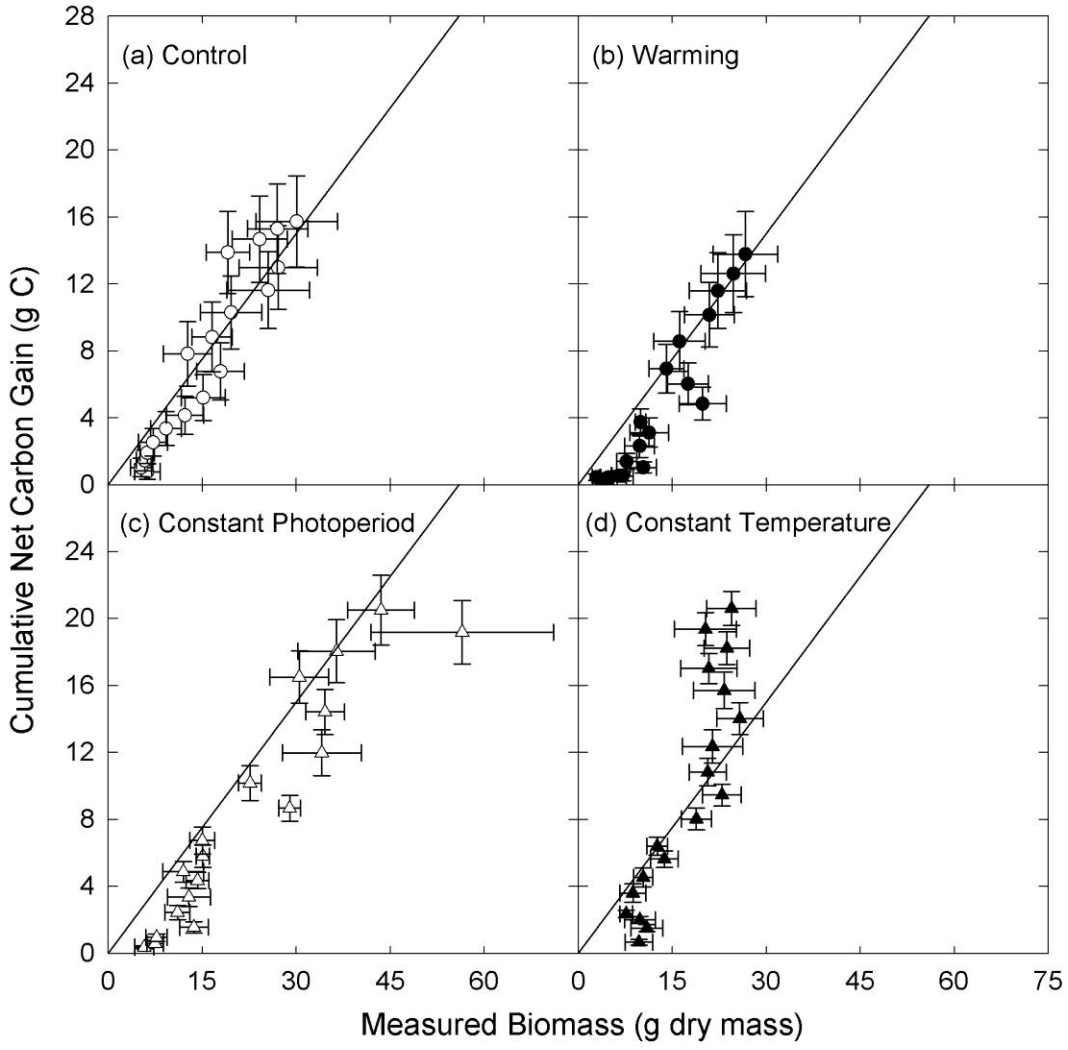

Figure 3.12. Modelled cumulative net carbon gain versus measured biomass. Solid line indicates the expected relationship if all carbon from cumulative net carbon gain was used in biomass (assumed to be 50% carbon). (a) control treatment, (b) warming treatment, (c) constant photoperiod treatment, (d) constant temperature treatment. Data presented as means ± s.e.m (of total number of individuals, *N* = 8). *N* = 4 trees per chamber and 2 chambers per point.

3.4 Discussion

Warmer temperatures caused the seedlings to maintain photosynthetic capacity even at low photoperiods, implying that climate warming could stimulate the duration of carbon uptake in seedlings, and possibly mature trees, in northern forests. Regardless of whether elevated temperatures were imposed with a 5°C warming or with a constant day/night temperature, both V_{cmax} and J_{max} were stimulated compared to control temperature treatments (control and constant photoperiod). In both the elevated temperature treatments (warming and constant temperature), these high photosynthetic capacities were associated with a constant ratio of V_{cmax}/N (per unit leaf area) and stable Rubisco concentrations. In the control temperature treatments, low photosynthetic capacities towards the end of the experiment were correlated with decreases in the ratio of V_{cmax}/N but an *increase* in Rubisco concentrations, implying that Rubisco accumulated as a nitrogen storage protein (which has been observed in *Eucalyptus* spp. (Warren *et al*., 2003), *Nicotiana tabacum* L. (Stitt & Schulze, 1994), *Pinus sylvestris* L. (Warren *et al*., 2000), and in the tropical species *Licania unguiculata* Prance (Bahar *et al.*, 2017)). In contrast to my photosynthetic results, biomass and respiration rates responded to photoperiod, while warmer temperatures suppressed growth.

3.4.1 Warming maintained photosynthetic capacity despite short photoperiods

Exposure to warmer temperatures under declining photoperiods representative of autumn field conditions maintained high photosynthetic capacity in white spruce seedlings, which should allow this species to continue fixing CO_2 at a high rate later into the autumn as the climate warms. I previously found that 4 °C warming stimulates V_{cmax} and J_{max} under short photoperiods in Norway spruce (Stinziano *et al.*, 2015), and the data presented here demonstrate that autumn temperatures affect photosynthetic and leaf biochemistry dynamics regardless of whether seedlings are exposed to long photoperiods or realistic declines in photoperiod. The stimulation of photosynthetic capacity under warming and short photoperiods in seedlings is also consistent with large-scale patterns of enhanced CO_2 uptake in northern forests in warmer autumns (e.g. Keenan *et al.*, 2014), hinting that these patterns may be more broadly applicable to mature trees as well.

In temperate deciduous trees, declines in photosynthetic capacity in the late summer and autumn were more strongly correlated with photoperiod than temperature (Bauerle *et al*., 2012). While I also found a stronger correlation between apparent V_{cmax} or J_{max} and photoperiod than with temperature, this relationship did not limit the ability of warming to stimulate photosynthetic capacity at short photoperiods, and I found no evidence for a direct effect of photoperiod on V_{cmax}. The difference between these two data sets may indicate that photosynthetic responses to photoperiod differ between plant functional types or vary with tree age.

3.4.2 Leaf biochemistry responses to temperature and photoperiod

Down regulation of photosynthetic capacity in the control temperature treatments was associated with a decline in photosynthetic nitrogen use efficiency (apparent V_{cmax}/nitrogen concentration). This decline in apparent V_{cmax} and the apparent V_{cmax}/N ratio occurred even though Rubisco concentrations increased over the experiment, leading to an uncoupling of the expected relationship between leaf N, apparent V_{cmax} and Rubisco concentration in the last weeks of the experiment, and a curvilinear relationship between apparent V_{cmax} and Rubisco concentrations (Fig. 3.8). The increasing Rubisco concentration and decreasing apparent V_{cmax} in the control temperature treatments suggests that Rubisco was used as a nitrogen storage protein (i.e. inactive Rubisco is accumulated for nitrogen storage; Stitt & Schulze, 1994; Warren *et al*., 2000, Bahar *et al*., 2017), which is common, especially in evergreen trees (Quick *et al.*, 1992; Warren *et al.*, 2003; Millard *et al.*, 2007).

In the warming treatments, high photosynthetic capacity was correlated with a high and stable apparent V_{cmax}/N ratio: on a leaf area basis, apparent V_{cmax} increased over the experiment and so did leaf nitrogen concentration. However, this did not result from an increase in Rubisco concentrations over the same time period. Instead, in both the elevated temperature treatments, Rubisco concentrations were constant, implying that cooler temperatures were required to initiate the build-up of Rubisco as a storage protein. Indeed, the break in the relationship between V_{cmax} and Rubisco in the control temperature treatments (Figs. 3.8b and h) occurred when day/night temperatures dropped

to 12.7/3.7 °C, temperatures cooler than those experienced in the elevated temperature treatments. As Rubisco concentrations were constant in the elevated temperature treatments, there was no correlation between Rubisco concentrations and apparent V_{cmax} or leaf nitrogen concentration. Rubisco is an intricately controlled enzyme whose *in vivo* activity is dependent on leaf energy status, the activity of a chaperone protein, Rubisco activase, and the CO_2 concentrations around the enzyme, among other factors (Carmo-Silva *et al.*, 2015). While I do not have Rubisco activation state data, increases in the activation state of Rubisco as the experiment progressed could have led to the higher apparent V_{cmax} measured in later weeks. High growth temperatures could also have increased mesophyll conductance, increasing chloroplastic CO_2 concentrations around Rubisco, thereby increasing my measurements of apparent V_{cmax}. High measurement temperatures generally increase mesophyll conductance, though the strength of this response varies between species (von Caemmerer & Evans, 2015), and the response of mesophyll conductance to growth temperature is variable and currently unclear (Lewis *et al*., 2015).

In contrast to the variable pattern of apparent V_{cmax} /Rubisco between treatments, apparent J_{max}/[Chl] declined over time in all treatments, a result driven mainly by increases in chlorophyll concentrations in all treatments. While chlorophyll and carotenoid concentrations often increase during autumn in conifers (Chang *et al*., 2015; Stinziano *et al.*, 2015; Wong & Gamon, 2015), pigment concentrations in my study were unaffected. The decrease in apparent J_{max}/[Chl] suggests an increase in energy dissipation away from photochemical quenching for CO_2 assimilation towards nonphotochemical quenching, which has been observed in *Pinus banksiana* Lamb. where both low temperature and short photoperiods can separately induce increased nonphotochemical quenching (Busch *et al*., 2007). Apparent J_{max} did not co-vary with pigment concentrations, but was co-regulated with apparent V_{cmax}, emphasizing the importance of maintaining a balance between electron transport and the Calvin cycle.

3.4.3 Growth was strongly stimulated by long photoperiods but not warming

Photoperiod, but not warming, stimulated biomass accumulation. Growth cessation in many conifers is known to be sensitive to photoperiod (Gyllenstrand *et al*., 2007; Holliday *et al*., 2008; Hamilton *et al*., 2016), so photoperiod cues may prevent north-temperate and boreal conifers from extending their growing season in warmer autumn. The stimulation of growth under constant photoperiod was not simply due to having more hours of light to photosynthesize, as growth plotted against accumulated irradiance shows the constant photoperiod seedlings grow faster for a given amount of light than in other treatments, and is thus likely related to photoperiod cues on growth *per se*. The rate of biomass accumulation was lowest in seedlings experiencing elevated temperatures, despite ample access to water and nutrients. Warming often suppresses growth in conifers (Way & Oren, 2010) and spruce may be particularly sensitive to temperature increases (Way & Sage, 2008b; Kroner & Way, 2016). Phytochrome activity may explain the reduced growth at high temperatures and the enhanced growth at long photoperiods, since phytochromes act as both temperature sensors and light sensors in regulating growth (Jung *et al*., 2016; Legris *et al*., 2016). Specifically, Legris *et al*. (2016) found that phytochrome B activity declined at higher temperatures, and since light is also required for phytochrome function, low photoperiods and high temperatures may suppress seedling growth by suppressing phytochrome signalling, while constant photoperiod maintains the phytochrome activity necessary for continued growth.

While growth rates varied between treatments, the relative biomass allocation strategy was remarkably constant across the different growth conditions. Although shoot growth may be more photoperiod-driven and root growth more correlated with temperature in some experiments (Bigras & D'Aoust, 1993; Hamilton *et al*., 2016), leaf, stem and root growth were all greatest under the long photoperiods of the constant photoperiod treatment. It is important to note however, that growth patterns change with age (Ununger *et al*., 1988), and can be quite different in first year seedlings than in older trees.

3.4.4 Carbon uptake and growth respond to different seasonal cues

Although elevated temperature maintained photosynthetic capacity in my study, it had little effect on growth, while long photoperiods allowed biomass to accumulate rapidly even at low temperatures. The differential responses of photosynthetic traits and growth to temperature and photoperiod could lead to a desynchronization of the carbon uptake period and the period of active growth as the climate warms. This desynchronization would have important implications for ecosystem-level carbon fluxes if these results hold in mature trees. The finding of increased carbon uptake rates and capacity but no concurrent stimulation of biomass under the elevated temperature treatments also suggests that the extra fixed carbon is being directed to processes other than growth. While this appears to be the case in the constant temperature treatment seedlings, where biomass accumulated more slowly than my cumulative net carbon gain model predicted, the reduced biomass in the (more ecologically realistic) warming treatment was predicted based on cumulative net carbon gain, implying that extreme warming is required to disrupt the carbon gain/growth relationship. The control of growth by photoperiod rather than temperature could be adaptive, as shutting down growth based on photoperiod could reduce the risk of frost damage to the seedling, while continued carbon uptake would allow for enhanced carbon storage to ensure adequate energy supplies for respiration during winter.

There was no evident thermal acclimation of R_{dark}, and R_{dark} at growth temperatures was higher in the elevated temperature treatments than the control temperature treatment, which had the lowest R_{dark}. Thus, instead of being allocated to biomass, the increase in carbon uptake went hand in hand with greater respiration rates and the extra carbon was invested in labile carbon pools with short residency times. If this holds true in natural systems, CO_2 fixed during warm autumns may cycle back to the atmosphere quickly, rather than entering recalcitrant carbon pools, limiting the impact of increased photosynthesis during the autumn on offsetting anthropogenic CO_2 emissions.

3.5 References

Aitchison J. **1986**. *The statistical analysis of compositional data*. Chapman and Hall: London, UK.

Amundson RG, Hadley JL, Funcher JF, Fellows S, Alscher RG. **1992**. Comparisons of seasonal changes in photosynthetic capacity, pigments, and carbohydrates of healthy sapling and mature red spruce and of declining and healthy red spruce. *Canadian Journal of Forest Research* **22**, 1605–1616.

Atkin OK, Tjoelker MG. **2003**. Thermal acclimation and the dynamic response of plant respiration to temperature. *Trends Plant Science* **8**, 343–351.

Ayub G, Smith RA, Tissue DT, Atkin OK. **2011**. Impacts of drought on leaf respiration in darkness and light in *Eucalyptus saligna* exposed to industrial-age atmospheric CO_2 and growth temperature. *New Phytologist* **190**, 1003–1018.

Badger MR, Collatz GJ. **1977**. Studies on the kinetic mechanism of ribulose-1,5-bisphosphate carboxylase and oxygenase reactions, with particular reference to the effect of temperature on kinetic parameters. *Carnegie Institution Washington Year Book* **76**, 355–361.

Bahar NHA, Ishida FY, Weerasinghe LK, *et al*. 2017. Leaf-level photosynthetic capacity in lowland Amazonian and high-elevation Andean tropical moist forests of Peru. *New Phytologist* **214**, 1002–1018.

Barichivich J, Briffa KR, Myeni RB, Osborn TJ, Melvin TM, Ciais P, Piao S, Tucker C. **2013**. Large-scale variations in the vegetation growing season and annual cycle of atmospheric CO_2 at high northern latitudes from 1950 to 2011. *Global Change Biology* **19**, 3167–3183.

Basler D, Körner C. **2012**. Photoperiod sensitivity of bud burst in 14 temperate forest tree species. *Agricultural & Forest Meteorology* **165**, 73–81.

Bauerle WL, Oren R, Way DA, Qian SS, Stoy PC, Thornton PE. **2012**. Photoperiodic regulation of the seasonal pattern of photosynthetic capacity and the implications for carbon cycling. *Proceedings of the National Academy of Sciences of the United States of America* **109**, 8612–8617.

Bigras FJ, D'Aoust AL. **1993**. Influence of photoperiod on shoot and root frost tolerance and bud phenology of white spruce seedlings (*Picea glauca*). *Canadian Journal of Forest Research* **23**, 219–228.

Bronson DR, Gower ST, Tanner M, Van Herk I. **2009**. Effect of ecosystem warming on boreal black spruce bud burst and shoot growth. *Global Change Biology* **15**, 1534–1543.

Buermann W, Bikash PR, Jung M, Burn DH, Reichstein M. **2013**. Earlier springs decrease peak summer productivity in North American boreal forests. *Environmental Research Letters* **8**, 24027–24036.

Busch F, Hüner NPA, Ensminger I. **2007**. Increased air temperature during simulated autumn conditions does not increase photosynthetic carbon gain but affects the dissipation of excess energy in seedlings of the evergreen conifer Jack pine. *Plant Physiology* **143**, 1242–51.

Busch F, Hüner NPA, Ensminger I. **2008**. Increased air temperature during simulated autumn conditions impairs photosynthetic electron transport between photosystem II and photosystem I. *Plant Physiology* **147**, 402–14.

Carmo-Silva E, Scales JC, Madgwick PJ, Parry MJ. **2015**. Optimizing Rubisco and its regulation for greater resource use efficiency. *Plant, Cell and Environment* **38**, 1817–1832.

Caspar T, Huber SC, Somerville C. **1985**. Alterations in growth, photosynthesis, and respiration in a starchless mutant of *Arabidopsis thaliana* (L.) deficient in chloroplast phosphoglucomutase activity. *Plant Physiology* **79**, 11–17.

Chang CY, Unda F, Zubilewich A, Mansfield SD, Ensminger I. **2015**. Sensitivity of cold acclimation to elevated autumn temperature in field-grown *Pinus strobus* seedlings. *Frontiers in Plant Science* **6**, 165.

Collins M, Knutti R, Arblaster J, *et al*. **2013**. Long-term climate change: projections, commitments and irreversibility. In: *Climate Change 2013: The Physical Science Basis. Contribution of Working Group I to the Fifth Assessment Report of the Intergovernmental Panel on Climate Change*, edited by **Stocker TF, Qin D, Plattner G-K, Tignor M, Allen SK, Boschung J, Nauels A, Xia Y, Bex V, Midgley PM**. Cambridge University Press: Cambridge, UK.

Danby RK, Hik DS. **2007**. Responses of white spruce (*Picea glauca*) to experimental warming at a subarctic alpine treeline. *Global Change Biology* **13**, 437–451.

Delpierre N, Vitasse Y, Chuine I, Guillemot J, Bazot S, Rutishauser T, Rathgeber CBK. **2016**. Temperate and boreal forest tree phenology: from organ-scale processes to terrestrial ecosystem models. *Annals of Forest Science* **73**, 5–25.

Deslauriers A, Beaulieu M, Balducci L, Giovannelli A, Gagnon MJ, Rossi S. **2014**. Impact of warming and drought on carbon balance related to wood formation in black spruce. *Annals of Botany* **114**, 335–345.

Dormling I, Gustafsson A, von Wettstein D. **1968**. The experimental control of the life cycle in *Picea abies* (L.) Karst. *Silvae Genetica* **17**, 44–64.

Downs RJ, Borthwick HA. **1956**. Effects of photoperiod on growth of trees. *Botanical Gazette* **117**, 310–326.

Evans JR. **1989**. Photosynthesis and nitrogen relationship in leaves of C_3 plants. *Oecologia* **78**, 9–19.

Farquhar GD, Wong SC. **1984**. An empirical model of stomatal conductance. *Australian Journal of Plant Physiology* **11**, 191–210.

Farquhar G, von Caemmerer S, Berry JA. **1980**. A biochemical model of photosynthetic CO_2 assimilation in leaves of C_3 species. *Planta* **149**, 78–90.

Fu YH, Piao S, Op de Beeck M, Cong N, Zhao H, Zhang Y, Menzel A, Janssens IA. **2014**. Recent spring phenology shifts in western Central Europe based on multiscale observations. *Global Ecology & Biogeography* **23**, 1255–1263.

Gitelson AA, Peng Y, Arkebauer TJ, Suyker AE. **2015**. Productivity, absorbed photosynthetically active radiation, and light use efficiency in crops: implications for remote sensing of crop primary production. *Journal of Plant Physiology* **177**, 100–109.

Gyllenstrand N, Clapham D, Källman T, Lagercrantz U. **2007**. A Norway spruce FLOWERING LOCUS T homolog is implicated in control of growth rhythm in conifers. *Plant Physiology* **144**, 248–257.

Hall M, Räntfors M, Slaney M, Linder S, Wallin G. **2009**. Carbon dioxide echange of buds and developing shoots of boreal Norway spruce exposed to elevated or ambient CO_2 concentration and temperature in whole-tree chambers. *Tree Physiology* **29**, 461–481.

Hall M, Medlyn BE, Abamowitz G, Franklin O, Räntfors M, Linder S, Wallin G. **2013**. Which are the most important parameters for modelling carbon assimilation in boreal Norway spruce under elevated [CO_2] and temperature conditions? *Tree Physiology* **33**, 1156–1176.

Hamilton JA, Kayal WE, Hart AT, Runcie DE, Arango-Velez A, Cooke JEK. **2016**. The joint influence of photoperiod and temperature during growth cessation and development of dormancy in white spruce (*Picea glauca*). *Tree Physiology* **36**, 1432–1448.

Hänninen H, Tanino K. **2011**. Tree seasonality in a warming climate. *Trends in Plant Science* **16**, 412–416.

Heide OM. **1974**. Growth and dormancy in Norway spruce ecotypes (*Picea abies*) I. interaction of photoperiod and temperature. *Physiologia Plantarum* **30**, 1–12.

Holm S. **1979**. A simple sequentially rejective multiple test procedure. *Scandinavian Journal of Statistics* **6**, 65–70.

Holliday JA, Ralph SG, White R, Bohlmann J, Aitken SN. **2008**. Global monitoring of autumn gene expression within and among phenotypically divergent populations of Sitka spruce (*Picea sitchensis*). *New Phytologist* **178**, 103–122.

Jordan DB, Ogren WL. **1981**. Species variation in the specificity of ribulose biphosphate carboxylase/oxygenase. *Nature* **291**, 513–515.

Jordan DB, Ogren WL. **1984**. The CO_2/O_2 specificity of ribulose 1,5-bisphosphate carboxylase/oxygenase. *Planta* **161**, 308–313.

Jung J-H, Domijan M, Klose C, *et al*. 2016. Phytochromes function as thermosensors in *Arabidopsis*. *Science* **354**, 886–889.

Kang H, Ekberg I, Eriksson G, Ununger J. **1994**. Second and third growth period responses of *Picea abies* families to first growth period photoperiodic, light intensity and temperature treatments. *Silva Fennica* **28**, 215–232.

Keenan T, Gray J, Friedl M. **2014**. Net carbon uptake has increased through warming-induced changes in temperate forest phenology. *Nature Climate Change* **4**, 598–604.

Kramer PJ. **1936**. Effect of variation in length of day on growth and dormancy of trees. *Plant Physiology* **11**, 127–137.

Kroner Y, Way DA. **2016**. Carbon fluxes acclimate more strongly to elevated growth temperatures than to elevated CO_2 concentrations in a northern conifer. *Global Change Biology* **22**, 2913–2928.

Laemmli UK. **1970**. Cleavage of structural proteins during the assembly of the head of bacteriophage T4. *Nature* **227**, 680–685.

Legris M, Klose C, Burgie ES, *et al*. 2016. Phytochrome B integrates light and temperature signals in *Arabidopsis*. *Science* **354**, 897–900.

Lewis JD, Phillips NG, Logan BA, *et al*. 2015. Rising temperature may negate the stimulatory effect of rising CO_2 on growth and physiology of Wollemi pine (*Pollemia nobilis*). *Functional Plant Biology* **42**, 836–850.

Medlyn BE, Dreyer E, Ellsworth D, Forstreuter M, Harley PC, Kirschbaum MUF, Roux XLE. **2002**. Temperature response of parameters of a biochemically based model of photosynthesis. II. A review of experimental data. *Plant, Cell & Environment* **25**, 1167–1179.

Millard P, Sommerkorn M, Grelet G-A. **2007**. Environmental change and carbon limitation in trees: a biochemical, ecophysiological and ecosystem appraisal. *New Phytologist* **175**, 11–28.

Niinemets Ü, Tenhunen JD. **1997**. A model separating leaf structural and physiological effects on carbon gain along light gradients for the shade-tolerant species *Acer saccharum*. *Plant, Cell & Environment* **20**, 845–866.

Öquist G, Hüner NPA. **1991**. Effects of cold acclimation on the susceptibility of photosynthesis to photoinhibition in Scots pine and in winter and spring cereals: a fluorescence analysis. *Functional Ecology* **5**, 91–100.

Öquist G, Hüner NPA. **2003**. Photosynthesis of overwintering evergreen plants. *Annual Review of Plant Biology* **54**, 329–55.

Park T, Ganguly S, Tommervik H, *et al*. 2016. Changes in growing season duration and productivity of northern vegetation inferred from long-term remote sensing data. *Environmental Research Letters* **11**, 084001.

Piao S, Ciais P, Friedlingstein P, *et al*. 2008. Net carbon dioxide losses of northern ecosystems in response to autumn warming. *Nature* **451**, 49–52.

Quick WP, Fichtner K, Schulze ED., *et al*. 1992. Decrease Ribulose-1,5-bisphosphate carboxylase-oxygenase in transgenic tobacco transformed with an antisense *RbcS*. 4. Impact on photosynthesis in conditions of altered nitrogen supply. *Planta* **188**, 522–531.

R Core Development Team. **2013**. R: a language and environment for statistical computing. R Foundation for Statistical Computing: Vienna, Austria. https://www.R-project.org.

Reich PB, Sendall KM, Rice K, Rich RL, Stefanski A, Hobbie SE Montgomery RA. **2015**. Geographic range predicts photosynthetic and growth response to warming in co-occurring tree species. *Nature Climate Change* **5**, 148–152.

Reich PB, Walters MB, Tjoelker MG, Vanderklein D, Buschena C. **1998**. Photosynthesis and respiration rates depend on leaf and root morphology and nitrogen concentration in nine boreal tree species differing in relative growth rate. *Functional Ecology* **12**, 395–405.

Reich PB, Walters MB, Ellsworth DS. **1997**. From tropics to tundra: global convergence in plant functioning. *Proceedings of the National Academy of Sciences of the United States of America* **94**, 13730–13734.

Reich PB, Walters MB, Kloeppel BD, Ellsworth DS. **1995**. Different photosynthesis-nitrogen relations in deciduous hardwood and evergreen coniferous tree species. *Oecologia* **104**, 24–30.

Reich PB, Walters MB, Ellsworth DS. **1991**. Leaf age and season influence the relationships between leaf nitrogen, leaf mass per area and photosynthesis in maple and oak trees. *Plant, Cell & Environment* **14**, 251–259.

Ununger J, Ekberg I, Kang H. **1988**. Genetic control and age-related changes of juvenile growth characters in *Picea abies*. *Scandinavian Journal of Forest Research* **3**, 55–66.

Slaney M, Wallin G, Medhurst J, Linder S. **2007**. Impact of elevated carbon dioxide concentration and temperature on bud burst and shoot growth of boreal Norway spruce. *Tree Physiology* **27**, 301–312.

Sigurdsson BD, Medhurst JL, Wallin G, Eggertsson O, Linder S. **2013**. Growth of mature boreal Norway spruce was not affected by elevated [CO_2] and/or air temperature unless nutrient availability was improved. *Tree Physiology* **33**, 1192–1205.

Stinziano JR, Way DA. **2014**. Combined effects of rising [CO_2] and temperature on boreal forests: growth, physiology and limitation. *Botany* **92**, 425–436.

Stinziano JR, Hüner NPA, Way DA. **2015**. Warming delays autumn declines in photosynthetic capacity in Norway spruce (*Picea abies*). *Tree Physiology* **35**, 1303–1313.

Stitt M, Schulze D. **1994**. Does Rubisco control the rate of photosynthesis and plant growth? An exercise in molecular ecophysiology. *Plant, Cell & Environment* **17**, 465–487.

von Caemmerer S, Evans JR. **2015**. Temperature responses of mesophyll conductance differ greatly between species. *Plant, Cell & Environment* **38**, 629–637.

Warren CR, Adams MA, Chen ZL. **2000**. Is photosynthesis related to concentrations of nitrogen and Rubisco in leaves of Australian native plants? *Australian Journal of Plant Physiology* **27**, 407–416.

Warren CR, Dreyer E, Adams MA. **2003**. Photosynthesis-Rubisco relationships in foliage of *Pinus sylvestris* in response to nitrogen supply and the proposed role of Rubisco and amino acids as nitrogen stores. *Trees* **17**, 359–366.

Way DA, Oren R. **2010**. Differential responses to changes in growth temperature between trees from different functional groups and biomes: a review and synthesis of data. *Tree Physiology* **36**, 669–688.

Way DA, Sage RF. **2008a**. Thermal acclimation of photosynthesis in black spruce [*Picea mariana* (Mill.) B.S.P.]. *Plant, Cell & Environment* **31**, 1250–1262.

Way DA, Sage RF. **2008b**. Elevated growth temperatures reduce the carbon gain of black spruce [*Picea mariana* (Mill.) B.S.P.]. *Global Change Biology* **14**, 624–636.

Way DA, Yamori W. **2014**. Thermal acclimation of photosynthesis: on the importance of adjusting our definitions and accounting for thermal acclimation of respiration. *Photosynthesis Research* **119**, 89–100.

Way DA, Montgomery RA. **2015**. Photoperiod constrains on tree phenology, performance and migration in a warming world. *Plant, Cell & Environment* **38**, 1725–1736.

Wellburn AR. **1994**. The spectral determination of chlorophyll a and chlorophyll b, as well as total carotenoids, using various solvents with spectrophotometers of different resolution. *Journal of Plant Physiology* **144**, 307–313.

Wilson KB, Baldocchi DD, Hanson PJ. **2000**. Spatial and seasonal variability of photosynthetic parameters and their relationship to leaf nitrogen in a deciduous forest. *Tree Physiology* **20**, 565–578.

Wong CYS, Gamon JA. **2015**. The photochemical reflectance index provides an optical indicator of spring photosynthetic activation in evergreen conifers. *New Phytologist* **206**, 196–208.

Wright IJ, Reich PB, Westoby M, *et al*. **2004**. The wordwide leaf economics spectrum. *Nature* **428**, 821–827.

Yamori W, Hikosaka K, Way DA. **2014**. Temperature response of photosynthesis in C_3, C_4, and CAM plants: temperature acclimation and temperature adaptation. *Photosynthesis Research* **119**, 101–117.

Yamori W, Suzuki K, Noguchi K, Nakai M, Terashima I. **2006**. Effects of Rubisco kinetics and Rubisco activation state on the temperature dependence of the photosynthetic rate in spinach leaves from contrasting growth temperatures. *Plant, Cell & Environment* **29**, 1659–1670.

Yin HJ, Liu Q, Lai T. **2008**. Warming effects on growth and physiology in the seedlings of the two conifers *Picea asperata* and *Abies faxoniana* under two contrasting light conditions. *Ecological Research* **23**, 459–469.

Zhang J, Huang S, He F. **2015a**. Half-century evidence from western Canada shows forest dynamics are primarily driven by competition followed by climate. *Proceedings of the National Academy of Sciences of the United States of America* **112**, 4009–4014.

Zhang Y-J, Cao K-F, Sack L, Li N, Wie X-M, Goldstein G. **2015b**. Extending the generality of leaf economic design principles in the cycads, an ancient lineage. *New Phytologist* **206**, 817–829.

Zhao C, Liu Q. **2009**. Growth and photosynthetic responses of two coniferous species to experimental warming and nitrogen fertilization. *Canadian Journal of Forest Research* **39**, 1–11.

Chapter 4

4 Improving models of photosynthetic thermal acclimation: which parameters are most important and how many should be modified?

This chapter was published in a similar form in *Global Change Biology* (Stinziano, Way & Bauerle, 2018, "Improving models of photosynthetic thermal acclimation: which parameters are most important and how many should be modified?", *Global Change Biology* **24**, 1580–1598), and addresses **Question 3** (do models that include multi-factor acclimation of photosynthesis improve estimates of gross primary productivity in conifers?) and **Hypotheses 2** and **3** (**2**: day length, not temperature, drives seasonal changes in photosynthetic capacity in evergreen conifers; **3**: evergreen conifers acclimate multiple parameters of the temperature response of photosynthetic capacity) in Chapter 1.

4.1 Introduction

Globally, the biosphere absorbs ~120 Gt carbon yr^{-1} from the atmosphere through photosynthesis, a significantly larger flux than the release of carbon from either autotrophic or heterotrophic respiration (each ~60 Gt carbon yr^{-1}) or anthropogenic emissions (~7.9 Gt carbon yr^{-1}) (Amthor, 1995; Schlesinger & Andrews, 2000; Ciais *et al.*, 2013). Given that net carbon uptake (i.e. photosynthetic carbon uptake minus (photo)respiratory carbon release) by terrestrial ecosystems is on the order of 2–4 Gt carbon yr^{-1} (Le Quéré *et al.*, 2016), relatively small changes in photosynthesis as the climate warms and atmospheric CO_2 concentrations increase in coming decades could mitigate or amplify the on-going increase in atmospheric CO_2 concentrations. Accurate modeling of photosynthesis and its response to climate drivers such as temperature are thus necessary to predict future carbon cycle dynamics and coupled vegetation-climate feedbacks.

Net CO_2 assimilation rates (A_{net}) increase with temperature up to a thermal optimum (T_{opt}, between 25-30 °C for C_3 plants), above which A_{net} declines (Way & Yamori, 2014). This temperature response is driven by the combination of increases in respiration (Atkin & Tjoelker, 2003), photorespiration, and photosynthesis with increasing leaf temperature,

which increase at different rates as temperature rises. Thermal acclimation of the photosynthetic temperature response shifts T_{opt} towards the recent growth temperature, as well as affecting maximum rates of A_{net} and the overall shape of the A_{net} temperature response curve (Way & Yamori, 2014; Yamori *et al.*, 2014). There are numerous studies addressing how photosynthesis acclimates to temperature changes (summarized in these meta-analyses: Hikosaka *et al.*, 2006; Kattge & Knorr, 2007; Way & Yamori, 2014; Yamori *et al.*, 2014; for examples of ecosystem-level responses, see Baldocchi *et al.*, 2001; Niu *et al.*, 2012), but thermal acclimation of photosynthesis still represents a key uncertainty in the Earth System Models used to predict future vegetation-atmosphere carbon exchange (Smith & Dukes, 2013; Lombardozzi *et al.*, 2015; Rogers *et al.*, 2017). Recent studies have shown the potential to improve Earth System Model performance by incorporating thermal acclimation of photosynthesis (e.g. Smith *et al.*, 2016), and photosynthetic temperature acclimation has been included in some Earth System Models (e.g. Oleson *et al.*, 2013), but the generality with which this acclimation can be incorporated is unclear.

As Earth System Models use photosynthetic capacity (which includes both maximum rates of Rubisco carboxylation (V_{cmax}) and electron transport (J_{max})) to estimate photosynthesis, any attempt to incorporate temperature acclimation of photosynthesis should be based on photosynthetic capacity. Thermal acclimation of photosynthetic capacity could occur in two fundamental ways: acclimation of the acute temperature response parameters that describe the shape of the temperature response of V_{cmax} and J_{max}, and acclimation of the basal photosynthetic capacity (k_{25}; i.e. V_{cmax} or J_{max} measured at 25 °C). The acute temperature response of photosynthetic capacity (i.e. the instantaneous response of V_{cmax} or J_{max} to a change in leaf temperature) is captured by a modified Arrhenius function (Johnson *et al.*, 1942; Harley *et al.*, 1985; Medlyn *et al.*, 2002), which can be described using activation and deactivation energies:

$$\mathbf{f(T_k) = k_{25} exp\left[\frac{E_a(T_k - 298)}{298RT_k}\right] \frac{1+\exp\left(\frac{298\Delta S - H_d}{298R}\right)}{1+\exp\left(\frac{T_k\Delta S - H_d}{T_k R}\right)}} \qquad \text{Equation 4.1}$$

where k_{25} is photosynthetic capacity at 25 °C (μmol m^{-2} s^{-1}), E_a is the activation energy of V_{cmax} or J_{max} (J mol^{-1}), T_k is the leaf temperature (K), 298 is the reference temperature (K), R is the universal gas constant (8.314 J K^{-1} mol^{-1}), ΔS is the entropy parameter (J mol^{-1}), and H_d is the deactivation energy of photosynthetic capacity (J mol^{-1}). An equivalent form of the modified Arrhenius function can also be used to describe the acute temperature response of V_{cmax} and J_{max} (Johnson *et al.*, 1942):

$$\mathbf{f(T_k) = k_{opt} \frac{H_d exp\left(E_a \frac{T_k - T_{optk}}{RT_kT_{optk}}\right)}{H_d - E_a\left[1 - exp\left(H_d \frac{T_k - T_{optk}}{RT_kT_{optk}}\right)\right]}} \quad \text{Equation 4.2}$$

where T_{optk} is the thermal optimum of V_{cmax} or J_{max} (K) and k_{opt} is the photosynthetic capacity at this optimum temperature (μmol m^{-2} s^{-1}). The relationship between Equations 4.1 and 4.2 can be described as (Medlyn *et al.*, 2002):

$$\mathbf{T_{optk} = \frac{H_d}{\Delta S - R ln\left[\frac{E_a}{H_d - E_a}\right]}} \quad \text{Equation 4.3}$$

In some cases, an unmodified Arrhenius equation is used to describe the temperature response of photosynthetic capacity (Medlyn *et al.*, 2002):

$$f(T_k) = k_{25} exp\left[\frac{E_a(T_k - 298)}{298RT_k}\right] \quad \text{Equation 4.4}$$

The acute temperature response of V_{cmax}, J_{max} and T_{optk} may therefore acclimate to prevailing temperatures through changes in E_a, H_d, ΔS, k_{25}, or some combination of these parameters (i.e. multifactor acclimation). While acclimation of other parameters, such as the Michaelis-Menten constants for Rubisco carboxylation (K_c) and oxygenation (K_o) can affect carbon gain, carbon gain tends to be more sensitive to changes in the acute temperature response parameters such as E_a, H_d, and ΔS (Maire *et al.*, 2012), which I focus on in the present study. For acclimation of E_a, Hikosaka *et al.* (2006) found a positive linear relationship between the E_a of V_{cmax} and leaf temperature, while Dillaway and Kruger (2010) found a nonlinear relationship between the E_a for both V_{cmax} and J_{max} and air temperature, with a minimum E_a between 25 and 28 °C. Acclimation of the H_d of photosynthetic capacity has not been explored to my knowledge: temperature response

parameters of V_{cmax} and J_{max} are laborious to measure, and H_d is often constrained to a specific value (i.e. 200,000 J mol^{-1} from Farquhar *et al.* (1980), based on data from Nolan and Smillie (1976) in barley, *Hordeum vulgare* L. cv. Abyssinian) which may not be appropriate for all species. The entropy parameter, ΔS, has been shown to decrease linearly when acclimating to increasing air temperature for both V_{cmax} and J_{max} (Kattge & Knorr, 2007); when acclimation of photosynthetic capacity is added to an Earth System Model (e.g. Oleson *et al.*, 2013) or the effect of photosynthetic thermal acclimation on plant carbon fluxes has been investigated in models (Smith *et al.*, 2016), it is usually accomplished by altering ΔS. However, the accuracy of ΔS may be problematic, as ΔS can be quite variable between species grown under similar conditions (up to 4-fold for ΔS of V_{cmax} and 8-fold for ΔS of J_{max}; Dreyer *et al.*, 2001). As well, since ΔS is estimated concurrently with H_d, there may be issues with current ΔS data as many studies assume that H_d is 200,000 J mol^{-1}, which should affect the value of ΔS. Lastly, while k_{25} can change when growth air temperature changes (e.g. Han *et al.*, 2004; Panek, 2004; Misson *et al.*, 2006; Han *et al.*, 2008; Stinziano *et al.*, 2015; Stinziano & Way, 2017), there is little evidence for a consistent pattern of thermal acclimation of k_{25} (Way & Oren, 2010; Way & Yamori, 2014), making it difficult to determine how thermal acclimation of k_{25} should be modelled.

Accurately modeling vegetation carbon fluxes requires that not only temperature, but other climate factors that influence photosynthetic capacity over the growing season are incorporated as well. While seasonal changes in temperature can affect photosynthetic capacity (e.g. Xu & Baldocchi, 2003; Stinziano *et al.*, 2015; Stinziano & Way, 2017), so can seasonal changes in day length (Bauerle *et al.*, 2012). In temperate, deciduous trees, photosynthetic capacity was better correlated with day length than temperature, and imposing a longer day length on *Acer rubrum* increased V_{cmax} (Bauerle *et al.*, 2012). However, this may not hold true for the longer-lived foliage of conifers, as seasonal trajectories of photosynthetic capacity in *Picea glauca* were driven by temperature and not day length (Stinziano & Way, 2017). Therefore, any attempts to investigate the impact of seasonal changes in temperature on photosynthetic capacity (via thermal acclimation) should also address possible impacts of seasonal changes in day length.

Given that incorporating thermal acclimation of ΔS can improve carbon flux estimates in Earth System Models (Smith *et al.*, 2016), I explored how incorporating thermal acclimation of E_a, H_d, ΔS, and k_{25} for photosynthetic capacity affected estimates of carbon uptake. I used a spatially explicit canopy model, MAESTRA (Wang & Jarvis, 1990a,b; Medlyn, 2004; Duursma & Medlyn, 2012), to model gross primary productivity (GPP) of a loblolly pine (*Pinus taeda*) stand, and used eddy covariance data from the same site to assess model performance. I hypothesized that an evergreen conifer would acclimate multiple parameters of the photosynthetic temperature response, i.e. acclimation of multiple parameters in the acute temperature response of photosynthetic capacity, which would cause large improvements in model performance when using multifactor models of thermal acclimation of photosynthetic capacity. I also investigated whether photosynthetic capacity was better correlated with day length or temperature in evergreen conifers to develop a model of seasonal acclimation for k_{25}. While day length appears to correlate well with photosynthetic capacity in deciduous broadleaf trees (Bauerle *et al.*, 2012), I hypothesized that this would not be the case in evergreen species, such as the loblolly pine stand used here, as photoperiod was not a strong driver of V_{cmax} or J_{max} in an evergreen conifer species grown under controlled conditions (Stinziano & Way, 2017).

4.2 Materials and methods

4.2.1 Meta-analysis of seasonal V_{cmax} for acclimation of basal V_{cmax}

First, I set out to determine whether seasonal thermal acclimation of basal photosynthetic capacity (k_{25}) occurs in evergreen conifers to allow us to derive seasonal trajectories of basal V_{cmax} (V_{cmax25}, measured at 25 °C) for the pine forest stand I was modeling. A comprehensive Google Scholar search was made, using the terms “seasonal” or “monthly” AND “V_{cmax}”. Since the site I modelled was a *Pinus taeda* forest, the secondary terms I used were the following genera of evergreen conifers: *Abies*, *Chamaecyparis*, *Juniperus*, *Libocedrus*, *Picea*, *Pinus*, *Pseudotsuga*, *Sequoia*, *Sequoiadendron*, *Thuja*, *Tsuga*, *Taxodium*, and *Taxus*. The search yielded 12 studies on 9

species, which were combined with one set of unpublished data on *Thuja canadensis* (Figs. B.1 and B.2, see Appendix B for methods) for data on a total of 10 species (Table 4.1). Studies all fit the following selection criteria: 1) contains seasonal V_{cmax} data or contains both seasonal light-saturated rates of net CO_2 assimilation (A_{sat}) data and either seasonal intercellular CO_2 concentrations (C_i) or the ratio of C_i to ambient CO_2 concentrations (C_a) (C_i/C_a) values to allow us to calculate V_{cmax} via the one-point A-C_i method (De Kauwe *et al.*, 2016); and 2) contains enough information to determine the daily temperatures and day length of the study site, to allow us to partition whether temperature, day length, or both factors explain seasonal acclimation in V_{cmax}. Data were extracted from published figures using Data Thief III v. 1.7 (Tummers, 2015).

Table 4.1. Species and studies used in the meta-analysis.

Species	Study
Chamaecyparis obtusa	Han *et al*., 2006; Han & Chiba, 2009
Picea abies	Stinziano *et al*., 2015
Picea glauca	Stinziano & Way, 2017
Picea mariana	Bigras & Bertrand, 2006
Pinus densiflora	Han *et al*., 2004; Han *et al*., 2008
Pinus ponderosa	Panek, 2004; Misson *et al*., 2006
Pinus rigida	Renninger *et al*., 2013
Pinus sylvestris	Strand *et al*., 2002
Pinus taeda	Lewis *et al*., 1996
Thuja canadensis	This study (Appendix B)

All but one study measured V_{cmax25} (i.e. k_{25}), and the V_{cmax} data of the remaining study on *Pinus sylvestris* were standardized to 25 °C using the E_a, H_d, and ΔS for V_{cmax} from *P. sylvestris* with Equation 4.1 (Medlyn *et al.*, 2002). The V_{cmax25} data were then plotted versus day of year and fit with second-order polynomials (Bauerle *et al.*, 2012) to estimate the annual peak V_{cmax25} for each species and study, on the assumption that the measured data were unlikely to capture the true peak of V_{cmax25}. V_{cmax25} data for each species in each study were then normalized to this peak annual V_{cmax25} to yield relative V_{cmax25} to account for large differences in the magnitude of V_{cmax} amongst conifers (Peaucelle *et al.*, 2017). Relative V_{cmax25} values were aggregated for all species and studies and examined as a response of mean daily air temperature (°C) for the preceding 10 days (calculated using 30 minute intervals of air temperature) and relative day length (as a proportion of the summer solstice day length for each location). I used 10 days for the acclimation time to ensure that acclimation will have occurred (i.e. 7 or more days; Smith & Dukes, 2017; Way *et al.*, 2017) and reflected seasonal changes in temperature to contrast the effects of seasonal changes in temperature and day length on V_{cmax25}.

Data were analyzed using multiple linear regression in R GUI (R Core Development Team, 2013), running all combinations (with and without each term and interactions) of the following model: Relative V_{cmax25} ~ Air Temperature * Relative Day Length. The best model was selected by choosing the model with the lowest Bayesian Information Criterion (BIC) using the {BIC} function on the models in R.

4.2.2 Sensitivity analysis of the Arrhenius temperature response model

To determine the potential importance of thermal response parameters, I investigated the sensitivity of the modified (Equation 4.1) and unmodified (Equation 4.4) Arrhenius function to the temperature response parameters E_a, H_d (modified Arrhenius function only), and ΔS (modified Arrhenius function only) for V_{cmax}. For simplicity, I started with the following base parameter values: k_{25} of 1 (to assess hypothetical rates of V_{cmax} relative to 25 °C) E_a of 60 kJ mol^{-1}, H_d of 200 kJ mol^{-1}, and ΔS of 650 J mol^{-1}. Next, I varied individual parameters, keeping everything else constant, by ± 5% of the base

value, and chose the highest (E_a: 224.47 kJ mol^{-1}, Leuning (2002); H_d: 415.551 kJ mol^{-1}, Leuning (2002); ΔS: 1341 J mol^{-1}, Leuning (2002)) and lowest (E_a: 33.92 kJ mol^{-1}, Medlyn *et al.* (2002); H_d: 90 kJ mol^{-1}, Leuning (2002); ΔS: 293 J mol^{-1}, Leuning (2002)) values for each parameter that I could find in the literature.

4.2.3 Model parameterization and validation

The MAESTRA model is a three-dimensional, spatially explicit model of tree canopy carbon flux, water balance, and radiation (Wang & Jarvis, 1990a, 1990b; Medlyn, 2004; Duursma & Medlyn, 2012). The model simulates individual trees within a stand and includes neighboring tree interactions. MAESTRA has been used to successfully simulate a range of species and canopy types, including *Pinus taeda* (Luo *et al.*, 2001), but also *Acer rubrum* (Bowden & Bauerle, 2008) and *Eucalyptus grandis* (Binkley *et al.*, 2010).

MAESTRA was used to test the effects of thermal acclimation of photosynthetic capacity on the model's ability to capture eddy covariance data from loblolly pine at the Duke Forest (lat.: 35.9782 N, long.: 79.0942 W) for 1998 to 2001 (available from ameriflux.ornl.gov). This model and dataset were chosen to compare my results with those of Luo *et al.* (2001) who modelled canopy carbon gain with MAESTRA at this site for 1996 to 1998. The site is a *Pinus taeda* forest that has been growing since 1983 (Ellsworth *et al.*, 1995), where *P. taeda* is responsible for most of the ecosystem carbon fixation (DeLucia *et al.*, 1999). The soil is a low-fertility Ultic Alfisol with a pH of 5.75 (Andrews *et al.*, 1999). Mean annual temperatures were 15.6 °C, 14.9 °C, 14.0 °C, and 14.7 °C and annual precipitation was 1305 mm, 1363 mm, 1132 mm, and 947 mm in 1998, 1999, 2000, and 2001, respectively. I parameterized the model per Luo *et al.* (2001), where V_{cmax} and J_{max} were scaled to leaf nitrogen in the canopy (Table 2). MAESTRA was validated by running the model for all four site-years to determine hourly GPP. I validated the data by performing a linear regression between modelled GPP and measured GPP for data averaged for each hour across August for all site years as per Luo *et al.* (2001). I did not perform a sensitivity analysis, as this was done in Luo

et al. (2001) for all parameters relevant to carbon uptake for the Duke Forest site from 1996 to 1998.

4.2.4 Acclimation scenarios

Acclimation of V_{cmax25} was performed as follows. V_{cmax25} was calculated on a leaf nitrogen basis (Equation 5; Ellsworth *et al.*, 1998) and measured at 25 °C on *P. taeda* at the Duke site (Luo *et al.*, 2001; Table 4.2):

$$V_{cmax25} = 25.3N_{area} + 28.6 \qquad \text{Equation 4.5}$$

where V_{cmax25} is the V_{cmax} at 25 °C (μmol m^{-2} s^{-1}) and N_{area} is the foliar nitrogen concentration on an area basis (g m^{-2}). This value of V_{cmax25} was assumed to represent the peak annual value of V_{cmax25} in the V_{cmax25}-air temperature relationship derived from the meta-analysis (Fig. 4.1a). This peak V_{cmax25} was then scaled to vary over the year using the regression developed above from the meta-analysis of V_{cmax} and air temperature. In this way, V_{cmax25} was first scaled with canopy nitrogen concentration, then scaled to the previous ten-day running mean air temperature to provide a seasonal trajectory of k_{25} for the study site. Basal J_{max} (J_{max} at 25 °C, J_{max25}, μmol m^{-2} s^{-1}) was also scaled with nitrogen within the canopy (Equation 4.6; Ellsworth *et al.*, 1998), then scaled against the seasonal V_{cmax25} values to preserve a J_{max25}:V_{cmax25} ratio of 2.1 (based on the ratio of Equations 4.6 and 4.5 calculated at the leaf nitrogen concentrations in each canopy position used in MAESTRA; Table 4.2):

$$J_{max25} = 53.1N_{area} + 60 \qquad \text{Equation 4.6}$$

Table 4.2. Parameter values used in MAESTRA, from Luo *et al*. (2001).

Parameter names and units	Abbreviation	Parameter value
Confile:		
Start Date	STARTDATE	January 1
End Date	ENDDATE	December 31
Number of layers in the crown	NOLAY	6
Number of points per layer	PPLAY	12
Number of zenith angles	NZEN	9
Number of azimuth angles	NAZ	6
Number of shading trees	NOTREES	8
Physiological File:		
Transmittance and Reflectance (PAR/NIR/IR):		
Soil reflectance (%)	RHOSOL	0.10/0.30/0.05
Needle transitivity (%)	ATAU	0.03/0.26/0.0
Needle reflectance (%)	ARHO	0.09/0.33/0.05
J_{max} *Parameter*		
J_{max}-Nitrogen Slope	JMAXA	53.1
J_{max}-Nitrogen Intercept	JMAXB	60
Curvature of light response curve of electron transport	THETA	0.7
Quantum yield of electron transport (mol e^- mol^{-1} CO_2)	AJQ	0.12
Activation energy (J mol^{-1})	EAVJ	37000
Deactivation energy (J mol^{-1})	ADVJ	220000
Entropy term (J K^{-1} mol^{-1})	DELSJ	710
V_{cmax} *Parameter:*		
V_{cmax}-Nitrogen Slope	VCMAXA	25.3
V_{cmax}-Nitrogen Intercept	VCMAXB	28.6

Activation energy (J mol^{-1})	EAVC	58500
Foliar dark respiration:		
Foliar dark respiration rate (μmol m^{-2} s^{-1} at 25 °C)	RD	0.804
Temperature (in °C) at which RD is specified	RTEMP	25
Fraction by which dark respiration is reduced in the light	DAYRESP	0.7
Foliage Q_{10} values	FOLQ10	0.07
Stomatal Conductance Model (Ball-Berry):		
Input parameter (mol m^{-2} s^{-1})	G0	0.0002
Input parameter (mol m^{-2} s^{-1})	G1	4.84
	NSIDES	2
Width of the leaf (m)	WLEAF	0.001
Nitrogen Concentration (for different canopy layers)	NFOL	2.1, 2.1, 1.92, 1.73, 1.55, 1.37
Structural File:		
Number of age classes		1
Shape of the canopy		ELIP
Leaf angle distribution (spherical)		1.64
Number of leaf area classes		1
Average leaf incidence angle		45
Beta distribution coefficients for leaf area density	BPT	5.5, 0.62, 1.4
Trees file:		
Height (m)	ALLHTCROWN	16
Stem diameter (m)	ALLDIAM	0.425
Crown Radius (m)	ALLRADY, ALLRADX	1.2
Trunk height (m)	ALLHTTRUNK	6
Leaf area index		2.63 to 4.67

Plot description:		
m	XMAX	25
m	YMAX	25
	XSLOPE	0
	YSLOPE	0
°	BEARING	180
	NOTREES	100
Aerodynamics:		
Measurement height (m)	ZHT	16
Zero-plane displacement (m)	ZPD	10.4
Roughness length (m)	Z0HT	1.6

Some parameters contain multiple parameters to specify canopy-layer values, values that change through time, or different components (e.g. reflectance and transmittance).

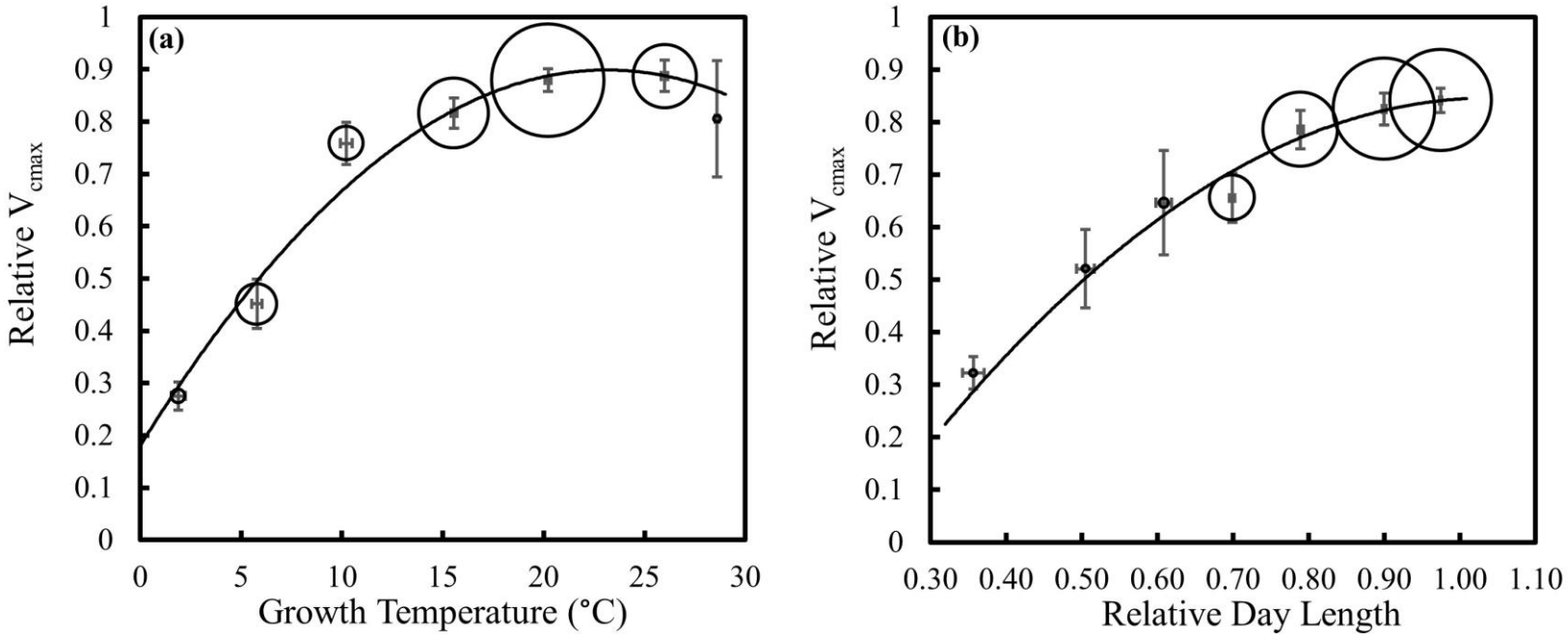

Figure 4.1. Relative maximum Rubisco carboxylation capacity (V_{cmax}) across air temperature (a) and relative day length (b) in evergreen conifers. Data presented as means ± 1 SD for 5 °C bins in (a) and for bins of 0.1 for relative day length except for peak (0.95 to 1.0) and below 0.45 (due to few data points at low day lengths). Circle size indicates the number of measurements per bin (between 5 and 101 measurements per bin). Solid line indicates quadratic regression for (a) Relative V_{cmax} = -0.0013 * (Air Temperature)^2 + 0.0621 * Air Temperature + 0.1808, R^2 = 0.359, P < 0.01, and (b) Relative V_{cmax} = -1.1917 * (Relative Day Length)^2 + 2.4826 * Relative Day Length – 0.4468, R^2 = 0.123, P < 0.001.

Thermal acclimation of ΔS was performed using the previous ten-day running mean air temperature (T_{growth}) (Kattge & Knorr, 2007):

$$\Delta S = d + e \times T_{growth} \quad \text{Equation 4.7}$$

where d is a constant with a value of 668.39 for V_{cmax} and 659.70 for J_{max} and e is a constant with values of -1.07 for V_{cmax} and -0.75 for J_{max}.

The E_a was thermally acclimated either linearly for V_{cmax} (Hikosaka *et al.*, 2006):

$$E_a = 34.1 + 1.01 \times T_{growth} \quad \text{Equation 4.8}$$

or non-linearly for both V_{cmax} and J_{max} (Dillaway & Kruger, 2010):

$$E_a = \frac{x}{T_{growth}^{\ 2}} - \frac{y}{T_{growth}} + z \quad \text{Equation 4.9}$$

where x, y, and z are constants equal to 45322 kJ mol^{-1} °C, 3368.2 kJ mol^{-1} °C, and 119.9 kJ mol^{-1} for V_{cmax}, and 80318.9 kJ mol^{-1} °C, 6093.6 kJ mol^{-1} °C, and 134.7 kJ mol^{-1} for J_{max}. Constants were derived from temperature responses for V_{cmax} and J_{max} for trembling aspen (*Populus tremuloides* Michx.), paper birch (*Betula papyrifera* Marsh.), eastern cottonwood (*Populus deltoides* Bartr ex. Marsh var. deltoides), and sweetgum (*Liquidambar styraciflua* L.) (Dillaway & Kruger, 2010).

I modified the intercepts of Equations 4.8 and 4.9 so that the E_a values intercepted with the values used in Luo *et al.* (2001) at 25 °C, then used the ten-day running average air temperature in Equations 4.8 and 4.9. I did this to preserve the original values of E_a for *Pinus taeda*, while maintaining the reported shape of the thermal acclimation responses.

Since Luo *et al.* (2001) used Equation 4.4 for V_{cmax} instead of Equation 4.1 and therefore had no H_d or ΔS for V_{cmax} in their results, my baseline "no acclimation" scenario also does not incorporate changes in H_d or ΔS for V_{cmax}, so that my "no acclimation" results can be directly compared to those in Luo *et al.* (2001). I built acclimation scenarios that incorporated acclimation of k_{25} (using the temperature response equation in Figure 1 and preserving a J_{max25}:V_{cmax25} of 2.1; these scenarios are denoted as k_{25} below), E_a (using

Equation 4.8 for V_{cmax} only (denoted as Eav below) or using Equation 4.9 for both V_{cmax} and J_{max} (denoted as Eavj below)), and ΔS (using Equation 4.7 for J_{max} only when Equation 4.4 was used to scale V_{cmax} as in Luo *et al.* (2001), or for both V_{cmax} and J_{max} when V_{cmax} was scaled with Equation 4.1; denoted as ΔS below). Scenarios using Equation 4.4 for V_{cmax} are denoted by '(-)' to indicate that these scenarios do not consider H_d or ΔS for V_{cmax}, while scenarios using Equation 1 for V_{cmax} are denoted by '(+)'.

I built up the scenarios from no thermal acclimation (NA; where V_{cmax25}, V_{cmax} E_a, J_{max25}, and the E_a and ΔS for J_{max} are all held constant) up to multifactor acclimation, combining acclimation of multiple parameters at the same time. I tested 18 different base acclimation scenarios (Table 4.3):

1) no acclimation; Equation 4.4 for V_{cmax} (NA (-));
2) no acclimation; Equation 4.1 for V_{cmax} (NA (+));
3) acclimation of k_{25}; Equation 4.4 for V_{cmax} (k_{25} (-));
4) acclimation of k_{25}; Equation 4.1 for V_{cmax} (k_{25} (+));
5) acclimation of the E_a of V_{cmax} using Equation 4.7; Equation 4.4 for V_{cmax} (Eav (-));
6) acclimation of the E_a of V_{cmax} using Equation 4.7; Equation 4.1 for V_{cmax} (Eav (+));
7) acclimation of the E_a of both V_{cmax} and J_{max} using Equation 4.9; Equation 4.4 for V_{cmax} (Eavj (-));
8) acclimation of the Ea of both V_{cmax} and J_{max} using Equation 4.9; Equation 4.1 for V_{cmax} (Eavj (+));
9) acclimation of ΔS using Equation 4.4; Equation 4.1 for V_{cmax} (ΔS);
10) k_{25}/Eav (-)
11) k_{25}/Eav (+)
12) k_{25}/Eavj (-)
13) k_{25}/Eavj (+)
14) k_{25}/ΔS
15) Eav/ΔS
16) Eavj/ΔS

17) k_{25}/Eav/ΔS
18) k_{25}/Eavj/ΔS

Note that anywhere that ΔS acclimation is included in a scenario, H_d for V_{cmax} is necessarily already included as well. These base scenarios all used an H_d value of 200,000 J mol^{-1} for V_{cmax} (as per Farquhar *et al.*, 1980) and of 220,000 J mol^{-1} for J_{max} (as per Luo *et al.*, 2001).

Table 4.3. Components used (indicated by an 'X') to build each acclimation scenario.

	Acclimated Parameters				
Scenario	Modified or unmodified Arrhenius for V_{cmax}	k_{25} (Fig. 4.1a)	V_{cmax} E_a (Hikosaka *et al*., 2006)	V_{cmax} and J_{max} E_a (Dillaway & Kruger, 2010)	ΔS (Kattge & Knorr, 2007)
1. NA (-)	Unmodified Eq. 4.4				
2. NA (+)	Modified Eq. 4.1				
3. k_{25} (-)	Unmodified Eq. 4.4	X Eq. Fig. 4.1a			
4. k_{25} (+)	Modified Eq. 4.1	X Eq. Fig. 4.1a			
5. Eav (-)	Unmodified Eq. 4.4		X Eq. 4.8		
6. Eav (+)	Modified Eq. 4.1		X Eq. 4.8		
7. Eavj (-)	Unmodified Eq. 4.4			X Eq. 4.9	
8. Eavj (+)	Modified Eq. 4.1			X Eq. 4.9	
9. ΔS	Modified Eq. 4.1				X Eq. 4.7
10. k_{25}/Eav (-)	Unmodified Eq. 4.4	X Eq. Fig. 4.1a	X Eq. 4.8		

11. k_{25}/Eav (+)	Modified Eq. 4.1	X Eq. Fig. 4.1a	X Eq. 4.8		
12. k_{25}/Eavj (-)	Unmodified Eq. 4.4	X Eq. Fig. 4.1a		X Eq. 9	
13. k_{25}/Eavj (+)	Modified Eq. 4.1	X Eq. Fig. 4.1a		X Eq. 9	
14. k_{25}/ΔS	Modified Eq. 4.1	X Eq. Fig. 4.1a			X Eq. 4.7
15. Eav/ΔS	Modified Eq. 4.1		X Eq. 4.8		X Eq. 4.7
16. Eavj/ΔS	Modified Eq. 4.1			X Eq. 4.9	X Eq. 4.7
17. k_{25}/Eav/ΔS	Modified Eq. 4.1	X Eq. Fig. 4.1a	X Eq. 4.8		X Eq. 4.7
18. k_{25}/Eavj/ΔS	Modified Eq. 4.1	X Eq. Fig. 4.1a		X Eq. 4.9	X Eq. 4.7

NA: no acclimation, (-) Equation 4.4 is used for V_{cmax}, (+), Equation 4.1 is used for V_{cmax}, k_{25}: basal acclimation of V_{cmax} and J_{max} at 25 °C, Eav: linear acclimation of V_{cmax} activation energy, Eavj: nonlinear acclimation of V_{cmax} and J_{max} activation energies, ΔS: acclimation of the entropy parameter.

4.2.5 Deactivation analysis

As all scenarios contained an H_d parameter for J_{max} (although a subset did not include H_d for V_{cmax} (i.e. the (-) scenarios)), I tested how sensitive modelled GPP was to the H_d values used. The 18 base acclimation scenarios were therefore rerun with both the highest and the lowest (non-zero) H_d values found in the literature (Scenarios 19 to 36 and 37 to 54, respectively; Table 4.4). The high value scenarios used a V_{cmax} H_d value of 415,551 J mol^{-1} (from *Brassica rapa*) and a J_{max} H_d value of 714,000 J mol^{-1} (from *Juglans regia*), while the low value scenarios used a V_{cmax} H_d value of 90,000 J mol^{-1} (from *Fraxinus excelsior*) and a J_{max} H_d value of 88,300 J mol^{-1} (from *Quercus robur*); all H_d values are from Leuning (2002).

Table 4.4. Outline of the thermal acclimation scenarios used.

Thermal Domain	Full Range			8 to 25 °C	18 to 31 °C
Scenario	Mid H_d	High H_d	Low H_d	Mid H_d	Mid H_d
NA (-)	1	19	37		
NA (+)	2	20	38		
k25 (-)	3	21	39		
k25 (+)	4	22	40		
Eav (-)	5	23	41	55	
Eav (+)	6	24	42	56	
Eavj (-)	7	25	43		61
Eavj (+)	8	26	44		62
ΔS	9	27	45		
k25/Eav (-)	10	28	46	57	
k25/Eav (+)	11	29	47	58	
k25/Eavj. (-)	12	30	48		63
k25/Eavj. (+)	13	31	49		64
k25/ΔS	14	32	50		
Eav/ΔS	15	33	51	59	
Eavj/ΔS	16	34	52		65
k25/Eav/ΔS	17	35	53	60	
k25/Eavj/ΔS	18	36	54		66

NA: no acclimation, (-) Equation 4.4 is used for V_{cmax}, (+), Equation 4.1 is used for V_{cmax}, k_{25}: basal acclimation of V_{cmax} and J_{max} at 25 °C, Eav: linear acclimation of V_{cmax} activation energy, Eavj: nonlinear acclimation of V_{cmax} and J_{max} activation energies, ΔS: acclimation of the entropy parameter.

4.2.6 Temperature domain analysis

Since the equations describing the thermal acclimation of E_a were developed from data measured under specific temperature ranges, I also tested the effect of restricting my modeling efforts to the appropriate temperature range. The linear acclimation for V_{cmax} E_a was restricted to 8-25 °C (Hikosaka *et al.*, 2006), while the nonlinear acclimation for V_{cmax} E_a and J_{max} E_a was restricted to 18-31 °C (Dillaway & Kruger, 2010) in this analysis. I compared all acclimation scenarios across the full temperature range at the Duke site, but also only ran MAESTRA for the times when the field air temperature data was between 8 and 25 °C for scenarios with Eav acclimation (Scenarios 55 to 60) and between 18 and 31 °C for acclimation scenarios with Eavj acclimation (Scenarios 61 to 66) (Table 4.4).

Each of the acclimation scenarios (Scenarios 1-66) were run for five separate days (February 1st, April 6th, August 8th, September 30th, and November 21st) for each year of the Duke eddy covariance data to match the periods of physiological measurements in Luo *et al.* (2001), and to provide a seasonal range over which to test the scenarios. Hourly modelled gross photosynthetic rates from MAESTRA were then compared against observed hourly GPP for the eddy covariance data. Model performance was evaluated based on model R^2 and BIC.

4.3 Results

4.3.1 Seasonal acclimation of V_{cmax25}

Relative V_{cmax25} was more strongly correlated with mean daily air temperature (R^2 = 0.36, Fig. 4.1a) for evergreen conifers than with relative day length (R^2 = 0.12, Fig. 4.1b), peaking at ~25 °C in the temperature correlation, while peaking at the longest day length in the day length correlation. The best model of seasonal changes in relative V_{cmax25} included only mean daily air temperature (Table 4.5). Temperature acclimation of k_{25} was therefore scaled using the quadratic relationship between relative V_{cmax25} and air temperature (Fig. 4.1a). This scaling may also account for within-season leaf age and

temperature effects on V_{cmax25} (see Wilson *et al.* (2000) for possible within-season aging effects on V_{cmax25}).

Table 4.5. Models of relative maximum Rubisco carboxylation capacity (V_{cmax}).

Model	BIC
Relative V_{cmax} ~ Air Temperature * Relative Day Length	16.9
Relative V_{cmax} ~ Air Temperature + Relative Day Length	14.5
Relative V_{cmax} ~ Air Temperature	9.4
Relative V_{cmax} ~ Relative Day Length	79.6

BIC, Bayesian information criterion.

4.3.2 The Arrhenius model is more sensitive to H_d and ΔS than E_a

The Arrhenius model is relatively insensitive to small changes in E_a, with 5% changes in E_a causing little difference for estimates of relative V_{cmax} with either the modified or unmodified Arrhenius equation (Fig. 4.2a). The highest E_a caused convergence of the modified and unmodified Arrhenius equations, while the lowest E_a value had a more pronounced effect on the estimates of relative V_{cmax} from the unmodified Arrhenius equation than the modified Arrhenius equation. Changing either H_d or ΔS caused substantial shifts in the temperature response function of relative V_{cmax}, with a 5% increase in H_d and a 5% decrease in ΔS shifting the temperature optimum upwards by ~20 °C, while a 5% decrease in H_d and a 5% increase in ΔS shifted the temperature optimum downwards by ~15 °C (Figs. 4.2b, c). The highest value of H_d and lowest value of ΔS caused the modified Arrhenius equation to resemble the unmodified Arrhenius equation at biologically relevant temperatures, while the lowest value of H_d and highest value of ΔS caused an exponential decline in relative V_{cmax} across the temperature range modelled.

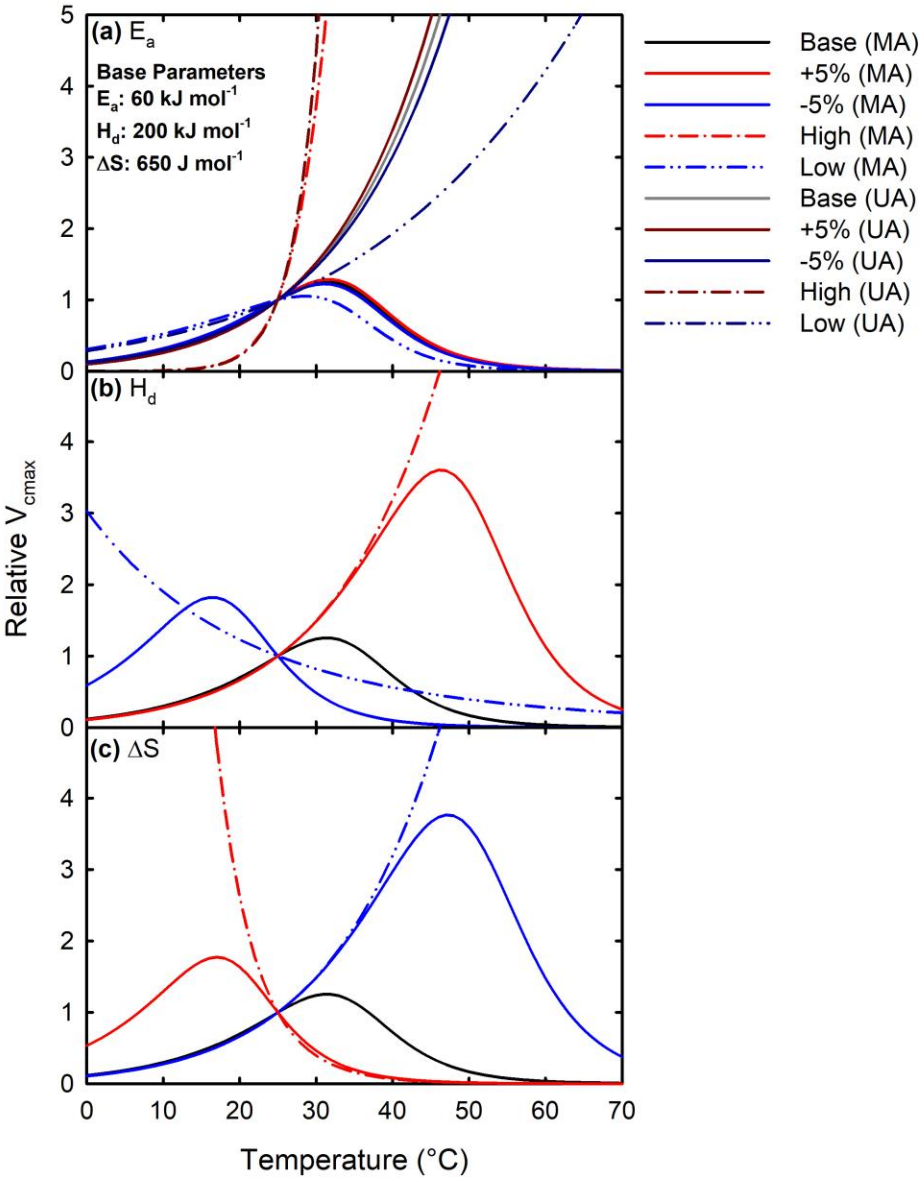

Figure 4.2. Sensitivity analysis of the Arrhenius temperature response models of relative V_{cmax} to changes in (a) activation energy (E_a), (b) deactivation energy (H_d), and (c) the entropy parameter (ΔS). Base parameter values were varied ± 5%, as well as using the highest (High) and lowest (Low) values available in the literature. Red indicates the parameter value has been increased, while blue indicates a decrease in the parameter value, relative to the base parameter value. MA: modified (peaked) Arrhenius function (Equation 4.1), UA: unmodified Arrhenius function (Equation 4.4).

4.3.3 Thermal acclimation improves model predictions

Modelled and measured GPP were strongly correlated (r = 0.95) with a slope of 1.048 (95% confidence interval: 1.017 to 1.080) and an intercept of 0.084 μmol m^{-2} s^{-1} (95% confidence interval: 0.012 to 0.156), indicating that the MAESTRA model slightly over-estimated GPP (Fig. 4.3). Incorporating photosynthetic temperature acclimation into MAESTRA had scenario-dependent effects on model performance, where single factor acclimation tended to improve model performance (Table 4.6, Fig. 4.4). In general, ΔS-based scenarios, which are currently used in efforts to acclimate photosynthesis in Earth System Models, improved explanatory power over the base model. However, including values for both H_d and ΔS for V_{cmax} to single factor acclimation scenarios (the '+' versus '–' scenarios in my analysis) generally reduced model performance (for example Figs. 4.4g, h). The best performing models under the full temperature domain all included acclimation of k_{25} (k_{25} (-), k_{25}/Eav (-), k_{25}/Eav/ΔS). While the two and three parameters scenarios that included k_{25} performed well, the addition of a second or third parameter generally led to relatively small improvements in model performance. Including Eav to the k_{25} (-) acclimation only improved R^2 by 0.2% (though it reduced carbon gain by 40 μmol m^{-2} relative to k_{25} (-); Table 4.6), while adding ΔS to the k_{25}/Eav scenario increased R^2 by 0.5% relative to k_{25} (-) (and reduced carbon gain by 6 μmol m^{-2} relative to k_{25} (-)). Including Eavj (the k_{25}/Eavj (-) scenario) to the k_{25} (-) scenario reduced model performance (reducing the R^2 by 6.4% and carbon gain by 189 μmol m^{-2} relative to k_{25} (-)), though adding ΔS as well (i.e. k_{25}/Eavj/ΔS) improved R^2 over the k_{25}/Eavj scenario by 1.1% (but still reduced R^2 by 5.3% and reduced carbon gain by 161 μmol m^{-2} relative to the k_{25} (-) scenario). Overall, multifactor models provided minimal improvements in model performance over the single factor model, and the greatest improvements in multifactor acclimation were due to the inclusion of k_{25} (Table 4.6). When summing carbon gain across all days for each scenario, incorporating photosynthetic thermal acclimation generally reduced modelled carbon gain compared to the NA (-) scenario (although ΔS increased carbon gain by 69 μmol m^{-2}) (Table 4.6). The two best scenarios (by R^2 and/or BIC), k_{25}/Eav (-) (lowest BIC) and k_{25}/Eav/ΔS (highest R^2), had five-day

carbon gain predictions that were 159 μmol m^{-2} and 125 μmol m^{-2} less, respectively, than the NA (-) model.

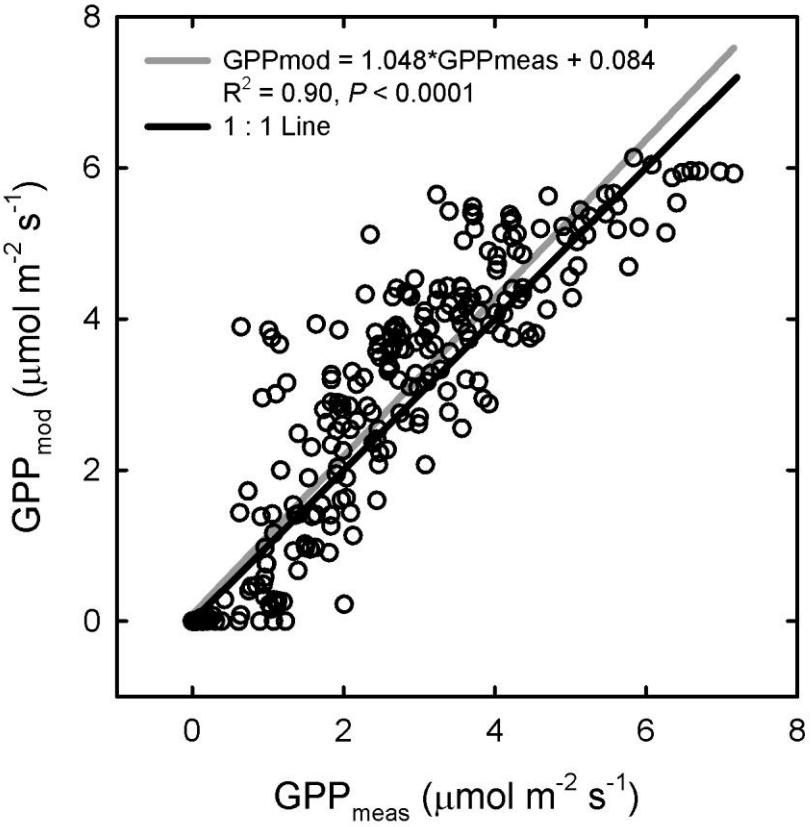

Figure 4.3. Modelled hourly gross primary productivity (GPP_{mod}) from MAESTRA corresponds well with hourly GPP measurements (GPP_{meas}) from eddy covariance for the Duke Forest site from each year between January 1st, 1998 and December 31st, 2001. Data were modelled using MAESTRA as per the parameterisation of Luo *et al*. (2001), without any acclimation. See Table 4.2 for the parameters used in MAESTRA. Grey line indicates the regression between modelled and measured GPP, while the black line indicates the 1:1 line. Note that the temperature range was -13.7 to 39.7 °C across the site years used.

Table 4.6. Slope and intercepts of photosynthetic acclimation scenarios across all temperature (Full) and under restricted temperature domains of the linear Ea (8 - 25 °C; Eav-containing scenarios) and the Eavj (18 - 31 °C; Eavj-containing) scenarios. The scenarios with the highest R^2 and/or lowest BIC are bolded within each temperature domain scenario.

Temperature Domain	Full					Restricted			
Scenario	Slope	Intercept	R^2	BIC	C Gain (μmol m^{-2})	Slope	Intercept	R^2	BIC
1. NA (-)	1.044	0.309	0.688	1551	746				
2. NA (+)	0.926	0.461	0.520	1777	751				
3. k25 (-)	0.950	0.712	0.799	1178	627				
4. k25 (+)	0.801	0.303	0.565	1550	604				
5. Eav (-)	1.142	0.220	0.720	1562	760	1.150	0.242	0.723	1303
6. Eav (+)	0.903	0.498	0.494	1802	756	0.883	0.396	0.530	1423
7. Eavj (-)	0.883	-0.042	0.730	1292	486	**0.977**	**0.132**	**0.885**	**432**
8. Eavj (+)	0.690	0.025	0.550	1437	407	0.672	0.222	0.553	639
9. ΔS	1.100	0.389	0.709	1552	817				
10. k25/Eav (-)	**0.922**	**0.124**	**0.801**	**1141**	**587**	0.933	0.207	0.825	916
11. k25/Eav (+)	0.802	0.302	0.566	1549	604	0.799	0.344	0.563	1294
12. k25/Eavj (-)	0.810	-0.054	0.735	1197	438	**0.926**	**0.123**	**0.879**	**422**
13. k25/Eavj (+)	0.618	0.014	0.559	1311	361	0.620	0.214	0.551	610
14. k25/ΔS	0.989	0.193	0.797	1222	660				
15. Eav/ΔS	1.078	0.308	0.749	1437	766	1.079	0.279	0.772	1154
16. Eavj/ΔS	0.906	-0.047	0.730	1317	496	1.004	0.133	0.883	447
17. k25/Eav/ΔS	**0.963**	**0.144**	**0.804**	**1175**	**621**	0.974	0.218	0.825	948
18. k25/Eavj/ΔS	0.845	-0.037	0.746	1210	466	0.965	0.124	0.882	433

C Gain: the total carbon uptake calculated by summing data across all simulated days; NA: no acclimation, (-) Equation 4.4 is used for V_{cmax}, (+), Equation 4.1 is used for V_{cmax}, k_{25}: basal acclimation of V_{cmax} and J_{max} at 25 °C, Eav: linear acclimation of V_{cmax} activation energy, Eavj: nonlinear acclimation of V_{cmax} and J_{max} activation energies, ΔS: acclimation of the entropy parameter.

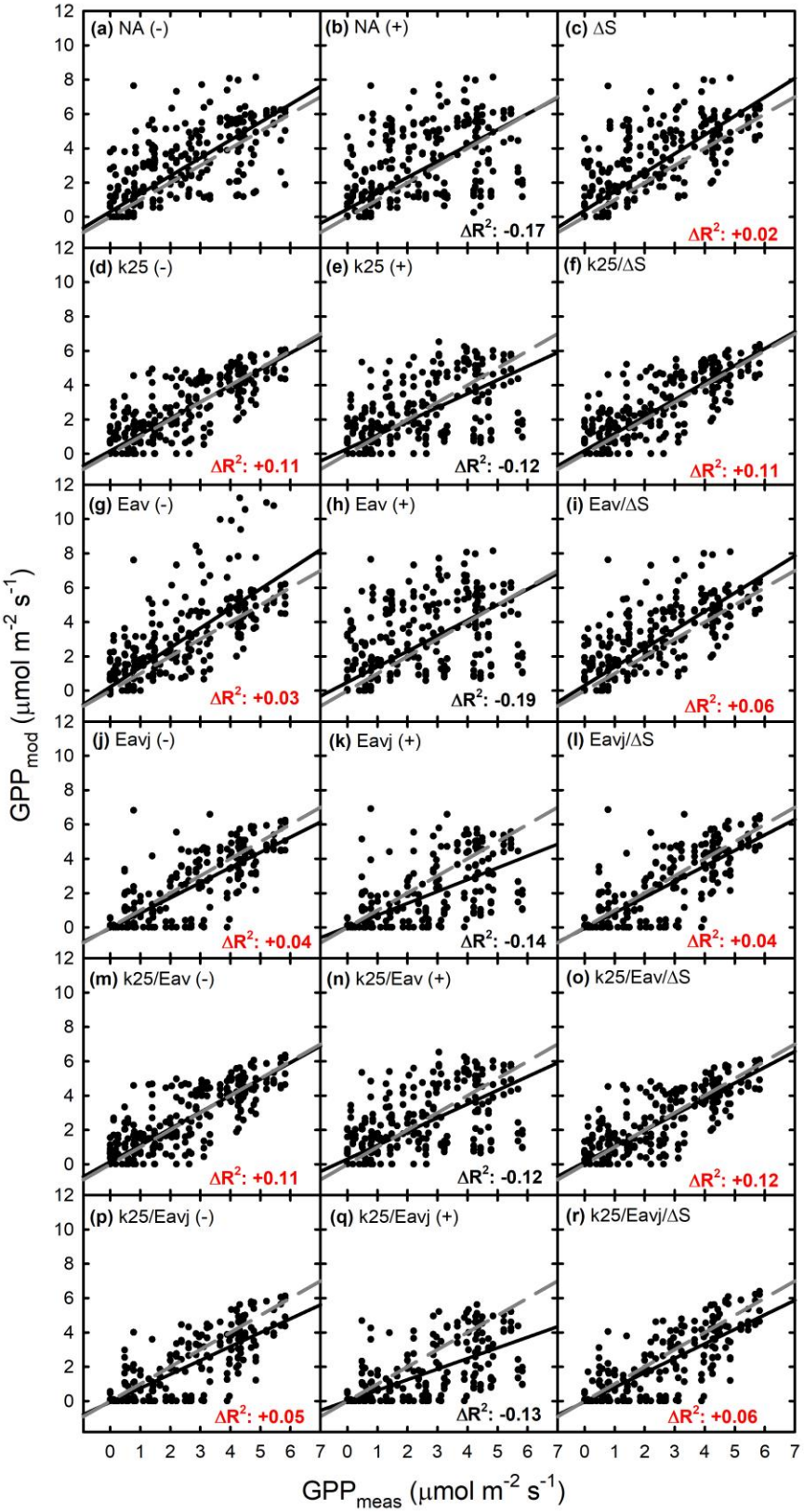
(a) NA (-)
(b) NA (+)
(c) ΔS
ΔR²: -0.17
ΔR²: +0.02
(d) k25 (-)
(e) k25 (+)
(f) k25/ΔS
ΔR²: +0.11
ΔR²: -0.12
ΔR²: +0.11
(g) Eav (-)
(h) Eav (+)
(i) Eav/ΔS
ΔR²: +0.03
ΔR²: -0.19
ΔR²: +0.06
(j) Eavj (-)
(k) Eavj (+)
(l) Eavj/ΔS
ΔR²: +0.04
ΔR²: -0.14
ΔR²: +0.04
(m) k25/Eav (-)
(n) k25/Eav (+)
(o) k25/Eav/ΔS
ΔR²: +0.11
ΔR²: -0.12
ΔR²: +0.12
(p) k25/Eavj (-)
(q) k25/Eavj (+)
(r) k25/Eavj/ΔS
ΔR²: +0.05
ΔR²: -0.13
ΔR²: +0.06
GPP_mod (μmol m-2 s-1)
GPP_meas (μmol m-2 s-1)

Figure 4.4. Modelled hourly gross primary productivity (GPP) from MAESTRA across scenarios with different types of photosynthetic temperature acclimation for February 1st, April 6th, August 8th, September 30th, and November 21st from each year between 1998 and 2001. Solid black lines represent significant linear regressions ($P < 0.001$). Grey dashed line indicates a 1:1 relationship. See Table 4.6 for slopes and intercepts. NA: no acclimation, (-) Equation 4.4 is used for V_{cmax}, (+), Equation 4.1 is used for V_{cmax}, k25: basal acclimation of V_{cmax} and J_{max} at 25 °C, Eav: linear acclimation of V_{cmax} activation energy, Eavj: nonlinear acclimation of V_{cmax} and J_{max} activation energies, ΔS: acclimation of the entropy parameter. ΔR^2 indicates the absolute change in R^2 compared to the base NA (-) scenario, with red text indicating an improvement.

4.3.4 Deactivation analysis

Next, I replaced the H_d value in MAESTRA for all base scenarios (1 to 18) with the highest or lowest H_d values for V_{cmax} and J_{max}. Under high H_d, scenarios using Equation 4.1 to describe V_{cmax} (i.e. (+)-containing scenarios) produced the greatest performance increases (up to 27.7% compared to the base H_d case), and the difference from describing V_{cmax} with Equation 4.1 instead of Equation 4.4 disappeared (i.e. it did not matter whether or not H_d and ΔS for V_{cmax} were included in the scenario; Fig. 4.5; Table 4.7). The best performing acclimation scenarios with the alternate H_d values (highest R^2 and/or BIC) all contained acclimation of k_{25}, corresponding to the best performing scenarios under the base H_d case.

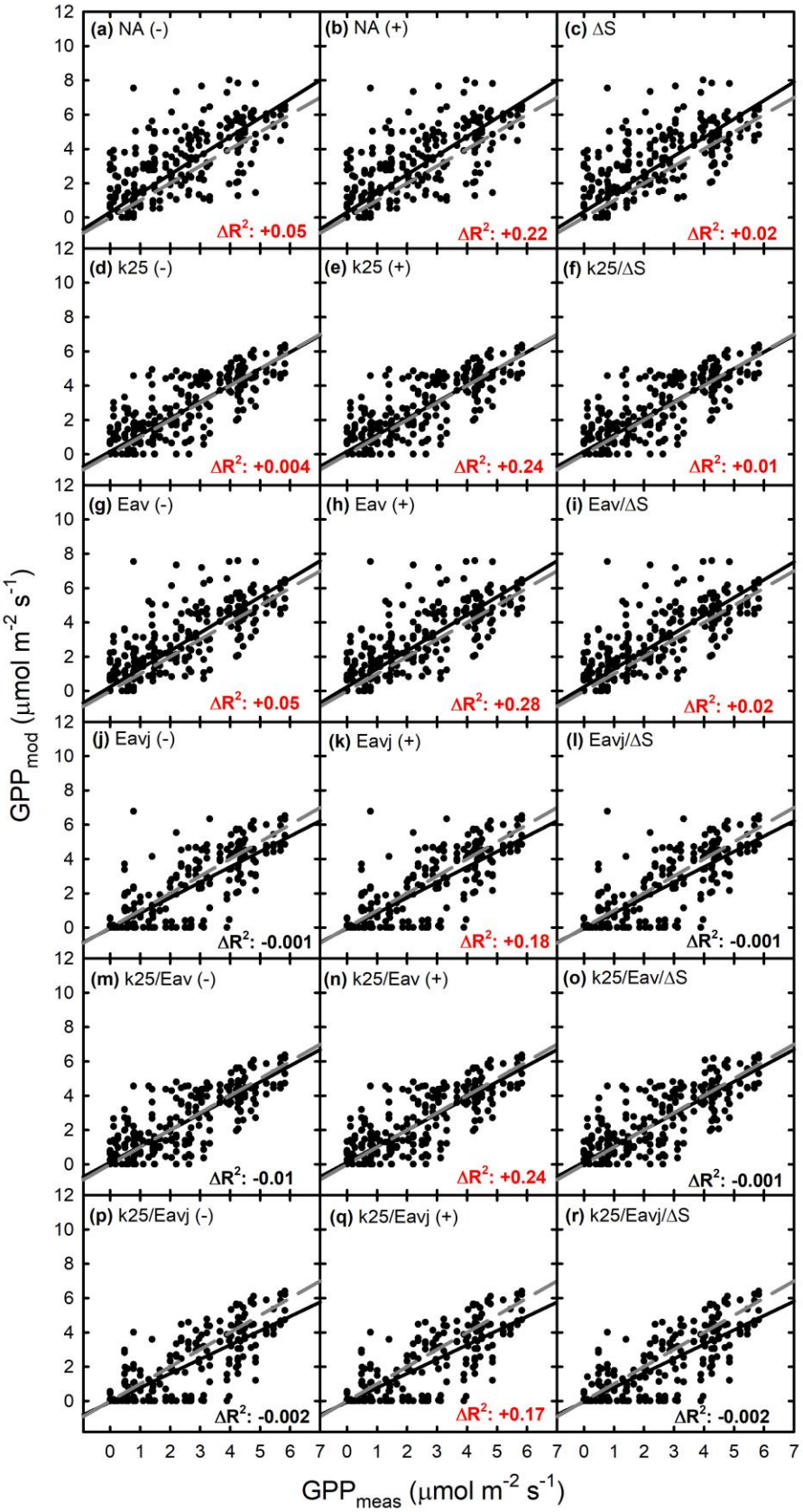
(a) NA (-)
ΔR²: +0.05
(b) NA (+)
ΔR²: +0.22
(c) ΔS
ΔR²: +0.02
(d) k25 (-)
ΔR²: +0.004
(e) k25 (+)
ΔR²: +0.24
(f) k25/ΔS
ΔR²: +0.01
(g) Eav (-)
ΔR²: +0.05
(h) Eav (+)
ΔR²: +0.28
(i) Eav/ΔS
ΔR²: +0.02
(j) Eavj (-)
ΔR²: -0.001
(k) Eavj (+)
ΔR²: +0.18
(l) Eavj/ΔS
ΔR²: -0.001
(m) k25/Eav (-)
ΔR²: -0.01
(n) k25/Eav (+)
ΔR²: +0.24
(o) k25/Eav/ΔS
ΔR²: -0.001
(p) k25/Eavj (-)
ΔR²: -0.002
(q) k25/Eavj (+)
ΔR²: +0.17
(r) k25/Eavj/ΔS
ΔR²: -0.002
GPP_mod (μmol m-2 s-1)
GPP_meas (μmol m-2 s-1)

Figure 4.5. High deactivation energy (H_d) scenario: modelled hourly gross primary productivity (GPP) from MAESTRA across scenarios with different types of photosynthetic temperature acclimation for February 1st, April 6th, August 8th, September 30th, and November 21st from each year between 1998 and 2001. Solid black lines represent significant linear regressions ($P < 0.001$). Grey dashed line indicates a 1:1 relationship. See Table 4.7 for slopes and intercepts. NA: no acclimation, (-) Equation 4.4 is used for V_{cmax}, (+), Equation 4.1 is used for V_{cmax}, k25: basal acclimation of V_{cmax} and J_{max} at 25 °C, Eav: linear acclimation of V_{cmax} activation energy, Eavj: nonlinear acclimation of V_{cmax} and J_{max} activation energies, ΔS: acclimation of the entropy parameter. ΔR^2 indicates the absolute change in R^2 compared to the same scenario with the original H_d value used in Fig. 4.4, with red text indicating an improvement.

Table 4.7. Acclimation scenario performance under the highest H_d for V_{cmax} and J_{max} (High H_d) and the lowest H_d (Low H_d). Slope and intercepts of photosynthetic acclimation scenarios across all temperature (Full) and under restricted temperature domains of the linear Ea (8 - 25 °C; Eav-containing scenarios) and the Eavj (18 - 31 °C; Eavj-containing scenarios) scenarios. The scenarios with the highest R^2 and/or lowest BIC are bolded within each temperature domain scenario.

H_d	High					Low			
Scenario	Slope	Intercept	R^2	BIC	Scenario	Slope	Intercept	R^2	BIC
19. NA (-)	1.100	0.312	0.737	1486	37. NA (-)	0.782	0.686	0.377	1893
20. NA (+)	1.100	0.312	0.737	1486	38. NA (+)	1.215	0.576	0.534	2011
21. k_{25} (-)	0.966	0.166	0.803	1181	39. k_{25} (-)	0.894	0.210	0.755	1243
22. k_{25} (+)	0.966	0.166	0.803	1181	40. k_{25} (+)	1.084	0.502	0.537	1894
23. Eav (-)	1.049	0.245	0.771	1353	41. Eav (-)	0.985	0.282	0.719	1424
24. Eav (+)	1.049	0.245	0.771	1353	42. Eav (+)	1.175	0.649	0.498	2047
25. Eavj (-)	0.896	-0.046	0.729	1308	43. Eavj (-)	0.842	-0.003	0.715	1282
26. Eavj (+)	0.896	-0.046	0.729	1308	44. Eavj (+)	0.968	0.008	0.652	1555
27. ΔS	1.080	0.349	0.732	1479	45. ΔS	1.164	0.653	0.493	2047
28. k_{25}/Eav (-)	0.937	0.128	0.790	1190	46. k_{25}/Eav (-)	**0.862**	**0.152**	**0.769**	**1168**
29. k_{25}/Eav (+)	**0.938**	**0.119**	**0.803**	**1152**	47. k_{25}/Eav (+)	1.069	0.470	0.560	1837
30. k_{25}/Eavj (-)	0.832	-0.060	0.733	1226	48. k_{25}/Eavj (-)	**0.764**	**-0.020**	**0.732**	**1147**
31. k_{25}/Eavj (+)	0.832	-0.060	0.733	1226	49. k_{25}/Eavj (+)	0.903	-0.010	0.657	1478
32. k_{25}/ΔS	0.966	0.166	0.803	1181	50. k_{25}/ΔS	1.084	0.498	0.541	1887
33. Eav/ΔS	1.040	0.246	0.768	1352	51. Eav/ΔS	1.175	0.650	0.498	2047
34. Eavj/ΔS	0.896	-0.046	0.729	1308	52. Eavj/ΔS	0.968	0.008	0.652	1555
35. k_{25}/Eav/ΔS	0.938	0.119	0.803	1152	53. k_{25}/Eav/ΔS	1.069	0.470	0.560	1837
36. k_{25}/Eavj/ΔS	0.836	-0.039	0.744	1205	54. k_{25}/Eavj/ΔS	0.922	0.064	0.626	1562

NA: no acclimation, (-) Equation 4.4 is used for V_{cmax}, (+), Equation 4.1 is used for V_{cmax}, k_{25}: basal acclimation of V_{cmax} and J_{max} at 25 °C, Eav: linear acclimation of V_{cmax} activation energy, Eavj: nonlinear acclimation of V_{cmax} and J_{max} activation energies, ΔS: acclimation of the entropy parameter.

Replacing H_d with the lowest available values had the greatest impact on scenario performance, reducing the R^2 in the NA (-) scenario by 0.311 (Fig. 4.6). In general, the spread of the data was increased (Fig. 4.6), and apart from Eavj (+) and k25/Eavj (+) scenarios (which had increased model performance of 10.2 and 9.8%, respectively), most other scenarios showed drastic reductions in performance (up to -25.6%) (Fig. 4.6; Table 4.7). As with the base H_d and the high H_d cases, scenarios containing k_{25} performed best, with minor improvements from multifactor acclimation in the k25/Eav (-) and k25/Eavj (-) scenarios (Table 4.7).

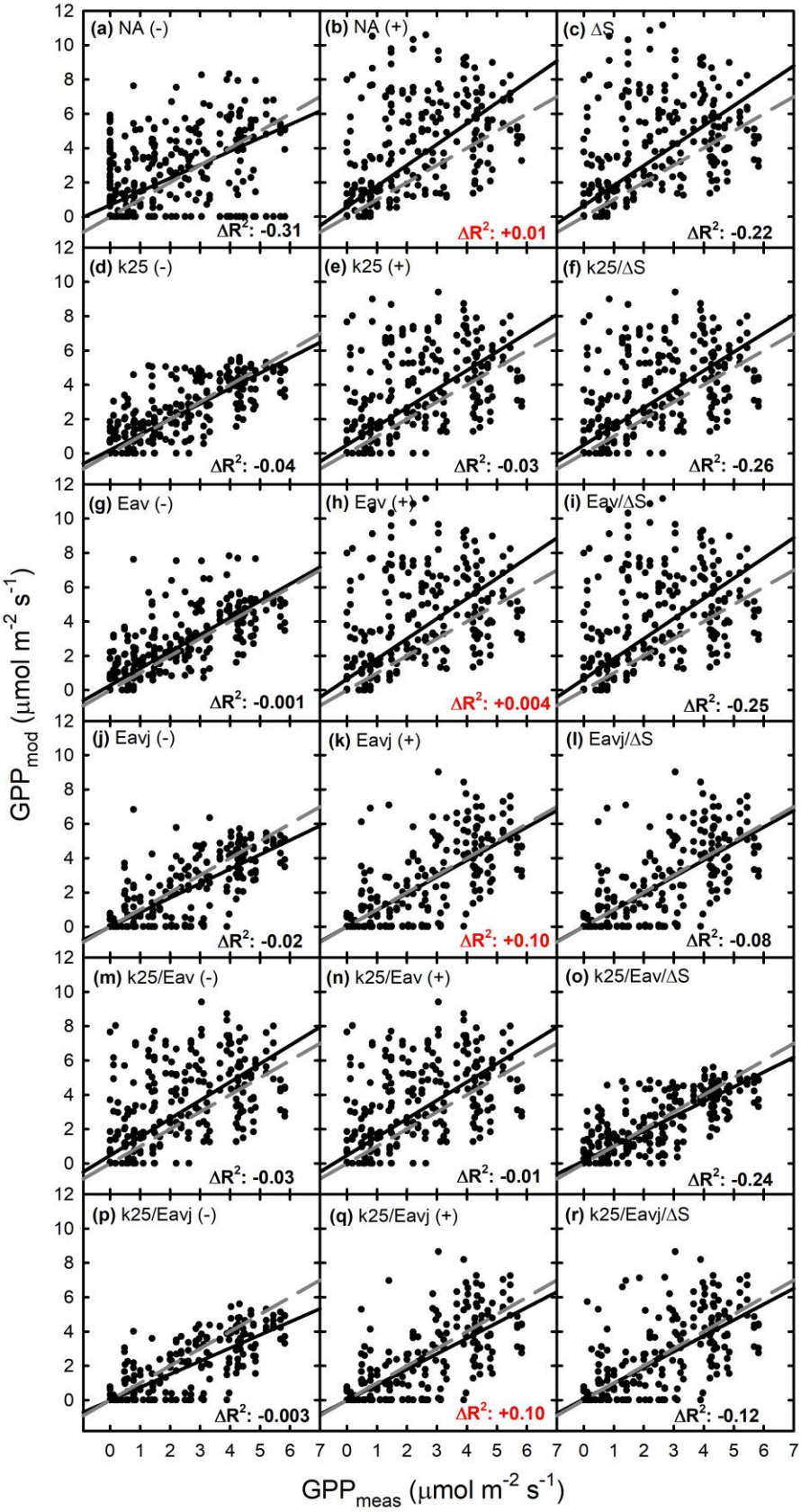
(a) NA (-)
ΔR²: -0.31
(b) NA (+)
ΔR²: +0.01
(c) ΔS
ΔR²: -0.22
(d) k25 (-)
ΔR²: -0.04
(e) k25 (+)
ΔR²: -0.03
(f) k25/ΔS
ΔR²: -0.26
(g) Eav (-)
ΔR²: -0.001
(h) Eav (+)
ΔR²: +0.004
(i) Eav/ΔS
ΔR²: -0.25
(j) Eavj (-)
ΔR²: -0.02
(k) Eavj (+)
ΔR²: +0.10
(l) Eavj/ΔS
ΔR²: -0.08
(m) k25/Eav (-)
ΔR²: -0.03
(n) k25/Eav (+)
ΔR²: -0.01
(o) k25/Eav/ΔS
ΔR²: -0.24
(p) k25/Eavj (-)
ΔR²: -0.003
(q) k25/Eavj (+)
ΔR²: +0.10
(r) k25/Eavj/ΔS
ΔR²: -0.12
GPP_mod (μmol m-2 s-1)
GPP_meas (μmol m-2 s-1)

Figure 4.6. Low deactivation energy (H_d) scenario: modelled hourly gross primary productivity (GPP) from MAESTRA across scenarios with different types of photosynthetic temperature acclimation for February 1st, April 6th, August 8th, September 30th, and November 21st from each year between 1998 and 2001. Solid black lines represent significant linear regressions ($P < 0.001$). Grey dashed line indicates a 1:1 relationship. See Table 4.7 for slopes and intercepts. NA: no acclimation, (-) Equation 4.4 is used for V_{cmax}, (+), Equation 4.1 is used for V_{cmax}, k25: basal acclimation of V_{cmax} and J_{max} at 25 °C, Eav: linear acclimation of V_{cmax} activation energy, Eavj: nonlinear acclimation of V_{cmax} and J_{max} activation energies, ΔS: acclimation of the entropy parameter. ΔR^2 indicates the absolute change in R^2 compared to the same scenario with the original H_d value used in Fig. 4.4, with red text indicating an improvement.

4.3.5 Restricting temperature domain improves performance of thermal acclimation scenarios

Since measurements of thermal acclimation of E_a for V_{cmax} and J_{max} are made over a restricted range of leaf temperatures, I investigated the effect of restricting the temperature domains to those matching the measurements of the E_a of V_{cmax} and J_{max} (i.e. if the ten-day running mean air temperature for a given date was outside of the temperature range used to generate the estimate from Equations 4.8 and 4.9, that date was excluded from the model run). Restricting the temperature domain to that of Equation 8 showed slight improvements of up to 3.6% in the performance of scenarios containing Eav relative to their performance under the full temperature domain (Figs. 4.7a-f; Table 4.6).

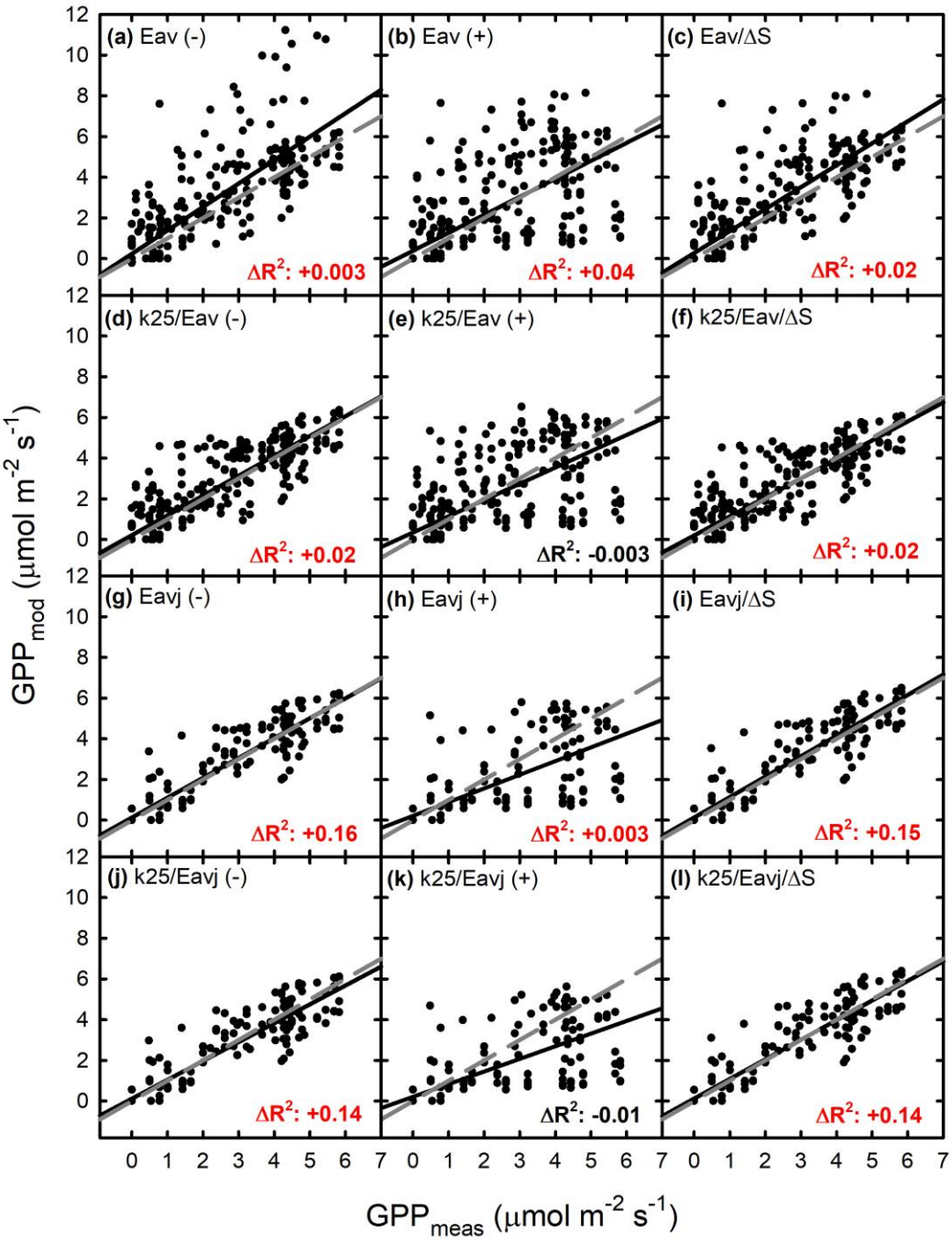

Figure 4.7. Modelled gross primary productivity (GPP) from MAESTRA with temperature ranges restricted to the respective domains of Equations 4.8 (Eav) and 4.9 (Eavj). Solid black lines represent significant linear regressions ($P < 0.001$). Grey dashed line indicates a 1:1 relationship. See Table 4.6 for slopes and intercepts. (-) Equation 4.4 was used for V_{cmax}, (+) Equation 4.1 was used for V_{cmax}, k_{25}: basal

acclimation of V_{cmax} and J_{max} at 25 °C, Eav: linear acclimation of V_{cmax} activation energy, Eavj: nonlinear acclimation of V_{cmax} and J_{max} activation energies, ΔS: acclimation of the entropy parameter. ΔR^2 denotes the absolute change in R^2 relative to the full temperature domain for that scenario in Fig. 4.4, with red text indicating an improvement.

Restricting the temperature domain to that of Equation 4.9 greatly improved the performance of the Eavj scenarios relative to their base case, with improvements of up to 15.5%. However, minimal effects of restricted temperature domain were seen in the Eavj (+) and k25/Eavj (+) scenarios (Figs. 4.7g-l; Table 4.6). The performance of the Eavj scenario under its temperature domain relates to the extreme values of E_a calculated from Equation 4.8 at low temperatures, which causes carbon assimilation in MAESTRA to collapse to 0 below moderately low (~10 °C) temperatures, reducing model performance.

4.4 Discussion

Incorporating thermal acclimation of photosynthesis generally improved scenario performance. Overall, the best acclimation scenarios generally overestimated GPP at low rates, and under-estimated GPP at high rates, since the intercepts were greater than zero and the slopes slightly less than 1. Multiple unaccounted-for factors that can affect photosynthetic carbon uptake could contribute to this, including stresses which could depress GPP in the measured data (Luo *et al.*, 2001), differences amongst leaf age classes (although the model performs well with a single age class; Fig. 4.3), uncertainties in how to partition GPP from net ecosystem exchange (Reichstein *et al.*, 2005; Schaefer *et al.*, 2012; Wohlfahrt & Gu, 2015), and not accounting for photosynthetic carbon uptake in the understory. Including the parameters H_d and ΔS for V_{cmax} had the most detrimental effects on model performance (see differences between + and – scenarios), while including k_{25} acclimation had the most positive effects. It is also important to consider the concept of equifinality here (Medlyn *et al.*, 2005), since different parameterizations of the model could give similar model results, as is illustrated by the ability to produce similar temperature responses of relative V_{cmax} by altering either H_d or ΔS. Therefore, while k_{25} acclimation is the most parsimonious way to include thermal acclimation of photosynthetic capacity, other acclimation functions could also be used. However, multifactor acclimation provided only modest improvements over single factor acclimation (<1% increase in R^2) (Table 4.6). Including ΔS acclimation (currently implemented in some Earth System Models; Oleson *et al.*, 2013; Smith & Dukes, 2013; Smith *et al.*, 2016) improved performance by only ~2% and when combined with acclimation of other parameters, provided some improvements over single factor

acclimation. This suggests that current implementations of photosynthetic temperature acclimation (Oleson *et al.*, 2013; Smith & Dukes, 2013; Smith *et al.*, 2016) may not be the best way to acclimate photosynthesis in models since single-factor acclimation of ΔS did not perform as well as single-factor acclimation of k_{25} (-), Eav (-) and Eavj (-). Overall the best performing multifactor acclimation scenarios included k_{25} acclimation, but these showed near-equivalent performance to single factor k_{25} acclimation. Including Eavj tended to reduce the performance of multifactor models compared to single- or dual-factor models that did not contain Eavj, while using Eav tended to improve multifactor models. The lack of large improvements in multifactor acclimation models may be related to the equations being derived from data on different species (i.e. 'mixing and matching' parameters) (Hikosaka *et al.*, 2006; Kattge & Knorr, 2007; Dillaway & Kruger, 2010). This supports the Rogers *et al.* (2017) recommendation that measured photosynthetic parameters cannot be mixed and matched – with my extension being that they should be used within the confines of their measurement environment. *Therefore, I recommend that multifactor thermal acclimation of photosynthesis not be used in large scale modeling efforts until the underlying physiology is better understood*.

4.4.1 Acclimation of k_{25} outperforms acclimation of other parameters

Our data show that k_{25} is the most important parameter to acclimate to temperature, as acclimation of k_{25} improves GPP predictions both under the full temperature range and when restricted to the temperature range of Equation 4.8. In addition, under the most restricted temperature range for Equation 4.9, acclimation of k_{25} still performed well. While previous studies found that k_{25} did not necessarily acclimate to changes in growth temperature in an easily described pattern (Way & Oren, 2010; Way & Yamori, 2014), Smith & Dukes (2017) found that short-term temperature acclimation caused acclimation of basal rates of V_{cmax} in 22 species, implying that photosynthetic responses to short- and long-term temperature changes may need to be addressed separately. My acclimation scenario is not developmental acclimation, but a combination of temperature effects and leaf age (i.e. seasonal acclimation) and specifically a short-term, air temperature acclimation. Leaf age effects, which include nitrogen reallocation, (e.g. Wilson *et al.*,

2000; Xu *et al.*, 2017) may explain why k_{25} tended to improve the scenarios in which it was included. Within-season leaf age is confounded with changes in air temperature in my k_{25} acclimation scenario, and without Rubisco concentration data, it is difficult to parse whether the k_{25} acclimation is capturing 1) a true temperature effect, 2) a shift of Rubisco function towards nitrogen storage, 3) within-season aging, or 4) all of these effects. However, my data, when combined with that from Smith & Dukes (2017), suggests that k_{25} acclimation should improve carbon gain predictions over seasonal timescales. I would like to note, however, that my acclimation function for k_{25} was derived from coniferous tree data, and conifers are not broadly represented in the data used to derive the other acclimation functions (Hikosaka *et al.*, 2006; Kattge & Knorr, 2007; Dillaway & Kruger, 2010). Given this, these other acclimation functions may perform better on other plant functional types than they do in my analysis.

4.4.2 V_{cmax25} was better correlated with air temperature than day length

My data suggest that photosynthetic capacity in evergreen conifers is regulated differently than in broadleaf deciduous trees, contrasting with the findings of Bauerle *et al.* (2012), which may be related to the use of Rubisco as a nitrogen storage protein during the winter in evergreen conifers (Quick *et al.*, 1992; Warren *et al.*, 2003; Millard *et al.*, 2007; Stinziano & Way, 2017). If this is the case, Earth System Models that incorporate a day length scalar for V_{cmax}, such as the Community Land Model(Oleson *et al.*, 2013), may need to use air temperature, as opposed to day length, to scale V_{cmax25} in evergreen conifers across the season. Currently, however, Earth System Models typically incorporate temperature acclimation of ΔS (Smith & Dukes, 2013; Smith *et al.*, 2016) and/or day length acclimation of V_{cmax} (Oleson *et al.*, 2013), and my data suggest that acclimating ΔS only minimally improves model performance for an evergreen conifer. In this regard, incorporating acclimation of k_{25} *in lieu* of ΔS acclimation for evergreen conifers may improve model performance.

4.4.3 H_d has strong impacts on model performance

In my investigation of using high and low H_d values, I found that the best acclimation scenarios tended to include acclimation of basal photosynthetic acclimation (k_{25}). Reducing H_d of both V_{cmax} and J_{max} from the commonly used values to low, but biologically realistic values had the greatest impact on model performance, reducing R^2 of NA (-) by almost half, and increasing the positive effect of temperature acclimation scenarios on model performance. Meanwhile, increasing H_d of both V_{cmax} and J_{max} from the commonly used values to high, but biologically realistic values generally improved the performance of all acclimation scenarios. Interestingly, the largest improvements were seen in scenarios that included H_d and ΔS for V_{cmax}, and using a high value for H_d eliminated the differences between using the modified (Equation 4.1) and unmodified (Equation 4.4) Arrhenius equation for V_{cmax} (Fig. 4.5; Table 4.7). This effect is due to the high H_d value pushing meaningful divergences between the modified and unmodified Arrhenius equations to high temperatures outside the range used in the present study (Fig. 4.2). Such responses illustrate the importance of H_d, a parameter often fixed to 200,000 J mol^{-1} due to overparameterization of the modified Arrhenius model and the difficulty in measuring it (due to the high temperatures required) (Medlyn *et al.*, 2002; Kattge & Knorr, 2007), which has limited systematic investigations into acclimation of H_d for V_{cmax} and J_{max} (although see Leuning, 2002, and Galmés *et al.*, 2015 for H_d data *in vivo* and *in vitro*, respectively). Therefore, understanding the degree of thermal acclimation of H_d, and whether it even occurs, remains an important knowledge gap. Given the sensitivity of model performance to the value of H_d used (Figs. 4.5, 4.6), the high sensitivity of the Arrhenius model to both H_d and ΔS relative to E_a (Fig. 4.2), and the (required) simultaneous fitting of H_d and ΔS, a renewed focus on quantifying values of H_d and determining to what extent H_d responds to changes in leaf temperature is needed. In light of this sensitivity to H_d and ΔS, and the similar model outputs obtained by changing these two parameters, it is necessary to address whether the modified Arrhenius model used here is the correct approach to modeling photosynthesis and assessing acclimation, since this function is embedded in larger models (Duursma & Medlyn, 2012; Oleson *et al.*, 2013). The Johnson *et al.* (1942) modified Arrhenius function requires

simultaneous fitting of H_d and ΔS, which may be modified relative to each other to achieve the same results (Figs. 4.2b, c). There may be other ways to model temperature responses that avoid this particular equifinality issue, such as the modified Arrhenius function from Kruse *et al.* (2017), which requires only two parameters to describe the curvature of the temperature response.

4.4.4 Temperature domains of acclimation functions affect modeling conclusions

Restricting the modeling results to the temperature domains of the E_a acclimation scenarios improved model performance. The greatest increases in performance under the limited temperature ranges were seen in scenarios containing Eavj acclimation (Equation 4.9; Tables 4.6, 4.7), which is likely due to the rapid increase in E_a values outside the temperature domain of the function. My data support the conclusion that using acclimation equations outside their temperature domain could adversely affect predictions (particularly regarding Equation 4.9 from Dillaway & Kruger, 2010), and should be discouraged. More research is needed, however, to expand the temperature domains for the parameters investigated here, as we currently lack data at temperature extremes.

4.4.5 Conclusions and future directions

To my knowledge, the present study is the first to compare the influence of acclimation of the individual parameters dictating the thermal response of A_{net} on predictions of canopy carbon flux. In my dataset, incorporating multifactor scenarios of thermal acclimation of photosynthesis into models of carbon uptake increased model complexity without improving performance. I therefore have two final recommendations that could improve photosynthetic modeling efforts in Earth System Models: 1) further research into the parameters that underlie photosynthetic thermal acclimation, particularly H_d, is needed to determine if these parameters co-acclimate across a broad range of species and plant functional types and across the range of temperatures experienced by the earth

system; and 2) thermal acclimation of basal rates of photosynthetic capacity should be incorporated into models.

4.5 References

Amthor JS. **1995**. Terrestrial higher-plant response to increasing atmospheric [CO_2] in relation to the global carbon cycle. *Global Change Biology* **1**, 243–274.

Andrews JA, Harrison KG, Matamala R, Schlesinger WH. **1999**. Separation of root respiration from total soil respiration using carbon-13 labeling during free-air carbon dioxide enrichment (FACE). *Soil Science Society of America Journal* **63**, 1429.

Atkin OK, Tjoelker MG. **2003**. Thermal acclimation and the dynamic response of plant respiration to temperature. *Trends in Plant Science* **8**, 343–351.

Baldocchi DD, Falge E, Gu L *et al*. **2001**. FLUXNET: a new tool to study the temporal and spatial variability of ecosystem-scale carbon dioxide, water vapor, and energy flux densities. *Bulletin of the American Meteorological Society* **82**, 2415–2434.

Bauerle WL, Oren R, Way DA *et al*. 2012. Photoperiodic regulation of the seasonal pattern of photosynthetic capacity and the implications for carbon cycling. *Proceedings of the National Academy of Sciences of the United States of America* **109**, 8612–8617.

Bigras FJ, Bertrand A. **2006**. Responses of *Picea mariana* to elevated CO_2 concentration during growth, cold hardening and dehardening: phenology, cold tolerance, photosynthesis and growth. *Tree Physiology* **26**, 875–888.

Binkley D, Stape JL, Bauerle WL, Ryan MG. **2010**. Explaining growth of individual trees: Light interception and efficiency of light use by *Eucalyptus* at four sites in Brazil. *Forest Ecology & Management* **259**, 1704–1713.

Bowden JD, Bauerle WL. **2008**. Measuring and modeling the variation in species-specific transpiration in temperate deciduous hardwoods. *Tree Physiology* **28**, 1675–1683.

Ciais P, Sabine C, Bala G *et al*. 2013. Carbon and other biogeochemical cycles. In: *Climate Change Science 2013: The Physical Science Basis. Contribution of Working Group I to the Fifth Assessment Report of the Intergovernmental Panel on Climate Change*, edited by **Stocker TF, Qin D, Plattner G-K, Tignor M, Allen SK, Boschung J, Nauels A, Xia Y, Bex V, Midgeley PM**, pp. 465–570. Cambridge University Press: Cambridge, UK.

DeLucia, Hamilton, Naidu *et al*. 1999. Net primary production of a forest ecosystem with experimental CO_2 enrichment. *Science* **284**, 1177–1179.

Dillaway DN, Kruger EL. **2010**. Thermal acclimation of photosynthesis: a comparison of boreal and temperate tree species along a latitudinal transect. *Plant, Cell & Environment* **33**, 888–899.

Dreyer E, Le Roux X, Montpied P, Daudet FA, Masson F. **2001**. Temperature response of leaf photosynthetic capacity in seedlings from seven temperate tree species. *Tree Physiology* **21**, 223–232.

Duursma R, Medlyn B. **2012**. MAESPA: a model to study interactions between water limitation, environmental drivers and vegetation function at tree and stand levels, with an example application to [CO_2] x drought interactions. *Geoscientific Model Development* **5**, 919–940.

Ellsworth DS, Oren R, Huang C, Phillips N, Hendrey GR. **1995**. Leaf and canopy responses to elevated CO_2 in a pine forest under free-air CO_2 enrichment. *Oecologia* **104**, 139–146.

Ellsworth DS, LaRoche J, Hendrey GR. **1998**. Elevated CO_2 in a prototype free-air CO_2 enrichment facility affects photosynthetic nitrogen relations in a maturing pine forest. *BNL 52545*. Brookhaven National Laboratory: Upton, NY, USA.

Farquhar GD, von Caemmerer S, Berry JA. **1980**. A biochemical model of photosynthetic CO_2 assimilation in leaves of C_3 species. *Planta* **149**, 78–90.

Galmés J, Karpalov MV, Copolovici LO, Hermida-Carrera C, Niinemets Ü. **2015**. Temperature responses of Rubisco maximum carboxylase activity across domains of life: phylogenetic signals, trade-offs, and importance for carbon gain. *Photosynthesis Research* **123**, 183–201.

Han Q, Chiba Y. **2009**. Leaf photosynthetic responses and related nitrogen changes associated with crown reclosure after thinning in a young *Chamaecyparis obtusa* stand. *Journal of Forest Research* **14**, 349–357.

Han Q, Kawasaki T, Nakano T, Chiba Y. **2004**. Spatial and seasonal variability of temperature responses of biochemical photosynthesis parameters and leaf nitrogen content within a *Pinus densiflora* crown. *Tree Physiology* **24**, 737–744.

Han Q, Araki M, Chiba Y. **2006**. Acclimation to irradiance of leaf photosynthesis and associated nitrogen reallocation in photosynthetic apparatus in the year following thinning of a young stand of *Chamaecyparis obtusa*. *Photosynthetica* **44**, 523–529.

Han Q, Kawasaki T, Nakano T, Chiba Y. **2008**. Leaf-age effects on seasonal variability in photosynthetic parameters and its relationships with leaf mass per area and leaf nitrogen concentration within a *Pinus densiflora* crown. *Tree Physiology* **28**, 551–558.

Harley PC, Weber JA, Gates DM. **1985**. Interactive effects of light, leaf temperature, CO_2 and O_2 on photosynthesis in soybean. *Planta* **165**, 249–263.

Hikosaka K, Ishikawa K, Borjigidai A, Muller O, Onoda Y. **2006**. Temperature acclimation of photosynthesis: mechanisms involved in the changes in temperature dependence of photosynthetic rate. *Journal of Experimental Botany* **57**, 291–302.

Johnson FH, Eyring H, Williams RW. **1942**. The nature of enzyme inhibitions in bacterial luminescence: Sulfanilamide, urethane, temperature and pressure. *Journal of Cellular & Comparative Physiology* **20**, 247–268.

Kattge J, Knorr W. **2007**. Temperature acclimation in a biochemical model of photosynthesis: a reanalysis of data from 36 species. *Plant, Cell & Environment* **30**, 1176–1190.

De Kauwe MG, Lin Y-S, Wright IJ *et al*. 2016. A test of the "one-point method" for estimating maximum carboxylation capacity from field-measured, light-saturated photosynthesis. *New Phytologist* **210**, 1130–1144.

Kruse J, Adams MA, Kadinov G, Arab L, Kreuzwieser J, Alfarraj S, Schulze W, Rennenberg H. **2017**. Characterization of photosynthetic acclimation in *Phoenix dactylifera* by a modified Arrhenius equation originally developed for leaf respiration. *Trees* **31**, 623–644.

Leuning R. **2002**. Temperature dependence of two parameters in a photosynthesis model. *Plant, Cell & Environment* **25**, 1205–1210.

Lewis JD, Tissue DT, Strain BR. **1996**. Seasonal response of photosynthesis to elevated CO_2 in loblolly pine (*Pinus taeda* L.) over two growing seasons. *Global Change Biology* **2**, 103–114.

Lombardozzi DL, Bonan GB, Smith NG, Dukes JS, Fisher RA. **2015**. Temperature acclimation of photosynthesis and respiration: A key uncertainty in the carbon cycle-climate feedback. *Geophysical Research Letters* **42**, 8624–8631.

Luo Y, Medlyn B, Hui D, Ellsworth D, Reynolds J, Katul G. **2001**. Gross primary productivity in Duke forest: modeling synthesis of CO_2 experiment and eddy–flux data. *Ecological Applications* **11**, 239–252.

Maire V, Martre P, Kattge J, Gastal F, Esser G, Fontaine S, Soussana JF. **2012**. The coordination of leaf photosynthesis links C and N fluxes in C_3 plant species. *PLoS ONE* **7**, e38345.

Medlyn BE, Dreyer E, Ellsworth D *et al*. 2002. Temperature response of parameters of a biochemically based model of photosynthesis. II. A review of experimental data. *Plant, Cell & Environment* **25**, 1167–1179.

Medlyn BE. **2004**. A MAESTRO retrospective. In: *Forests at the Land-Atmosphere Interface*, edited by **McNaughton K**, pp. 105–121. CAB International: Wallingford, UK.

Medlyn BE, Robinson AP, Clement R, McMurtrie RE. **2005**. On the validation of models of forest CO_2 exchange using eddy covariance data: some perils and pitfalls. *Tree Physiology* **25**, 839–857.

Millard P, Sommerkorn M, Grelet G-A. **2007**. Environmental change and carbon limitation in trees: a biochemical, ecophysiological and ecosystem appraisal. *New Phytologist* **175**, 11–28.

Misson L, Tu KP, Boniello RA, Goldstein AH. **2006**. Seasonality of photosynthetic parameters in a multi-specific and vertically complex forest ecosystem in the Sierra Nevada of California. *Tree Physiology* **26**, 729–741.

Niu S, Luo Y, Fei S *et al*. **2012**. Thermal optimality of net ecosystem exchange of carbon dioxide and underlying mechanisms. *New Phytologist* **194**, 775–783.

Nolan WG, Smillie RM. **1976**. Multi-temperature effects on Hill reaction activity of barley chloroplasts. *Biochimica et Biophysica Acta (BBA) - Bioenergetics* **440**, 461–475.

Oleson KW, Lawrence DM, Bonan GB, *et al*. **2013**. Technical description of version 4.5 of the Community Land Model (CLM). National Center for Atmospheric Research: Boulder, CO.

Panek JA. **2004**. Ozone uptake, water loss and carbon exchange dynamics in annually drought-stressed *Pinus ponderosa* forests: measured trends and parameters for uptake modeling. *Tree Physiology* **24**, 277–290.

Le Quéré C, Andrew RM, Canadell JG *et al*. **2016**. Global Carbon Budget 2016. *Earth System Science Data* **8**, 605–649.

Peaucelle M, Bellassen V, Ciais P, Peñuelas J, Viovy N. **2017**. A new approach to optimal discretization of plant functional types in a process-based ecosystem model with

forest management: a case study for temperate conifers. *Global Ecology & Biogeography* **26**, 486–499.

Quick WP, Chaves MM, Wendler R *et al*. 1992. The effect of water stress on photosynthetic carbon metabolism in four species grown under field conditions. *Plant, Cell & Environment* **15**, 25–35.

Reichstein M, Falge E, Baldocchi D *et al*. 2005. On the separation of net ecosystem exchange into assimilation and ecosystem respiration: review and improved algorithm. *Global Change Biology* **11**, 1424–1439.

Renninger HJ, Clark KL, Skowronski N, Schäfer KVR. **2013**. Effects of a prescribed fire on water use and photosynthetic capacity of pitch pines. *Trees* **27**, 1115–1127.

Rogers A, Medlyn BE, Dukes JS *et al*. 2017. A roadmap for improving the representation of photosynthesis in Earth system models. *New Phytologist* **213**, 22–42.

Schaefer K, Schwalm CR, Williams C *et al*. 2012. A model-data comparison of gross primary productivity: results from the North American Carbon Program site synthesis. *Journal of Geophysical Research* **117**, G3.

Schlesinger WH, Andrews JA. **2000**. Soil respiration and the global carbon cycle. *Biogeochemistry* **48**, 7–20.

Smith NG, Dukes JS. **2013**. Plant respiration and photosynthesis in global-scale models: incorporating acclimation to temperature and CO_2. *Global Change Biology* **19**, 45–63.

Smith NG, Dukes JS. **2017**. Short-term acclimation to warmer temperatures accelerates leaf carbon exchange processes across plant types. *Global Change Biology* **23**, 4840–4853.

Smith NG, Malyshev SL, Shevliakova E, Kattge J, Dukes JS. **2016**. Foliar temperature acclimation reduces simulated carbon sensitivity to climate. *Nature Climate Change* **6**, 407–411.

Stinziano JR, Way DA. **2017**. Autumn photosynthetic decline and growth cessation in seedlings of white spruce are decoupled under warming and photoperiod manipulations. *Plant, Cell & Environment* **40**, 1296–1316.

Stinziano JR, Hüner NPA, Way DA. **2015**. Warming delays autumn declines in photosynthetic capacity in a boreal conifer, Norway spruce (*Picea abies*). *Tree Physiology* **35**, 1303–1313.

Strand M, Lundmark T, Söderbergh I, Mellander P-E. **2002**. Impacts of seasonal air and soil temperatures on photosynthesis in Scots pine trees. *Tree Physiology* **22**, 839–847.

Wang YP, Jarvis PG. **1990a**. Description and validation of an array model — MAESTRO. *Agricultural & Forest Meteorology* **51**, 257–280.

Wang YP, Jarvis PG. **1990b**. Influence of crown structural properties on PAR absorption, photosynthesis, and transpiration in Sitka spruce: application of a model (MAESTRO). *Tree Physiology* **7**, 297–316.

Warren CR, Dreyer E, Adams MA. **2003**. Photosynthesis-Rubisco relationships in foliage of *Pinus sylvestris* in response to nitrogen supply and the proposed role of Rubisco and amino acids as nitrogen stores. *Trees* **17**, 359–366.

Way DA, Oren R. **2010**. Differential responses to changes in growth temperature between trees from different functional groups and biomes: a review and synthesis of data. *Tree Physiology* **30**, 669–688.

Way DA, Yamori W. **2014**. Thermal acclimation of photosynthesis: on the importance of adjusting our definitions and accounting for thermal acclimation of respiration. *Photosynthesis Research* **119**, 89–100.

Way DA, Stinziano JR, Berghoff H, Oren R. **2017**. How well do growing season dynamics of photosynthetic capacity correlate with leaf biochemistry and climate fluctuations? *Tree Physiology* **37**, 879–888.

Wilson KB, Baldocchi DD, Hanson PJ. **2000**. Spatial and seasonal variability of photosynthetic parameters and their relationship to leaf nitrogen in a deciduous forest. *Tree Physiology* **20**, 565–578.

Wohlfahrt G, Gu L. **2015**. The many meanings of gross photosynthesis and their implication for photosynthesis research from leaf to globe. *Plant, Cell & Environment* **38**, 2500–2507.

Xu L, Baldocchi DD. **2003**. Seasonal trends in photosynthetic parameters and stomatal conductance of blue oak (*Quercus douglasii*) under prolonged summer drought and high temperature. *Tree Physiology* **23**, 865–877.

Xu X, Medvigy D, Wright SJ, Kitajima K, Wu J, Albert LP, Martins GA, Saleska SR, Pacala SW. **2017**. Variations of leaf longevity in tropical moist forests predicted by a trait-driven carbon optimality model. *Ecology Letters* **20**, 1097–1106.

Yamori W, Hikosaka K, Way DA. **2014**. Temperature response of photosynthesis in C_3, C_4, and CAM plants: temperature acclimation and temperature adaptation. *Photosynthesis Research* **119**, 101–117.

Chapter 5

5 Variation in photosynthetic physiology among boreal trees leads to divergent modelled carbon gain responses to climate change

A version of this chapter has been submitted to *Global Change Biology* (Manuscript ID: GCB-18-0412), and addresses **Question 4** (how do climate variation (seasonal and annual) and physiological variation interact to affect projections of boreal tree net carbon gain responses to climate change?) and **Hypothesis 1** (boreal trees are limited in growth and photosynthesis by low temperatures) from Chapter 1.

5.1 Introduction

Boreal forests account for ~30% of the globe's forested area (FAO, 2001) and contain ~32% of the world's forest carbon (Bradshaw & Warkentin, 2015). These high latitude forests also exhibit high sensitivity to climate variability (Seddon *et al*., 2016) and will experience greater and more seasonally variable warming than temperate or tropical forests (Collins *et al*., 2013). The response of boreal forests to climate change is particularly important as photosynthetic and respiratory fluxes from high latitude forests strongly influence the global carbon cycle, as evidenced by the impact that the seasonality of these carbon fluxes has on the amplitude of annual atmospheric CO_2 oscillations (Graven *et al*., 2013; Forkel *et al*., 2016). As such, understanding how carbon fluxes respond to rising CO_2 and temperature in the small number of tree species that dominate the boreal forest is necessary for modeling how climate change will impact future atmospheric CO_2 trajectories.

The Earth system models used to predict future climate scenarios group plant species according to plant functional types to model climate responses of carbon fluxes in the boreal forest and other biomes (Sitch *et al*., 2008; Fisher *et al*., 2014; Rogers *et al*., 2017). This simplification assumes that all species within a plant functional type are physiologically similar, and thus these models use an identical set of parameter values to model photosynthesis and respiration for all the species in a given plant functional type (Bonan *et al*., 2002). However, the physiological parameters used to estimate plant

carbon fluxes in these models, such as the maximum carboxylation rate of Rubisco (V_{cmax}), can vary by more than 350% between species within the boreal evergreen needle-leaved tree plant functional type (Warren *et al*., 2003; Goodine *et al*., 2008). Variability in the physiology of species represented by a given plant functional type thus introduces large uncertainties into our predictions of vegetation responses to climate change (Wullschleger *et al*., 2014; Ali *et al*., 2015; Atkin *et al*., 2015). However, it is unclear whether ignoring this variation in photosynthetic and respiratory parameterizations significantly impacts predictions of how boreal forest carbon fluxes will be affected by climate change, or whether the large increases in high latitude temperature will have such a strong effect on tree carbon fluxes that these physiological differences between species are trivial in comparison.

Modeling the responses of vegetation carbon fluxes to climate requires estimates of how photosynthetic CO_2 uptake and CO_2 losses from respiration respond to short-term changes in leaf temperature. The temperature response of photosynthetic capacity can be described by a modified Arrhenius function (Medlyn *et al*., 2002):

$$f(T_k) = k_{25}\exp\left[\frac{E_a(T_k-298)}{298RT_k}\right]\frac{1+\exp\left(\frac{298\Delta S-H_d}{298R}\right)}{1+\exp\left(\frac{T_k\Delta S-H_d}{T_kR}\right)} \qquad \text{Equation 5.1}$$

where $f(T_k)$ is the photosynthetic capacity (either the maximum rate of Rubisco carboxylation, V_{cmax}, or the maximum rate of electron transport, J_{max}, both in μmol CO_2 m^{-2} s^{-1}), k_{25} is the photosynthetic capacity at 25 °C (μmol CO_2 m^{-2} s^{-1}), T_k is the temperature (K), R is the universal gas constant (8.314 J mol^{-1} K^{-1}), E_a is the activation energy (J mol^{-1}), H_d is the deactivation energy (J mol^{-1}), and ΔS is the entropy parameter (J mol^{-1}). The E_a determines the steepness of the slope of the temperature response of photosynthetic capacity below the thermal optimum, while H_d describes the steepness of the slope above the thermal optimum, and ΔS affects the temperature at which the thermal optimum occurs. The temperature response of photosynthetic capacity can also be described with an unmodified Arrhenius equation (Johnson *et al*., 1942):

$$f(T_k) = k_{25}\exp\left[\frac{E_a(T_k-298)}{298RT_k}\right] \qquad \text{Equation 5.2}$$

which assumes that $f(T_k)$ increases monotonically with temperature (i.e. the temperatures used in scaling are far below the thermal optimum where modifications to Equation 2 are needed). In contrast to photosynthetic capacity, the temperature response of respiration can be described by (Atkin & Tjoelker, 2003):

$$R_2 = e^{\left[\frac{T_2 - T_1}{10} \log Q_{10} + \log R_1\right]} \qquad \text{Equation 5.3}$$

where R_1 and R_2 are respiration rates (μmol CO_2 m^{-2} s^{-1}) at temperatures T_1 and T_2 (°C), respectively, and Q_{10} is the thermal sensitivity coefficient, representing a fold change in the rate of respiration per 10 °C temperature increase.

The approaches to modeling leaf carbon fluxes described above are widely used in describing plant responses to their thermal environment. But the parameter values describing these temperature responses are not necessarily static, as they may change when plants are exposed to different environmental conditions. Both photosynthesis and respiration can acclimate to higher temperatures in plants that are exposed to warm conditions for weeks or longer (Berry & Björkman, 1980; Atkin & Tjolker, 2003; Hikosaka *et al*., 2006; Kattge & Knorr, 2007; Yamori *et al*., 2014; Heskel *et al*., 2016), and incorporating thermal acclimation of these processes improves model predictions of ecosystem CO_2 exchange and tends to increase net carbon gain (Smith *et al*., 2016a). Photosynthetic acclimation tends to shift the thermal optimum of photosynthetic capacity to a higher temperature, where a shift in the temperature optimum can be related to a change in the ΔS parameter of the modified Arrhenius response in Equation 5.1 (Kattge & Knorr, 2007). But there is conflicting evidence as to how thermal acclimation of the photosynthetic temperature response occurs (Dillaway & Kruger, 2010): values for the E_a and ΔS parameters of Equation 5.1 have been proposed to change in leaves acclimated to warmer temperatures (Hikosaka *et al*., 2006; Kattge & Knorr, 2007; Dillaway & Kruger, 2010), and it remains unknown whether acclimation of H_d occurs (Chapter 4; Stinziano *et al*., 2018). Thermal acclimation to warmer temperature also tends to reduce respiration rates (Slot & Kitajima, 2015), which can reduce the effect of climate warming on respiration by 80% in boreal and temperate tree species (Reich *et al*., 2016). Temperature

acclimation of respiration can be achieved by a reduction in the Q_{10} of respiration (Slot & Kitajima, 2015; Heskel *et al*., 2016), described by (Atkin & Tjoelker, 2003):

$$Q_{10} = 3.090 - 0.043T \qquad \text{Equation 5.4}$$

where T is the acclimation temperature (°C).

While the methods for incorporating thermal acclimation of plant carbon fluxes are still debated (and are therefore the focus of the present study), photosynthetic capacity can also respond to both elevated CO_2 (Ainsworth & Rogers, 2007; Chapter 2; Stinziano & Way, 2014) and seasonal changes in day length (Bauerle *et al*., 2012). In general, photosynthetic capacity declines with acclimation to elevated CO_2, an effect that is relatively well understood and can be implemented in models via reductions in leaf N (and therefore photosynthetic capacity) at elevated CO_2 (Ainsworth & Rogers, 2007; Rogers *et al*. 2017). With regard to the effects of seasonal changes in day length, both V_{cmax} and J_{max} show a stronger correlation with the day of year (DOY) than with temperature for deciduous broadleaf trees, such that decreasing day length causes a reduction in photosynthetic capacity (Bauerle *et al*., 2012). In an evergreen conifer, there is a stronger correlation of photosynthetic capacity with day length than with temperature, although there does not appear to be a causative relationship with day length (Stinziano & Way, 2017). Scaling photosynthetic capacity with DOY improves global and regional models of vegetative carbon uptake (Bauerle *et al*., 2012; Stoy *et al*., 2014), and provides a way to account for seasonal variation of photosynthetic capacity that is separate from the temperature acclimation described above, as implemented in the Community Land Model (Oleson *et al*., 2013) and the Ecosystem Demography 2 model (Medvigy *et al*., 2013).

Here I assess how net carbon gain (the sum of photosynthesis, respiration, and photorespiration) is affected by considering species-level physiological variation and thermal acclimation of photosynthesis and respiration under a range of climate scenarios at five sites across a latitudinal gradient in the boreal forest. I used a spatially-explicit three-dimensional model (MAESTRA; Duursma & Medlyn, 2012) to predict net carbon gain in 20 x 20 m plots for seven boreal conifer species (*Abies balsamea*, *Larix laricina*,

Picea abies, *Picea glauca*, *Picea mariana*, *Pinus banksiana*, and *Pinus sylvestris*) under a set of climate change scenarios for the year 2100. I hypothesized that: 1) modelled net carbon gain would be stimulated by both warming and elevated CO_2 in boreal trees species; 2) all the species modeled would have similar responses to climate change, but the magnitude of the effect of increasing CO_2 and temperature would vary between species; 3) the effect of incorporating species variation in physiological parameter values on modeled net carbon gain would be smaller than the effect of simulated climate change; and 4) thermal acclimation of photosynthesis and respiration would enhance net carbon gain across all climate scenarios at all sites.

5.2 Materials and methods

5.2.1 Meteorological data

To test how physiological variability of boreal conifers affected modelled net carbon gain across a range of climate conditions, I compiled average hourly air temperature, relative humidity and wind speed data for 2011 to 2015 for each month from June to October (climate.weather.gc.ca/, Environment Canada, 2016) at five locations across the Canadian boreal forest: Trenton, ON (44°07'00" N, 77°32'00" W) (Site 1), Moosonee, ON (51°17'28" N, 80°36'28" W) (Site 2), Peawanuck, ON (54°59'00" N, 85°26'00" W) (Site 3), Churchill, MB (58°44'21" N, 94°03'59" W) (Site 4), and Fort Good Hope, NT (66°14'32" N, 128°38'39" W) (Site 5) (Fig. 5.1). Solar insolation was estimated in 15 minute intervals using an online calculator (http://www.pveducation.org/pvcdrom/calculation-of-solar-insolation) that estimates maximum solar insolation based on latitude and day of year.

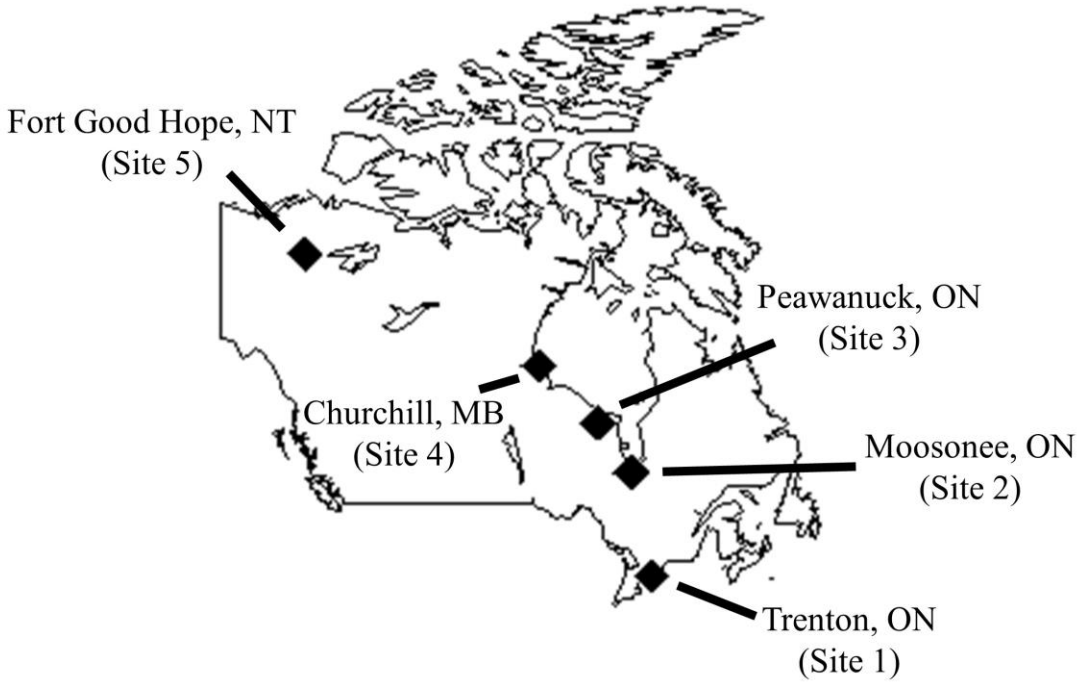

Figure 5.1. Locations of climatological stations used for MAESTRA simulations to provide a breadth of seasonal changes in temperature and day length.

5.2.2 Model description and parameterization

I used a process-based model of radiation absorption and carbon balance for individual trees (MAESPA, run in MAESTRA mode) that scales tissue-level measurements of carbon flux to the whole tree, by integrating data on canopy structure, radiation, weather, and physiology (Duursma & Medlyn, 2012). For each boreal conifer species (*Abies balsamea* (L.) Mill., *Larix laricina* (Du Roi) K. Koch., *Picea abies* (L.) H. Karst., *Picea glauca* (Moench) Voss, *Picea mariana* (Mill.) B.S.P., *Pinus banksiana* Lamb, and *Pinus sylvestris* L.) where I could find sufficient photosynthetic and respiratory data in the literature (i.e. photosynthetic capacity at 25 °C, leaf respiration at 25 °C), I parameterized MAESTRA to estimate net carbon gain for that species (Table 5.1). For species where data on necessary parameters were missing (e.g. photosynthetic temperature response parameters, stomatal conductance model parameters), parameter data from the same genus was used, and if no genus-specific parameter values were available, a mean value of that parameter from all other boreal conifer species was used. I used a value for quantum yield of electron transport (AJQ) of 0.218 (mean value from Wallin *et al*., 1992; Long *et al*., 1993, and Marek *et al*., 2002 for *Picea* spp.), and a thermal sensitivity coefficient (Q_{10}) for respiration (leaf, stem, and root) of 2.0, which has been found to be stable across a range of elevated growth temperatures and CO_2 concentrations in a boreal conifer species (Kroner & Way, 2016). However, since the focus of my study was on the interplay between physiological traits and climate variability, I kept tree dimension parameter values constant across species in MAESTRA, a similar approach to canopy structure as that used in larger-scale models like the Community Land Model (Oleson *et al*., 2013). Both V_{cmax} and J_{max} were calculated for June 16 (DOY 167), July 16 (DOY 197), August 16 (DOY 228), September 16 (DOY 259) and October 16 (DOY 289) as a function of day of year. I used an equation to scale photosynthetic capacity from the literature with day length, assuming the literature value to be a maximum photosynthetic capacity. This day of year scaling equation (and the values for the equation constants) were based on an evergreen conifer (*Picea glauca*; Chapter 3; Stinziano & Way, 2017):

$$PC = P_{max} \times \frac{aDOY^2 + bDOY + g}{P_{max,pg}} \qquad \text{Equation 5.5}$$

where PC is either V_{cmax} or J_{max} on a given DOY, P_{max} is the maximum value of PC for a given species (assumed to be equal to the literature value), and $P_{max,pg}$ is the maximum value of PC for *Picea glauca*. The equation constants a, b and g are -0.0003 and -0.0022 for a, 0.2968 and 1.2992 for b, and -8.8682 and -97.2139 for g, for V_{cmax} and J_{max}, respectively.

Table 5.1. Species-specific mean parameter values used in MAESTRA to model carbon gain for each boreal conifer species at the stand level.

Parameter names and units	Abbreviation	Species						
		Abies balsamea	*Larix laricina*	*Picea abies*	*Picea glauca*	*Picea mariana*	*Pinus banksiana*	*Pinus sylvestris*
Maximum rate of electron transport at 25 °C (μmol m^{-2} s^{-1})	Maximum J_{max}	54.3[1]	61.25[2]	70.9[3]	97.9[4]	154.5[5-7]	245[7,8]	143[9-11]
Curvature of light response curve of electron transport	THETA	0.71[12]						
Quantum yield of electron transport (mol e^- mol^{-1} CO_2)	AJQ	0.218[13-15]						
Activation energy of J_{max} (J mol^{-1})	EAVJ	50820[16]	50820[16]	40000[17]	40000[17]	40000[17]	100280[16]	100280[16]
Deactivation energy of J_{max} (J mol-1)	EDVJ	200000[16]	200000[16]	220000[17]	220000[17]	220000[17]	147920[16]	147920[16]
Entropy term of J_{max} (J K^{-1} mol^{-1})	DELSJ	710[17]						
Maximum rate of Rubisco carboxylation at 25 °C (μmol m^{-2} s^{-1})	Maximum V_{cmax}	23.3[1]	41.2[2]	51.6[3]	44.5[4]	46[5-7]	73.7[7,8]	84[9-11]
Activation energy of V_{cmax} (J mol^{-1})	EAVC	60020[16]	60020[16]	56000[17]	56000[17]	56000[17]	69830[16]	69830[16]
Foliar dark respiration rate at 25 °C (μmol m^{-2} s^{-1})	RD	1.2[18]	0.62[2]	0.53[19]	2.78[4]	0.62[5,6]	1.15[20]	2.31[10]
R_{light} as proportion of R_D	DAYRESP	0.7[21]						
Foliage Q_{10} values (exponential form)	FOLQ10	0.862[22]						
Stem respiration at 25 °C (μmol m^{-2} s^{-1})		1.77[28]	1.59[29]	1.92[30]	1.92[30]	1.92[30]	1.09[31]	1.09[31]
Root respiration at 25 °C (μmol g^{-1} s^{-1})		0.0216[29]	0.0221[32]	0.0063[33]	0.0095[34]	0.0299[32]	0.0244[32]	0.0194[35]
Intercept of the Ball Berry model (mol m^{-2} s^{-1})	G0	0.0395[29]	0.0364[2]	0.025[36]	0.0256[4]	0.0974[37]	0.01[38]	0.01[38]
Slope of the Ball Berry model (mol m^{-2} s^{-1})	G1	5.92[29]	5.68[2]	6[36]	9.84[4]	2.85[37]	5[38]	5[38]

CO_2 compensation point in the absence of mitochondrial respiration at 25 °C (μmol mol^{-1})	GAMMA	40.8[29]	40.8[29]	36.9[36]	36.9[36]	36.9[36]	44.7[38]	44.7[38]
Soil reflectance (%) (PAR/NIR/IR)	RHOSOL	0.10, 0.30, 0.05[17]						
Needle transitivity (%) (PAR/NIR/IR)	ATAU	0.03, 0.26, 0.0[17]						
Needle reflectance (%) (PAR/NIR/IR)	ARHO	0.09, 0.33, 0.05[17]						
Number of sides for leaf	NSIDES	1[17]						
Width of the leaf	WLEAF	0.001[17]						
Number of age classes		1[4]						
Foliage clumping factor		0.64[12]						
Shape of canopy		CONE[39]						
Leaf angle distribution		1[39]						
Number of leaf area classes		1[39]						
Mean leaf incidence angle		45[39]						
Crown radius (y-axis, m)	ALLRADY	1.38[40]						
Crown radius (x-axis, m)	ALLRADX	1.38[40]						
Height (m)	ALLHTCROWN	7.84[41-44]						
Trunk height (m)	ALLHTTRUNK	1.46[45]						
Stem diameter (m)	ALLDIAM	0.0912[41-44]						
Leaf area (m)	ALLLAREA	16.3[46]						
Plot x-dimension (m)	XMAX	20						
Plot y-dimension (m)	YMAX	20						
Slope x-dimension (°)	XSLOPE	0						
Slope y-dimension (°)	YSLOPE	0						
(°)	BEARING	180						

Number of trees	NOTREES	81[41-44]
Measurement height (m)	ZHT	7.84[47]
Zero-plane displacement (m)	ZPD	5.09[47]
Roughness length (m)	Z0HT	0.78[47]

Note: data listed in one column only were used for all species. In cases where data were not available, means of the species for which data are available were used instead. For calculation parameters, I used 10, 12, 9, 6, and 8 for number of layers in the crown, number of points per layer, number of zenith angles, number of azimuth angles, and number of shading trees, respectively. [1]Goodine *et al*., 2008; [2]This study (Table C.1); [3]Stinziano *et al*., 2015; [4]Stinziano & Way, 2017; [5]Major *et al*., 2014; [6]Rayment *et al*., 2002; [7]Cai & Dang, 2002; [8]Zhang & Dang, 2005; [9]Warren *et al*., 2003; [10]Jach & Ceulemans, 2000; [11]Kellomäki & Wang, 1996; [12]Medlyn *et al*., 2005; [13]Marek *et al*., 2002; [14]Long *et al*., 1993; [15]Wallin *et al*., 1992; [16]Medlyn *et al*., 2002; [17]Ibrom *et al*., 2006; [18]Lusk & Reich, 2000; [19]Tarvainen *et al*., 2013; [20]Busch *et al*., 2007; [21]Ayub *et al*., 2011; [22]Stockfors & Linder, 1998; [23]Scheller & Mladenoff, 2004; [24]Richardson *et al*., 2001; [25]Tjoelker *et al*., 1998; [26]Way & Sage, 2008; [27]Wuytack *et al*., 2013; [28]Lavigne *et al*., 2004; [29]Mean of other parameters; [30]Acosta *et al*., 2008; [31]Zha *et al*., 2004; [32]Tjoelker *et al*., 1999; [33]Weger & Guy, 1991; [34]Koch *et al*., 2007; [35]Crookshanks *et al*., 1998; [36]Zheng *et al*., 2002; [37]Way *et al*., 2011; [38]Thum *et al*., 2007; [39]Gspaltl *et al*., 2013; [40]Vezina, 1962; [41]Peichl *et al*., 2007; [42]Fournier *et al*., 1997; [43]Harrell *et al*., 1995; [44]Robertson, 1987; [45]Riano *et al*., 2004; [46]Chen *et al*., 2002; [47]Calculated from Norman & Campbell, 1998.

In MAESTRA, model plots of forest stands were set up as uniform monocultures based on mean height, diameter at breast height, leaf area index, and mean stand density data for boreal conifers (Vezina, 1962; Robertson, 1987; Harrell *et al*., 1995; Fournier *et al*., 1997; Chen *et al*., 2002; Riano *et al*., 2004; Peichl *et al*., 2007; Table 5.1). Using a consistent set of structural values for all species allowed for an assessment of the direct impacts of physiological and biochemical variability between species on net carbon gain in the absence of tree structural variation.

5.2.3 Assessing how boreal tree physiology affects net carbon gain responses to climate change

I used warming predictions for the representative concentration pathway 8.5 scenario (75^{th} percentile predictions for 2081-2100 from Annex I from Working Group 1 of Assessment Report 5 for the Intergovernmental Panel on Climate Change (Figs. AI.SM8.5.28, AI.SM8.5.31, AI.SM8.5.32, AI.SM8.5.36, AI.SM8.5.39, AI.SM8.5.40 from IPCC, 2013)) to construct eight climate scenarios of increasing spatiotemporal resolution. 1) Global average annual warming (+4.5 °C) represents the simplest case and is often used in experimental investigations of warming effects on vegetation. 2) Regional average annual warming (varying from +6 to 10 °C across the latitudinal gradient examined here) accounts for regional variation in warming predictions; since higher latitudes experience greater warming, this scenario represents a more accurate depiction of warming at high latitude locations than does global average annual warming. 3) Seasonal regional warming (varying from +6 to 8 °C) represents a spatiotemporally explicit warming scenario that accounts for differential warming expected across seasons; peak warming is less than the regional average annual warming because I did not run simulations during the winter season, and the temporal resolution is three months for this scenario instead of one year for the annual warming. I constructed the control (2011 to 2015 climate data) and the three warming scenarios with and without elevated CO_2 of 936 ppm (average representative concentration pathway 8.5 prediction) for a total of eight climate scenarios (Table C.2). These scenarios were run for each species separately at each of the five locations across the boreal forest (see Meteorological Data above). Each model simulation consisted of one day in June, July, August, September, and

October (with climate data reflecting the average climate data for the whole month) such that one monoculture stand of each species was simulated for each climate scenario, location, and time. The range of climate scenarios, locations, and times were selected to achieve a wide range of climate conditions (minimum mean 24-hr temperature: -2.7 °C, maximum mean 24-hr temperature: 27.49 °C; Table C.2) to adequately assess differences among physiological parameter sets. With seven species (Table 5.1), eight climate scenarios, five locations, and five time points, a total of 1400 simulations were run for the interspecies comparison. Climate change effects on net carbon gain were calculated by taking the ratio of net carbon gain under the climate change scenario relative to net carbon gain under the current climate data.

5.2.4 How do species-specific parameter values and metabolic acclimation affect carbon gain responses to climate change scenarios?

Given the relative lack of data on thermal response parameters for photosynthetic capacity, I next assessed the effect of modifying the thermal response parameters from Equations 5.1 and 5.2 (i.e. E_a for V_{cmax} and both E_a and H_d for J_{max}) on net carbon gain in MAESTRA. I used the extensive physiological dataset available for *Picea glauca* in Stinziano and Way (2017) for this in-depth modeling. I tested the effect of varying E_a and H_d on net carbon gain responses to climate scenarios by running MAESTRA with the full *Picea glauca* parameter set, then substituted the thermal response parameter sets from *Picea glauca* for those of *Abies* and *Pinus*. I then quantified the total variance in net carbon gain within a climate scenario (across all time points and locations) for each of the three species-specific parameter sets (for a total of 600 simulations). To test the impact of the photosynthetic capacity values on modelled net carbon gain among boreal trees, I used a *Picea glauca* parameterization of MAESTRA and switched out V_{cmax} and J_{max} values from *P. glauca* for those from *Abies balsamea* (the lowest V_{cmax} and J_{max} values in my study) and *Pinus banksiana* (the highest V_{cmax} and J_{max} values in my study), then ran MAESTRA for all 200 combinations of location, month, and climate scenario for each photosynthetic capacity parameterization of MAESTRA (for a total of 600 simulations for the V_{cmax}/J_{max} swapping).

To test the effect of photosynthetic thermal acclimation on net carbon gain, total carbon gain, and variability in net carbon gain, I tested two separate acclimation approaches. For the first approach, activation energies for V_{cmax} and J_{max} were scaled with average monthly temperature as per Dillaway & Kruger (2010):

$$E_{a,Vcmax} = {45322}/{T_{air}{}^2} - {3368.2}/{T_{air}} + 119.9 \quad \text{Equation 5.6}$$

$$E_{a,Jmax} = {80318.9}/{T_{air}{}^2} - {6093.6}/{T_{air}} + 134.7 \quad \text{Equation 5.7}$$

where $E_{a,Vcmax}$ and $E_{a,Jmax}$ are the activation energies for V_{cmax} and J_{max} (in kJ mol^{-1}), respectively, and T_{air} is the mean air temperature (°C) for the simulated month. The equations were translated (by changing the constants for $E_{a,Vcmax}$ and $E_{a,Jmax}$, respectively) to intersect with the activation energies for *Picea*, which changed the constants for $E_{a,Vcmax}$ and $E_{a,Jmax}$ from 119.9 to 118.2 and from 134.7 to 155.2. Note that the parameterizations of MAESTRA with Equations 5.6 and 5.7 use Equation 5.2 for V_{cmax} and Equation 5.1 for J_{max}. For the second approach, I tested the effects of acclimating ΔS for V_{cmax} and J_{max} on net carbon gain; this required a value for H_d for V_{cmax} (which is present only in Equation 5.1), which I set to 200 kJ mol^{-1} (Medlyn *et al*., 2002). I then acclimated photosynthesis according to Kattge & Knorr (2007):

$$\Delta S = d + e \times T_{air} \quad \text{Equation 5.8}$$

where d and e are constants with separate values for V_{cmax} (668.39 J mol^{-1} and -1.07 J mol^{-1} °C^{-1}, respectively) and J_{max} (659.70 J mol^{-1} and -0.75 J mol^{-1} °C^{-1}, respectively).

The two photosynthetic thermal acclimation scenarios and the control (no acclimation) scenario were also run with and without respiratory acclimation, where the Q_{10} of respiration was scaled to the monthly mean air temperature using Equation 5.4 (for a total of 1200 simulations for comparing acclimation scenarios).

5.2.5 Statistical analysis

Data analyses were carried out using R GUI Version 3.3.3 (R Core Development team, 2017). To determine whether net carbon gain varied by: 1) species-specific physiologcial parameter sets, 2) species-specific photosynthetic capacity (i.e. swapping out V_{cmax} and J_{max} while holding all other parameters constant), or 3) species-specific Arrhenius parameters, I ran ANOVAs with the following structure, treating all variables as fixed effects: Net Carbon Gain ~ Warming Scenario * CO_2 Scenario * Mean 24-hr Temperature * Species, where species represents the parameter set used (1) or the photosynthetic capacity or Arrhenius parameters used (for 2 & 3, respectively). To determine whether net carbon gain varied with acclimation of photosynthesis and respiration across the climate scenarios, the ANOVA structure was: Net Carbon Gain ~ Warming Scenario * CO_2 Scenario * Mean 24-hr Temperature * Pn * Rn, where Pn respresents photosynthetic temperature acclimation (either E_a or ΔS), and Rn represents respiratory temperature acclimation. ANOVA models were stepwise-reduced, removing parameters until the lowest Bayesian Information Criterion (BIC) was achieved. The model with the lowest BIC was then used for final interpretation. Tukey's HSD was used to determine differences in net carbon gain between species, parameters, and acclimation types within the respective ANOVAs.

5.3 Results

Under current climate conditions and CO_2, the timing and rates of net carbon gain showed considerable and realistic latitudinal variation, with a shorter and more intense period of peak net carbon gain at higher latitudes (Fig. C.1a). Warming of +4.5 °C enhanced carbon gain and extended the period of carbon gain at all latitudes except the most southerly site (where net carbon gain was reduced in the summer for most species), with larger increases in peak net carbon gain at higher latitudes (Figs. 5.2b, C.1b). Annual regional warming reduced summer net carbon gain at the lowest and highest latitude sites, but enhanced net carbon gain during autumn at all sites and during all months at Sites 3 and 4 (Figs. 5.2d, C.1c). Seasonal regional warming, the most complex and realistic warming scenario, showed a *less* complex effect on net carbon gain, strongly increasing net carbon gain at higher latitudes, particularly in the autumn, while reducing

net carbon gain during summer at the lowest latitudes, similar to the 4.5 °C warming scenario (Figs. 5.2f, C.1d). In general, warming had the most positive effect on net carbon gain across all species in the autumn, and tended to reduce net carbon gain at the lowest latitude site during the warm summer months (Figs. 5.2, C.1). Increasing the atmospheric CO_2 concentrations in these scenarios preserved the patterns seen in net carbon gain changes across time and space (Figs. C.1e-h). Unsurprisingly, elevated CO_2 generally enhanced net carbon gain relative to the ambient CO_2 scenario, although it had the greatest effect mid-summer and at the lowest latitudes, where temperatures were warmest (Fig. 5.2a). When the two climate change factors were considered together, elevated CO_2 attenuated reductions in net carbon gain at high temperatures compared to the ambient CO_2 scenarios (Figs. 5.2a, c, e, g, C.1e-h), while also increasing the differences seen between species across the climate scenarios (Fig. C.1). The seasonal regional warming with elevated CO_2 increased net carbon gain and the period of carbon uptake relative to current climate conditions, except for two species (*Larix laricina* and *Abies balsamea*) at the lowest latitude site (Figs. 5.2g, C.1h).

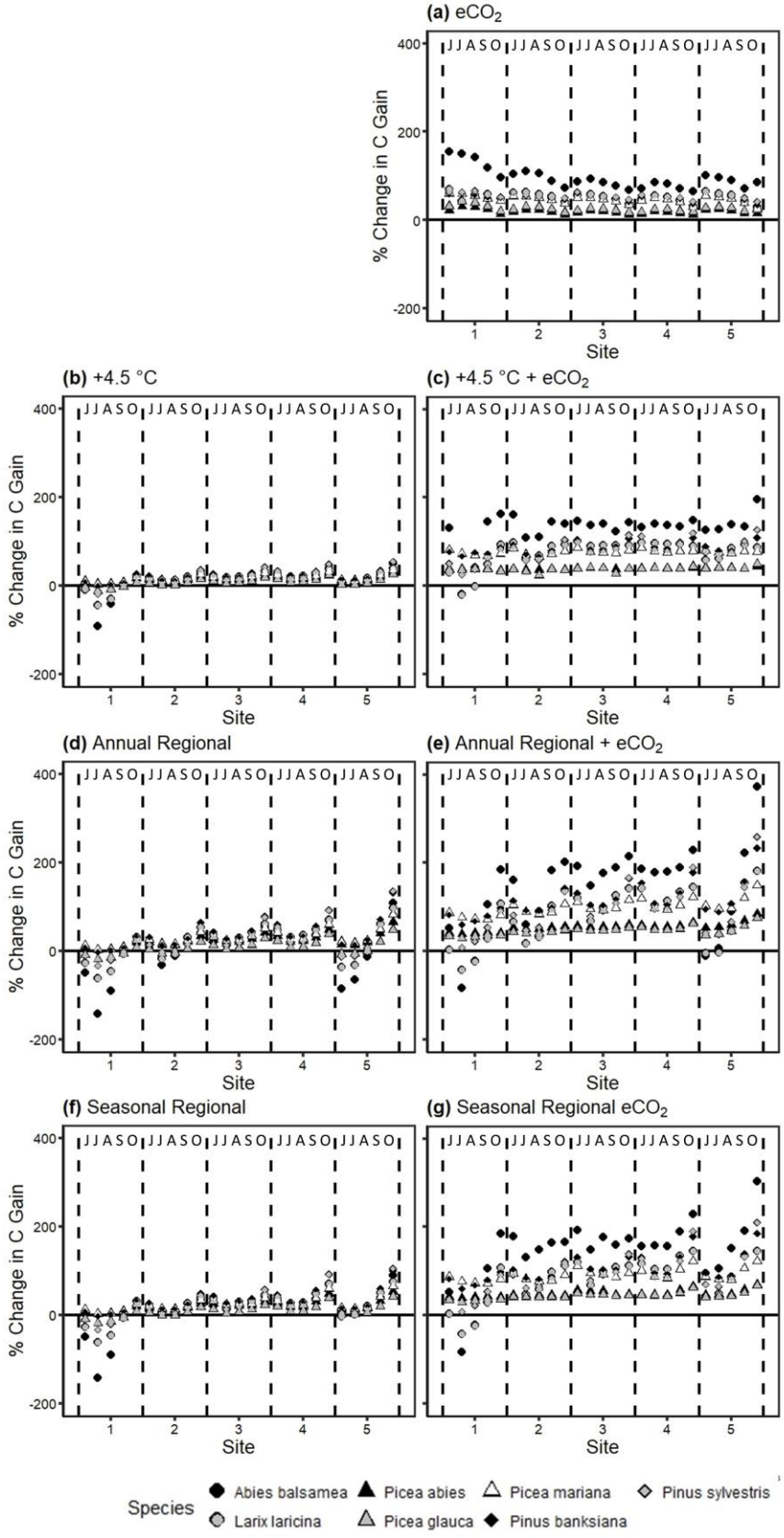
(a) eCO2
(b) +4.5 °C
(c) +4.5 °C + eCO2
(d) Annual Regional
(e) Annual Regional + eCO2
(f) Seasonal Regional
(g) Seasonal Regional eCO2
% Change in C Gain
Site
J J A S O
Species
Abies balsamea
Picea abies
Picea mariana
Pinus sylvestris
Larix laricina
Picea glauca
Pinus banksiana

Figure 5.2. Percent change in net daily carbon (C) gain of boreal trees across time and site relative to current climate conditions under (a, c, e, g) elevated CO_2, (b, c) 4.5 °C of warming, (d, e) annual regional warming, and (f, g) seasonal regional warming, at (a, b, c, d) ambient or (e, f, g, h) elevated CO_2 for the year 2100. Data represent the means of simulations run with monoculture stands of seven boreal tree species at five sites and five time points. 0 °C indicates current climate conditions, +4.5 °C indicates global average warming for 2100, annual regional indicates spatially explicit annual warming, and seasonal regional indicates spatiotemporally explicit warming, while eCO2 indicates elevated CO_2 concentrations. JJASO stands for June, July, August, September, October, and indicate the date for each point within a site. Sites are delineated with dashed lines.

Under current CO_2 concentrations in all species, changes in net carbon gain relative to current climates started to approach 0% when mean monthly 24-hr temperatures increased above ~21 °C (Fig. 5.3). However, elevated CO_2 ameliorated most of the negative effects of the warming scenarios at high temperatures (Fig. 5.3).

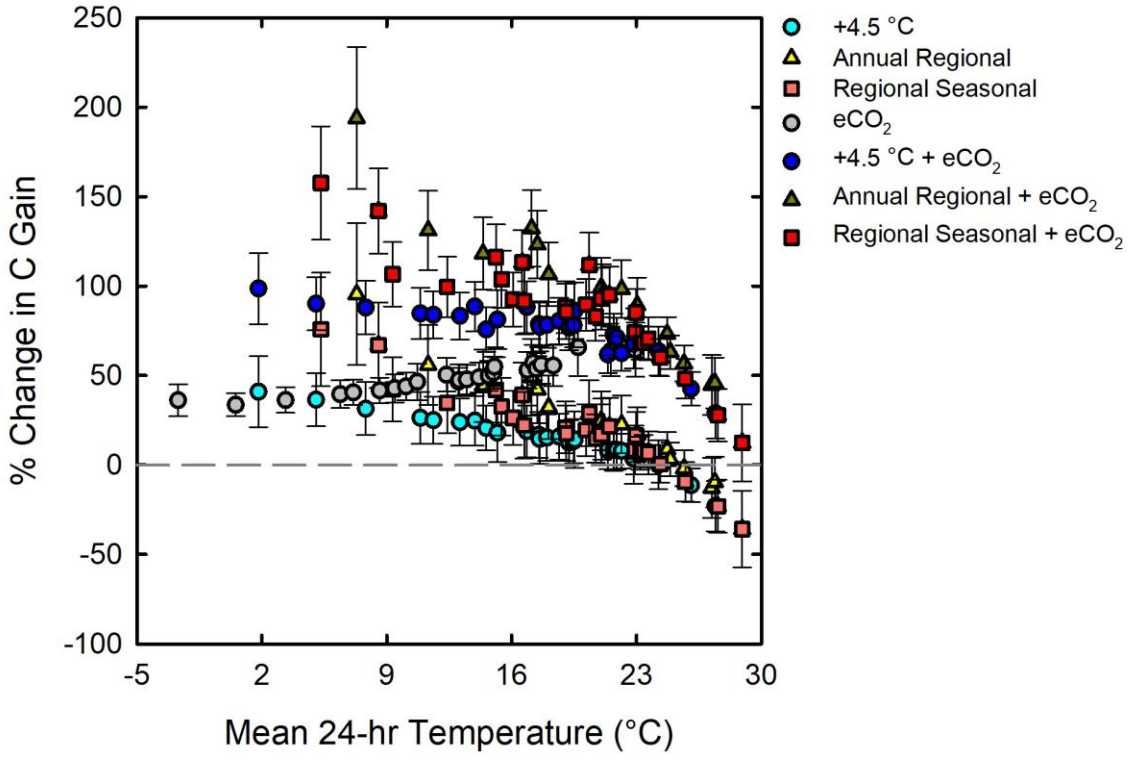

Figure 5.3. Percent change in net carbon (C) gain of boreal trees relative to current climate conditions under different climate change scenarios is reduced at higher average daily temperatures. Dashed grey line represents 0% change. Each point is one mean of one simulation of each of seven species per month per latitude per species, *N* = 175 per climate scenario. +4.5 °C indicates global average warming for 2100, annual regional indicates spatially explicit annual warming, regional seasonal indicates spatiotemporally explicit warming, and +eCO2 indicates elevated CO_2.

5.3.1 Differences in species responses to climate change correlates with species' physiology

There were notable differences between species responses to the climate scenarios (Figs. 5.2, C.1, Table 5.2), with the relative order from highest net carbon gain across the climate scenarios to the lowest being: *Pinus banksiana* > *Pinus sylvestris* > *Picea mariana* > *Picea abies* > *Picea glauca* = *Larix laricina* > *Abies balsamea* (Table 5.2; Tukey's HSD for $P < 0.05$). *Abies balsamea* had the lowest net carbon gain and the greatest reductions in net carbon gain in the warming scenarios, as well as the strongest stimulations and suppressions of net carbon gain in response to combined elevated CO_2 and warming (Fig. 5.2). This translated into *Abies balsamea* having the lowest summed carbon gain across all months and sites (Table 5.3), more than 50% less than the next lowest value (seen in *Larix laricina*). Responses of net carbon gain to the climate scenarios in *Larix laricina* also showed considerable variation: net carbon gain was strongly stimulated at high latitudes in the autumn but suppressed at low latitudes in the summer under warming-only scenarios, while tending towards the median response of all species under elevated CO_2 (Fig. 5.2). The highest summed carbon gain under all climate scenarios was found in the pine species (*Pinus sylvestris* and *Pinus banksiana*) (Table 5.3). The pine species both showed strong stimulations of net carbon gain across all latitudes and months under the elevated CO_2 scenarios, and under most sites and months in the warming only scenarios. Net carbon gain in the three *Picea* species was less responsive to warming than in the other species, and *Picea abies* and *Picea glauca* showed the least response to the elevated CO_2 scenarios, either with or without warming (Figs. 5.2, C.1).

Table 5.2. ANOVA output comparing the effects of species parameters, acclimation, and climate scenario on net carbon gain, with the number of simulations in parentheses.

	All Species (1400)			V_{cmax} and J_{max} Swap (600)			Arrhenius Swap (600)			Acclimation (1200)		
	df	*F*	*P*	df	*F*	*P*	df	*F*	*P*	df	*F*	*P*
Warming	3, 1330	71	**<0.0001**	3, 573	32	**<0.0001**	3, 572	1.4	0.23	3, 1167	92	**<0.0001**
CO_2	1, 1330	1990	**<0.0001**	1, 573	1047	**<0.0001**	1, 572	242	**<0.0001**	1, 1167	473	**<0.0001**
24-hr T	1, 1330	2990	**<0.0001**	1, 573	1507	**<0.0001**	1, 572	371	**<0.0001**	1, 1167	2658	**<0.0001**
Species	6, 1330	772	**<0.0001**	2, 573	2527	**<0.0001**	2, 572	11	**<0.0001**			
Pn										2, 1167	505	**<0.0001**
Rn										1, 1167	10	**0.0016**
Warming * CO_2				3, 573	5.3	**0.0013**				3, 1167	9.7	**<0.0001**
Warming * 24-hr T	3, 1330	13	**<0.0001**	3, 573	3.8	**0.0105**	3, 572	11	**<0.0001**	3, 1167	0.5	0.6662
Warming * Species	18, 1330	5.5	**<0.0001**	6, 573	16	**<0.0001**	6, 572	1.5	0.179			
CO_2 * 24-hr T	1, 1330	209	**<0.0001**	1, 573	124	**<0.0001**	1, 572	15	**0.002**	1, 1167	130	**<0.0001**
CO_2 * Species	6, 1330	42	**<0.0001**	2, 573	90	**<0.0001**	2, 572	6	**0.0025**			
24-hr T* Species	6, 1330	80	**<0.0001**	2, 573	243	**<0.0001**	2, 572	5.1	**0.0062**			
Warming * Pn										6, 1167	42	**<0.0001**
CO_2 * Pn										2, 1167	3.6	**0.0284**
24-hr T * Pn										2, 1167	186	**<0.0001**
24-hr T * Rn										1, 1167	5.9	**0.0152**
Warming * 24-hr T * Species	18, 1330	3.1	**<0.0001**				6, 572	2.5	**0.0206**			
Warming * 24-hr T * Pn										6, 1167	3.9	**0.0008**

CO_2 * 24-hr T * Species	6, 1330	6.3	**<0.0001**	2, 573	14	**<0.0001**

All Species: each species-specific parameter set from Table 5.1; V_{cmax} and J_{max} Swap: switching out V_{cmax} and J_{max} within a *Picea glauca* modeling framework; Arrhenius Swap: switching out the Arrhenius temperature response parameters for V_{cmax} and J_{max} within a *Picea glauca* framework; Acclimation: comparing the effects of acclimating activation energy or the entropy parameter of the Arrhenius response and/or respiratory acclimation within a *Picea glauca* modeling framework; Warming: degree of warming, average annual, regional annual, regional seasonal; CO_2: elevated CO_2; 24-hr T: mean 24-hr temperature; Species: parameter sets for each species (or effect of swapping in different species parameters); Pn Acclimation: acclimation of activation energy or the entropy parameter; Rn acclimation: respiratory acclimation; BIC: Bayesian Information Criterion.

Table 5.3. Total carbon gain (mol tree^{-1}) summed across all latitudes and months for each species under each scenario. Bolded values indicate the highest total carbon gain within a climate scenario, italicized values indicate the lowest total carbon gain within a climate scenario.

	Species						
Climate Scenario	*Abies balsamea*	*Larix laricina*	*Picea abies*	*Picea glauca*	*Picea mariana*	*Pinus banksiana*	*Pinus sylvestris*
Current	*26.3*	75.6	92.1	89.8	93	**103**	101
+4.5°C	*27.4*	84.2	103.5	94.3	106	**122**	113
Annual Regional	*22.9*	81.2	110.3	93.4	115	**132**	114
Seasonal Regional	*26.3*	84.7	107.8	94.5	112	**128**	115
eCO_2	*52.2*	116.8	110.9	113.6	138	**158**	**158**
+4.5°C + eCO_2	*58.9*	128.6	128.3	123.5	162	**190**	176
Annual Regional + eCO_2	*55.7*	122.3	140.7	129.3	180	**210**	179
Seasonal Regional + eCO_2	*60*	128.4	136.0	128.1	173	**203**	182

Current indicates current climate conditions, +4.5°C indicates global average warming for 2100, annual regional indicates spatially explicit annual warming, regional seasonal indicates spatiotemporally explicit warming, and +eCO_2 indicates elevated CO_2.

I switched the *Picea glauca* V_{cmax} and J_{max} values to those of either *Abies balsamea* or *Pinus banksiana* while holding all other parameter values constant in a *Picea glauca* parameterization to evaluate the effect of changing V_{cmax} and J_{max} on the patterns seen in net carbon gain. Unsurprisingly, I found that V_{cmax} and J_{max} explained the large differences in net and total carbon gain across species, since modeling *Picea glauca* with the low *Abies balsamea* V_{cmax} and J_{max} values generated very low net carbon gain and total carbon gain (< 30% of that compared to using *Picea glauca* values for photosynthetic capacity) while using the high *Pinus banksiana* V_{cmax} and J_{max} values in a *Picea glauca* framework increased total carbon gain up to 75% (net carbon gain: Fig. 5.4, Table 5.2; total carbon gain: Table 5.4).

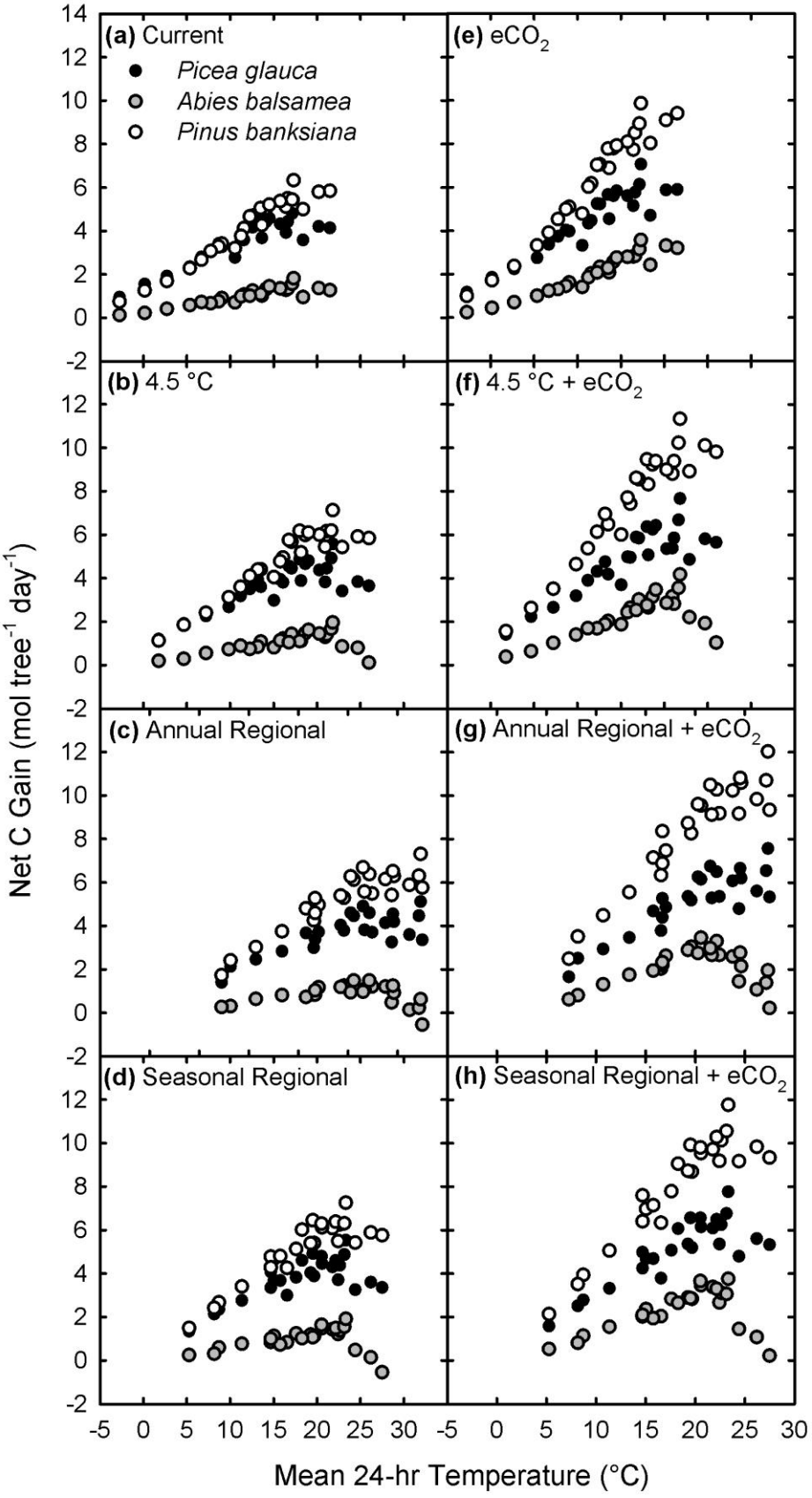
(a) Current
Picea glauca
Abies balsamea
Pinus banksiana
(e) eCO2
(b) 4.5 °C
(f) 4.5 °C + eCO2
(c) Annual Regional
(g) Annual Regional + eCO2
(d) Seasonal Regional
(h) Seasonal Regional + eCO2
Net C Gain (mol tree-1 day-1)
Mean 24-hr Temperature (°C)

Figure 5.4. Net carbon (C) gain across 24-hr temperature using three sets of V_{cmax} and J_{max} (*Picea glauca*, *Abies balsamea*, *Pinus banksiana*) in a *Picea glauca* parameterization of MAESTRA under (a, e) current climate conditions, (b, f) 4.5 °C of warming, (c, g) annual regional warming, (d, h) seasonal regional warming, at (a, b, c, d) current ambient CO_2 or (e, f, g, h) elevated CO_2 for the year 2100. +4.5 °C indicates global average warming for 2100, annual regional indicates spatially explicit annual warming, and seasonal regional indicates spatiotemporally explicit warming, while eCO2 indicates elevated CO_2 concentrations.

Table 5.4. Total carbon gain (mol tree^{-1}) summed across latitude and time for each Arrhenius temperature response parameter set (or V_{cmax} and J_{max} parameter set) within a *Picea glauca* modeling framework. For comparisons between Arrhenius parameter sets, bolded values indicate the highest total carbon gain within a climate scenario, italicized values indicate the lowest total carbon gain within a climate scenario. For comparisons between V_{cmax} and J_{max} parameter sets, starred (*) values indicate the highest total carbon gain within a climate scenario, underlined values indicate the lowest total carbon gain within a climate scenario.

Arrhenius Parameters	*Abies balsamea*	*Picea glauca*	*Picea glauca*	*Picea glauca*	*Pinus banksiana*
V_{cmax} and J_{max} Set	*Picea glauca*	*Abies balsamea*	*Picea glauca*	*Pinus banksiana*	*Picea glauca*
Current	**103**	25	90	103*	*87*
+4.5°C	**103**	26	*94*	122*	96
Annual Regional	*87.8*	19	**93**	132*	92
Seasonal Regional	**98**	24	*95*	129*	96
eCO_2	**156**	52	*114*	158*	135
+4.5°C + eCO_2	**158**	57	*124*	190*	146
Annual Regional + eCO_2	139	46	*129*	210*****	**142**
Seasonal Regional + eCO_2	**152**	58	*128*	202*	148

Current indicates current climate conditions, +4.5°C indicates global average warming for 2100, annual regional indicates spatially explicit annual warming, regional seasonal indicates spatiotemporally explicit warming, and +eCO_2 indicates elevated CO_2.

5.3.2 Arrhenius parameters strongly influence net carbon gain responses to climate

Switching the Arrhenius parameters in the MAESTRA parameterization used to model *Picea glauca*, I found that climatic effects on net carbon gain were smallest when using the set of *Picea* Arrhenius parameter values, largest with the *Abies* Arrhenius parameter values, and intermediate for the *Pinus* values (Figs. 5.5, C.2). In general, using the *Abies* and *Pinus* Arrhenius parameter values led to greater net carbon gain than using the *Picea* parameters, although *Abies* parameters led to the absolute highest total carbon gain (Figs. 5.5, C.2 Tables 5.2, 5.4). The total carbon gain was increased up to ~30% just by switching Arrhenius parameters from *Picea* to *Abies*. However, there were no differences in the responses of net carbon gain to warming scenarios amongst the model runs using different Arrhenius parameter sets (Fig. 5.5, Table 5.2), although the *Abies* and *Pinus* parameter values led to more positive net carbon gain responses to elevated CO_2 than were seen with the *Picea* Arrhenius parameter values (Figs. 5.5, C.2, Table 5.2; Tukey's HSD at $P < 0.05$).

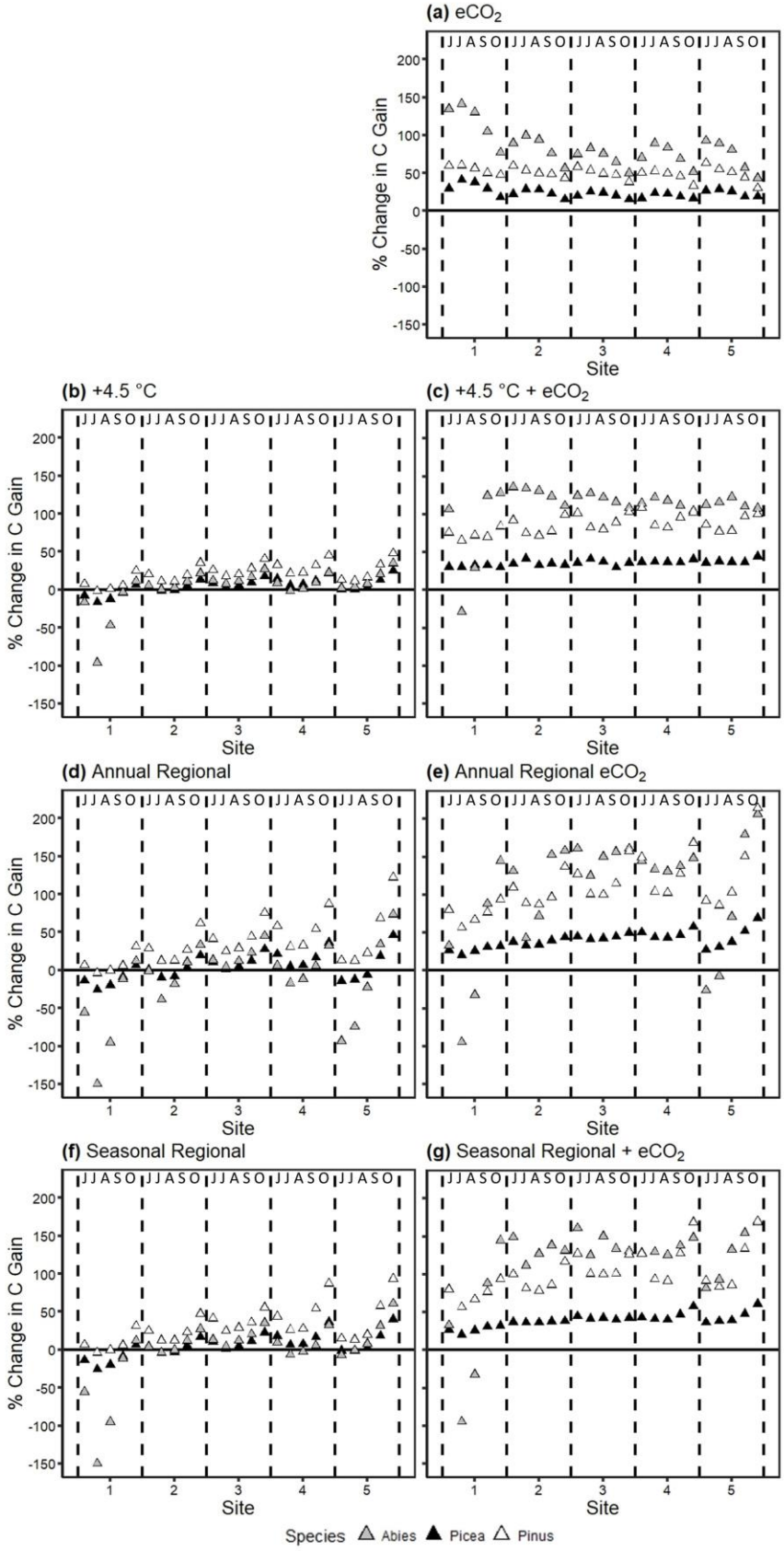
(a) eCO2
(b) +4.5 °C
(c) +4.5 °C + eCO2
(d) Annual Regional
(e) Annual Regional eCO2
(f) Seasonal Regional
(g) Seasonal Regional + eCO2
J J A S O
% Change in C Gain
Site
Species Abies Picea Pinus

Figure 5.5. Percent change in net daily carbon (C) gain of boreal trees across time and site relative to current climate conditions under (a, c, e, g) elevated CO_2, (b, c) 4.5 °C of warming, (d, e) annual regional warming, and (f, g) seasonal regional warming, at (a, b, c, d) ambient or (e, f, g, h) elevated CO_2 for the year 2100. Data represent simulations run with monoculture stands of *Picea glauca* at five sites and five time points using one of the Arrhenius temperature response parameters for *Picea*, *Abies*, or *Pinus*. 0 °C indicates current climate conditions, +4.5 °C indicates global average warming for 2100, annual regional indicates spatially explicit annual warming, and seasonal regional indicates spatiotemporally explicit warming, while eCO2 indicates elevated CO_2 concentrations. JJASO stands for June, July, August, September, October, and indicate the date for each point within a site. Sites are delineated with dashed lines.

5.3.3 Photosynthetic temperature acclimation has variable effects across climate scenarios

Using the *Picea glauca* parameterization of MAESTRA, I investigated how thermal acclimation of photosynthesis (via E_a or ΔS of both V_{cmax} and J_{max}) and respiration altered net carbon gain. Across the full temperature range investigated in the modeled climate scenarios, acclimation of E_a for V_{cmax} and J_{max} caused a convergence in the temperature response of net carbon gain at low temperatures, and large reductions in total carbon gain of up to 175% compared to the non-acclimated control (Figs. 5.6a,c , 5.7a, Tables 5.2, 5.5). Restricting the analysis to the temperature domain at which the E_a acclimation functions for V_{cmax} and J_{max} were determined (i.e. 18 – 31 °C), these effects largely disappeared: there was no convergence in net carbon gain responses to temperature across climate scenarios, and total carbon gain was reduced by only ~10–15% (Fig. 5.6c, 5.7a, Table 5.5). Acclimation of ΔS for V_{cmax} and J_{max} had little effect on the temperature response of net carbon gain (Table 5.2; Tukey's HSD at $P > 0.05$), although it slightly reduced total carbon gain within some of the elevated CO_2 climate scenarios compared to the non-acclimated control (Figs. 5.6e, 5.7b, Table 5.5). The effect of acclimating ΔS for V_{cmax} and J_{max} on net carbon gain showed two divergent patterns (Fig. 5.7b): a positive stimulation of net carbon gain occurred at temperatures below ~21 °C in climate scenarios without elevated CO_2, while a positive stimulation of net carbon gain occurred above ~21 °C in scenarios with elevated CO_2, explaining the reductions in total carbon gain for the elevated CO_2 scenarios (Table 5.5). Restricting the temperature range of this analysis to the thermal domain of the ΔS acclimation functions for V_{cmax} and J_{max} (11 – 35 °C) had no effect on the patterns observed above (Figs. 5.6e, 5.7b; Table 5.5).

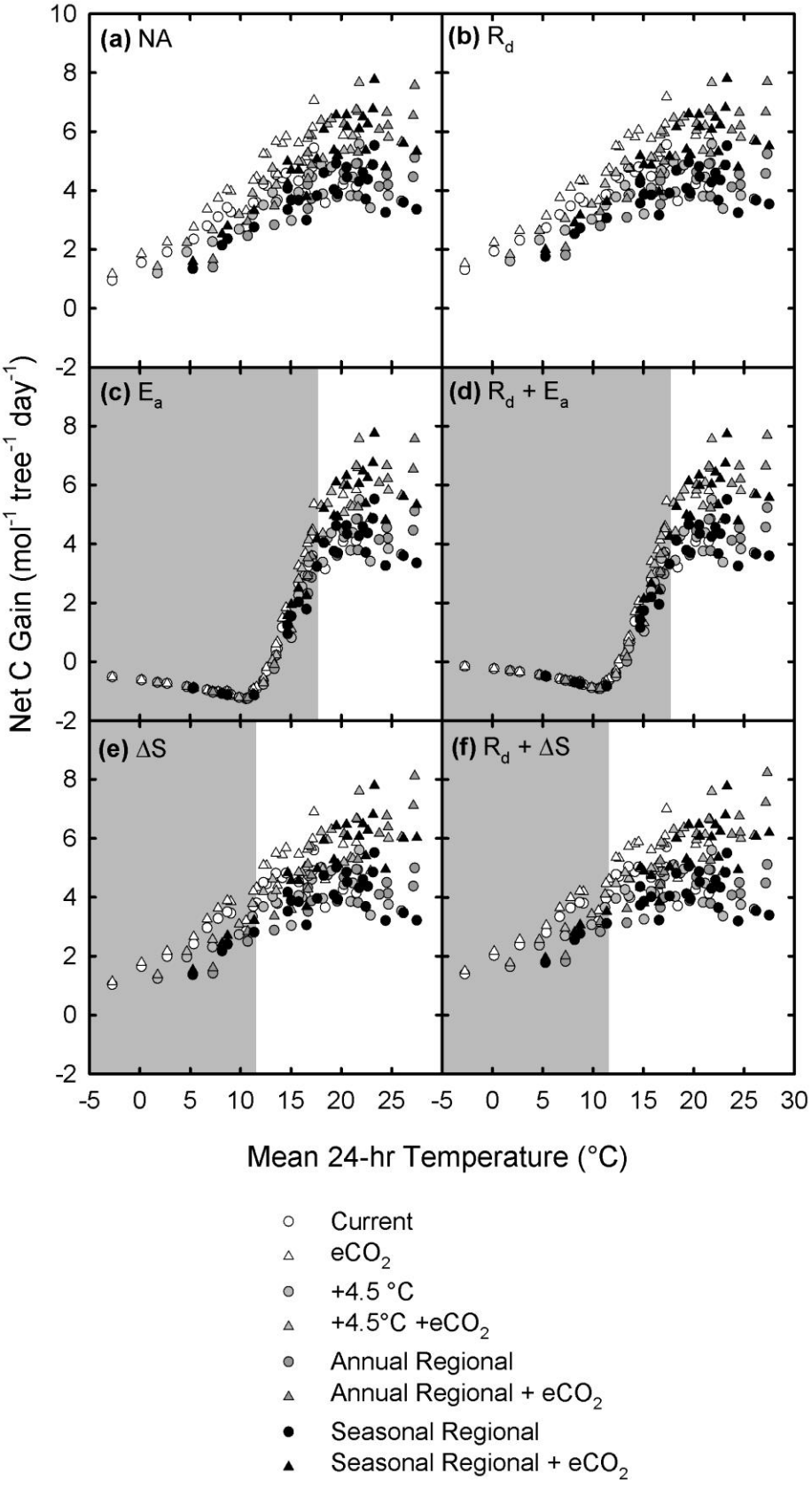
(a) NA
(b) R_d
(c) E_a
(d) R_d + E_a
(e) ΔS
(f) R_d + ΔS
Net C Gain (mol^{-1} tree^{-1} day^{-1})
Mean 24-hr Temperature (°C)
Current
eCO$_2$
+4.5 °C
+4.5°C +eCO$_2$
Annual Regional
Annual Regional + eCO$_2$
Seasonal Regional
Seasonal Regional + eCO$_2$

Figure 5.6. Net carbon (C) gain predictions for a monoculture stand of *Picea glauca* under (a) no acclimation, (b) temperature acclimation of respiration (R_d) according to Equation 5.4, (c) temperature acclimation of the activation energy (E_a) of photosynthetic capacity according to Equations 5.6 and 5.7 (Dillaway & Kruger, 2010), (d) thermal acclimation of both respiration and E_a for photosynthetic capacity, (e) acclimation of the entropy parameter of the photosynthetic temperature response (ΔS) according to Equation 5.8 (Kattge & Knorr, 2007), and (f) acclimation of both respiration and ΔS. Each point is one simulation of one stand of *Picea glauca* for one time point and latitude. *N* = 25 per climate scenario. Current indicates current climate conditions, +4.5 °C indicates global average warming for 2100, annual regional indicates spatially explicit annual warming, regional seasonal indicates spatiotemporally explicit warming, and +eCO2 indicates elevated CO_2. Grey regions in c-f indicate regions outside of the temperature domains of the photosynthetic acclimation equations (18 to 31 °C for Equations 5.6 and 5.7; 11 to 35 °C for Equation 5.8).

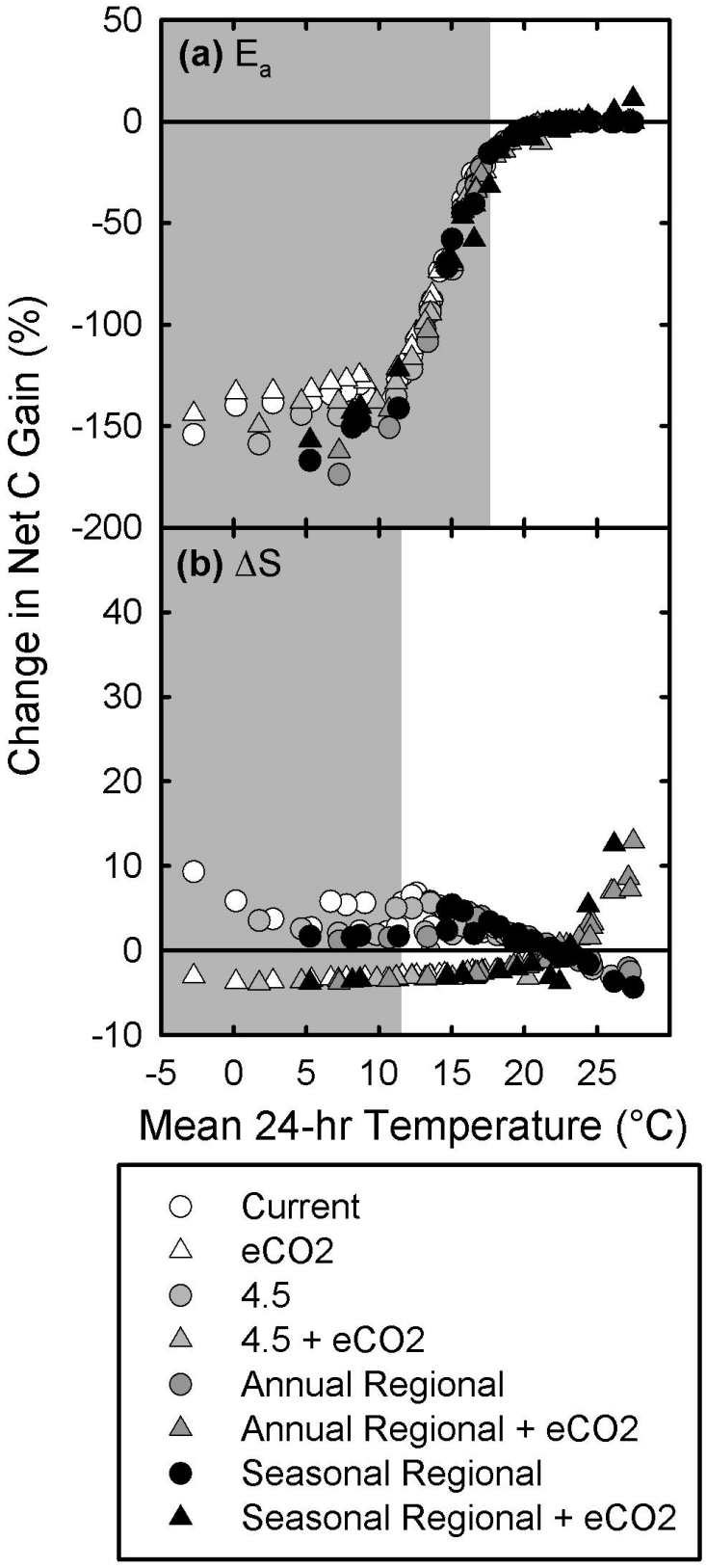
(a) E_a
(b) ΔS
Change in Net C Gain (%)
Mean 24-hr Temperature (°C)
50
0
-50
-100
-150
-200
40
30
20
10
0
-10
-5
0
5
10
15
20
25
Current
eCO2
4.5
4.5 + eCO2
Annual Regional
Annual Regional + eCO2
Seasonal Regional
Seasonal Regional + eCO2

Figure 5.7. Percent change in net carbon (C) gain predictions for a monoculture stand of *Picea glauca* under (a) temperature acclimation of the activation energy (E_a) of photosynthetic capacity according to Equations 5.6 and 5.7 (Dillaway & Kruger, 2010), and (b) acclimation of the entropy parameter of the photosynthetic temperature response (ΔS) according to Equation 5.8 (Kattge & Knorr, 2007). Each point is one simulation of one stand of *Picea glauca* for one time point and latitude. N = 25 per climate scenario. Current indicates current climate conditions, +4.5 °C indicates global average warming for 2100, annual regional indicates spatially explicit annual warming, regional seasonal indicates spatiotemporally explicit warming, and +eCO2 indicates elevated CO_2. Grey regions indicate regions outside of the temperature domains of the photosynthetic acclimation equations (18 to 31 °C for Equations 5.6 and 5.7; 11 to 35 °C for Equation 5.8).

Table 5.5. Total carbon gain (mol tree^{-1}) summed across latitude and time for each acclimation scenario under each climate scenario, and under one of: full temperature range, temperature range of Equations 5.6 and 5.7 (for V_{cmax} E_a and J_{max} E_a; 18 - 31°C), and temperature range of Equation 5.8 (ΔS; 11 - 35°C). Bolded values indicate the highest total carbon gain within a climate scenario, italicized values indicate the lowest total carbon gain within a climate scenario.

Full Temperature Range	Acclimation Scenario					
Climate Scenario	None	E_a	ΔS	R_d	E_a + R_d	ΔS + R_d
Current	90	*20*	93	96	27	**99**
+4.5°C	94	*57*	96	98	60	**100**
Annual Regional	93	*74*	94	**96**	78	**96**
Seasonal Regional	95	*69*	96	97	72	**98**
eCO_2	114	*30*	111	**120**	36	117
+4.5°C + eCO_2	123	*77*	121	**128**	83	127
Annual Regional + eCO_2	129	*106*	131	132	108	**133**
Seasonal Regional + eCO_2	128	*97*	128	**131**	100	**131**
18 - 31°C						
Current	12	*11*	12	**16**	14	**16**
+4.5°C	52	*50*	**53**	**53**	*50*	**53**
Annual Regional	67	*66*	*66*	**71**	69	**71**
Seasonal Regional	64	*63*	64	**69**	66	**69**
eCO_2	*16*	*16*	*16*	**22**	19	21
+4.5°C + eCO_2	71	*67*	70	**73**	69	**73**
Annual Regional + eCO_2	96	*94*	98	101	99	**103**
Seasonal Regional + eCO_2	90	*88*	91	**92**	91	**92**
11 - 35°C						
Current	68	*29*	70	70	31	**73**
+4.5°C	86	*61*	88	88	63	**90**
Annual Regional	87	*77*	88	**92**	78	**92**

Seasonal Regional	89	*72*	90	90	74	**91**
eCO_2	87	*38*	85	**90**	41	88
+4.5°C + eCO_2	114	*81*	112	**117**	85	116
Annual Regional + eCO_2	122	*109*	124	127	110	**128**
Seasonal Regional + eCO_2	121	*100*	121	**123**	102	**123**

Current indicates current climate conditions, +4.5°C indicates global average warming for 2100, annual regional indicates spatially explicit annual warming, regional seasonal indicates spatiotemporally explicit warming, and +eCO_2 indicates elevated CO_2. None indicates no acclimation, E_a indicates acclimation of the activation energies for photosynthetic capacity according to Equations 5.6 and 5.7, ΔS indicates acclimation of the entropy parameter according to Equation 5.8, and R_d indicates acclimation of respiration according to Equation 5.4.

Acclimating respiration (as per Equation 5.4) increased total carbon gain across the photosynthetic acclimation and climate scenarios (Tables 5.2, 5.5; Tukey's HSD at $P < 0.05$). But incorporating thermal acclimation of respiration had only a relatively small effect on the patterns of the temperature response of net carbon gain (Figs. 5.6b, d, f, Table 5.2). There was no interaction between respiration acclimation and photosynthetic acclimation, so there were no complex effects of combining photosynthetic and respiratory acclimation on the observed patterns of net carbon gain (Table 5.2).

5.4 Discussion

I hypothesized that modeled net carbon gain would increase under warming and elevated CO_2 scenarios in all the boreal tree species I evaluated. While total carbon gain (summed across all sites and months) was indeed stimulated by elevated CO_2 and by elevated CO_2 combined with warming, warming alone had relatively little, and sometimes a negative, effect on net carbon gain in species like *Abies balsamea*, but had large positive effects on others (like *Pinus banksiana*) (Figs. 5.2, C.1, Table 5.3). This same pattern was seen across the sites and months, where most species responded positively to future climate projections, but some species showed decreased net carbon gain in a warmer climate. Reductions in net carbon gain were most common at the southerly sites and during midsummer, and occurred even when the scenario included elevated CO_2. Thus, at the warmest sites and months, leaf temperatures in *Abies balsamea* and *Larix laricina* likely exceeded their thermal optima for photosynthesis, leading to declines in modeled net carbon gain. My results highlight that even within species from a single plant functional type, differences in physiological parameter values can produce highly varied responses to climate change. These results are also in agreement with studies that find plants at lower latitudes within their range have reduced or non-existent thermal safety margins where negative growth responses to warming tend to occur (Goldblum & Rigg, 2005; Girardin *et al*., 2016a; Girardin *et al*., 2016b; O'Sullivan *et al*., 2017). Based on the relative order of species in their modelled net carbon gain, we hypothesize that the boreal forest will experience compositional changes in conifer species under climate change, with *Pinus* spp. increasing in relative abundance, while *Abies balsamea* and *Larix laricina* will decline in relative abundance.

5.4.1 Boreal conifers show divergent modelled responses of net carbon gain to climate change

Using species-specific physiological parameters from the literature, I found that differences in net carbon gain between species under current climates across the boreal forest were more pronounced under future climate scenarios (Fig. C.1). But rather than finding that only the magnitude of the effect of rising CO_2 and warming varied between species as I hypothesized, I found that both magnitude and sometimes the direction of the response of net carbon gain to climate change varied. Species like *Picea glauca* and *Picea abies* showed a small, but consistent stimulation of net carbon gain in response to the seasonal regional warming with elevated CO_2 scenario in all months and sites, while *Abies balsamea* had suppressed net carbon gain at the most southerly site in the summer and a 303% increase in net carbon gain at the most northerly site in October under that same climate scenario (Fig. 5.2g). These differences in how species respond to the climate scenarios are correlated with the Arrhenius parameter values for the species. When net carbon gain is modeled using a common physiological framework with species-specific Arrhenius parameter values (Figs. 5.5, C.2), net carbon gain shows similar patterns across the climate scenarios, sites and months for the assessed species as it does in the full model analysis. In the seasonal regional warming, elevated CO_2 scenario, the *Picea glauca* Arrhenius parameter values generate a small increase in net carbon gain across all sites and months, while the *Abies balsamea* Arrhenius parameter values reduce net carbon gain in the warmer sites and months, but strongly stimulate net carbon gain in the northern sites in the autumn months. My analysis therefore highlights the importance of these relatively poorly characterized parameters for correctly predicting how vegetation will respond to climate change. But my analysis also highlights that all the boreal conifers I studied fix more carbon at high latitudes in the autumn, where temperature is currently limiting, as evidenced by strong increases in net carbon gain in future climate scenarios. As well, the elevated CO_2 scenarios enhanced the seasonality of net carbon gain at higher temperatures, implying that the increasing amplitude of atmospheric CO_2 concentrations that have been linked to boreal forest carbon fluxes (Graven *et al*., 2013; Forkel *et al*., 2016) may be related to the CO_2 fertilization effect on photosynthesis.

5.4.2 Physiological variability introduces greater variability in net carbon gain than climate variability

In contrast to my third hypothesis, physiological variability across species introduced greater variability in net carbon gain than did temperature changes in the climate scenarios, and the variability introduced by considering species-specific physiology was further enhanced under elevated CO_2 (Fig. 5.4). Simply using realistic V_{cmax} values from another boreal evergreen conifer species net carbon gain could be changed from 1 to 6 mol tree^{-1} day^{-1} under a current climate scenario (*Abies balsamea* to *Pinus banksiana*, Fig. 5.4a), a six-fold difference, while maximum net carbon gain was increased by warming from 6 to 7.5 mol tree^{-1} day^{-1} and by warming with elevated CO_2 from 6 to 12 mol tree^{-1} day^{-1} in *Pinus banksiana*, a two-fold difference or less (Fig. 5.4). Total carbon gain varied across these three V_{cmax} values by almost seven-fold in the annual regional climate scenario (Table 5.4). My data therefore support the importance of using the correct V_{cmax} value in modeling carbon fluxes, as discussed in Rogers *et al*. (2017). My findings also have important implications for the use of a plant functional type approach in models, where a mean value for a physiological parameter is often used to describe a suite of species with similar ecological and life history traits. While six of the seven species modelled here are in the boreal evergreen needleleaf tree plant functional type (and all species are in the family Pinaceae), the large variation in physiology and net carbon gain responses to climate could not be captured by a single set of physiological parameters. This raises a question on whether differences in population-level photosynthetic physiology may be important, however it appears that at least for evergreen conifers, photosynthetic physiology is consistent across populations (Johnsen & Seiler, 1996; Centritto & Jarvis 1999). My data support the growing movement away from plant functional types towards using plant functional traits (Yang *et al*., 2015; Butler *et al*., 2017; Peaucelle *et al*., 2017), since the physiological variation within a plant functional group could introduce large uncertainties into estimates of carbon uptake. Approaches incorporating variability in leaf traits can improve model estimates of gross primary productivity (Reich *et al*., 2014). Other modeling approaches that embrace this physiological variation across species within a plant functional type are also likely to produce realistic predictions of vegetation responses to climate change, since using trait

distributions for plant functional types can reproduce global patterns in leaf traits (Butler *et al*., 2017). However, a key challenge to better incorporate plant traits into vegetation models involves ensuring that the added complexity reduces, rather than increases, uncertainties in model predictions.

5.4.3 Photosynthetic thermal acclimation has a stronger impact on net carbon gain than respiratory thermal acclimation

While I hypothesized that thermal acclimation of photosynthesis and respiration would consistently improve net carbon gain, incorporating thermal acclimation had mixed effects on net carbon gain depending on how it was implemented (Figs. 5.6, 5.7; Table 5.5). In general, thermal acclimation of photosynthesis had much larger impacts on net and total carbon gain than acclimation of respiration (Fig. 5.6, Table 5.5), although these impacts were often negative, indicating the importance of properly implementing this process in models. I also demonstrate that acclimation functions need to be implemented within the temperature domain of the equations being used, otherwise they can produce highly unrealistic results (e.g. acclimation of E_a for V_{cmax} and J_{max}; Fig. 5.6) (Stinziano *et al*., 2018). Acclimation of the E_a for V_{cmax} and J_{max} caused severe reductions in net carbon gain when used outside the thermal domain where the acclimation equation was derived, but had relatively small negative effects on net carbon gain from 18-31 °C (Table 5.5). In contrast, acclimation of ΔS had little effect on net carbon gain regardless of whether the acclimation was implemented within or outside of the temperature domain of that acclimation function (Fig. 5.6, Table 5.2). Thermal acclimation of respiration did increase net carbon gain, but had little effect on the patterns in net carbon gain in response to climate scenarios (Fig. 5.6, Tables 5.2 and 5.5). The greatest total carbon gain within a climate scenario was consistently achieved when temperature acclimation of respiration was included in the model, either alone or with photosynthetic thermal acclimation using the ΔS approach (Table 5.5). Campbell *et al*. (2007) found that thermal acclimation of respiration is generally greater than acclimation of photosynthesis, while I found that acclimation of photosynthesis has a greater impact on net carbon gain. These data are not at odds with my findings here, as Campbell *et al*. (2007) used light-saturated net CO_2 assimilation as a proxy for photosynthesis, such that thermal acclimation of

photosynthesis may act in a compensatory way on net CO_2 assimilation, reducing the apparent acclimation of net CO_2 assimilation. However, whether and how coordination between thermal acclimation of photosynthesis and respiration occurs remains to be determined.

5.4.4 Caveats on statistics

It is important to note that the data presented here come from a deterministic model, and may violate the assumption of independence of observations. Thus, even though the assumptions of linearity, homogeneity of variances, and normality were met, care should be taken in interpreting the statistics, as the statistical output may be misleading (e.g. variables and their interactions may be significant when they are not, or vice versa). The statistics used to aid in the interpretation of the model output show that responses to environmental variables may be highly contigent on the individual species. This means that predictions on the responses of boreal trees to climate change may need to be considered on a species by species basis, as the underlying physiology may have a strong influence on directionality and magnitude of the response of carbon gain to climate.

5.4.5 Conclusions and future directions

While my data suggest that carbon accumulation will be enhanced under the representative concentration pathway 8.5 climate change scenario, realized responses to climate change will be strongly influenced by other extrinsic factors, such as water (Smith *et al*., 2016b), nutrient limitations (Sigurdsson *et al*., 2013) and disturbances (Randerson *et al*., 2006)). Given that my results were modeled under non-limiting nutrient and water conditions, and without photosynthetic CO_2 acclimation, they represent a “best-case scenario”, implying that declines in net carbon gain may be more extensive under the more ecologically realistic conditions outlined above. Better representation of V_{cmax} and J_{max}, as well as further development of our understanding of physiological thermal acclimation, should be high-priority research targets to improve the accuracy and precision in coupled climate-vegetation models, because this current knowledge gap can introduce large uncertainties into models. There is also a growing body of literature showing the efficacy of acclimation in improving vegetative models

(e.g. Lombardozzi *et al*., 2015; Smith *et al*., 2016a; Smith & Dukes, 2017), which would benefit from improved acclimation functions. Lastly, my work highlights that a one-size fits all approach for plant functional types (e.g. boreal evergreen conifer) will introduce significant uncertainties in estimates of tree carbon gain. Approaches that increase the specificity of traits in models (e.g. Yang *et al*., 2015; Peaucelle *et al*., 2017) should be favoured over the traditional plant functional type approach.

5.5 References

Acosta M, Pavelka M, Pokorny R, Janous D, Marek MV. **2008**. Seasonal variation in CO_2 efflux of stems and branches of Norway spruce trees. *Annals of Botany* **101**, 469–477.

Ainsworth EA, Rogers A. **2007**. The response of photosynthesis and stomatal conductance to rising [CO_2]: mechanisms and environmental interactions. *Plant, Cell & Environment* **30**, 258–270.

Ali AA, Xu C, Rogers A, *et al*. 2015. Global-scale environmental control of plant photosynthetic capacity. *Ecological Applications* **25**, 2349–2365.

Atkin OK, Tjoelker MG. **2003**. Thermal acclimation and the dynamic response of plant respiration to temperature. *Trends in Plant Science* **8**, 343–351.

Atkin OK, Bloomfield KJ, Reich PB, *et al*. 2015. Global variability in leaf respiration in relation to climate, plant functional types and leaf traits. *New Phytologist* **206**, 614–636.

Ayub G, Smith RA, Tissue DT, Atkin OK. **2011**. Impacts of drought on leaf respiration in darkness and light in *Eucalyptus saligna* exposed to industrial-age atmospheric CO_2 and growth temperature. *New Phytologist* **190**, 1003–1018.

Bauerle WL, Oren R, Way DA, Qian SS, Stoy PC, Thornton PE, Bowden JD, Hoffman FM, Reynolds RF. **2012**. Photoperiodic regulation of the seasonal pattern of photosynthetic capacity and the implications for carbon cycling. *Proceedings of the National Academy of Sciences of the United States of America* **109**, 8612–8617.

Berry J, Björkman O. **1980**. Photosynthetic response and adaptation to temperature in higher plants. *Annual Review of Plant Physiology* **31**, 491–543.

Bonan GB, Levis S, Kergoat L, Oleson KW. **2002**. Landscapes as patches of plant functional types: an integrating concept for climate and ecosystem models. *Global Biogeochemical Cycles* **16**, 5-1–5-18.

Bradshaw CJA, Warkentin IG. **2015**. Global estimates of boreal forest carbon stocks and flux. *Global & Planetary Change* **128**, 24–30.

Busch F, Hüner NPA, Ensminger I. **2007**. Increased air temperature during simulated autumn conditions does not increase photosynthetic carbon gain but affects the dissipation of excess energy in seedlings of the evergreen conifer Jack pine. *Plant Physiology* **143**, 1242–1251.

Butler EE, Datta A, Flores-Moreno H, *et al*. 2017. Mapping local and global variability in plant trait distributions. *Proceedings of the National Academy of Sciences of the United States of America* **114**, E10937–E10946.

Cai T, Dang Q-L. **2002**. Effects of soil temperature on parameters of a coupled photosynthesis-stomatal conductance model. *Tree Physiology* **22**, 819–827.

Campbell C, Atkinson L, Zaragoza-Castells J, Lundmark M, Atkin O, Hurry V. **2007**. Acclimation of photosynthesis and respiration is asynchronous in response to changes in temperature regardless of plant functional group. *New Phytologist* **176**, 375–389.

Centritto M, Jarvis PG. **1999**. Long-term effects of elevated carbon dioxide concentration and provenance on four clones of Sitka spruce (*Picea sitchensis*). II. Photosynthetic capacity and nitrogen use efficiency. *Tree Physiology* **19**, 807–814.

Chen JM, Pavlic G, Brown L, *et al*. 2002. Derivation and validation of Canada-wide coarse-resolution leaf area index maps using high-resolution satellite imagery and ground measurements. *Remote Sensing of Environment* **80**, 165–184.

Collins M, Knutti R, Arblaster J, *et al*. 2013. Long-term climate change: projections, commitments and irreversibility. In: *Climate Change 2013: The Physical Science Basis*. *Contribution of Working Group I to the Fifth Assessment Report of the Intergovernmental Panel on Climate Change*, edited by **Stocker TF, Qin D, Plattner G-K, Tignor M, Allen SK, Boschung J, Nauels A, Xia R, Bex V, Midgley PM**. Cambridge University Press: Cambridge, UK.

Crookshanks M, Taylor G, Broadmeadow M. **1998**. Elevated CO_2 and tree root growth: contrasting responses in *Fraxinus excelsior*, *Quercus petaea* and *Pinus sylvestris*. *New Phytologist* **138**, 241–250.

Dillaway DN, Kruger EL. **2010**. Thermal acclimation of photosynthesis: a comparison of boreal and temperate tree species along a latitudinal transect. *Plant, Cell & Environment* **33**, 888–899.

Duursma RA, Medlyn BE. **2012**. MAESPA: a model to study interactions between water limitation, environmental drivers and vegetation function at tree and stand levels, with an example application to [CO_2] x drought interactions. *Geoscientific Model Development* **5**, 919–940.

Fisher JB, Huntzinger DN, Schwalm CR, Sitch S. **2014**. Modeling the terrestrial biosphere. *Annual Review of Environment & Resources* **39**, 91–123.

Food & Agricultural Organization (FAO). **2001**. Global forest resources assessment 2000: Main report. *FAO*, For.Pap.140.

Forkel M, Carvalhais N, Rodenbeck C, Keeling R, Heimann M, Thonicke K, Zaehle S, Reichstein M. **2016**. Enhanced seasonal CO_2 exchange cause by amplified plant productivity in northern ecosystems. *Science* **351**, 696–699.

Fournier RA, Rich PM, Landry R. **1997**. Hierarchical characterization of canopy architecture for boreal forest. *Journal of Geophysical Research* **102**, 29445–29454.

Girardin MP, Bouriaud O, Hogg EH, *et al*. 2016a. No growth stimulation of Canada's boreal forest under half-century of combined warming and CO_2 fertilization. *Proceedings of the National Academy of Science of the United States of America* **113**, E8406–E8414.

Girardin MP, Hogg EH, Bernier PY, Kurs WA, Guo XJ, Cyr G. **2016b**. Negative impacts of high temperatures on growth of black spruce forests intensify with the anticipated climate warming. *Global Change Biology* **22**, 627–643.

Goldblum D, Rigg LS. **2005**. Tree growth response to climate change at the deciduous-boreal forest ecotone, Ontario, Canada. *Canadian Journal of Forest Research* **35**, 2709–2718.

Goodine GK, Lavigne MB, Krasowski MJ. **2008**. Springtime resumption of photosynthesis in balsam fir (*Abies balsamea*). *Tree Physiology* **28**, 1069–1076.

Graven HD, Keeling RF, Piper SC, *et al*. 2013. Enhanced seasonal exchange of CO_2 by northern ecosystems since 1960. *Science* **341**, 1085–1089.

Gspaltl M, Bauerle WL, Binkley D, Sterba H. **2013**. Leaf area and light use efficiency patterns of Norway spruce under different thinning regimes and age classes. *Forest Ecology & Management* **288**, 49–59.

Harrell PA, Bourgeau-Chavez LL, Kasischke ES, French NHF, Christensen Jr NL. **1995**. Sensitivity of ERS-1 and JERS-1 radar data to biomass and stand structure in Alaskan boreal forest. *Remote Sensing of the Environment* **54**, 247–260.

Heskel MA, O'Sullivan OS, Reich PB, *et al*. 2016. Convergence in the temperature response of leaf respiration across biomes and plant functional types. *Proceedings of the National Academy of Sciences of the United States of America* **113**, 3832–3837.

Hikosaka K, Ishikawa K, Borjigidai A, Muller O, Onoda Y. **2006**. Temperature acclimation of photosynthesis: mechanisms involved in the changes in temperature dependence of photosynthetic rate. *Journal of Experimental Botany* **57**, 291–302.

Ibrom A, Jarvis PG, Clement R, Morgenstern K, Iktchev A, Medlyn BE, Wang YP, Wingate L, Moncrieff JB, Gravenhorst G. **2006**. A comparative analysis of simulated and observed photosynthetic CO_2 uptake in two coniferous forest canopies. *Tree Physiology* **26**, 845–864.

Intergovernmental Panel on Climate Change (IPCC). **2013**. Annex I: atlas of global and regional climate projections supplementary material RCP8.5. In: *Climate Change 2013: The Physical Science Basis. Contribution of Working Group I to the Fifth Assessment Report of the Intergovernmental Panel on Climate Change*, edited by **van Oldenborgh GJ, Collins M, Arblaster J, Christensen JH, Marotzke J, Power SB, Rummukainen M, Zhou T**. Cambridge University Press: Cambridge, UK.

Jach ME, Ceulemans R. **2000**. Effects of season, needle age and elevated atmospheric CO2 on photosynthesis in Scots pine (*Pinus sylvestris*). *Tree Physiology* **20**, 145–157.

Johnsen KH, Seiler JR. **1996**. Growth, shoot phenology and physiology of diverse seed sources of black spruce: I. Seedling responses to varied atmospheric CO_2 concentrations and photoperiods. *Tree Physiology* **16**, 367–373.

Kellomäki S, Wang K-L. **1996**. Photosynthetic responses to needle water potentials in Scots pine after a four-year exposure to elevated CO_2 and temperature. *Tree Physiology* **16**, 765–772.

Koch N, Andersen CP, Raidl S, Agerer R, Matyssek R, Grams TEE. **2007**. Temperature-respiration relationships differ in mycorrhizal and non-mycorrhizal root systems of *Picea abies* (L.) Karst. *Plant Biology* **9**, 545–549.

Kroner Y, Way DA. **2016**. Carbon fluxes acclimate more strongly to elevated growth temperatures than to elevated CO_2 concentrations in a northern conifer. *Global Change Biology* **22**, 2913–2928.

Lavigne MB, Little CHA, Riding RT. **2004**. Changes in stem respiration rate during cambial reactivation can be used to refine estimates of growth maintenance respiration. *New Phytologist* **162**, 81–93.

Lombardozzi DL, Bonan GB, Smith NG, Dukes JS, Fisher RA. **2015**. Temperature acclimation of photosynthesis and respiration: a key uncertainty in the carbon cycle-climate feedback. *Geophysical Research Letters* **42**, 8624–8631.

Long SP, Postl WF, Bolhar-Nordenkampf HR. **1993**. Quantum yields for uptake of carbon dioxide in C_3 vascular plants of contrasting habitats and taxonomic groupings. *Planta* **189**, 226–234.

Lusk CH, Reich PB. **2000**. Relationships of leaf dark respiration with light environment and tissue nitrogen content in juveniles of 11 cold-temperate tree species. *Oecologia* **123**, 318–329.

Major JE, Mossler A, Barsi DC, Campbell M, Malcolm J. **2014**. Carbon assimilation variation and control in *Picea rubens*, *Picea mariana*, and their hybrids under ambient and elevated CO_2. *Trees* **28**, 329–334.

Medlyn BE, Dreyer E, Ellsworth D, *et al*. 2002. Temperature response of parameters of a biochemically based model of photosynthesis. II. A review of experimental data. *Plant, Cell & Environment* **25**, 1167–1179.

Medlyn BE, Berbigier P, Clemen, R, Grelle A, Loustau D, Linder S, Wingate L, Jarvis PJ, Sigurdsson BD, McMurtie RE. **2005**. Carbon balance of coniferous forests growing in contrasting climates: model-based analysis. *Agricultural & Forest Meteorology* **131**, 97–124.

Medvigy D, Jeong S-J, Clark KL, Skowronski NS, Schäfer KVR. **2013**. Effects of seasonal variation of photosynthetic capacity on the carbon fluxes of a temperate deciduous forest. *Journal of Geophysical Research: Biogeosciences* **118**, 1703–1714.

Norman JM, Campbell GS. **1998**. *An introduction to environmental biophysics*. Springer: New York, NY.

Oleson KW, Lawrence DM, Bonan GB, *et al*. 2013. *Technical description of version 4.5 of the Community Land Model (CLM)*. National Center for Atmospheric Research: Boulder, CO.

Peaucelle M, Bellassen V, Ciais P, Peñuelas J, Viovy N. **2017**. A new approach to optimal discretization of plant functional types in a process-based ecosystem model with forest management: a case study for temperate conifers. *Global Ecology & Biogeography* **26**, 486–499.

Peichl M, Moore TR, Arain MA, Dalva M, Brodkey D, McLaren J. **2007**. Concentrations and fluxes of dissolved organic carbon in an age-sequence of white pine forests in Southern Ontario, Canada. *Biogeochemistry* **86**, 1–17.

R Core Development Team. **2017**. R: a language and environment for statistical computing. R Foundation for Statistical Computing: Vienna, Austria. Retrieved from https://www.R-project.org.

Randerson JT, Liu H, Flanner MG, *et al*. 2006. The impact of boreal forest fire on climate warming. *Science* **314**, 1130–1132.

Rayment MB, Loustau D, Jarvis PJ. **2002**. Photosynthesis and respiration of black spruce at three organizational scales: shoot, branch and canopy. *Tree Physiology* **22**, 219–229.

Reich PB, Sendall KM, Stefanski A, Wei X, Rich RL, Montgomery RA. **2016**. Boreal and temperate trees show strong acclimation of respiration to warming. *Nature* **531**, 633–636.

Reich PB, Rich RL, Lu X, Wang Y-P, Oleksyn J. **2014**. Biogeographic variation in evergreen conifer needle longevity and impacts on boreal forest carbon cycle projections. *Proceedings of the National Academy of Sciences of the United States of America* **111**, 13703–13708.

Riano D, Chucieco E, Chondés S, Gonzalez-Matesanz J, Ustin SL. **2004**. Generation of crown bulk density for *Pinus sylvestris* L. from lidar. *Remote Sensing of Environment* **92**, 345–352.

Richardson AD, Berlyn GP, Gregoire TG. **2001**. Spectral reflectance of *Picea rubens* (Pinaceae) and *Abies balsamea* (Pinaceae) needles along an elevational gradient, Mt. Moosilauke, New Hampshire, USA. *American Journal of Botany* **88**, 667–676.

Robertson A. **1987**. The centroid of tree crowns as an indicator of abiotic processes in a balsam fir wave forest. *Canadian Journal of Forest Research* **17**, 746–755.

Sage RF, Kubien DS. **2007**. The temperature response of C_3 and C_4 photosynthesis. *Plant, Cell & Environment* **30**, 1086–1106.

Sage RF, Way DA, Kubien DS. **2008**. Rubisco, Rubisco activase, and global climate change. *Journal of Experimental Botany* **59**, 1581–1595.

Scheller RM, Mladenoff DJ. **2004**. A forest growth and biomass module for a landscape simulation model, LANDIS: design, validation, and application. *Ecological Modelling* **180**, 211–229.

Seddon AWR, Macias-Fauria M, Long PR, Benz D, Willis KJ. **2016**. Sensitivity of global terrestrial ecosystems to climate variability. *Nature* **531**, 229–232.

Sigurdsson BD, Medhurst JL, Wallin G, Eggertsson O, Linder S. **2013**. Growth of mature boreal Norway spruce was not affected by elevated [CO_2] and/or temperature unless nutrient availability was improved. *Tree Physiology* **33**, 1192–1205.

Sitch S, Huntingford C, Geney N, *et al*. 2008. Evaluation of the terrestrial carbon cycle, future plant geography and climate-carbon cycle feedbacks using five Dynamic Global Vegetation Models (DGVMs). *Global Change Biology* **14**, 2015–2039.

Slot M, Kitajima K. **2015**. General patterns of acclimation of leaf respiration to elevated temperatures across biomes and plant types. *Oecologia* **177**, 885–900.

Smith NG, Dukes JS. **2017**. Short-term acclimation to warmer temperatures accelerates leaf carbon exchange processes across plant types. *Global Change Biology* **23**, 4840–4853.

Smith NG, Malyshev SL, Shevliakova E, Kattge J, Dukes JS. **2016a**. Foliar temperature acclimation reduces simulated carbon sensitivity to climate. *Nature Climate Change* **6**, 407–411.

Smith NG, Pold G, Goranson C, Dukes JS. **2016b**. Characterizing the drivers of seedling leaf gas exchange responses to warming and altered precipitation: indirect and direct effects. *Annals of Botany Plants* **8**, plw066.

Stinziano JR, Way DA. **2017**. Autumn photosynthetic decline and growth cessation in seedlings of white spruce are decoupled under warming and photoperiod manipulations. *Plant, Cell & Environment* **40**, 1296–1316.

Stinziano JR, Way DA. **2014**. Combined effects of rising [CO_2] and temperature on boreal forests: growth, physiology and limitations. *Botany* **92**, 425–436.

Stinziano JR, Way DA, Bauerle WL. **2017**. Improving models of photosynthetic thermal acclimation: which parameters are most important and how many should be modified? *Global Change Biology* **Early View**

Stinziano JR, Hüner NPA, Way DA. **2015**. Warming delays autumn declines in photosynthetic capacity in a boreal conifer, Norway spruce (*Picea abies*). *Tree Physiology* **35**, 1303–1313.

Tarvainen L, Wallin G, Rantfors M, Uddling J. **2013**. Weak vertical canopy gradients of photosynthetic capacities and stomatal responses in a fertile Norway spruce stand. *Oecologia* **173**, 1179–1189.

Thum T, Aalto T, Laurila T, Aurela M, Kolari P, Hari P. **2007**. Parameterization of two photosynthesis models at the canopy scale in a northern boreal Scots pine forest. *Tellus B* **59**, 874–890.

Tjoelker MG, Oleksyn J, Reich PB. **1999**. Acclimation of respiration to temperature and CO_2 in seedlings of boreal tree species in relation to plant size and relative growth rate. *Global Change Biology* **49**, 679–691.

Tjoelker MG, Oleksyn J., Reich PB. **1998**. Seedlings of five boreal tree species differ in acclimation of net photosynthesis to elevated CO_2 and temperature. *Tree Physiology* **18**, 715–726.

Vezina PE. **1962**. Crown width-D.B.H. relationships for open-grown balsam fir and white spruce in Quebec. *Forestry Chronicle* **38**, 463–473.

Vitasse Y, Basler D. **2014**. Is the use of cuttings a good proxy to explore phenological responses of temperate forests in warming and photoperiod experiments? *Tree Physiology* **34**, 174–183.

Warren CR, Dreyer E, Adams MA. **2003**. Photosynthesis-Rubisco relationships in foliage of *Pinus sylvestris* in response to nitrogen supply and the proposed role of Rubisco and amino acids as nitrogen stores. *Trees* **17**, 359–366.

Way DA, Sage RF. **2008**. Thermal acclimation of photosynthesis in black spruce [*Picea mariana* (Mill.) B.S.P.]. *Plant, Cell & Environment* **31**, 1250–1262.

Way DA, Yamori W. **2014**. Thermal acclimation of photosynthesis: on the importance of adjusting our definitions and accounting for thermal acclimation of respiration. *Photosynthesis Research* **119**, 89–100.

Way DA, Oren R, Kim H-S, Katul GG. **2011**. How well do stomatal conductance models perform on closing plant carbon budgets? A test using seedlings grown under current and elevated temperatures. *Journal of Geophysical Research* **116**, G04031.

Wullschleger SD, Epstein HE, Box EO, Euskirchen ES, Goswami S, Iversen CM, Kattge J, Norby RJ, van Bodegom PM, Xu X. **2014**. Plant functional types in Earth system models: past experiences and future direction for application of dynamic vegetation models in high-latitude ecosystems. *Annals of Botany* **114**, 1–16.

Wuytack T, Samson R, Wuyts K, Adriaenssens S, Kardel F, Verheyen K. **2013**. Do leaf characteristics of white willow (*Salix alba* L.), northern red oak (*Quercus rubra* L.), and Scots pine (*Pinus sylvestris* L.) respond differently to ambient air pollution and other environmental stressors? *Water, Air & Soil Pollution* **224**, 1635.

Yamori W, Hikosaka K, Way DA. **2014**. Temperature response of photosynthesis in C_3, C_4, and CAM plants: temperature acclimation and temperature adaptation. *Photosynthesis Research* **119**, 101–117.

Yang Y, Zhu Q, Peng C, Wang H, Chen H. **2015**. From plant functional types to plant functional traits: a new paradigm in modelling global vegetation dynamics. *Progress in Physical Geography* **39**, 514–535.

Zha T, Kellomäki S, Wang K-Y, Ryyppo A, Niinisto S. **2004**. Seasonal and annual stem respiration of Scots pine trees under boreal conditions. *Annals of Botany* **94**, 889–896.

Zhang S, Dang Q-L. **2005**. Effects of soil temperature and elevated atmospheric CO_2 concentration on gas exchange, *in vivo* carboxylation and chlorophyll fluorescence in jack pine and white birch seedlings. *Tree Physiology* **25**, 523–531.

Zheng D, Freeman M, Bergh J, Rosberg I, Nilsen P. **2002**. Production of *Picea abies* in south-east Norway in response to climate change: a case study using process-based model simulation with field validation. *Scandinavian Journal of Forest Research* **17**, 35–46.

Chapter 6

6 Discussion

6.1 Thesis summary

There are relatively few data available on photosynthetic and growth responses of boreal trees to climate change. In Chapter 2, I addressed what we know about these responses (**Question 1** and **Hypothesis 1** in Chapter 1), and showed that moderate warming is likely to increase biomass accumulation in the boreal forest (Chapter 2, Fig. 2.2; Stinziano & Way, 2014). This observation provided one line of support for **Hypothesis 1** in Chapter 1, that boreal trees are limited in growth and photosynthesis by low temperatures. In Chapter 3, I addressed **Question 2** and **Hypotheses 1** and **2** from Chapter 1, and showed that warming during autumn has the potential to disrupt seasonal patterns in photosynthesis by delaying the autumn decline in carbon gain, but not growth, causing a decoupling between photosynthesis and growth in white spruce (*Picea glauca*) (Chapter 3, Figs. 5.2, 5.9; Stinziano & Way, 2017). This was due to photoperiodic control of the timing of growth. Whether this decoupling is an issue for all boreal trees remains an open question; however, a decoupling of photosynthesis and growth could lead to increased respiratory carbon losses during both spring and autumn (Chapter 3; Stinziano & Way, 2017). This decoupling of growth and photosynthesis could alter carbon flux dynamics across the boreal forest, possibly turning forests from a net sink to a net source of carbon for part of the year, which could amplify anthropogenic climate change. Chapter 3 further addressed the hypothesis that day length drives changes in photosynthetic capacity. While photosynthetic capacity was better correlated with day length, it was not a causative relationship, and photosynthetic capacity was primarily modulated by growth temperature (Figs. 3.2, 3.4, 6.1). In Chapter 4, I addressed **Question 3** and **Hypotheses 2** and **3** from Chapter 1. I showed that photosynthetic capacity was better correlated with temperature than day length in evergreen conifers (Fig. 4.1), the opposite of the effect found in broadleaf deciduous trees (Bauerle *et al*., 2012), and contrary to my predictions for **Hypothesis 2**. I also showed that amongst 18 acclimation scenarios, acclimation of basal photosynthetic capacity had the strongest impact on modeling performance, with multifactor acclimation adding only minimal

returns on explanatory power for increased complexity (Fig. 4.4). While this finding supports **Hypothesis 3** (that multifactor acclimation should improve model performance), the practical implication is that adding two additional acclimation equations only yields a 1% increase in explained variation (Stinziano *et al*., 2018) and this improvement is not great enough to justify additional equations in Earth System models. Furthermore, changes in deactivation energy of the temperature responses of V_{cmax} and J_{max} (H_d) strongly impacted model performance, although thermal acclimation of basal photosynthetic capacity remained one of the top performing acclimation functions (Figs. 4.5, 4.6). In Chapter 5, I addressed **Question 4** and **Hypothesis 1** from Chapter 1, and I show that thermal acclimation of photosynthetic capacity (within appropriate thermal conditions) tends to reduce modelled net carbon gain in boreal trees (Figs. 5.6, 5.7, 6.1). I also showed that warming has differential effects on net carbon gain across seasons and latitudes, with greater increases in net carbon gain through warming at higher latitudes and in the autumn (Fig. 5.2). Finally, I found that physiological variability in photosynthetic parameters led to greater variability in net carbon gain than did predicted climatic change (Figs. 5.4, C.1). These findings support **Hypothesis 1** (that boreal trees are low temperature limited in net carbon gain), although specifically later in the growing season and at higher latitudes. This provides further support for the findings from Chapter 2 that more extreme warming can have less positive, or even negative, effects on carbon gain (Stinziano & Way, 2014). These data underlie the importance of considering seasonal, latitudinal, and physiological variation in climate change experiments and modeling of carbon gain.

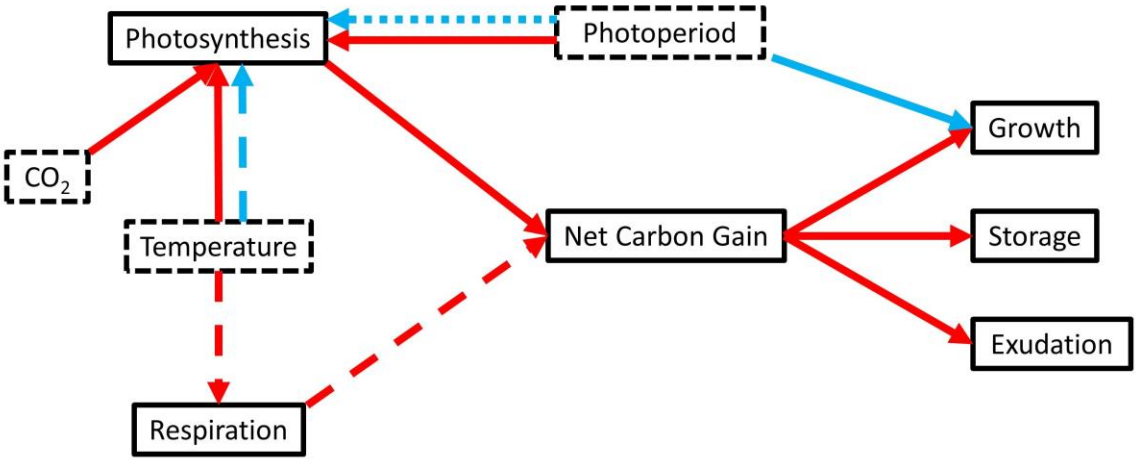

Figure 6.1. Overview of the response of net carbon gain in boreal trees to temperature, CO_2, and photoperiod. Temperature was expected to have a positive effect on photosynthesis, increasing net carbon gain, however my data suggest that boreal trees may not be low temperature limited and photosynthesis could respond negatively to warming (either through acclimation or exceeding the thermal optimum), causing a decrease in net carbon gain, but not necessarily a decline in growth. Photoperiod was known to limit growth in some species (Oleksyn *et al.*, 2001; Chen *et al.*, 2012; Hamilton *et al.*, 2016) and was assumed to have a positive effect on photosynthesis (Bauerle *et al.*, 2012), however my data in Chapter 3 call the effect on photosynthesis into question, pointing to a photoperiod limitation only on growth. Based on my data, increasing temperatures may not impact growth due to photoperiod constraints, contributing instead to changes in carbon storage and exudation. Red lines indicate state of knowledge prior to my thesis, blue lines indicate the contribution of my thesis. Solid lines indicate positive effects, dashed lines indicate negative effects, and dotted lines indicate unclear effects.

6.2 Boreal forest responses to climate change

Due to the influence of day length on tree growth, we may expect complex interactions between rising temperatures and CO_2, and the impact of day length on tree responses to climate change (Fig. 6.2). Currently, day length and temperature signals co-occur (i.e. shorter day lengths and low temperatures), such that when growth is shut down below a certain critical day length (Fig. 6.2a), carbon gain is relatively low and potential carbon losses (from fixed carbon allocated to pools other than biomass) are minimized (Fig. 6.2b, blue line). However, warming will potentially increase carbon gain during the period of growth limitations (Fig. 6.2b, light red line). But without biomass growth to use the extra carbon, this may lead to increased release of carbon through respiration, volatile organic compound production, absorbed light energy as heat and root exudates. Carbon exudation into the soil could stimulate ('prime') microbial activity in boreal soils, enhancing carbon efflux from the soil, reducing carbon storage, and contributing to a change in boreal forests from a carbon sink to a carbon source (Chapin *et al*., 2009). Meanwhile, elevated CO_2 enhances carbon gain further (Fig. 6.2b, grey line), with combined elevated CO_2 and warming causing increases in carbon gain during cool seasons and reductions during the summer (Fig. 6.2b, dark red line). Thermal acclimation (Fig. 6.2b, dashed lines in all scenarios) could reduce net carbon gain during the active growth season when temperatures are higher, and increase carbon gain when growth ceases and temperatures are lower, leading to a reduction in carbon that is allocated to biomass. Combined, these effects could lead to enhanced carbon uptake during the photosynthetically active period, but the greater uptake of carbon during the growth-limited period could lead to a greater efflux of carbon during winter. The net effect of these processes would be a greater difference between total carbon fixed (which would be increased) and total carbon efflux (which would also be increased due to carbon allocation to more labile pools).

The data in my thesis support the idea by Piao *et al*. (2017) that increased seasonal oscillations in atmospheric CO_2 are due to a CO_2 fertilization effect at high latitudes. Piao *et al*. (2017) used a combination of atmospheric CO_2 oscillations and dynamic global vegetation models to explain the increasing seasonal amplitude of atmospheric CO_2 seen

by other papers (Graven *et al.*, 2013; Forkel *et al.*, 2016), and suggest that rising CO_2 concentrations are driving the increased seasonal amplitude in atmospheric CO_2. Piao *et al.* (2017) further suggested that carbon release during the non-growing season is responsible for increased net carbon efflux at higher latitudes, and that climate explains latitudinal differences in the seasonal amplitude of atmospheric CO_2. I showed that there is enhanced seasonality of carbon gain under rising CO_2 and temperatures in boreal forests (Chapter 5; Fig. C.1), and a decoupling of growth and carbon gain in the autumn that could lead to greater carbon efflux during winter (Chapter 3; Stinziano & Way, 2017). Combined, these findings suggest that enhanced seasonal oscillations in atmospheric CO_2 (Graven *et al.*, 2013) may be partly due to CO_2 stimulation of photosynthesis in boreal trees and enhanced winter efflux (possibly due to stimulation of microbial activity and soil respiration, Chapin *et al*., 2009) of CO_2 fixed after growth cessation.

Increased seasonality of net carbon uptake due to CO_2 fertilization of photosynthesis may not necessarily be correlated with increased growth at high latitudes. Recent data using tree rings to estimate stem growth from Girardin *et al.* (2016) suggest that, on average, there has been no net growth response of the boreal forest to climate change over the past 50 years. This may be related to day length-mediated control of growth, which could limit any increases in carbon gain from being retained and used for growth. Furthermore, if day length provides a control over growth (instead of temperature) such that warming and rising CO_2 increase net carbon uptake after growth ceases, there may be a diversion of the CO_2 to more labile pools where the carbon is respired off in the winter.

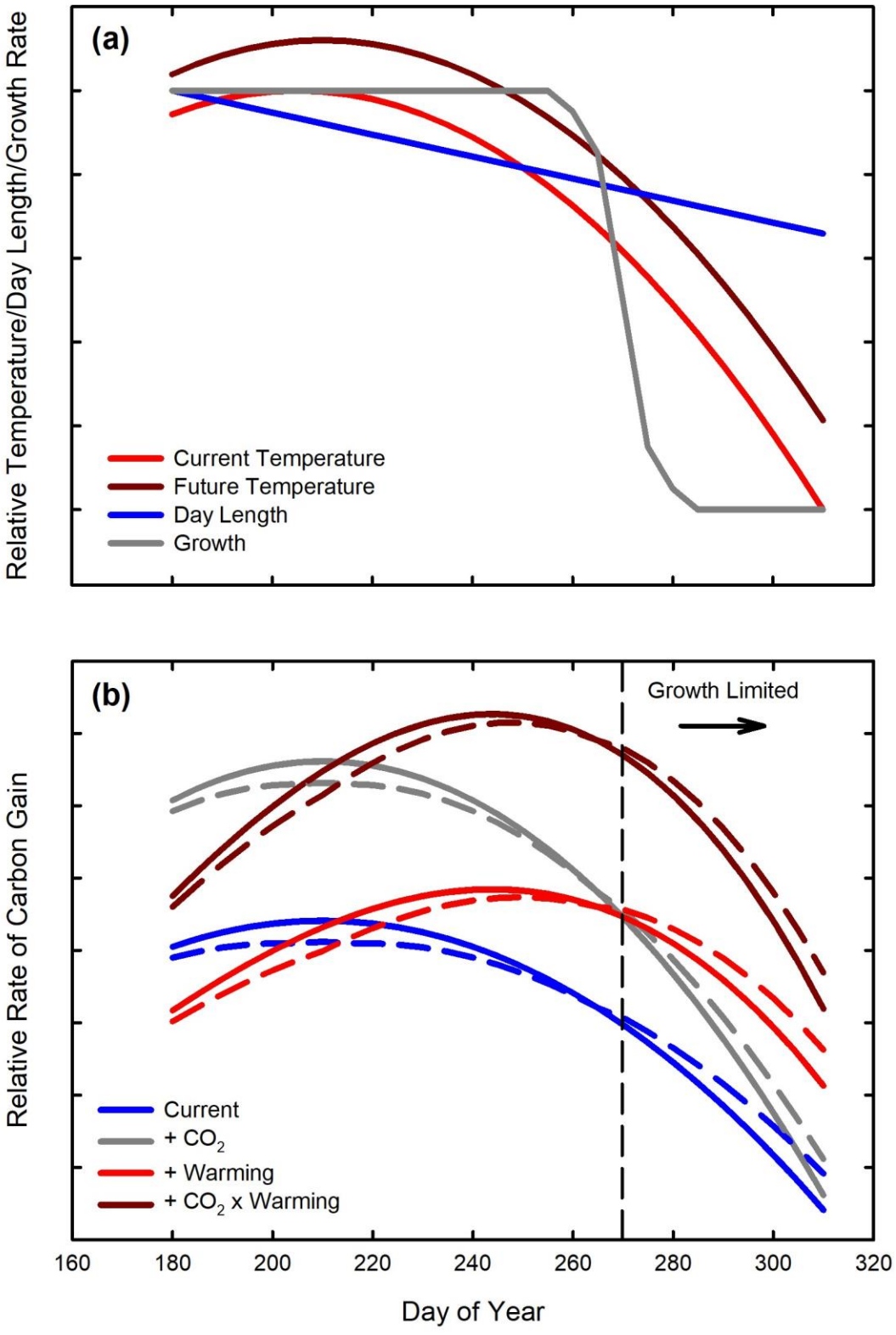
(a)
Relative Temperature/Day Length/Growth Rate
Current Temperature
Future Temperature
Day Length
Growth
(b)
Growth Limited
Relative Rate of Carbon Gain
Current
+ CO2
+ Warming
+ CO2 x Warming
160
180
200
220
240
260
280
300
320
Day of Year

Figure 6.2. (a) Growth is controlled by day length in many boreal evergreen conifers (Clapham *et al*., 1998; Oleksyn *et al*., 2001; Sogaard *et al*., 2008; Hamilton *et al*., 2016), and climate warming will greatly affect temperatures under the shorter days during the growth limited seasons. (b) Climate warming could decrease carbon gain during the warmest seasons, while increasing carbon gain during cold seasons (Chapter 5). Elevated CO_2 will generally increase carbon gain. However, growth limitations (denoted by the dashed vertical line) may prevent fixed carbon from being allocated to biomass (Chapter 3), meaning that under warming and elevated CO_2 a large amount of carbon may be allocated to more labile pools and may be released from boreal trees into the ecosystem. Furthermore, thermal acclimation (dashed lines, all scenarios) may reduce net carbon gain during the warmest seasons and stimulate net carbon gain during the cooler seasons (Chapter 5), leading to a net reduction in carbon gain during the active growth season.

The meta-analysis in Chapter 2 (Stinziano & Way, 2014) and modeling study in Chapter 5 predict an increase in growth from moderate warming and elevated CO_2, in contrast to the findings of Girardin *et al.* (2016). However, individual species showed divergent responses in the Girardin *et al*. (2016) study (as found in Chapter 5), which was focused on mature trees growing in a field setting. In Chapters 2 and 5, I used physiological data collected mainly from seedlings, and given that seedling phenology can be more sensitive to environmental conditions than mature trees (Vitasse & Basler, 2014), it is possible that seedlings would show a stronger response to climate change than mature trees. Mature trees have large energy and nutrient stores, which may buffer the trees from environmental stresses. Such redundancies could dampen environmental responses, especially if the tree responds to an internal parameter (e.g. carbohydrate status) that is affected by the external parameter (e.g. temperature). Recently, O'Leary *et al.* (2017) found that leaf night respiration is strongly correlated to carbon compounds across accessions in *Arabidopsis thaliana*. If this holds true for trees, then carbon stores in mature trees may help to buffer respiratory responses to environmental change for a period of time. Furthermore, my data focus on tree responses to climate change in the absence of nutritional, water, or light limitations. Given that much of the boreal forest may be nutrient-limited (Van Cleve & Zasada, 1976; Bonan, 1990), especially relative to other forest types (Foster & Bhatti, 2002), this could explain the lack of a mean growth response of boreal forests to climate change (Jarvis & Linder, 2000; Sigurdsson *et al.*, 2013; Girardin *et al.*, 2016). As such, the experimental data and modeling predictions should represent an upper bound on carbon uptake for boreal and coniferous tree responses to climate change.

The seasonality of boreal forests may have a strong impact on the responses of net carbon uptake to climate change. Hadden and Grelle (2016) found that increases in respiration during the shoulder seasons at a boreal plot in Sweden since 1997 reduced net carbon fixation since there were no corresponding changes in gross carbon fixation. This contrasts with my modeling in Chapter 5, where I found increases in net carbon gain during autumn months under climate warming. Hadden and Grelle (2016) argue that their data indicate a change in the temperature response of the boreal ecosystem causing an increase in respiration at low temperatures. Meanwhile Zhang *et al.* (2017), using eddy

covariance data from over 100 sites in boreal and temperate forests, found that net carbon uptake is likely to increase with climate warming. Combined, these studies suggest that there will be spatial heterogeneity in the response of boreal forest carbon gain to climate warming. The extent of such heterogeneity in carbon gain responses will be directly related to seasonality in climate change (see section 6.3–6.4 below) and other environmental limitations (see section 6.5.2 below).

6.3 Disruption of seasonal environmental cues

Tree phenology and photosynthesis are regulated throughout the year by a seasonally changing environment, and trees may use one or more of a combination of environmental variables to trigger new growth, senescence, or photosynthesis (Gyllenstrand *et al*., 2007; Holliday *et al*., 2008 Bigras & D'Aoust, 1993; Stinziano *et al*., 2015; Hamilton *et al*., 2016). The most common environmental parameters used are day length, light quality, temperature, and water availability. In the boreal forest, light and temperature cues can have strong regulatory effects on growth and photosynthesis. In broadleaf angiosperm trees, photoperiod can directly affect photosynthetic capacity (Bauerle *et al.*, 2012). Regarding growth for broadleaf angiosperm trees, a certain photoperiod may be required for growth cessation while the timing could be modified by growing temperatures (reviewed by Maurya & Bhalerao, 2017). The interaction between photoperiod and temperature signals in angiosperms is supported by data in *Arabidopsis* showing temperature modulation of photoperiod signaling (Legris *et al.*, 2016; Jung *et al.*, 2016). However, based on my data in Chapter 3 it appears that in white spruce (*Picea glauca* Moench Voss.) growth cessation is regulated strictly by photoperiod, while photosynthesis is more strongly regulated by temperature. This resulted in a decoupling of growth from photosynthesis under a climate warming scenario in seedlings (Stinziano & Way, 2017), however it is important to note that seedlings may respond differently than older trees (Ununger *et al*., 1988). Furthermore, coordinated temperature and photoperiod signals are required to achieve maximum cold hardiness during autumn in conifers (Öquist & Hüner, 2003). As such, disruptions of seasonal temperature cues from climate change could have consequences for growth (e.g. by limiting potential growth),

survival (e.g. by increasing the risk of frost damage; Way & Montgomery, 2015), and carbon cycling of forests, by reducing the proportion of carbon allocated to growth.

6.4 Thermal versus photoperiod acclimation in models

Bauerle *et al.* (2012) and Stoy *et al.* (2014) demonstrated the importance of including photoperiod acclimation of photosynthetic capacity into coupled vegetation-climate models. However, such work was based on responses in broadleaf trees, and my work in Chapter 3 demonstrates that while photosynthetic capacity in an evergreen conifer is well correlated with photoperiod, photoperiod effects on photosynthetic capacity are not causative (as they are in red maple, Bauerle *et al.*, 2012). Therefore, any improvement in modelled carbon gain in evergreen conifer-dominated regions when using photoperiod acclimation may be due to the autocorrelation of changes in photoperiod with some biotic (and/or abiotic) process(es) including, but not limited to: within-season aging of leaf tissue, feedbacks between growth and photosynthesis, temperature, and water availability. This photoperiod acclimation however, is separate from thermal acclimation of photosynthetic capacity in Earth System models.

Including thermal acclimation of photosynthetic capacity improves the ability of coupled vegetation-climate models to capture net ecosystem exchange of CO_2 (Smith *et al.*, 2016). However, there are many possible implementations of thermal acclimation of photosynthetic capacity as I outline in Chapter 4, including different formulations for acclimating the activation energy (E_a) of the temperature response (Hikosaka *et al.*, 2006; Dillaway & Kruger, 2010), acclimation of the entropy parameter (ΔS, Kattge and Knorr, 2007), and acclimation of basal photosynthetic capacity (Chapter 4). Studies addressing thermal acclimation in Earth System models currently ignore the possibility of multifactor acclimation, which I show using MAESTRA in Chapter 4 provides diminishing returns for enhanced model complexity. It is important to note that the multifactor acclimation used in Chapter 4 necessarily compiled acclimation responses of individual parameters based on data from different sets of species for each parameter. This mixing and matching of data from different species could have introduced a bias against multifactor thermal acclimation improving the ability of MAESTRA to model gross primary productivity of a forest stand (Chapter 4).

To properly assess multifactor acclimation, we need to understand whether deactivation energy of the temperature responses of V_{cmax} and J_{max} (H_d), which affects the modeling of ΔS, acclimates to temperature. In Chapter 4, I show that unnecessarily fixing H_d of the temperature response of photosynthetic capacity can affect the performance of thermal acclimation scenarios. An experimental test of multifactor thermal acclimation is needed: this would involve measuring temperature responses of photosynthetic capacity across a broad range of temperatures (with enough data to prevent the issue of overparameterization) that encompass the high temperature decline in photosynthetic capacity. This experimental design would need to be coupled with a large number of species to have the statistical power to detect acclimation in E_a, H_d, and ΔS, which can have high variability in their estimates (Leuning, 2002; Hikosaka *et al.*, 2006; Kattge & Knorr, 2007; Dillaway & Kruger, 2010).

It is crucial to consider whether the modified Arrhenius equation is appropriate and/or biologically relevant. The H_d and ΔS terms are incorporated in a way that suggests the equation is based on the Gibbs free energy of the reaction. In this case, the ΔS term would represent the change in entropy of the reaction, while H_d would represent the change in enthalpy of the reaction rather than the deactivation energy. However, the Arrhenius equation was developed to interpret single-enzyme reactions (Arrhenius, 1915). Medlyn *et al*. (2002) interpreted the Arrhenius modification with ΔS and H_d to relate to temperature-induced changes in enzyme conformation, with H_d representing the slope of decline above the thermal optimum of the temperature response and ΔS specifically being left out of a biological interpretation. Since V_{cmax} and J_{max} determined on a gas exchange basis integrate myriad biological processes (Farquhar *et al*., 1980), the interpretation of these terms may change. It is unclear whether E_a would represent the E_a of the rate-limiting reaction for V_{cmax} and J_{max} under a given set of conditions, or whether it would indeed actually represent the E_a of a single reaction. For V_{cmax}, E_a is more likely to represent the E_a for the Rubisco-catalyzed carboxylation reaction based on its derivation according to Farquhar *et al*. (1980). For J_{max}, the interpretation is unclear: does E_a pertain to the oxidation or reduction of PQ, cytochrome b_6/f, plastocyanin, NAD^+? These same arguments apply to both the ΔS and H_d terms so that the modified Arrhenius temperature response parameters may retain their biological meaning for V_{cmax} (i.e.

activation energy, the change in entropy, and the change in enthalpy of the Rubisco-catalyzed RuBP carboxylation), while the biological meaning of these parameters in relation to J_{max} is unclear. Thus, when interpreting changes in the Arrhenius temperature response parameters for gas exchange-derived photosynthetic capacity, it is important to recognize that the parameters may not have mechanistic relevance to the temperature response of photosynthetic capacity. It is also crucial to note that the equation differs markedly (with a '1 + exponential function') from the latest temperature response function from macromolecular rate theory that describes temperature responses enzyme-catalyzed reactions on the basis of Gibbs free energy (Arcus *et al*., 2016). This suggests that the modified Arrhenius equation may not contain biologically relevant terms, and that a switch to a new temperature response function with biologically relevant terms is needed.

In addition to our lack of understanding about whether multifactor thermal acclimation of photosynthetic capacity actually occurs, the effects of photoperiod on thermal acclimation are relatively unknown. However, the meta-analysis in Chapter 4 provides a clue as to what the effects of photoperiod may be. Many studies have shown that thermal acclimation of basal rates of photosynthetic capacity does not occur in a consistent manner (see meta-analyses by Way & Oren, 2010; Way & Yamori, 2014) – however, nearly all the data in these studies were from thermal acclimation under constant photoperiod. The meta-analysis in Chapter 4 includes only seasonal data where temperature and photoperiod are changing, and shows that basal photosynthetic capacity acclimates to temperature, as is also shown by Smith and Dukes (2017). It is possible that this discrepancy between Chapter 4 and the meta-analyses by Way and Oren (2010) and Way and Yamori (2014) is partly due to a photoperiod-modulation of thermal acclimation of photosynthetic capacity. To address this, an experiment measuring temperature responses of photosynthetic capacity across different photoperiods would be needed, however this experiment would require a control treatment with no changes in photoperiod to account for possible aging effects on thermal acclimation of photosynthetic capacity.

6.5 Future directions to improve vegetative models

6.5.1 Photosynthetic acclimation

Current models of vegetative carbon uptake tend to include (if at all) only one type of photosynthetic temperature acclimation, and almost exclusively the entropy parameter of the acute temperature response (Oleson *et al*., 2013; Smith *et al*., 2016). However, there may be acclimation of all parameters in the acute temperature response of photosynthesis, as well as acclimation of the basal rates. There are also significant hurdles to incorporating more comprehensive photosynthetic temperature acclimation into vegetation models, rooted in the paucity of data on the acclimation of the temperature response of photosynthesis.

The main parameter used in photosynthetic models in dynamic global vegetation models/Earth system models is the maximum rate of Rubisco carboxylation (V_{cmax}) (e.g. Cox, 2001; Sitch *et al*., 2008; Oleson *et al.*, 2013). However, under the Farquhar *et al.* (1980) paradigm, V_{cmax} represents only one limitation-state of photosynthesis (CO_2-limited). Other limitation states include ribulose-1,5-bisphosphate regeneration limitations (i.e. the maximum rate of electron transport, J_{max}, is limiting), and phosphate regeneration limitations where ATP production is limited by the dephosphorylation and export of triose phosphates from the chloroplast (triose phosphate utilization limitation, TPU). Acclimation of these other limitation states must occur to some extent, as manipulation of limitation states is one mechanism through which a chloroplast can be energetically balanced (Hüner *et al.*, 2012). However, thermal acclimation studies focus mostly on V_{cmax} and J_{max} (e.g. Hikosaka *et al.*, 2006; Kattge & Knorr, 2007; Dillaway & Kruger, 2010; Smith & Dukes, 2017; Stinziano *et al.*, 2018), and almost none on acclimation of TPU. The primary limitation to photosynthesis changes across the acute temperature response at a given intercellular CO_2 concentration in the leaf (C_i), such that V_{cmax} limitations are important at high temperatures, while TPU limitations are important at low temperatures (Sage & Kubien, 2007; Busch & Sage, 2017). In this way, ignorance of TPU limitations and its acclimation may be introducing as-yet unquantified uncertainties into our modeling of high latitude systems characterized by lower temperatures.

6.5.2 Environmental interactions

Beyond the impact of rising temperatures on growth and photosynthesis in boreal trees, there are other environmental factors projected to change with climate change, including precipitation, fire, drought, nutrient availability, and insect pests. These factors could interact with temperature and CO_2 effects on tree physiology and growth (Allen *et al.*, 2010), and I will address some of those interactions here.

Climate warming has led to increased risks of drought and fire in the boreal forest. In the boreal forest, drought-induced tree mortality has increased by over 4% $year^{-1}$ since 1963 (Peng *et al.*, 2011). Fire intensity (annual burned area) and frequency have increased more than two-fold (Kasischke & Turetsky, 2006), while stand-level carbon accumulation has decreased (Ma *et al.*, 2012; Hogg *et al.*, 2017). Forest fires have a very strong influence on boreal forest carbon balance in Canada (Bond-Lamberty *et al.*, 2007). Nonetheless, Canada's boreal forests remained a carbon sink between 1990 and 2008 (Kurz *et al.*, 2013), and even though fire emissions may quadruple by 2100, CO_2 stimulation of photosynthesis may maintain the boreal carbon sink (Balshi *et al.*, 2009).

Nutrient availability is also known to restrict forest carbon uptake (Fernández-Martínez *et al.*, 2014), and there are some experiments investigating interactions of nutrient status with climate change (Sigurdsson *et al.*, 2013; Ellsworth *et al.*, 2017). In mature Norway spruce (*Picea abies*), nutrient limitations prevented a biomass response to elevated temperatures and CO_2 (Sigurdsson *et al.*, 2013).

Given that my thesis focuses on tree responses to climate change under high water and nutrient availability, drought would likely constrain carbon uptake at the tree and stand level, reducing any increases in carbon gain with warming and elevated CO_2, and leading to negative carbon gain in some cases. Current greening and browning trends across the boreal forest are linked to water availability (Bi *et al*., 2013), and given that modelled carbon gain can decline at high temperatures even under ideal moisture conditions (Chapter 5), future drought events in a warmer climate could cause large reductions in growth and carbon uptake in boreal trees, further enhancing the moisture-induced browning of the boreal forest. Meanwhile fire effects have greater meaning at the stand-

level, where fire may destroy photosynthetically active tissue and change whole stands from carbon sinks to carbon sources. Thus, the increases in net carbon uptake predicted under future climate conditions in my thesis (Chapters 2, 3, 5), and specifically in areas that are low temperature-limited, represent an upper limit on future carbon gain in boreal trees.

6.6 Concluding remarks

In conclusion, moderate future warming, especially under elevated CO_2, is likely to enhance photosynthetic carbon uptake in conifers (Chapters 2, 3) with the timing of more extreme warming being important in whether climate change enhances carbon uptake (Chapter 5), while day length may dictate whether that additional carbon is fixed into more or less labile pools by modulating growth (Chapter 3). When looking into possible vegetation-atmosphere feedbacks, it appears as though photosynthetic temperature acclimation may reduce carbon gain (Chapters 4, 5) compared to an unacclimated state. However, our understanding of photosynthetic thermal acclimation is poor, and current functions available to incorporate acclimation of photosynthetic capacity in Earth System models may be unsuitable for conifers (Chapter 4). Furthermore, current Earth System models assume that at least some proportion of fixed carbon is used to produce new biomass. If photoperiod limits the allocation of carbon to longer-term stores such as growth, leading to an efflux of recently fixed carbon during the non-growth season, then current Earth System models may be overestimating annual carbon uptake in high latitude ecosystems by excluding such an effect. Overall, the experimental and modeling data in this thesis are consistent with the hypothesis that CO_2 stimulation of photosynthesis is a primary contributor to the increasing amplitude of atmospheric CO_2 oscillations (Piao *et al*., 2017). Meanwhile, improving our ability to model photosynthetic thermal acclimation will require extensive collaborative research to capture the thermal response parameters of all the biochemical and diffusional limitations to photosynthesis, including V_{cmax}, J_{max}, TPU, stomatal conductance, and mesophyll conductance, and across a large range of biological and geographical diversity so as to be useful in modeling efforts. Modeling necessarily requires some simplifying assumptions, however at some point more complexity will be needed to improve model predictions of reality.

6.7 References

Allen CD, Macalady AK, Chenchouni H, *et al*. 2010. A global overview of drought and heat-induced tree mortality reveals emerging climate change risks for forests. *Forest Ecology & Management* **259**, 660–684.

Arcus VL, Prentice EJ, Hobbs JK, *et al*. 2016. On the temperature dependence of enzyme-catalyzed rates. *Biochemistry* **55**, 1681–1688.

Arrhenius S. **1915**. *Quantitative laws in biological chemistry*. Bell: London.

Atkin OK, Tjoelker MG. **2003**. Thermal acclimation and the dynamic response of plant respiration to temperature. *Trends in Plant Science* **8**, 343–351.

Bauerle WL, Oren R, Way DA, Qian SS, Stoy PC, Thornton PE. **2012**. Photoperiodic regulation of the seasonal pattern of photosynthetic capacity and the implications for carbon cycling. *Proceedings of the National Academy of Sciences of the United States of America* **109**, 8612–8617.

Balshi MS, McGuire AD, Duffy P, Flannigan M, Kicklighter DW, Melillo J. **2009**. Vulnerability of carbon storage in North American boreal forests to wildfires during the 21st century. *Global Change Biology* **15**, 1491–1510.

Bi J, Xu L, Samanta A, Zhu Z, Myneni R. **2013**. Divergent arctic-boreal vegetation changes between North American and Eurasia over the past 30 years. *Remote Sensing* **5**, 2093–2112.

Bigras FJ, D'Aoust AL. **1993**. Influence of photoperiod on shoot and root frost tolerance and bud phenology of white spruce seedlings (*Picea glauca*). *Canadian Journal of Forest Research* **23**, 219–228.

Bonan G. **1990**. Carbon and nitrogen cycling in North American boreal forests. II. Biogeographic patterns. *Canadian Journal of Forest Research* **20**, 1077–1088.

Bond-Lamberty B, Peckham SD, Ahl DE, Gower ST. **2007**. Fire as the dominant driver of central Canadian boreal forest carbon balance. *Nature* **450**, 89–92.

Busch FA, Sage RF. **2017**. The sensitivity of photosynthesis to O_2 and CO_2 concentration identifies strong Rubisco control above the thermal optimum. *New Phytologist* **213**, 1036–1051.

Chapin III FS, McFarland J, McGuire AD, Euskirchen ES, Ruess RW, Kielland K. **2009**. The changing global carbon cycle: linking plant-soil carbon dynamics to global consequences. *Journal of Ecology* **97**, 840–850.

Chen J, Källman T, Ma X, *et al*. 2012. Disentangling the roles of history and local selection in shaping clinal variation of allele frequencies and gene expression in Norway spruce (*Picea abies*). *Genetics* **191**, 865–881.

Clapham DH, Dormling I, Ekberg L, Eriksson G, Qamaruddin M, Vince-Prue D. **1998**. Latitudinal cline of requirement for far-red light for the photoperiodic control of budset and extension growth in *Picea abies* (Norway spruce). *Physiologia Plantarum* **102**, 71–78.

Cox PM. **2001**. Description of the "TRIFFID" dynamic global vegetation model. *Hadley Centre Technical Note 24*. Hadley Centre: Berks, UK.

Dillaway DN, Kruger EL. **2010**. Thermal acclimation of photosynthesis: a comparison of boreal and temperate tree species along a latitudinal transect. *Plant, Cell & Environment* **33**, 888–899.

Ellsworth DS, Anderson IC, Crous KY, *et al.* 2017. Elevated CO_2 does not increase eucalypt forest productivity on a low-phosphorus soil. *Nature Climate Change* **7**, 279–282.

Farquhar GD, von Caemmerer S, Berry JA. **1980**. A biochemical model of photosynthetic CO_2 assimilation in leaves of C_3 species. *Planta* **149**, 78–90.

Fernández-Martínez M, Vicca S, Janssens IA, *et al.* 2014. Nutrient availability as the key regulator of global forest carbon balance. *Nature Climate Change* **4**, 471–476.

Forkel M, Carvalhais N, Rödenbeck C, Keeling R, Heimann M, Thonicke K, Zaehle S, Reichstein M. **2016**. Enhanced seasonal CO_2 exchange caused by amplified plant productivity in northern ecosystems. *Science* **351**, 696–699.

Foster NW, Bhatti JS. **2002**. Forest ecosystems: nutrient cycling. In: *Encyclopedia of Soil Science*, edited by **Lal R**, vol. 1, pp. 718–720. Dekker: New York, NY.

Girardin MP, Bouriaud O, Hogg EH, *et al.* 2016. No growth stimulation of Canada's boreal forest under half-century of combined warming and CO_2 fertilization. *Proceedings of the National Academy of Sciences of the United States of America* **113**, E8406–E8414.

Graven HD, Keeling RF, Piper SC, *et al.* 2013. Enhanced seasonal exchange of CO_2 by northern ecosystems since 1960. *Science* **341**, 1085–1089.

Gyllenstrand N, Clapham D, Källman T, Lagercrantz U. **2007**. A Norway spruce FLOWERING LOCUS T homolog is implicated in control of growth rhythm in conifers. *Plant Physiology* **144**, 248–257.

Hadden D, Grelle A. **2016**. Changing temperature response of respiration turns boreal forest from carbon sink into carbon source. *Agricultural & Forest Meteorology* **223**, 30–38.

Hamilton JA, El Kayal W, Hart AT, Runcie DE, Arango-Velez A, Cooke JEK. **2016**. The joint influence of photoperiod and temperature during growth cessation and development of dormancy in white spruce (*Picea glauca*). *Tree Physiology* **36**, 1432–1448.

Hikosaka K, Ishikawa K, Borjigidai A, Muller O, Onoda Y. **2006**. Temperature acclimation of photosynthesis: mechanisms involved in the changes in temperature dependence of photosynthetic rate. *Journal of Experimental Botany* **57**, 291–302.

Hogg EH, Michaelian M, Hook TI, Undershultz ME. **2017**. Recent climatic drying leads to age-independent growth reductions of white spruce stands in western Canada. *Global Change Biology* **23**, 5297–5308.

Holliday JA, Ralph SG, White R, Bohlmann J, Aitken SN. **2008**. Global monitoring of autumn gene expression within and among phenotypically divergent populations of Sitka spruce (*Picea sitchensis*). *New Phytologist* **178**, 103–122.

Hüner NPA, Bode R, Dahal K, Hollis L, Rosso D, Krol M, Ivanov AG. **2012**. Chloroplast redox imbalance governs phenotypic plasticity: the "grand design of photosynthesis" revisited. *Frontiers in Plant Science* **3**, 1–12.

Jarvis P, Linder S. **2000**. Botany: constraints to growth of boreal forests. *Nature* **405**, 904–905.

Jung J-H, Domijan M, Klose C, *et al.* 2016. Phytochromes function as thermosensors in *Arabidopsis*. *Science* **354**, 886–889.

Kasischke ES, Turetsky MR. **2006**. Recent changes in the fire regime across the North American boreal region – spatial and temporal patterns of burning across Canada and Alaska. *Geophysical Research Letters* **33**, L09703.

Kattge J, Knorr W. **2007**. Temperature acclimation in a biochemical model of photosynthesis: a reanalysis of data from 36 species. *Plant, Cell & Environment* **30**, 1176–1190.

Kurz WA, Shaw CH, Boisvenue C, Stinson G, Metsaranta J, Leckie D, Dyk A, Smyth C, Neilson ET. **2013**. Carbon in Canada's boreal forest – a synthesis. *Environmental Reviews* **21**, 260–292.

Legris M, Klose C, Burgie ES, *et al.* 2016. Phytochrome B integrates light and temperature signals in *Arabidopsis*. *Science* **354**, 897–900.

Leuning R. **2002**. Temperature dependence of two parameters in a photosynthesis model. *Plant, Cell & Environment* **25**, 1205–1210.

Ma Z, Peng C, Zhu Q, Chen H, Yu G, Li W, Zhou X, Wang W, Zhang W. **2012**. Regional drought-induced reduction in the biomass carbon sink of Canada's boreal forests. *Proceedings of the National Academy of Sciences of the United States of America* **109**, 2423–2427.

Maurya JP, Bhalerao RP. **2017**. Photoperiod- and temperature-mediated control of growth cessation and dormancy in trees: a molecular perspective. *Annals of Botany* **120**, 351–360.

Medlyn BE, Dreyer E, Ellsworth D, *et al*. **2002**. Temperature response of parameters of a biochemically based model of photosynthesis. II. A review of experimental data. *Plant, Cell & Environment* **25**, 1167–1179.

O'Leary BM, Lee CP, Atkin OK, Cheng R, Brown TB, Millar AH. **2017**. Variation in leaf respiration rates at night correlates with carbohydrate and amino acid supply. *Plant Physiology* **174**, 2261–2273.

Oleksyn J, Reich PB, Tjoelker MG, Chalupka W. **2001**. Biogeographic differences in shoot elongation pattern among European Scots pine populations. *Forest Ecology & Management* **148**, 207–220.

Oleson KW, Lawrence DM, Bonan GB *et al.* 2013. *Technical description of version 4.5 of the Community Land Model (CLM)*. National Center for Atmospheric Research: Boulder, CO.

Öquist G, Hüner NPA. **2003**. Photosynthesis of overwintering evergreen plants. *Annual Review of Plant Biology* **54**, 329–355.

Peng C, Ma Z, Lei X, Zhu Q, Chen H, Wang W, Liu S, Li W, Fang X, Zhou X. **2011**. A drought-induced pervasive increase in tree mortality across Canada's boreal forests. *Nature Climate Change* **1**, 467–471.

Piao S, Liu Z, Wang Y, *et al.* 2017. On the causes of trends in the seasonal amplitude of atmospheric CO_2. *Global Change Biology* **Early View**

Sage RF, Kubien DS. **2007**. The temperature response of C_3 and C_4 photosynthesis. *Plant, Cell & Environment* **30**, 1086–1106.

Sigurdsson BD, Medhurst JL, Wallin G, Eggertsson O, Linder S. **2013**. Growth of mature boreal Norway spruce was not affected by elevated [CO_2] and/or air temperature unless nutrient availability was improved. *Tree Physiology* **33**, 1192–1205.

Smith NG, Dukes JS. **2017**. Short-term acclimation to warmer temperatures accelerates leaf carbon exchange processes across plant types. *Global Change Biology* **23**, 4840–4853.

Smith NG, Malyshev SL, Shevliakova E, Kattge J, Dukes JS. **2016**. Foliar temperature acclimation reduces stimulated carbon sensitivity to climate. *Nature Climate Change* **6**, 407–411.

Sogaard G, Johnsen O, Nilsen J, Junttila O. **2008**. Climatic control of bud burst in young seedlings of nine provenances of Norway spruce. *Tree Physiology* **28**, 311–320.

Stinziano JR, Way DA. **2014**. Combined effects of rising [CO_2] and temperature on boreal forests: growth, physiology and limitations. *Botany* **92**, 425–436.

Stinziano JR, Way DA. **2017**. Autumn photosynthetic decline and growth cessation in seedlings of white spruce are decoupled under warming and photoperiod manipulations. *Plant, Cell & Environment* **40**, 1296–1316.

Stinziano JR, Hüner NPA, Way DA. **2015**. Warming delays autumn declines in photosynthetic capacity in Norway spruce (*Picea abies*). *Tree Physiology* **35**, 1303–1313.

Stinziano JR, Way DA, Bauerle WL. **2018**. Improving models of photosynthetic thermal acclimation: which parameters are most important and how many should be modified? *Global Change Biology* **24**, 1580–1598.

Stoy PC, Trowbridge AM, Bauerle WL. **2014**. Controls on seasonal patterns of maximum ecosystem carbon uptake and canopy-scale photosynthetic light response:

contributions from both temperature and photoperiod. *Photosynthesis Research* **119**, 49–64.

Ununger J, Ekberg I, Kang H. **1988**. Genetic control and age-related changes of juvenile growth characters in *Picea abies*. *Scandinavian Journal of Forest Research* **3**, 55–66.

Van Cleve K, Zasada JC. **1976**. Response of 70-year-old white spruce to thinning and fertilization in interior Alaska. *Canadian Journal of Forest Research* **6**, 145–152.

Vitasse Y, Basler D. **2014**. Is the use of cuttings a good proxy to explore phenological responses of temperate forests in warming and photoperiod experiments? *Tree Physiology* **34**, 174–183.

Way DA, Oren R. **2010**. Differential responses to changes in growth temperature between trees from different functional groups and biomes: a review and synthesis of data. *Tree Physiology* **30**, 669–688.

Way DA, Montgomery RA. **2015**. Photoperiod constraints on tree phenology, performance and migration in a warming world. *Plant, Cell & Environment* **38**, 1725–1736.

Way DA, Yamori W. **2014**. Thermal acclimation of photosynthesis: on the importance of adjusting our definitions and accounting for thermal acclimation of respiration. *Photosynthesis Research* **119**, 89–100.

Zhang Z, Zhang R, Cescatti A, *et al.* 2017. Effect of climate warming on the annual terrestrial net ecosystem CO_2 exchange globally in the boreal and temperate regions. *Scientific Reports* **7**, 3108.

Appendix A: Chapter 4 supplementary material

A.1 Materials and methods

Rubisco large subunit standard curves and immunoblotting were used to quantify Rubisco in leaves of *Picea glauca* in Chapter 3. The standard curve contained 0.12 pmol, 0.24 pmol, and 0.48 pmol of Rubisco large subunit. Samples were initially loaded on an equal extract volume basis (4 μL), and samples were re-run (by either diluting or loading more sample) whenever the Rubisco content was outside the quantification range of the standard curve until the samples were within the quantifiable range (Fig. A.1a). Rubisco quantities were determined first by measuring the peak area of the optical density of the immunoblot bands using the Gels > Plot Lanes function in ImageJ (Fig. A.1b). The peak areas of the Rubisco large subunit standards were then used to generate a standard curve with which to quantify the Rubisco content of the samples (Fig. A.1c).

A.2 Figures

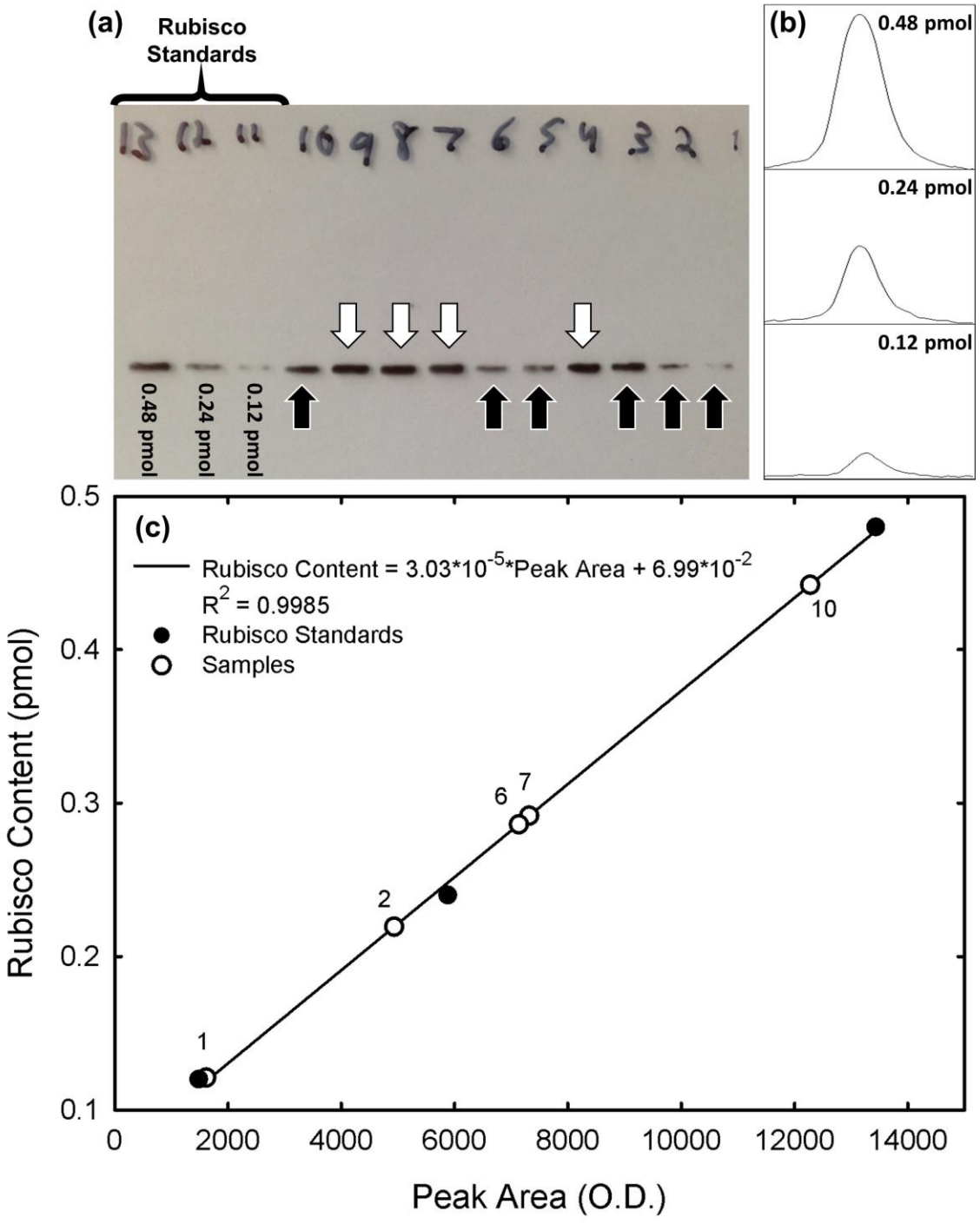

Figure A.1. Example analysis of immunoblot for quantifying Rubisco. (a) Immunoblot for Rubisco large subunit showing the quantity of Rubisco large subunit standard loaded (lanes 11 to 13) and ten samples (lanes 1 to 10). Black

arrows indicate quantifiable samples where Rubisco content falls within the range of the Rubisco standards, while white arrows indicate unquantifiable samples due to too much Rubisco. (b) Optical density peaks for the Rubisco standards in (a) from the gel analysis function in ImageJ. Total Rubisco quantity is represented by the area under the curve. (c) Rubisco content as a function of peak area (O.D.: optical density), with the Rubisco large subunit standards as black points, quantifiable samples as white points, and standard curve as the black line. Numbers near the sample points indicate the sample lane from (a).

Appendix B: Chapter 4 supplementary material

B.1 Materials and methods

Six 2-year old seedlings of *Thuja canadensis* were grown in a rooftop greenhouse with ambient temperature and lighting conditions at the Biotron Centre for Climate Change Research in London, Ontario, Canada (lat.: 42.9849 N, long.: 81.2453 W) during the summer of 2015. Irradiance during the day peaked between 700 and 1000 W m^{-2}, and temperatures ranged from 10 to 37 °C, coincident with outdoor conditions (Fig. B1). Photosynthetic CO_2 response curves were measured approximately every two weeks from July 20th until September 22nd. Net CO_2 assimilation was measured with a LI-6400XT portable photosynthesis system equipped with a 6400-22 L opaque conifer chamber and a 6400-02B LED light source (Licor Biosciences, Lincoln, NE) at 25 °C under saturating light (of 1000 μmol m^{-2} s^{-1} determined from light response curves) with a vapor pressure deficit held constant at a value between 0.9 and 1.8 kPa, and reference CO_2 concentrations of 400, 300, 200, 150, 100, 50, 400, 800, 1200, 1600, and 2000 μmol mol^{-1} CO_2. Maximum Rubisco carboxylation capacity was determined by fitting the model of Farquhar *et al.* (1980) to the CO_2 response data. The CO_2 compensation point in the absence of mitochondrial respiration (Γ*), and the Michaelis-Menten constants for Rubisco carboxylation and oxygenation (K_c and K_o, respectively) for cold-acclimated *Spinacia oleracea* were used (Yamori *et al.*, 2006) as per Way and Sage (2008).

B.2 References

Farquhar GD, von Caemmerer S, Berry JA. **1980**. A biochemical model of photosynthetic CO_2 assimilation in leaves of C_3 species. *Planta* **149**, 78–90.

Way DA, Sage RF. **2008**. Elevated growth temepratures reduce the carbon gain of black spruce [*Picea mariana* (Mill.) B.S.P.]. *Global Change Biology* **14**, 624–636.

Yamori W, Suzuki K, Noguchi K, Nakai M, Terashima I. **2006**. Effects of Rubisco kinetics and Rubisco activation state on the temperature dependence of the photosynthetic rate in spinach leaves from contrasting growth temperatures. *Plant, Cell & Environment* **29**, 1659–1670.

B.3 Figures

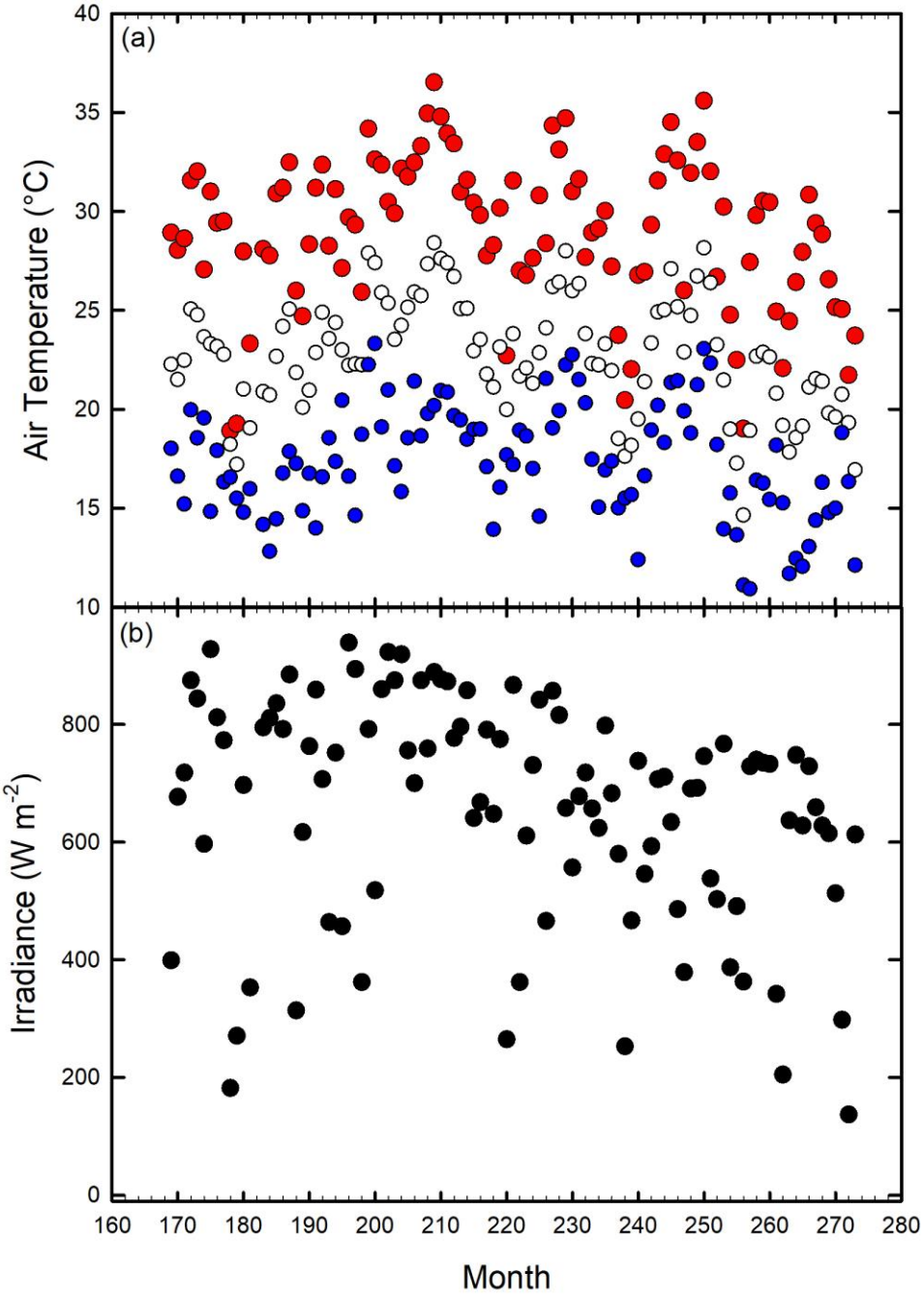

Figure B.1. Environmental data in the greenhouse over the experiment with *Thuja canadensis*. (a) maximum (red), mean (white) and minimum (blue) daily air temperatures and (b) maximum daily irradiance.

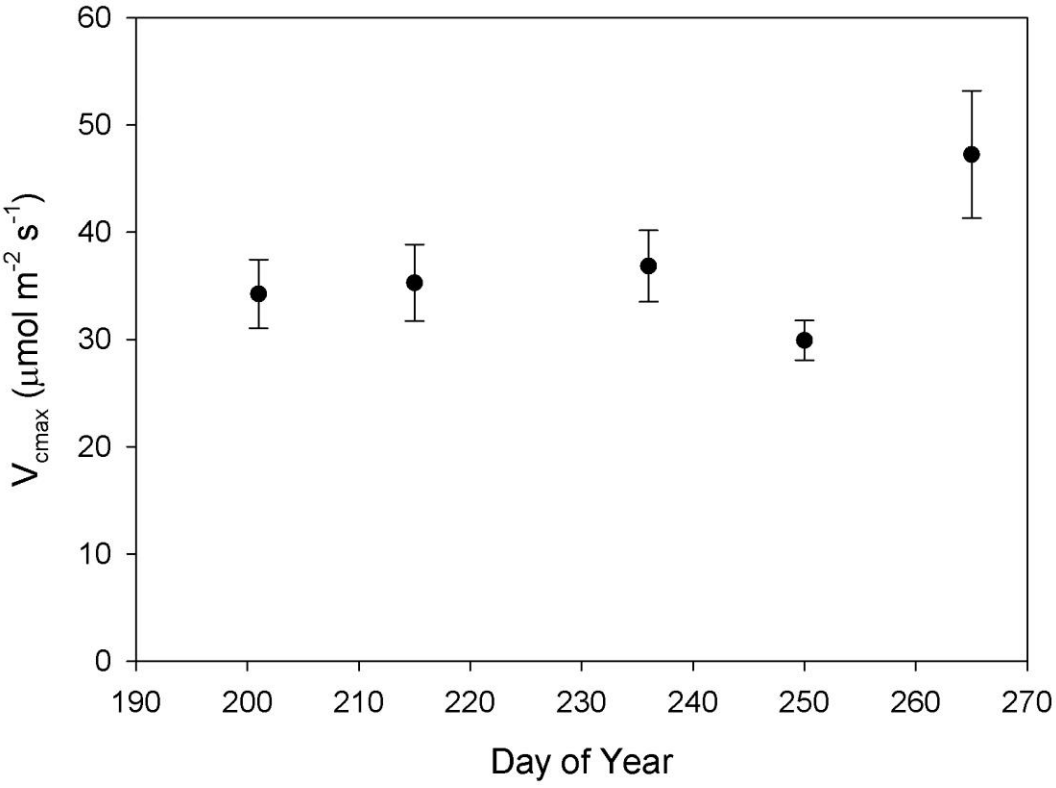

Figure B.2. Maximum Rubisco carboxylation rates (V_{cmax}) for *Thuja canadensis*. Data presented as means ± s.e.m. *N* = 6 per point.

Appendix C: Chapter 5 supplementary material

C.1 Materials and methods

Six 2-year old seedlings of *Larix laricina* were grown in a rooftop greenhouse, which was allowed to vary with ambient environmental conditions from June 18th to July 21st, 2015 at the Biotron Centre for Climate Change Research in London, Ontario, Canada (lat.: 42.9849 °N, long.: 81.2453 °W). Temperatures ranged from 12.5 to 35 °C, while irradiance peaked between 700 and 1000 W m^{-2}. The CO_2 response of net CO_2 assimilation was measured on July 21st. Gas exchange measurements were performed with a LI-6400 XT portable photosynthesis system with a 6400-22L opaque conifer chamber and a 6400-02B LED light source (Licor Biosciences, Lincoln, NE) at 25 °C under predetermined saturating light of 1000 μmol m^{-2} s^{-1}, and vapor pressure deficit held constant between 1.0 and 1.5 kPa, with measurements performed at reference CO_2 concentrations of 400, 300, 200, 150, 100, 50, 400, 800, 1200, 1600, and 2000 μmol mol^{-1} CO_2. Biochemical limitations to photosynthesis, including maximum rates of Rubisco carboxylation (V_{cmax}) and electron transport (J_{max}) were fit to the CO_2 response data using the model of Farquhar *et al*. (1980). Data from cold-acclimated *Spinacia oleracea* (Yamori *et al*., 2006) for the CO_2 compensation point in the absence of mitochondrial respiration (Γ*), and the Michaelis-Menten constants for Rubisco carboxylation and oxygenation (K_c and K_o, respectively) were used as per Way and Sage (2008). Dark respiration (R_{dark}) was measured at 25 °C in the middle of the night on July 20th.

We parameterized the stomatal conductance (g_s) response to relative humidity (RH) according to the Ball Berry model of g_s (Ball *et al*., 1987) using g_s measured at a reference CO_2 of 400 μmol mol^{-1}:

$$g_s = m_1 \frac{A}{C_a - \Gamma} RH + b_1 \qquad \text{Equation C.1}$$

where m_1 and b_1 are treatment-specific parameters (Table C.1).

Table C.1. Gas exchange parameters measured in *Larix laricina* at 25°C. Data presented as means ± s.e.m. Ball-Berry parameters were derived from data pooled from all individuals (*N* = 6).

Parameter	Value
V_{cmax} (μmol m^{-2} s^{-1})	41.2 ± 2.9
J_{max} (μmol m^{-2} s^{-1})	61.3 ± 7.5
R_{dark} (μmol m^{-2} s^{-1})	0.62 ± 0.05
Intercept of the Ball-Berry model (mol m^{-2} s^{-1})	0.0364 ± 0.0105
Slope of the Ball-Berry model (mol m^{-2} s^{-1})	5.68 ± 0.84

V_{cmax}: maximum Rubisco carboxylation capacity; J_{max}: maximum rate of electron transport; R_{dark}: dark respiration.

Table C.2. Temperature (°C) conditions used in modeling for each warming scenario in Chapter 5. All warming scenarios were run with current (400 µmol mol^{-1}) and elevated (936 µmol mol^{-1}) CO_2.

Scenario		Current			+4.5 °C			Annual Regional			Seasonal Regional		
Site	DOY	Min.	Mean	Max.	Min.	Mean	Max.	Min.	Mean	Max.	Min.	Mean	Max.
1	167	13.8	18.4	22.2	18.3	22.9	26.7	19.8	24.4	28.2	19.8	24.4	28.2
	197	16.8	21.5	25.5	21.3	26.0	30.0	22.8	27.5	31.5	22.8	27.5	31.5
	228	16.0	20.2	24.0	20.5	24.7	28.5	22.0	26.2	30.0	22.0	26.2	30.0
	259	12.6	16.4	20.8	17.1	20.9	25.3	18.6	22.4	26.8	18.6	22.4	26.8
	289	7.3	10.6	13.6	11.8	15.1	18.1	13.3	16.6	19.6	13.3	16.6	19.6
2	167	8.7	13.7	18.3	13.2	18.2	22.8	16.7	21.7	26.3	14.7	19.7	24.3
	197	12.5	16.6	20.5	17.0	21.1	25.0	20.5	24.6	28.5	18.5	22.6	26.5
	228	12.0	15.8	19.8	16.5	20.3	24.3	20.0	23.8	27.8	18.0	21.8	25.8
	259	8.2	11.6	15.7	12.7	16.1	20.2	16.2	19.6	23.7	14.2	17.6	21.7
	289	3.0	5.4	8.5	7.5	9.9	13.0	11.0	13.4	16.5	9.0	11.4	14.5
3	167	6.1	11.3	16.2	10.6	15.8	20.7	14.1	19.3	24.2	14.1	19.3	24.2
	197	9.8	14.2	18.3	14.3	18.7	22.8	17.8	22.2	26.3	17.8	22.2	26.3
	228	8.9	12.6	16.8	13.4	17.1	21.3	16.9	20.6	24.8	16.9	20.6	24.8
	259	6.6	9.0	12.3	11.1	13.5	16.8	14.6	17.0	20.3	12.6	15.0	18.3
	289	1.1	2.7	5.0	5.6	7.2	9.5	9.1	10.7	13.0	7.1	8.7	11.0
4	167	4.9	8.7	12.0	9.4	13.2	16.5	12.9	16.7	20.0	10.9	14.7	18.0
	197	10.3	13.5	16.4	14.8	18.0	20.9	18.3	21.5	24.4	16.3	19.5	22.4
	228	9.6	12.3	14.7	14.1	16.8	19.2	17.6	20.3	22.7	15.6	18.3	20.7
	259	5.8	7.8	10.3	10.3	12.3	14.8	13.8	15.8	18.3	13.8	15.8	18.3
	289	-0.7	0.2	1.3	3.8	4.7	5.8	7.3	8.2	9.3	7.3	8.2	9.3
5	167	11.7	17.2	21.6	16.2	21.7	26.1	21.7	27.2	31.6	17.7	23.2	27.6
	197	12.7	17.3	21.3	17.2	21.8	25.8	22.7	27.3	31.3	18.7	23.3	27.3
	228	10.0	14.5	18.4	14.5	19.0	22.9	20.0	24.5	28.4	16.0	20.5	24.4

259	3.4	6.7	10.6	7.9	11.2	15.1	13.4	16.7	20.6	11.4	14.7	18.6
289	-4.2	-2.7	-0.8	0.3	1.8	3.7	5.8	7.3	9.2	3.8	5.3	7.2

Current: current temperature conditions for each site x month combination; +4.5 °C: temperature increase of 4.5 °C compared to current climate conditions; Annual Regional: spatially explicit annual warming projections for 2100; Seasonal Regional: spatially and temporally explicit warming projections for 2100; Min.: minimum daily temperature; Mean: mean 24-hr temperature; Max.: maximum daily temperature; Site 1: Trenton, ON; Site 2: Moosonee, ON; Site 3: Peawanuck, ON; Site 4: Churchill, MB; Site 5: Fort Good Hope, NT; DOY: day of year; DOY 167: June 16th; DOY 197: July 16th; DOY 228: August 16th; DOY 259: September 16th; DOY 289: October 16th.

C.2 References

Ball JT, Woodrow IE, Berry JA. **1987**. A model predicting stomatal conductance and its contribution to the control of photosynthesis under different environmental conditions. In: *Progress in Photosynthesis Research, Proceedings of the VII International Congress on Photosynthesis*, vol. 4, edited by **Biggins I**, pp. 221–224. Martinus Nijhoff: Dordrecht, Netherlands.

Farquhar GD, von Caemmerer S, Berry JA. **1980**. A biochemical model of photosynthetic CO_2 assimilation in leaves of C_3 species. *Planta* **149**, 78–90.

Way DA, Sage RF. **2008**. Elevated growth temperatures reduce the carbon gain of black spruce [*Picea mariana* (Mill.) B.S.P.]. *Global Change Biology* **14**, 624–636.

Yamori W, Suzuki K, Noguchi K, Nakai M, Terashima I. **2006**. Effects of Rubisco kinetics and Rubisco activation state on the temperature dependence of the photosynthetic rate in spinach leaves from contrasting growth temperatures. *Plant, Cell & Environment* **29**, 1659–1670.

C.3 Figures

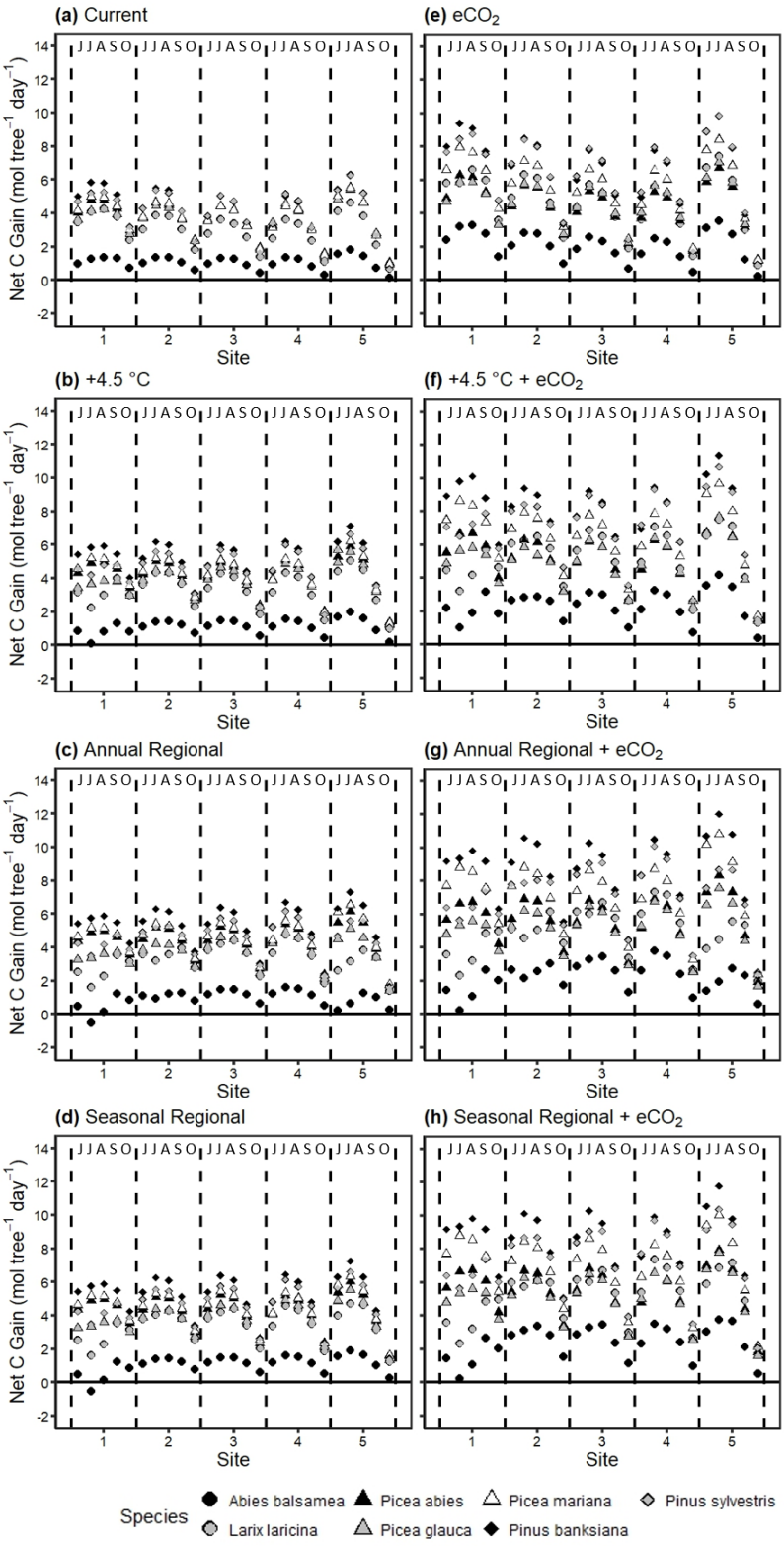
(a) Current
(e) eCO2
(b) +4.5 °C
(f) +4.5 °C + eCO2
(c) Annual Regional
(g) Annual Regional + eCO2
(d) Seasonal Regional
(h) Seasonal Regional + eCO2
Net C Gain (mol tree−1 day−1)
Site
J J A S O
Species
Abies balsamea
Picea abies
Picea mariana
Pinus sylvestris
Larix laricina
Picea glauca
Pinus banksiana

Figure C.1. Projected net daily carbon (C) gain of boreal trees across time and site under (a, e) current climate, (b, f) 4.5 °C of warming, (c, g) annual regional warming, and (d, h) seasonal regional warming, at (a, b, c, d) ambient or (e, f, g, h) elevated CO_2 for the year 2100. Data represent the means of simulations run with monoculture stands of seven boreal tree species at five sites and five time points. 0 °C indicates current climate conditions, +4.5 °C indicates global average warming for 2100, annual regional indicates spatially explicit annual warming, and seasonal regional indicates spatiotemporally explicit warming, while eCO2 indicates elevated CO_2 concentrations. JJASO stands for June, July, August, September, October, and indicate the date for each point within a site. Sites are delineated with dashed lines.

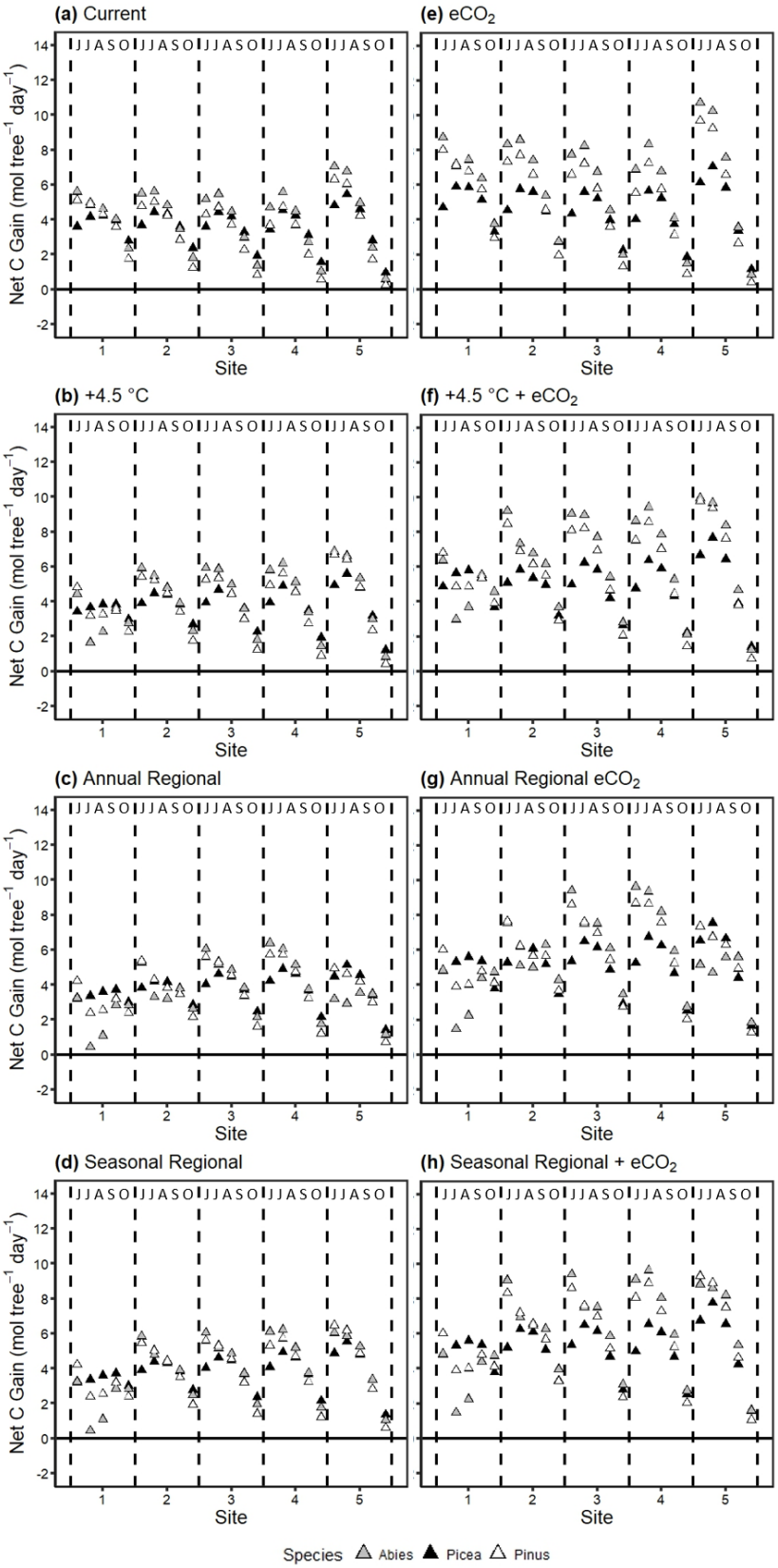
(a) Current
(e) eCO2
(b) +4.5 °C
(f) +4.5 °C + eCO2
(c) Annual Regional
(g) Annual Regional eCO2
(d) Seasonal Regional
(h) Seasonal Regional + eCO2
J J A S O J J A S O J J A S O J J A S O J J A S O
Net C Gain (mol tree−1 day−1)
Site
Species Abies Picea Pinus

Figure C.2. Projected net daily carbon (C) gain of boreal trees across time and site under (a, e) current climate, (b, f) 4.5 °C of warming, (c, g) annual regional warming, and (d, h) seasonal regional warming, at (a, b, c, d) ambient or (e, f, g, h) elevated CO_2 for the year 2100. Data represent simulations run with monoculture stands of *Picea glauca* at five sites and five time points using one of the Arrhenius temperature response parameters for *Picea*, *Abies*, or *Pinus*. 0 °C indicates current climate conditions, +4.5 °C indicates global average warming for 2100, annual regional indicates spatially explicit annual warming, and seasonal regional indicates spatiotemporally explicit warming, while eCO2 indicates elevated CO_2 concentrations. JJASO stands for June, July, August, September, October, and indicate the date for each point within a site. Sites are delineated with dashed lines.

Appendix D: Reprint permissions

D.1 Reprint permission for chapter 2

NRC RESEARCH PRESS LICENSE

TERMS AND CONDITIONS

Jan 27, 2018

This Agreement between Mr. Joseph Stinziano ("You") and NRC Research Press ("NRC Research Press") consists of your license details and the terms and conditions provided by NRC Research Press and Copyright Clearance Center.

License Number	4277311281996
License date	Jan 27, 2018
Licensed Content Publisher	NRC Research Press
Licensed Content Publication	Botany
Licensed Content Title	Combined effects of rising [CO2] and temperature on boreal forests: growth, physiology and limitations
Licensed Content Author	Joseph R. Stinziano, Danielle A. Way
Licensed Content Date	Jun 1, 2014
Licensed Content Volume	92
Licensed Content Issue	6
Type of Use	Thesis/Dissertation
Requestor type	Author (original work)
Format	Print and electronic
Portion	Full article
Order reference number	

Title of your thesis / dissertation	Effects of elevated temperature, elevated CO2 and photoperiod on conifer carbon fluxes
Expected completion date	Apr 2018
Estimated size(pages)	357
Requestor Location	Mr. Joseph Stinziano 1151 Richmond St Biological & Geological Sciences Rm 2035 London, ON N6A 5B7 Canada Attn: Mr. Joseph Stinziano
Billing Type	Invoice
Billing Address	Mr. Joseph Stinziano 1151 Richmond St Biological & Geological Sciences Rm 2035 London, ON N6A 5B7 Canada Attn: Mr. Joseph Stinziano
Total	0.00 CAD
Terms and Conditions	

General Terms & Conditions

Permission is granted upon the requester's compliance with the following terms and conditions:

1. A credit line will be prominently placed in your product(s) and include: for books the author, book title, editor, copyright holder, year of publication; for journals the author, title of article, title of journal, volume number, issue number, and the

inclusive pages. The credit line must include the following wording: "© 2008 Canadian Science Publishing or its licensors. Reproduced with permission," except when an author of an original article published in 2009 or later is reproducing his/her own work.

2. The requester warrants that the material shall not be used in any manner that may be derogatory to the title, content, or authors of the material or to Canadian Science Publishing, including but not limited to an association with conduct that is fraudulent or otherwise illegal.
3. Permission is granted for the term (for Books/CDs-Shelf Life; for Internet/Intranet-In perpetuity; for all other forms of print-the life of the title) and purpose specified in your request. Once term has expired, permission to renew must be made in writing.
4. Permission granted is nonexclusive, and is valid throughout the world in English and the languages specified in your original request. A new permission must be requested for revisions of the publication under current consideration.
5. Canadian Science Publishing cannot supply the requester with the original artwork or a "clean copy."
6. If the Canadian Science Publishing material is to be translated, the following lines must be included: The authors, editors, and Canadian Science Publishing are not responsible for errors or omissions in translations.

v1.4

D.2 Reprint permission for chapter 3

JOHN WILEY AND SONS LICENSE

TERMS AND CONDITIONS

Jan 27, 2018

This Agreement between Mr. Joseph Stinziano ("You") and John Wiley and Sons ("John Wiley and Sons") consists of your license details and the terms and conditions provided by John Wiley and Sons and Copyright Clearance Center.

License Number	4277320167598
License date	Jan 27, 2018
Licensed Content Publisher	John Wiley and Sons
Licensed Content Publication	Plant, Cell & Environment
Licensed Content Title	Autumn photosynthetic decline and growth cessation in seedlings of white spruce are decoupled under warming and photoperiod manipulations
Licensed Content Author	Joseph R. Stinziano, Danielle A. Way
Licensed Content Date	Mar 20, 2017
Licensed Content Pages	21
Type of use	Dissertation/Thesis
Requestor type	Author of this Wiley article
Format	Print and electronic
Portion	Full article
Will you be translating?	No

Title of your thesis / dissertation	Effects of elevated temperature, elevated CO2 and photoperiod on conifer carbon fluxes
Expected completion date	Apr 2018
Expected size (number of pages)	357
Requestor Location	Mr. Joseph Stinziano 1151 Richmond St Biological & Geological Sciences Rm 2035 London, ON N6A 5B7 Canada Attn: Mr. Joseph Stinziano
Publisher Tax ID	EU826007151
Total	0.00 CAD
Terms and Conditions	

TERMS AND CONDITIONS

This copyrighted material is owned by or exclusively licensed to John Wiley & Sons, Inc. or one of its group companies (each a"Wiley Company") or handled on behalf of a society with which a Wiley Company has exclusive publishing rights in relation to a particular work (collectively "WILEY"). By clicking "accept" in connection with completing this licensing transaction, you agree that the following terms and conditions apply to this transaction (along with the billing and payment terms and conditions established by the Copyright Clearance Center Inc., ("CCC's Billing and Payment terms and conditions"), at the time that you opened your RightsLink account (these are available at any time at http://myaccount.copyright.com).

Terms and Conditions

rent, sell, loan, lease, pledge, offer as security, transfer or assign the Wiley Materials on a stand-alone basis, or any of the rights granted to you hereunder to any other person.

- The Wiley Materials and all of the intellectual property rights therein shall at all times remain the exclusive property of John Wiley & Sons Inc, the Wiley Companies, or their respective licensors, and your interest therein is only that of having possession of and the right to reproduce the Wiley Materials pursuant to Section 2 herein during the continuance of this Agreement. You agree that you own no right, title or interest in or to the Wiley Materials or any of the intellectual property rights therein. You shall have no rights hereunder other than the license as provided for above in Section 2. No right, license or interest to any trademark, trade name, service mark or other branding ("Marks") of WILEY or its licensors is granted hereunder, and you agree that you shall not assert any such right, license or interest with respect thereto

- NEITHER WILEY NOR ITS LICENSORS MAKES ANY WARRANTY OR REPRESENTATION OF ANY KIND TO YOU OR ANY THIRD PARTY, EXPRESS, IMPLIED OR STATUTORY, WITH RESPECT TO THE MATERIALS OR THE ACCURACY OF ANY INFORMATION CONTAINED IN THE MATERIALS, INCLUDING, WITHOUT LIMITATION, ANY IMPLIED WARRANTY OF MERCHANTABILITY, ACCURACY, SATISFACTORY QUALITY, FITNESS FOR A PARTICULAR PURPOSE, USABILITY, INTEGRATION OR NON-INFRINGEMENT AND ALL SUCH WARRANTIES ARE HEREBY EXCLUDED BY WILEY AND ITS LICENSORS AND WAIVED BY YOU.

- WILEY shall have the right to terminate this Agreement immediately upon breach of this Agreement by you.

- You shall indemnify, defend and hold harmless WILEY, its Licensors and their respective directors, officers, agents and employees, from and against any actual or

threatened claims, demands, causes of action or proceedings arising from any breach of this Agreement by you.

- IN NO EVENT SHALL WILEY OR ITS LICENSORS BE LIABLE TO YOU OR ANY OTHER PARTY OR ANY OTHER PERSON OR ENTITY FOR ANY SPECIAL, CONSEQUENTIAL, INCIDENTAL, INDIRECT, EXEMPLARY OR PUNITIVE DAMAGES, HOWEVER CAUSED, ARISING OUT OF OR IN CONNECTION WITH THE DOWNLOADING, PROVISIONING, VIEWING OR USE OF THE MATERIALS REGARDLESS OF THE FORM OF ACTION, WHETHER FOR BREACH OF CONTRACT, BREACH OF WARRANTY, TORT, NEGLIGENCE, INFRINGEMENT OR OTHERWISE (INCLUDING, WITHOUT LIMITATION, DAMAGES BASED ON LOSS OF PROFITS, DATA, FILES, USE, BUSINESS OPPORTUNITY OR CLAIMS OF THIRD PARTIES), AND WHETHER OR NOT THE PARTY HAS BEEN ADVISED OF THE POSSIBILITY OF SUCH DAMAGES. THIS LIMITATION SHALL APPLY NOTWITHSTANDING ANY FAILURE OF ESSENTIAL PURPOSE OF ANY LIMITED REMEDY PROVIDED HEREIN.

- Should any provision of this Agreement be held by a court of competent jurisdiction to be illegal, invalid, or unenforceable, that provision shall be deemed amended to achieve as nearly as possible the same economic effect as the original provision, and the legality, validity and enforceability of the remaining provisions of this Agreement shall not be affected or impaired thereby.

- The failure of either party to enforce any term or condition of this Agreement shall not constitute a waiver of either party's right to enforce each and every term and condition of this Agreement. No breach under this agreement shall be deemed waived or excused by either party unless such waiver or consent is in writing signed by the party granting such waiver or consent. The waiver by or consent of a party to a breach of any provision of this Agreement shall not operate or be construed as a waiver of or consent to any other or subsequent breach by such other party.

- This Agreement may not be assigned (including by operation of law or otherwise) by you without WILEY's prior written consent.
- Any fee required for this permission shall be non-refundable after thirty (30) days from receipt by the CCC.
- These terms and conditions together with CCC's Billing and Payment terms and conditions (which are incorporated herein) form the entire agreement between you and WILEY concerning this licensing transaction and (in the absence of fraud) supersedes all prior agreements and representations of the parties, oral or written. This Agreement may not be amended except in writing signed by both parties. This Agreement shall be binding upon and inure to the benefit of the parties' successors, legal representatives, and authorized assigns.
- In the event of any conflict between your obligations established by these terms and conditions and those established by CCC's Billing and Payment terms and conditions, these terms and conditions shall prevail.
- WILEY expressly reserves all rights not specifically granted in the combination of (i) the license details provided by you and accepted in the course of this licensing transaction, (ii) these terms and conditions and (iii) CCC's Billing and Payment terms and conditions.
- This Agreement will be void if the Type of Use, Format, Circulation, or Requestor Type was misrepresented during the licensing process.
- This Agreement shall be governed by and construed in accordance with the laws of the State of New York, USA, without regards to such state's conflict of law rules. Any legal action, suit or proceeding arising out of or relating to these Terms and Conditions or the breach thereof shall be instituted in a court of competent jurisdiction in New York County in the State of New York in the United States of America and each party hereby consents and submits to the personal jurisdiction of such court, waives any objection to venue in such court and consents to service of

process by registered or certified mail, return receipt requested, at the last known address of such party.

WILEY OPEN ACCESS TERMS AND CONDITIONS

Wiley Publishes Open Access Articles in fully Open Access Journals and in Subscription journals offering Online Open. Although most of the fully Open Access journals publish open access articles under the terms of the Creative Commons Attribution (CC BY) License only, the subscription journals and a few of the Open Access Journals offer a choice of Creative Commons Licenses. The license type is clearly identified on the article.

The Creative Commons Attribution License

The Creative Commons Attribution License (CC-BY) allows users to copy, distribute and transmit an article, adapt the article and make commercial use of the article. The CC-BY license permits commercial and non-

Creative Commons Attribution Non-Commercial License

The Creative Commons Attribution Non-Commercial (CC-BY-NC)License permits use, distribution and reproduction in any medium, provided the original work is properly cited and is not used for commercial purposes.(see below)

Creative Commons Attribution-Non-Commercial-NoDerivs License

The Creative Commons Attribution Non-Commercial-NoDerivs License (CC-BY-NC-ND) permits use, distribution and reproduction in any medium, provided the original work is properly cited, is not used for commercial purposes and no modifications or adaptations are made. (see below)

Use by commercial "for-profit" organizations

Use of Wiley Open Access articles for commercial, promotional, or marketing purposes requires further explicit permission from Wiley and will be subject to a fee.

D.3 Reprint permission for chapter 4

JOHN WILEY AND SONS LICENSE

TERMS AND CONDITIONS

Jan 27, 2018

This Agreement between Mr. Joseph Stinziano ("You") and John Wiley and Sons ("John Wiley and Sons") consists of your license details and the terms and conditions provided by John Wiley and Sons and Copyright Clearance Center.

License Number	4277320462598
License date	Jan 27, 2018
Licensed Content Publisher	John Wiley and Sons
Licensed Content Publication	Global Change Biology
Licensed Content Title	Improving models of photosynthetic thermal acclimation: Which parameters are most important and how many should be modified?
Licensed Content Author	Joseph R. Stinziano, Danielle A. Way, William L. Bauerle
Licensed Content Date	Nov 1, 2017
Licensed Content Pages	1
Type of use	Dissertation/Thesis
Requestor type	Author of this Wiley article
Format	Print and electronic
Portion	Full article
Will you be translating?	No
Title of your thesis / dissertation	Effects of elevated temperature, elevated CO2 and photoperiod on conifer carbon fluxes

Expected completion date	Apr 2018
Expected size (number of pages)	357
Requestor Location	Mr. Joseph Stinziano 1151 Richmond St Biological & Geological Sciences Rm 2035 London, ON N6A 5B7 Canada Attn: Mr. Joseph Stinziano
Publisher Tax ID	EU826007151
Total	0.00 CAD
Terms and Conditions	

TERMS AND CONDITIONS

This copyrighted material is owned by or exclusively licensed to John Wiley & Sons, Inc. or one of its group companies (each a"Wiley Company") or handled on behalf of a society with which a Wiley Company has exclusive publishing rights in relation to a particular work (collectively "WILEY"). By clicking "accept" in connection with completing this licensing transaction, you agree that the following terms and conditions apply to this transaction (along with the billing and payment terms and conditions established by the Copyright Clearance Center Inc., ("CCC's Billing and Payment terms and conditions"), at the time that you opened your RightsLink account (these are available at any time at http://myaccount.copyright.com).

Terms and Conditions

- The materials you have requested permission to reproduce or reuse (the "Wiley Materials") are protected by copyright.

Materials on a stand-alone basis, or any of the rights granted to you hereunder to any other person.

- The Wiley Materials and all of the intellectual property rights therein shall at all times remain the exclusive property of John Wiley & Sons Inc, the Wiley Companies, or their respective licensors, and your interest therein is only that of having possession of and the right to reproduce the Wiley Materials pursuant to Section 2 herein during the continuance of this Agreement. You agree that you own no right, title or interest in or to the Wiley Materials or any of the intellectual property rights therein. You shall have no rights hereunder other than the license as provided for above in Section 2. No right, license or interest to any trademark, trade name, service mark or other branding ("Marks") of WILEY or its licensors is granted hereunder, and you agree that you shall not assert any such right, license or interest with respect thereto

- NEITHER WILEY NOR ITS LICENSORS MAKES ANY WARRANTY OR REPRESENTATION OF ANY KIND TO YOU OR ANY THIRD PARTY, EXPRESS, IMPLIED OR STATUTORY, WITH RESPECT TO THE MATERIALS OR THE ACCURACY OF ANY INFORMATION CONTAINED IN THE MATERIALS, INCLUDING, WITHOUT LIMITATION, ANY IMPLIED WARRANTY OF MERCHANTABILITY, ACCURACY, SATISFACTORY QUALITY, FITNESS FOR A PARTICULAR PURPOSE, USABILITY, INTEGRATION OR NON-INFRINGEMENT AND ALL SUCH WARRANTIES ARE HEREBY EXCLUDED BY WILEY AND ITS LICENSORS AND WAIVED BY YOU.

- WILEY shall have the right to terminate this Agreement immediately upon breach of this Agreement by you.

- You shall indemnify, defend and hold harmless WILEY, its Licensors and their respective directors, officers, agents and employees, from and against any actual or

threatened claims, demands, causes of action or proceedings arising from any breach of this Agreement by you.

- IN NO EVENT SHALL WILEY OR ITS LICENSORS BE LIABLE TO YOU OR ANY OTHER PARTY OR ANY OTHER PERSON OR ENTITY FOR ANY SPECIAL, CONSEQUENTIAL, INCIDENTAL, INDIRECT, EXEMPLARY OR PUNITIVE DAMAGES, HOWEVER CAUSED, ARISING OUT OF OR IN CONNECTION WITH THE DOWNLOADING, PROVISIONING, VIEWING OR USE OF THE MATERIALS REGARDLESS OF THE FORM OF ACTION, WHETHER FOR BREACH OF CONTRACT, BREACH OF WARRANTY, TORT, NEGLIGENCE, INFRINGEMENT OR OTHERWISE (INCLUDING, WITHOUT LIMITATION, DAMAGES BASED ON LOSS OF PROFITS, DATA, FILES, USE, BUSINESS OPPORTUNITY OR CLAIMS OF THIRD PARTIES), AND WHETHER OR NOT THE PARTY HAS BEEN ADVISED OF THE POSSIBILITY OF SUCH DAMAGES. THIS LIMITATION SHALL APPLY NOTWITHSTANDING ANY FAILURE OF ESSENTIAL PURPOSE OF ANY LIMITED REMEDY PROVIDED HEREIN.

- Should any provision of this Agreement be held by a court of competent jurisdiction to be illegal, invalid, or unenforceable, that provision shall be deemed amended to achieve as nearly as possible the same economic effect as the original provision, and the legality, validity and enforceability of the remaining provisions of this Agreement shall not be affected or impaired thereby.

- The failure of either party to enforce any term or condition of this Agreement shall not constitute a waiver of either party's right to enforce each and every term and condition of this Agreement. No breach under this agreement shall be deemed waived or excused by either party unless such waiver or consent is in writing signed by the party granting such waiver or consent. The waiver by or consent of a party to a breach of any provision of this Agreement shall not operate or be construed as a waiver of or consent to any other or subsequent breach by such other party.

- This Agreement may not be assigned (including by operation of law or otherwise) by you without WILEY's prior written consent.

- Any fee required for this permission shall be non-refundable after thirty (30) days from receipt by the CCC.

- These terms and conditions together with CCC's Billing and Payment terms and conditions (which are incorporated herein) form the entire agreement between you and WILEY concerning this licensing transaction and (in the absence of fraud) supersedes all prior agreements and representations of the parties, oral or written. This Agreement may not be amended except in writing signed by both parties. This Agreement shall be binding upon and inure to the benefit of the parties' successors, legal representatives, and authorized assigns.

- In the event of any conflict between your obligations established by these terms and conditions and those established by CCC's Billing and Payment terms and conditions, these terms and conditions shall prevail.

- WILEY expressly reserves all rights not specifically granted in the combination of (i) the license details provided by you and accepted in the course of this licensing transaction, (ii) these terms and conditions and (iii) CCC's Billing and Payment terms and conditions.

- This Agreement will be void if the Type of Use, Format, Circulation, or Requestor Type was misrepresented during the licensing process.

- This Agreement shall be governed by and construed in accordance with the laws of the State of New York, USA, without regards to such state's conflict of law rules. Any legal action, suit or proceeding arising out of or relating to these Terms and Conditions or the breach thereof shall be instituted in a court of competent jurisdiction in New York County in the State of New York in the United States of America and each party hereby consents and submits to the personal jurisdiction of such court, waives any objection to venue in such court and consents to service of

process by registered or certified mail, return receipt requested, at the last known address of such party.

WILEY OPEN ACCESS TERMS AND CONDITIONS

Wiley Publishes Open Access Articles in fully Open Access Journals and in Subscription journals offering Online Open. Although most of the fully Open Access journals publish open access articles under the terms of the Creative Commons Attribution (CC BY) License only, the subscription journals and a few of the Open Access Journals offer a choice of Creative Commons Licenses. The license type is clearly identified on the article.

The Creative Commons Attribution License

The Creative Commons Attribution License (CC-BY) allows users to copy, distribute and transmit an article, adapt the article and make commercial use of the article. The CC-BY license permits commercial and non-

Creative Commons Attribution Non-Commercial License

The Creative Commons Attribution Non-Commercial (CC-BY-NC)License permits use, distribution and reproduction in any medium, provided the original work is properly cited and is not used for commercial purposes.(see below)

Creative Commons Attribution-Non-Commercial-NoDerivs License

The Creative Commons Attribution Non-Commercial-NoDerivs License (CC-BY-NC-ND) permits use, distribution and reproduction in any medium, provided the original work is properly cited, is not used for commercial purposes and no modifications or adaptations are made. (see below)

Use by commercial "for-profit" organizations

Use of Wiley Open Access articles for commercial, promotional, or marketing purposes requires further explicit permission from Wiley and will be subject to a fee.

Curriculum Vitae

Name: Joseph Ronald Stinziano

Post-secondary Education and Degrees:
University of Western Ontario
London, Ontario, Canada
2013-2018 Ph.D.

The University of Western Ontario
London, Ontario, Canada
2009-2013 B.Sc.

Honours and Awards:
Fulbright Student Award, 2016
ISPR Travel Grant, 2016
NSERC Michael Smith Foreign Study Supplement, 2016
American Society of Plant Biologists Travel Grant, 2015
NSERC Doctoral Canada Graduate Scholarship, 2014
Julie Payette-NSERC Research Scholarship, 2013

Related Work Experience
Teaching Assistant
The University of Western Ontario
2013-2017

Member-at-large
Environmental and Ecological Planning Advisory Committee (EEPAC)
The City of London
2014-2018

Publications:
10 peer-reviewed publications, 160 citations, h-index: 6, i-10 index: 5

Des Marteaux L, **Stinziano JR**, Sinclair BJ. **2018**. Effects of cold acclimation on rectal micromorphology, ultrastructure, and cytoskeletal stability in *Gryllus pennsylvanicus* crickets. *Journal of Insect Physiology* **104**, 15–24. doi: 10.1016/j.jinsphys.2017.11.004.

Stinziano, JR, Way DA, Bauerle WL. **2018**. Improving models of photosynthetic thermal acclimation: which parameters are most important and how many should be modified? *Global Change Biology* **24**, 1580–1598. doi: 10.1111/gcb.13924.

Way DA, **Stinziano JR**, Berghoff H, Oren R. **2017**. How well do seasonal dynamics of photosynthetic capacity correlate with leaf proxies and climate fluctuations? *Tree Physiology* **37**, 879–888. doi: 10.1093/treephys/tpx086.

Stinziano JR, Way DA. **2017**. Autumn photosynthetic decline and growth cessation are decoupled under warming and photoperiod manipulations. *Plant, Cell & Environment* **40**, 1296–1316. doi: 10.1111/pce.12917

Stinziano JR, Morgan PB, Lynch DJ, Saathoff AJ, McDermitt DK, Hanson DT. **2017**. The rapid A/Ci response (RACiR): photosynthesis in the phenomic era. *Plant, Cell & Environment* **40**, 1256–1262. doi: 10.1111/pce.12911.

Stinziano JR, Hüner NPA, Way DA. **2015**. Warming delays autumn declines in photosynthetic capacity in a boreal conifer, Norway spruce (*Picea abies*). *Tree Physiology* 35, 1303–1313. doi: 10.1093/treephys/tpv118.

Quentin AG, Pinkard EA, Ryan MG, … **Stinziano JR** (52nd author of 60), *et al*. **2015**. Non-structural carbohydrates in woody plants compared among laboratories. *Tree Physiology* **35**, 1146–1165. doi: 10.1093/treephys/tpv073.

Stinziano JR, Sové RJ, Rundle HD, Sinclair BJ. **2015**. Rapid desiccation hardening changes the cuticular hydrocarbon profile of *Drosophila melanogaster*. Comparative Biochemistry and Physiology: Part A **180**, 38–42. doi: 10.1016/j.cbpa.2014.11.004.

Stinziano JR, Way DA. **2014**. Combined effects of rising CO_2 and temperature on Canada's boreal forest: growth, physiology and limitations. *Botany* **92**, 425–436. doi: 10.1139/cjb-2013-0314.

Sinclair BJ, **Stinziano JR**, Williams CM, MacMillan HA, Marshall KE, Storey KB. **2013**. Real-time measurement of metabolic rate during freezing and thawing of the wood frog, *Rana sylvatica*: implications for overwinter energy use. *Journal of Experimental Biology* **216**, 292–302. doi: 10.1241/jeb.076331.